



HAL
open science

Discovering Conglomerates for Chiral Resolution by Crystallization

Aliou Mbodji

► **To cite this version:**

Aliou Mbodji. Discovering Conglomerates for Chiral Resolution by Crystallization. Cristallography. Normandie Université, 2020. English. NNT : 2020NORMR006 . tel-02917352

HAL Id: tel-02917352

<https://theses.hal.science/tel-02917352v1>

Submitted on 19 Aug 2020

HAL is a multi-disciplinary open access archive for the deposit and dissemination of scientific research documents, whether they are published or not. The documents may come from teaching and research institutions in France or abroad, or from public or private research centers.

L'archive ouverte pluridisciplinaire **HAL**, est destinée au dépôt et à la diffusion de documents scientifiques de niveau recherche, publiés ou non, émanant des établissements d'enseignement et de recherche français ou étrangers, des laboratoires publics ou privés.



Normandie Université

THÈSE

Pour obtenir le diplôme de doctorat

Spécialité Chimie

Préparée au sein de l'Université de Rouen Normandie

Discovering Conglomerates for Chiral Resolution by Crystallization

**Présentée et soutenue par
Aliou MBODJI**

**Thèse soutenue publiquement le 14 Mai 2020
devant le jury composé de**

M. Johan WOUTERS	Professeur Université de Namur	Rapporteur
Mme. Jeanne CRASSOUS	Directeur de Recherche Université de Rennes 1	Rapporteur
Mme. Mihaela POP	Docteur Entreprise TeraCrystal	Examineur
Mme. Valérie DUPRAY	MCF – HDR Université de Rouen Normandie	Directeur de Thèse
M. Gérard COQUEREL	Professeur Université de Rouen Normandie	Président
M. Gabin GBABODE	MCF Université de Rouen Normandie	Membre invité
M. Richard M KELLOGG	Professeur Entreprise Syncom BV	Membre invité

Thèse dirigée par Valérie DUPRAY MCF-HDR et Co-encadrée par le Dr. Gabin GBABODE au laboratoire Sciences et Méthodes Séparatives (EA 3233 SMS)



To my wife Boury,

To my aunt Marianne,

To my Family,

To all my Friends,

**« L'intensité de ta foi augmente en
fonction de la profondeur de tes
pensées » Cheikh Ahmadou BAMB**

Acknowledgments

First of all, I want to thank Professor Gérard Coquerel for allowing me to do my PhD thesis in his group: Science et Méthodes Séparatives (SMS laboratory) but also for making me discover a lot of concepts on heterogeneous equilibria, preferential crystallization and more that had so far escaped me. I would like to thank you for the candidate compound you proposed to me for this work and for your daily take home wise lessons during our discussion. I am sure that they will bright my future carrier.

I would like to take this opportunity to say a very big thank to my two supervisors, Dr Valérie Dupray and Dr Gabin Gbabode, for giving me the opportunity to achieve a so rewarding thesis, giving me the possibility to progress in the field of Material Chemistry and to discover a new speciality of chemistry: Crystallization. Both of you have shared with me knowledge on nonlinear optics, identification of critical crystallization parameters, solving crystal structure from crystals and powders etc. Discussing with both of you were immediately easy and your daily comments, suggestions and recommendations on my experimental results were always fruitful to pursue the work. You have inspired me for your humble and simplicity with great rigor.

Specially, I would like to thank Dr Morgane Sanselme for helping to solve all the crystal structures. Without your collaboration, this work could not be achieved, I appreciate a lot your valuable work.

I thank all the permanent members of the laboratory (Dr Clément Brandel, Dr Ivo Rietveld, Dr Nicolas Couvrat, Dr Yohann Cartigny, Prof. Samuel Petit, and Prof. Pascal Cardinael and colleagues of chromatography team) for the constructive discussions we have in their offices or during seminar. They were a source of motivation and thus give me courage to pursue this work and improve my results.

Special thanks to Dr Simon Clevers and Dr Lina Yuan for their tutorials on SHG technique at the beginning of my PhD thesis. Thanks also to Dr Antoine Burel, Dr Bienvenu Atawa, Dr Clément De Saint Jores and Dr François Xavier Gendron for their help and support during their PhD period in the SMS laboratory.

I thank all my colleagues: CORE members (Dr Ryusei Oketani and Lina Harfouche), Dr Manon Shindler, other PhD students (Kangli Li, Chloé Sainlaud, Laurérine Marc, Aurélien Lemerrier,

Marine Hoquante and Mélody Briard), the members of the laboratory (Lucie Dautreaux, Celine Bensakoun and Marie Vaccaro) that allow daily to advance the science and all trainees who have crossed my path and helped to research and to the life of laboratory.

I would like to thank Professor Richard M Kellogg, Dr Michel Leeman and Syncom BV, Groningen-The Netherlands, for providing me one of the compounds used for this work. Thanks a lot, to Prof. Kellogg and Dr Leeman for their valuable contribution to the publications of this work.

During my thesis, I had the chance to spend one month in Nijmegen, The Netherlands, in the IMM laboratory, one month in Manchester, UK, in the CCAPPE laboratory, for my academic secondments and one month in Cluj-Napoca, Romania, TeraCrystal for my industrial secondment. I would like to thank respectively Professor Elias Vlieg and his group, Dr Thomas Vetter and his group, and Dr Mihaela Pop and his group which gave me the opportunity to discover more techniques and facilities for the characterization and chiral separation of organic compounds.

I would like to thank the European Commission by funding this research through the CORE project (October 2016–September 2020) from the Horizon 2020 Research and Innovation Programme of the European Union under Marie Skłodowska-Curie Grant Agreement No. 722456 CORE ITN. This research and innovation programme gave me the opportunity to accomplish a PhD degree and to build a very important scientific network and to travel across Europe.

Finally, I thank my mom Soukeye Dieng for all the love and support you have showed me, long life mommy and my dad Ibrahima who passed away in 2010. Special thanks to my aunt and mom Marianne Barry who passed away at the end of my PhD (beginning of 2020). I used to call you “Maman Barry”. For this auspicious occasion, I am indeed very grateful for all the love and support you have showed me since day one. You were my confident, my everything, you have done a lot for me, I will never forget to pray for you. Thanks to my other aunty Fambaye and other members of the family for their support always.

Special thanks to my pretty wife Penda Boury Ndao Mbodji, my life. Your warm support is always with me, I love you, my heart.

TABLE OF CONTENTS

TABLE OF CONTENTS	7
GENERAL INTRODUCTION	12
DEFINITION OF SOME BASIC CONCEPTS USED IN THE MANUSCRIPT	14
CHAPTER 1: GENERALITIES	16
PART 1 : THE CRYSTALLINE STATE	17
1.1. CRYSTALLINE STATE OF SOLIDS	17
1.2. THE GROUP THEORY	18
1.2.1. Unit cell, crystal systems and Bravais lattices.....	18
1.2.2. Symmetry and symmetry operations	19
1.2.3. Space groups.....	21
1.3. STRUCTURAL CHARACTERIZATION OF CRYSTALLINE SOLIDS	22
1.3.2. X-ray powder diffraction (XRPD).....	23
1.3.3. Single Crystal X-Ray Diffraction (SC-XRD).....	23
PART 2: THERMODYNAMICS AND HETEROGENEOUS EQUILIBRIA	25
2.1. CRYSTAL GENESIS	25
2.1.1. Precipitation.....	25
2.1.1.1. Supersaturation.....	25
2.1.2. Nucleation	25
2.1.2.1. Primary nucleation.....	25
2.1.2.2. Secondary nucleation.....	27
2.1.3. Growth.....	27
2.2. HETEROGENEOUS EQUILIBRIA AND STABILITY	27
2.2.1. Phase equilibria	27
2.2.2. Phase rule	28
2.2.3. Gibbs free energy	28
2.2.4. Equilibrium and stability	29
PART 3 : CHIRALITY	31
3.1. CHIRALITY AND STEREOISOMERS	31
3.1.1. History of chirality	31
3.1.2. Definition of chirality	32
3.1.3. Stereogenic centre and stereoisomers.....	33
3.1.3.1. Enantiomers.....	34
3.1.3.2. Diastereomers	35
3.1.3.3. Atropisomers	35
3.2. THERMODYNAMICS OF CHIRAL SYSTEMS	36
3.2.1. Binary phase diagrams of racemic mixtures.....	36
3.2.2. Ternary phase diagrams of racemic mixtures.....	38
3.3. CRYSTALLOGRAPHY OF CHIRAL MOLECULES	39
PART 4: RESOLUTION OF RACEMIC MIXTURES	42
4.1. CHROMATOGRAPHIC RESOLUTION.....	42
4.2. DIRECT RESOLUTION.....	42
4.2.1. Preferential crystallization (PC)	42
4.2.2. Deracemization.....	44

4.3. DIASTEREOMERIC RESOLUTION	44
PART 5: INTRODUCTION TO NONLINEAR OPTICS.....	45
5.1. GENERALITIES.....	45
5.1.1. Origin of optical nonlinearity	45
5.1.2. Theoretical explanation of nonlinear optics	45
5.1.3. Quadratic nonlinear phenomena.....	47
5.2. SECOND HARMONIC GENERATION (SHG)	48
5.2.1. Principle of SHG	48
5.2.2. Requirements for SHG	49
5.2.2.1. Non-centrosymmetry	49
5.2.2.2. Neumann principle	49
5.2.2.3. Kleinman symmetry rules.....	50
5.2.3. Conversion efficiency.....	51
5.2.4. Phase matching conditions	51
5.3. CLASSIFICATION OF NONLINEAR OPTICAL MATERIALS.....	52
5.3.1. Inorganic NLO materials	52
5.3.2. Organic NLO materials	53
5.3.3. Semi-organic materials.....	53
5.3.4. Organo-metallic NLO crystals	53
5.4. APPLICATIONS OF NLO CRYSTALS	53
PART 6 : CONCLUSION.....	55
REFERENCES	56
CHAPTER 2: DEVELOPMENT OF <i>IN SITU</i> SHG SET-UP AND ITS APPLICABILITY FOR CHIRAL COMPOUNDS.....	64
PART 1 : INTRODUCTION.....	65
PART 2: PRINCIPLE OF SCREENING OF CONGLOMERATE FORMING SYSTEM BY SHG	66
2.1. CLASSICAL TECHNIQUES	66
2.1.1. Comparison of spectroscopic data.....	66
2.1.2. Thermal behaviour analyses	66
2.1.3. Solubility data.....	67
2.2. SECOND HARMONIC GENERATION (SHG) TECHNIQUE	67
2.2.1 Principle of SHG pre-screening.....	67
2.2.2. Experimental Powder-SHG set-up	67
2.2.3. SHG responses	68
2.2.4. Detection of SHG signal in suspension (<i>in situ</i>).....	70
PART 3: FEASIBILITY STUDY	71
3.1. DETECTION OF SHG SIGNAL FOR NON-CENTROSYMMETRIC CRYSTALS IN SUSPENSION.....	71
3.1.1. Choice of α -quartz as a reference.....	71
3.1.2. Preliminary tests	71
3.2. SHG INTENSITY DEPENDENCIES.....	72
3.3.1. Influence of the amount of crystalline phase.....	72
3.3.2. Influence of the nature of solvent.....	73
3.3.2.1. Refractive index.....	73

3.3.2.2. Absorption coefficient	74
3.3. CONCLUSION OF THE FEASIBILITY STUDY	75
PART 4: EXPERIMENTAL SHG SET-UP FOR <i>IN SITU</i> MEASUREMENTS.....	77
4.1. DESCRIPTION OF THE SET-UP AND PRINCIPLE OF THE MEASUREMENTS.....	77
4.2. SELECTION OF CRYSTALLIZATION SYSTEMS	78
PART 5: CRYSTALLIZATION OF POTASSIUM DIHYDROGEN PHOSPHATE (KDP) MONITORED BY <i>IN SITU</i> SHG	79
5.1. REASONS OF THE CHOICE	79
5.2. EXPERIMENTAL CONDITIONS	79
5.3. RESULTS AND DISCUSSION.....	79
5.4. CONCLUSION AND POSSIBILITY TO EXTEND TO CHIRAL ORGANIC SYSTEMS	81
PART 6: INVESTIGATION OF A PHASE TRANSITION BY <i>IN SITU</i> SHG FOR CHIRAL COMPOUNDS.....	82
6.1. INTRODUCTION ON POLYMORPHIC PHASE CHANGE	82
6.2. HISTIDINE MONOHYDROCHLORIDE HYDRATE (S).....	82
6.2.1. Histidine monohydrochloride.....	82
6.2.2. Histidine monohydrochloride hydrate (s).....	83
6.2.3. Salt formation and characterizations	83
6.2.3.1. Salt formation	83
6.2.3.2. Powder-SHG technique.....	83
6.2.3.3. XRPD measurements.....	84
6.2.3.4. DSC and TGA-DSC analyses.....	84
6.2.3.5. <i>In situ</i> SHG analyses	85
6.2.4. Conclusion.....	86
6.3. IMEGLIMIN PROPIONATE	86
6.3.1. Salt formation and characterizations	87
6.3.1.1. Salt formation	87
6.3.1.2. Solid state NMR analyses.....	87
6.3.1.3. Powder-SHG technique.....	88
6.3.1.4. XRPD measurements.....	89
6.3.1.5. DSC and TGA-DSC analyses.....	90
6.3.2. Relative stability of the phases	92
6.3.3. Solubility studies	92
6.3.4. Phase change monitored by <i>in situ</i> SHG	93
6.3.5. Conclusion.....	96
PART 7 : CONCLUSION AND PROSPECTS.....	98
REFERENCES	100
CHAPTER 3: CHIRAL RESOLUTION OF CHLOCYPHOS VIA ITS SALT DERIVATIVES	103
PART 1: INTRODUCTION.....	104
PART 2: CHLOCYPHOS	106
2.1. CYCLIC PHOSPHORIC ACIDS.....	106
2.2. CHLOCYPHOS: THERMAL AND STRUCTURAL CHARACTERIZATIONS.....	106
2.2.1. DSC analyses.....	106

2.2.2. XRPD measurements.....	107
2.2.3. Crystal structure determination by SC-XRD.....	107
2.3. SOLUBILITY STUDIES OF CHLOCYPHOS	111
PART 3 : CHLOCYPHOS SALTS.....	113
3.1. SALT FORMATION AND SHG RESPONSES.....	113
3.2. IDENTIFICATION OF CONGLOMERATES	114
3.2.1. Methylammonium chlocyphos	114
3.2.2. Ethylammonium chlocyphos.....	116
3.2.3. Propylammonium chlocyphos	118
3.2.4. Butylammonium, Isobutylammonium, Pentylammonium, Hexylammonium and Cyclohexylammonium chlocyphos	120
3.2.5. Octylammonium chlocyphos.....	121
3.2.6. Calculation of the eutectic temperature for the conglomerate derivatives	123
3.3. CRYSTAL STRUCTURE DETERMINATION BY SC-XRD	125
3.3.1. Butylammonium, Isobutylammonium, Pentylammonium, Hexylammonium, Cyclohexylammonium and Propylammonium chlocyphos.....	125
3.3.1.1. Crystallographic data.....	125
3.3.1.2. Crystal structures description	126
3.3.2. Methylammonium chlocyphos	129
3.3.2.1. Crystallographic data.....	129
3.3.2.2. Crystal structure description.....	130
3.3.3. Ethylammonium chlocyphos.....	132
3.3.3.1. Crystallographic data.....	132
3.3.3.2. Crystal structure description.....	133
3.4. INVESTIGATION OF THE PARTIAL SOLID SOLUTION OF ETHYLAMMONIUM CHLOCYPHOS	134
3.4.1. DSC measurements of different mixtures	134
3.4.2. Construction of the binary phase diagram and Tammann graph.....	135
3.4.3. Investigation by XRPD measurements of the limit of the solid solution	136
3.5. TRENDS OF CONGLOMERATE FORMATION IN ALKYL-AMMONIUM CHLOCYPHOS SALTS	139
PART 4: RESOLUTION BY PREFERENTIAL CRYSTALLIZATION (PC)	141
4.1. EXPERIMENTAL CONDITIONS	141
4.1.1. Seeded Isothermal Preferential Crystallization (SIPC mode)	141
4.1.2. Auto Seeded Polythermic Programmed Preferential Crystallization (AS3PC mode)...	142
4.1.3. Auto-Seeded Preferential Crystallization Induced by Solvent Evaporation (ASPreCISE)	142
4.1.4. Solubility measurements	143
4.1.5. Polarimetric measurements	143
4.2. RESOLUTION OF BUTYLAMMONIUM CHLOCYPHOS	143
4.3. RESOLUTION OF ISOBUTYLAMMONIUM CHLOCYPHOS	144
4.3.1. SIPC mode.....	144
4.3.2. AS3PC mode	145
4.4. RESOLUTION OF HEXYLAMMONIUM CHLOCYPHOS	146
4.4.1. SIPC mode.....	146
4.4.2. AS3PC mode	147
4.5. RESOLUTION OF CYCLOHEXYLAMMONIUM CHLOCYPHOS.....	149

4.6. SUMMARY OF THE ENTRAINMENT PERFORMANCES	150
4.7. PARAMETERS LIMITING THE PC PERFORMANCES OF CHLOCYPHOS DERIVATIVES.....	151
4.7.1. High value of Flack parameter	151
4.7.2. Evidence of multi-epitaxy	151
4.7.3. The problem of insufficient solubility variation over temperature.....	153
PART 5. CONCLUSION AND PROSPECTS.....	154
REFERENCES	156
CHAPTER 4: GENERAL CONCLUSION AND PROSPECTS	160
REFERENCES	165
APPENDICES	166
APPENDIX I : EXPERIMENTAL CONDITIONS	167
1. X-Ray Powder Diffraction (XRPD)	167
2. Single Crystal X-Ray Diffraction (SC-XRD).....	168
3. Differential Scanning Calorimetry (DSC).....	169
4. Thermogravimetric Analysis (TGA)-DSC	169
5. Polarimetry	170
6. Second Harmonic Generation Microscopy (SHGM)	170
APPENDIX II: DEVELOPMENT OF <i>IN SITU</i> MONITORING	171
<i>In situ</i> SHG set-up.....	171
APPENDIX III: CHLOCYPHOS SALTS	172
1. Calculated and experimental XRPD patterns	172
2. Crystal structure packing.....	175
3. Crystallographic data from the enantiopure salts	177
APPENDIX IV : SCIENTIFIC VALORISATION	178
1. Publications	178
2. Oral communications	180
3. Poster communications.....	180

GENERAL INTRODUCTION

Chirality and its consequences on the human body has been known for more than one century and access to enantiomerically pure compounds is essential for obtaining pharmaceutically active products. Stereoselective crystallization is increasingly employed in the preparation of enantiopure organic compounds since it offers practical benefits. Within this context, it is effective to think about methods and techniques based on innovative technologies that enable the access to enantiopure compounds.

CORE, a four year Marie Skłodowska-Curie Innovative Training Network (ITN) on Continuous Resolution and Deracemization of Chiral Compounds by Crystallization, brings together 8 beneficiary partners and 6 associate partners from 6 European countries resulting in an unparalleled combination of chirality, synthesis and crystallization training and research covering the areas of Chemical Engineering, Chemistry and Applied Physics.

The CORE network employs 15 Early Stage Researchers (ESRs) on a challenging research-training programme, which is to be completed with a PhD thesis. The SMS laboratory of the University of Rouen-Normandie in which I belong is one of the beneficiary partners of this European project. As one of the ESRs, my main contribution to this CORE project was to provide experimental methods that enable to identify conglomerates in a large survey of chiral organic compounds.

This thesis is focused on the development of an experimental method based on the nonlinear optical phenomenon of second harmonic generation (SHG) to quickly identify conglomerates rather than racemic compounds or solid solutions. The method should be applicable for various media and at different temperatures i.e. with the aim of spotting conglomerates (whether stable or metastable) at the early stages of the crystallization process. In parallel, a second goal of this research is to investigate the trends of conglomerate formation.

Chapter 1 depicts the properties of the crystalline solid state, the basic notions of heterogeneous equilibria, the different resolution processes of chiral molecules, the principle of nonlinear techniques as well as basic notions that help their comprehension.

Chapter 2 of the manuscript is dedicated to the development of the experimental method of detection of conglomerate in suspension based on SHG technique. The *in situ* SHG technique is further used to study phase transition between a racemic compound and a conglomerate and vice-versa.

Chapter 3 is dedicated to the chiral separation by crystallization of a compound of industrial interests for the associate partners SYNCOM BV of the CORE project: Chlocyphos. The characterization of the chiral compound chlocyphos, the search and identification of its conglomerate derivatives and their chiral separation by using preferential crystallization are successively reported. The elaboration of the binary phase diagram of conglomerate with partial solid solutions in ethylammonium chlocyphos is also presented in this chapter. Based on this thorough study of chlocyphos derivatives, some trends of conglomerate formation are also proposed.

Chapter 4 is the general conclusions that reflect the amount of work that has been generally accomplished. It particularly summarizes the achievements provided in the two previous chapters with a critical analysis of the results obtained and of the advantages and drawbacks of the *in situ* SHG technique developed herein. Some prospects for future works on the search of potential candidates for the *in situ* SHG set-up and the chiral resolution of chlocyphos conglomerate derivatives will also be considered.

DEFINITION OF SOME BASIC CONCEPTS USED IN THE MANUSCRIPT

Chirality

It derives from the Greek work *cheir* meaning “hand” because, like hands, the molecules and objects in general are not superimposable with their mirror images.

Chirality is defined as the geometry of a spatial arrangement of atoms being non-superimposable on its mirror-image.

Enantiomers

If a pair of stereoisomers are *non-superimposable mirror images* of each other, then they are enantiomers.

Racemic mixture

An equal mixture of opposite enantiomers is called a racemic mixture. When the racemic mixture is a solid salt, it can be called a racemate.

Conglomerate

A racemic mixture of crystals, each one of which contains only one of the two enantiomers present in the racemic mixture (it is a biphasic mixture).

Racemic compound

A single solid phase in which the two enantiomers are present in equal amounts within the crystal lattice of every particle.

(Complete) Solid solution

A single solid phase in which the two enantiomers are distributed with two complementary Statistical Occupancy Factor (SOF) within the crystal lattice.

Polymorphism:

Polymorphism is defined as the ability of a substance to crystallize in several crystalline phases (named as polymorphs) that have different arrangements of the molecules while retaining the same chemical composition.

A polymorphic transition can be reversible (enantiotropy) or irreversible (monotropy). Two polymorphs can be enantropically or monotropically related.

Solvation / hydration

A solvate can be defined as a crystalline solid made of molecules of solute and solvent. When the solvent is water it is commonly called a hydrate. Solvates can be stoichiometric or non-stoichiometric.

Binary Eutectic Invariant

A three-phase domain which exists at a fixed temperature, a liquid phase transforms simultaneously and reversibly into two solid phases. The three phases have definite compositions and from the eutectic liquid to the two solid phases the transfer of matter is associated with a negative heat transfer ($\Delta H < 0$).

Binary Eutectoid Invariant

A three-phase domain which exists at a fixed temperature, a solid phase transforms simultaneously and reversibly into two solid phases. The three phases have definite compositions and from the single solid phase to the two solid phases the transfer of matter is associated with a (small) negative heat transfer ($\Delta H < 0$).

Binary Peritectoid Invariant

A three-phase domain which exists at a fixed temperature, a solid phase transforms simultaneously and reversibly into two solid phases. The three phases have definite compositions and from the single solid phase to the two solid phases the transfer of matter is associated with a (small) positive heat transfer ($\Delta H > 0$).

Binary Peritectic Invariant

A three-phase domain which exists at a fixed temperature, a solid phase transforms simultaneously and reversibly into a saturated liquid phase and a solid phase. The three phases have definite compositions and from the single solid phase to the two mixtures of the saturated liquid and solid phases the transfer of matter is associated with a positive heat transfer ($\Delta H > 0$).

CHAPTER 1: GENERALITIES

In this chapter, we introduce the general concepts necessary for a good understanding of the present work in terms of properties of the crystalline state of solids, thermodynamic and heterogeneous equilibria, chirality and thermodynamic chiral systems. Then, we will present the principles of the different methods of resolution of racemic mixtures to access to their pure enantiomers. The principle of nonlinear optical techniques and the screening of conglomerate forming systems using these techniques (second harmonic generation) will be finally described in this chapter.

PART 1 : THE CRYSTALLINE STATE

1.1. CRYSTALLINE STATE OF SOLIDS

The matter (atoms and molecules) can be arranged into three different states: solid, liquid and gaseous states. In solids and liquids, also referred to as condensed matters, the distance between adjacent atoms is of the order of a few Angstroms. It means that they contain 10^{22} - 10^{23} atoms per cm^3 . This may be compared with a density of about 2.7×10^{19} molecules per cm^3 in a gas at room temperature under 1 atm, corresponding to an average distance of approximately 30 Å between molecules¹. Interatomic or intermolecular interactions in the solid state are stronger than that in the liquid state. Indeed, in solids, atoms/molecules are usually more densely packed than in liquids. The solid state can be classified structurally into two categories: crystalline materials with long-range order characterized by the presence of a 3D periodic lattice and glasses (amorphous solids) with short-range order limited to the first closest neighbours of a given molecule as in liquids²⁻⁴.

To illustrate the difference between the two types of solids, a 2D representation of arrangement of the same compound (SiO_2) in crystal and glass forms: the molecular arrangement in crystalline (i) and amorphous (ii) SiO_2 is shown in Figure 1.1⁴.

In this present work, we are essentially interested in crystalline solids and particularly organic crystalline materials possessing nonlinear optical properties. We shall now discuss somewhat further the formalisms used to describe periodicity of structure, which is the fundamental feature of a crystal.

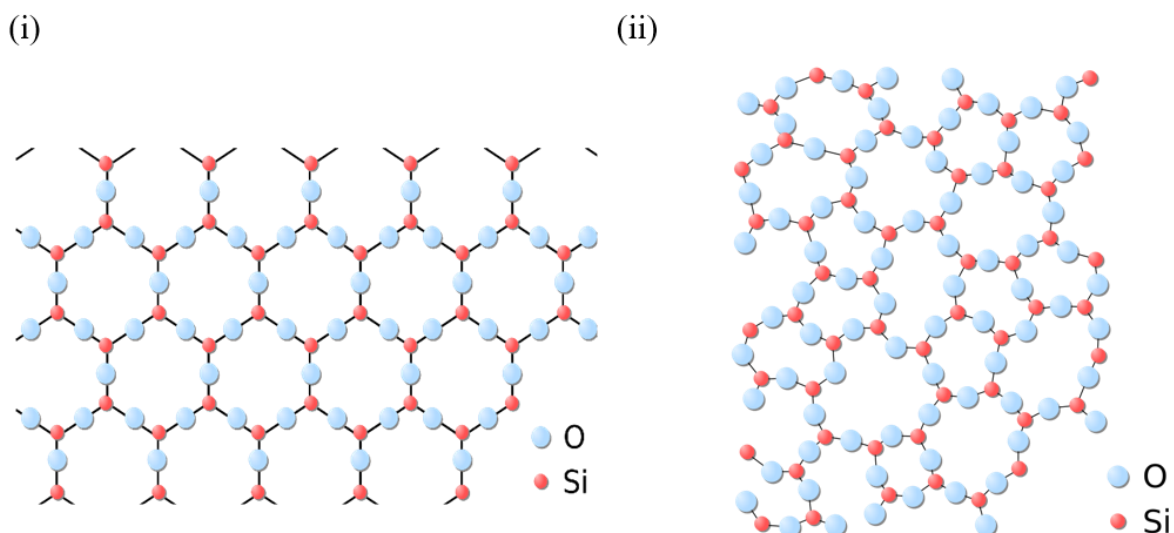


Figure 1.1. 2D representation of a two-dimensional arrangement of SiO_2 : (i) crystal form (quartz) and (ii) amorphous solid (adapted from reference 4).

1.2. THE GROUP THEORY

1.2.1. Unit cell, crystal systems and Bravais lattices

A unit cell is the repeating unit of smallest volume which; when filled up with itself along the 3 directions of space, builds ultimately the crystalline solid. The shape and size of the unit cell is defined by the cell parameters a , b , c (the magnitude of the translation vectors \mathbf{a} , \mathbf{b} , and \mathbf{c} respectively), α , β and γ (the angles between \mathbf{b} and \mathbf{c} , \mathbf{a} and \mathbf{c} , \mathbf{a} and \mathbf{b} translation vectors respectively). The unit cell contains the atoms and molecules necessary to generate the crystal. A unit cell with its cell parameters is represented in Figure 1.2. Each crystalline solid can be classified as a member of one of the seven possible crystal systems that are defined by the constraints or the values of the cell parameters a , b , c , α , β and γ .

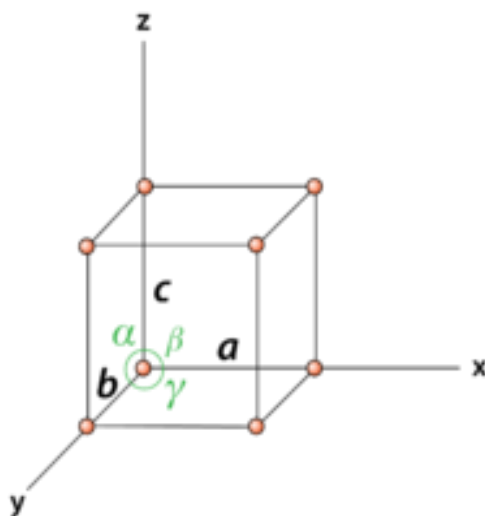
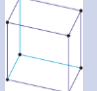
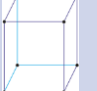
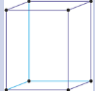
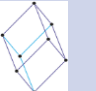
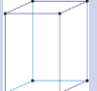
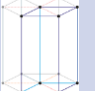
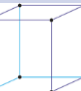
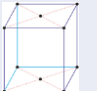
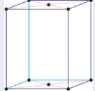
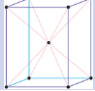
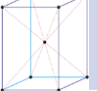
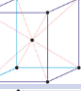
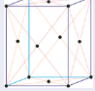
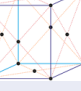


Figure 1.2: Representation of the unit cell of a crystal lattice with the lengths a , b and c and the angles α , β and γ .

The simplest and most symmetric is the cubic system and has the symmetry of a cube. The other six systems, in order of decreasing symmetry, are hexagonal, tetragonal, trigonal (also known as rhombohedral), orthorhombic, monoclinic and triclinic (conditions on cell parameters in Table 1.1).

Table 1.1: Crystal systems and 14 Bravais lattices

Crystal systems	Triclinic	Monoclinic	Orthorhombic	Trigonal	Tetragonal	hexagonal	Cubic	
Essential symmetry	No planes, no axes	One 2-fold axis Or one plane	3 mutually \perp 2-fold axes, intersecting in a 2-fold axis	One 3-fold axis	One 4-fold axis or a 4-fold inversion axis	One 6-fold axis	Four 3-fold axes	
Point group or crystal class	1 or $\bar{1}$	2; m ($= \bar{2}$); 2/m	222, mm2, mmm	3; $\bar{3}$; 32; 3m; $\bar{3}m$	4; $\bar{4}m$; 4/m; 4mm; 422; $\bar{4}2m$; 4/mmm	6; $\bar{6}$; 6/m; 6mm; 622; $\bar{6}m2$; 6/mmm	23; m3; 432; $\bar{4}3m$; m3m	
Equivalent	2	4	8	12	16	24	48	
Cell parameters	$a \neq b \neq c$ $\alpha \neq \beta \neq \gamma \neq 90^\circ$	$a \neq b \neq c$ $\alpha = \gamma = 90^\circ \neq \beta$	$a \neq b \neq c$ $\alpha = \beta = \gamma = 90^\circ$	$a = b = c$ $\alpha = \beta = \gamma \neq 90^\circ$	$a = b \neq c$ $\alpha = \beta = \gamma = 90^\circ$	$a = b \neq c$ $\alpha = \beta = 90^\circ$ $\gamma = 120^\circ$	$a = b = c$ $\alpha = \beta = \gamma = 90^\circ$	
Bravais Lattices	Primitive (P)							
	Base-centered (C)							
	Body-centered (I)							
	Face-centered (F)							

Bravais introduced the concept of space-lattice. Simply speaking, Bravais lattice is a set of points constructed by translating a single point in discrete steps by a set of basis vector (e.g. lattice modes). Bravais established that in 3D space only four different lattice modes exist.

By combining the four lattice modes and the seven crystal systems, Bravais demonstrated that 14 Bravais lattices can be constructed since, due to symmetry, all lattice modes are not compatible with each crystal system (see Table 1.1.). All crystalline materials recognised till now fit in one of these arrangements.

1.2.2. Symmetry and symmetry operations

Here, we focus on symmetry operations consistent with the 7 crystal systems. The only symmetry operations are rotation, inversion or rotation-inversion. Furthermore, the groups (in a mathematical sense) containing one or several symmetry elements which leave a point

unchanged after applying these symmetry operations a finite number of times, are called point groups.

- (i) A crystal is said to possess an n -fold rotation axis when the rotation over $360^\circ/n$ brings the crystal into self-coincidence.
- (ii) A crystal possesses an inversion centre when for each point located at \mathbf{r} relative to the centre, there exists an identical point located at $-\mathbf{r}$.
- (iii) A rotation-inversion axis exists when the crystal can be brought into self-coincidence by a combined rotation and inversion (noted \bar{n} that is rotation of $360^\circ/n$ plus an inversion symmetry).

In particular, the $\bar{2}$ axis corresponds to a mirror symmetry which is noted \mathbf{m} (see Table 1.1.). According to the inherent symmetry of the unit cell of each crystal system, only some point groups can be assigned to each crystal system. For example; point groups with 6-fold axes (rotation of 60°) are possible only for hexagonal lattices (see Table 1.1.). In total 32-point groups are distributed among the 7 crystal systems (Table 1.1.).

The description of crystal symmetry as summarized in the International Tables of Crystallography⁵ specifies two kind of rotation axes and mirror planes: Axes or planes for which the rotation or mirror is a symmetry of the crystal without an accompanying translation. Such rotation axes or mirror planes are simple; Axes or planes for which the rotation or mirror is only a symmetry of the crystal when accompanied by a translation parallel to the axis or plane. Such rotation axes or mirror planes are called screw axes or glide planes. Two new symmetry operations i.e. screw axes and glide planes are thus introduced.

- (i) A screw axis noted \mathbf{n}_t is a rotation followed by a translation parallel to this axis (\mathbf{n}_t means rotation $2\pi/n$ + translation of t/n ; n and t are integers with $t < n$). Example: 2_1 is a rotation of 180° followed by a translation of $1/2$ of the shortest crystallographic vector parallel to the translation.
- (ii) Glide plane is a mirror symmetry followed by a translation, parallel to the plane, of half of a basis vector or half of two basis vectors and one quarter of two basis vectors. Example: footprints of someone walking.

The 14 Bravais lattices + 32 point groups + symmetry operations with translation form the 230 possible space groups^{6,7} in a 3D space.

1.2.3. Space groups

A space group is a group according to group theory. The symmetry operations (not the symmetry elements) are the group elements that make up the space group. It is a combination of point symmetry plus translational symmetry⁸.

The generally low molecular symmetry of organic compounds often does not permit packings with molecules occupying special positions enforcing a corresponding symmetry reduction because molecules strive to attain densest packing possible. The statistics given by Belsky and co-workers⁹ show that centrosymmetric space groups are predominant, and the most frequent space group is $P2_1/c$. For chiral molecules, which may only adopt one of the 65 Sohncke space groups, the most frequent is $P2_12_12_1$. Sohncke space groups are the class of space groups that contains only symmetry operations of the first kind.

A more detail survey is available in the Cambridge Structure Data (CSD). The Space group frequency ranking for the 986,061 CSD structures for which the space group is fully defined. From CSD, the space group frequency ranking for January 2019, is summarized as follows in Table 1.2.

In the CSD, 87.8% of the structure entries crystallize in these common space groups and 22% adopt non-centrosymmetric space groups in which 16% adopt Sohncke space groups.

Table 1.2: Most common space groups of molecular crystals^a in the CSD released in January 2019

Rank	N° Space group	Space group	N° of structures in CSD	% of CSD
1	14	$P2_1/c$	339542	34.4
2	2	$P \bar{1}$	245703	24.9
3	15	$C2/c$	82346	8.3
4	19	$P2_12_12_1$	69645	7.1
5	4	$P2_1$	50570	5.1
6	61	$Pbca$	32371	3.3
7	33	$Pna2_1$	13570	1.4
8	62	Cc	10292	1.0
9	9	$Pnma$	10286	1.0
10	1	$P1$	9493	1.0
...				

^aOnly space group accounting for $\geq 1\%$ are given. Non-centrosymmetric space groups are in bold.

The common crystalline forms found for a given drug substance are polymorphs and solvates and one-third of the stable conglomerates exhibits polymorphism^{10,11} (i.e. possess different physicochemical properties). Polymorphism has important commercial and/or industrial implications in various fields. A solvate can be defined as a crystalline solid made of molecules of solute and solvent. When the solvent is water it is commonly called a hydrate.

Solvates also are of great importance in pharmaceutical and food industries since many compounds are obtained by crystallization from a solvent (leading sometimes to incorporation of solvent molecule in the crystal structure in stoichiometric or non-stoichiometric proportion). The stability of a solvate depends on its mechanism of desolvation (temperature, pressure, energy and RH).

1.3. STRUCTURAL CHARACTERIZATION OF CRYSTALLINE SOLIDS

1.3.1. Principle of X-ray diffraction

The use of X-rays as a tool for investigating the crystal structure was first suggested by von Laue in 1912 and was later further developed by W. H. and W. L. Bragg¹².

When an electron is interacted with a monochromatic beam of X-ray, the electric field vector of the radiation forces it to carry out vibrations at a frequency equal to that of the incident beam. As a consequence of the acceleration of the electron, it will emit radiation of the same wavelength in all directions. Thus, in an atom, all electrons contribute to the scattering of X-rays in this way. The intensity of the scattering for a given atom is thus proportional to its number of electrons.

Let us consider a set of parallel atomic planes of Miller indices (hkl), the distance between successive planes being d_{hkl} . As Bragg postulated, let us assume that an X-ray beam is reflected by an atomic plane according to Snell's law (i.e. the incident and reflected beams make the same angle with the normal plane). From the figure 1.3, we see that the rays 1 and 2 can reinforce each other in the reflected direction only if their path difference is an integer time the wavelength λ . Furthermore, the path difference for waves reflected by successive planes is $2d_{hkl}\sin\theta$. This is necessary because wave crests are points of equal phase.

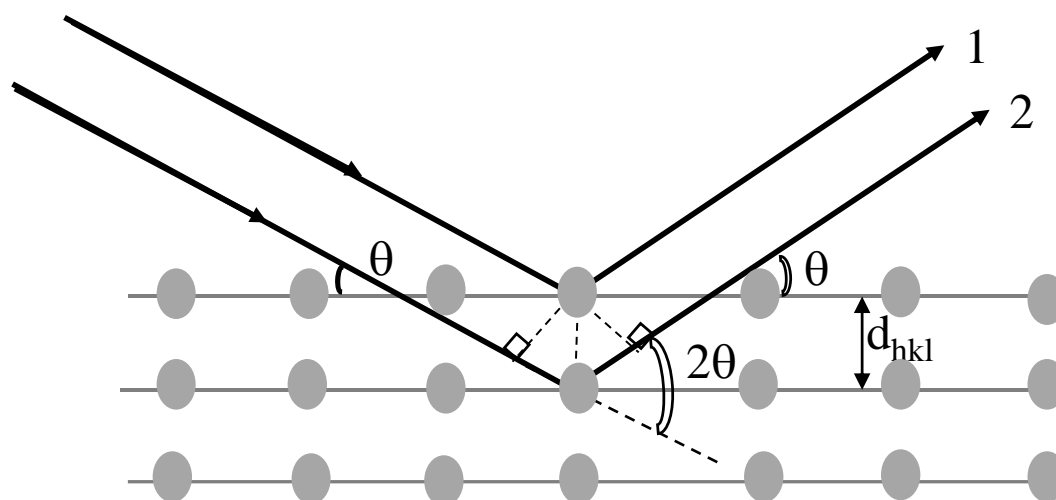


Figure 1.3: Principle of X-ray diffraction: Beams reflected from successive planes

Thus, the condition for reflection (Bragg condition) from the set of planes under consideration is given by

$$2d_{hkl} \sin \theta = n \lambda \quad (1.1)$$

Where n is an integer (0; 1; 2; 3, ...) and indicates the order of reflection, θ diffraction or Bragg angle, λ is the wavelength of incident beam.

For a given value of n , d_{hkl} and λ , the reflection can be observable only at a particular angle θ . Therefore, the diffraction is possible only in a particular direction for a set of particular diffraction planes.

1.3.2. X-ray powder diffraction (XRPD)

X-ray powder diffraction is a non-destructive technique widely used for the characterization of a variety of crystalline materials. This method has been conventionally used for phase identification of drug molecule and its polymorphs. However, about 20-30 years ago, the applications have been extended to the determination of crystal structures. The amount of information which is possible to extract depends on the nature of the sample microstructure (crystallite size and texture) and the quality of the experimental data (instrument performances and counting statistics)¹³. Basically, this method involves the diffraction of monochromatic X-ray by a powdered sample. Usually 'monochromatic' means the strong characteristic K component of the filtered radiation from an X-ray tube operated above the K excitation potential of the target material. In the powder (Debye-Scherrer) method, the X-ray fall on a mass of tiny crystals in all orientations, and the diffracted beams of each order h , k , l form a cone. Arcs of the cones are intercepted by a film surrounding the specimen.

When single crystals are not always available, this method is also suitable for structural determination of drug substances.

1.3.3. Single Crystal X-Ray Diffraction (SC-XRD)

Single crystal X-ray diffraction is one of the most powerful methods for crystal structure determination. The X-ray diffraction pattern can be obtained by only one single crystal. The selected single crystal is mounted on a three-circles goniometer allowing stepwise change in the orientation of the crystal versus the incident X-ray beam. CCD camera detects each diffraction directions. An indexation is used to identify the values h , k and l for each diffraction spot and therefore to determine the space group of the crystal structure via the extinction conditions. For the refinement, a Fourier transformation of experimental intensities is applied to determine the electronic density distribution in the unit cell of the direct lattice. SC-XRD is considered as the best method to derive unambiguously the chemical structure of molecules.

In the present work, operating conditions for XRPD, SC-XRD and the methods to grow single crystals are detailed on the chapter 3 and Appendix I.

PART 2: THERMODYNAMICS AND HETEROGENEOUS EQUILIBRIA

2.1. CRYSTAL GENESIS

The formation of crystalline solids from solution, melt or vapor state, is a process that underlies natural phenomena (for example rock formation or biomineralization). This process, called crystallization, refers to the first-order transition from a disordered state to a crystalline state. Crystallization involves nucleation and growth and plays an important role in industrial processes, such as the synthesis and purification of drugs.

2.1.1. Precipitation

Precipitation is usually a fast crystallization. It is generally hard to control crystal properties such as polymorphic structure, crystal morphology, and crystal size distribution¹⁴. The strongly nonlinear dependence of the nucleation rate on supersaturation combined with the large variations in this supersaturation explains the difficulty in achieving control over crystal properties.

2.1.1.1. Supersaturation

Nucleation of the particles takes place when a saturation threshold is reached. Saturation corresponds to a thermodynamic equilibrium. Nevertheless, it is possible to reach higher concentrations. Supersaturation is the driving force on crystallization, it is named β (supersaturation ratio)¹⁵ and expressed as given in equation (1. 2).

$$\beta = \frac{C}{S} \quad (1. 2)$$

Where **C** is the concentration of the solution and **S** is the solubility.

A supersaturation ratio greater than one is theoretically enough to induce a crystallization. Different ways such as evaporation, cooling or anti-solvent addition can be used to create a supersaturated state. In practice, supersaturation must be at a certain limit called Ostwald metastable limit¹⁶ to induce a spontaneous nucleation and crystallization; if not, the system is out of equilibrium.

2.1.2. Nucleation

Crystallization begins with the nucleation, a random formation of supercritical clusters of atoms. Nucleation can be divided in two categories: primary and secondary.

2.1.2.1. Primary nucleation

Primary nucleation is the process in which crystals form spontaneously from a supersaturated solution or a supercooled melt. It is difficult to observe the actual nucleation process since the nuclei are too small to be observed with any instrument.

Small aggregates (nuclei) form and dissolve again in the supersaturated solution. When the nuclei reach a critical size, they can grow into actual crystals. By assuming that nuclei adopt a spherical shape of r radius, the free enthalpy variation $\Delta G_{\text{nucleation}}$ related to spherical nuclei is given by the equation (1.3).

$$\Delta G_{\text{nucleation}} = - \frac{4}{3}\pi r^3 \Delta g_v + 4\pi r^2 \gamma \quad (1.3)$$

Where Δg_v stands for the volume energy term and γ for the interfacial tension (surface energy) of the crystal.

The free energy of nucleation involves two contribution terms¹⁷:

- Solute/solute interaction energy (volume contribution: stabilizing effect; growth of the nuclei).
- Solute/solution interaction energy (surface contribution : destabilizing effect : dissolution of the nuclei).

Figure 1.4¹⁸ depicts the evolution of the free energy difference of the surface term, the volume term and the total free energy difference as a function of the radius of the nucleus.

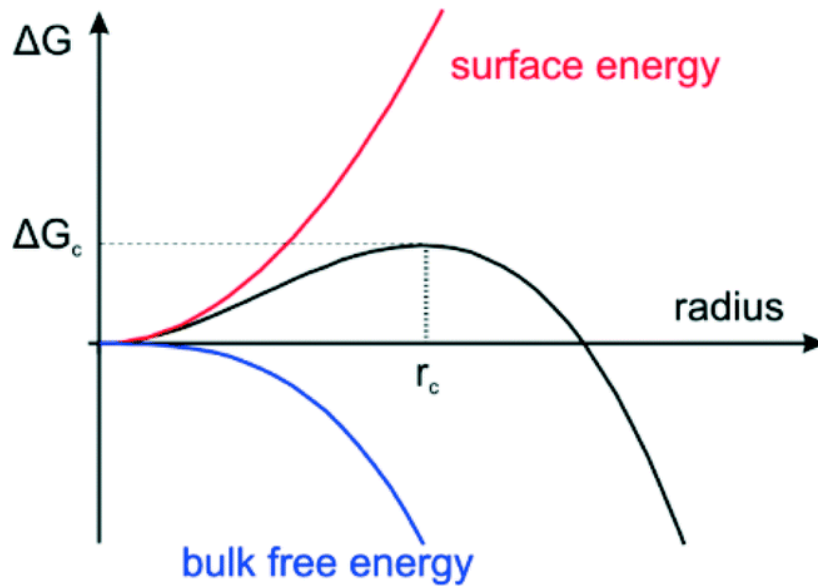


Figure 1. 4. Evolution of the free energy of a nucleus function of its radius (adapted from reference 18).

When $r = r_c$; $d(\Delta G_{\text{nucleation}})/dr = 0$; $r_c = \frac{2\gamma}{\Delta g_v}$; $\Delta G_c = \frac{16\pi\gamma^3}{3(\Delta g_v)^2}$ (1. 4)

Where r_c is the critical radius and ΔG_c is the maximum free energy (energy barrier for nucleation that nuclei must overcome to start their growth).

When the crystal has a radius smaller than r_c , it is energetically more favourable for the nucleus to re-dissolve and for larger sizes than r_c , the crystal grows.

As the critical radius is related to a maximum of free energy (ΔG_c), an activation energy is needed to generate nucleation. Heterogeneous nucleation occurs for lower energy barrier since the destabilizing crystal/solution surface is reduced for the benefit of solute/foreign surface interface (foreign surface being impurity, reactor wall, ...).

2.1.2.2. Secondary nucleation

One speaks of secondary nucleation when a supersaturated medium is in contact with an appropriate surface on which the supersaturated compound can crystallize.

Indeed, when a crystal is submitted to liquid shear stress or collisions (with another crystal or with the reactor wall...) small parts of the mother crystal are swept away and generate daughter crystals¹⁹. From a chiral point of view, the secondary nucleation generates daughter crystals of the same handedness as the mother crystal²⁰.

2.1.3. Growth

Once the critical radius is reached, the nucleus grows into a crystal by organizing and assembling ions or molecules with specific interaction and bonding at the crystal/solution interface. Growth processes and grown crystals (size) differ widely and depend on the roughness (at molecular scale) of the crystal surface. The crystal can grow continuously on irregular (kinked) surfaces or layer by layer on flat surfaces. In the second case, the growth by two-dimensional nucleation²¹ is favoured at high supersaturation, and the spiral growth around screw dislocations is often observed at moderate supersaturation^{22,23}. Growth depends in one hand on extrinsic factors such as, nature of solvent, solubility, temperature and presence of impurity, and the other hand on intrinsic factors such as crystal structure, nature of the bonds and defects.

Traditionally, supersaturation, nucleation and growth have often been considered in isolation with the implicit assumption that one process is essentially complete before the next one begins.

2.2. HETEROGENEOUS EQUILIBRIA AND STABILITY

2.2.1. Phase equilibria

Phase equilibria exist or are being strived for all around us. Most industrial processes are designed for and operate at equilibrium conditions; even when it is not so; it is important to know what would happen at equilibrium.

A phase is a homogeneous portion of a system with uniform physical and chemical characteristics, in principle separable from the rest of the system.

When two phases are brought into contact, they tend to exchange their components until the composition of each phase attains a constant value; when that state is reached, we say that the

phases are in equilibrium. The equilibrium composition of two phases are often different from one another. Phase equilibrium thermodynamics seeks to establish the relations among the various properties (temperature, pressure and composition) that ultimately prevail when two or more phases reach a state of equilibrium. The equilibria between phases can be visualized as a geometrical representation of the stable and metastable heterogeneous equilibria which satisfy several rules such as Gibbs phase rule. When the system is homogeneous, the unique phase in equilibrium is always the one with the lowest free energy.

2.2.2. Phase rule

The Phase rule describes the possible number of degrees of freedom in a (closed) system at equilibrium, in terms of the number of separate phases and the number of chemical constituents in the system. It was deduced from thermodynamic principles by Josiah Willard Gibbs. The equation states as equation (1. 5) is known as Gibb's phase rule²⁴.

$$\mathbf{V} = \mathbf{C} + \mathbf{N} - \boldsymbol{\phi} \quad (1. 5)$$

Where **V** is the variance, the number of intensive variables that can be changed independently without modifying the state of equilibrium; **C** is the number of independent constituents; **φ** is the number of phases present in the equilibrium and **N** refers to the number of intensive variables considered (Pressure and Temperature; indeed, N = 2).

The system is: invariant for V = 0; monovariant for V = 1; bivariant for V = 2...

2.2.3. Gibbs free energy

Gibbs free energy is the maximum work that may be done by a system at constant temperature and pressure. It is a thermodynamic variable (extensive) that was defined in 1876 by J. W. Gibbs²⁴ to predict whether a process will occur spontaneously at constant temperature and pressure. The free enthalpy or Gibbs free energy G is defined as follows in equation (1.6).

$$\mathbf{G} = \mathbf{H} - \mathbf{TS} \quad (1. 6)$$

Where **H**, is the enthalpy i.e. total energy of the system, **T** is the temperature, and **S** is the entropy associated to the disorder at the given temperature and pressure.

The change in Gibbs free energy (ΔG) is the difference between the free energy of the final state and the initial one in a closed system. For example, for a phase transformation between state A (G_A is its corresponded free energy) to state B (G_B is its corresponded free energy); the free energy difference is given as follows: $\Delta G = G_A - G_B$.

- i. $\Delta G > 0$; $G_A > G_B$; transformation is not favourable.
- ii. $\Delta G < 0$; $G_A < G_B$; transformation is favourable.
- iii. $\Delta G = 0$; $G_A = G_B$; A and B are in equilibrium.

The most stable state of a thermodynamic system is attained when its molar free energy is at its lowest possible value (i.e. for $\Delta G = 0$).

2.2.4. Equilibrium and stability

From a thermodynamic viewpoint the equilibrium state is a state of maximum stability toward which a closed physicochemical system proceeds by irreversible processes²⁵. The concepts of stability and instability for a simple mechanical system serve as an illustrative step toward development of the thermodynamic concept of equilibrium.

The figure 1.5²⁶ represents the different levels of equilibria in mechanical (a) and thermodynamic (b) systems.

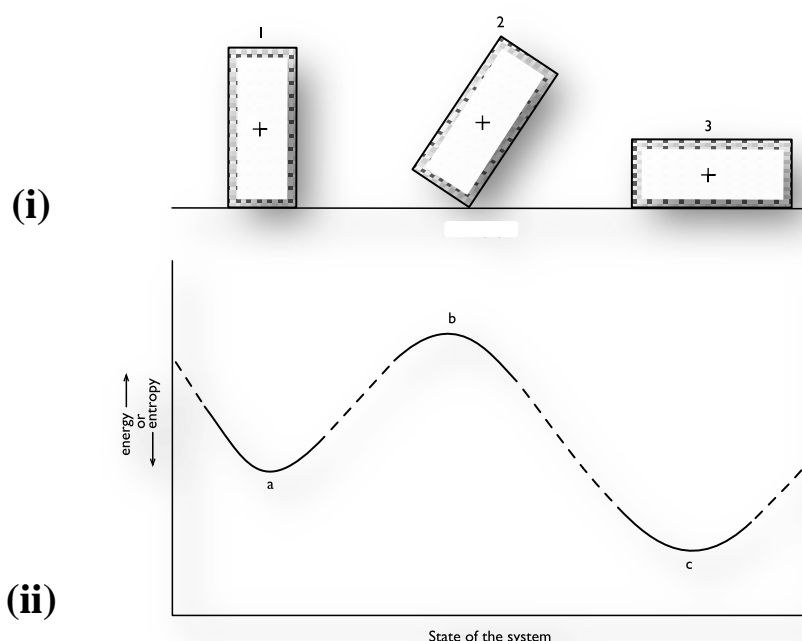


Figure 1.5: Concepts in mechanical and chemical equilibrium. (i) Metastable, unstable, and stable equilibrium in a mechanical system. (ii) Metastability, instability, and stability for different energetic states of a thermodynamic system (adapted from reference 26).

From Figure 1.5 (i), several levels of equilibria can be reached. Thus, one can define:

- **Metastable** equilibrium (position **1**): the box reaches a local minimum of the free energy; it is at a metastable state. It is at equilibrium but not the lowest one. The box would need activation energy to leave this equilibrium to a more stable one (metastable or stable).
- **Unstable state** (position **2**): a small movement can disturb the box, the free energy is not at a minimum value, the box is unstable and will evolve to reach the nearest equilibrium.

- **Stable** equilibrium (position **3**): the global free energy minimum corresponds to the stable equilibrium.

Thermodynamically viewpoint, as illustrated in Figure 1.5 (ii), **c** is at **stable** equilibrium with the lowest free energy and **a** is at a local minimum of free energy but does not have the lowest possible value of energy. It is at the **metastable** equilibrium state.

Based on the Ostwald rule of stages¹⁶, when the system is out of equilibrium, the intermediate metastable states will be involved before reaching the final stable state. Generally, the metastable state should irreversibly change to the stable state. But the time spent in the metastable state can vary from seconds to hours.

Therefore, thermodynamic equilibrium is found in metastable and stable conditions of equilibrium but not in unstable equilibrium.

PART 3 : CHIRALITY

3.1. CHIRALITY AND STEREOISOMERS

3.1.1. History of chirality

In 1801, René-Just Haüy, a French mineralogist observed that quartz crystals showed hemihedral behaviour²⁷ i.e. certain facets of the crystals are mirror images of each other (Figure 1.6).

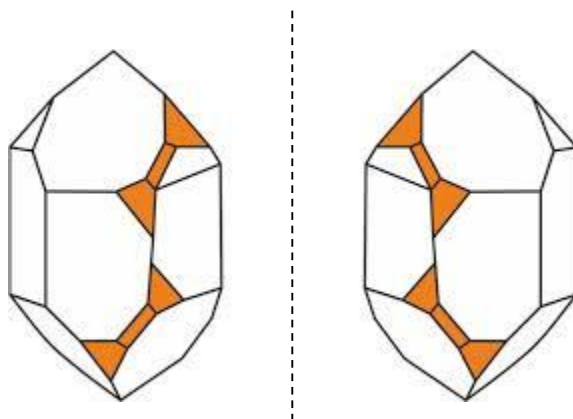


Figure 1.6. Enantiomorphous crystals of quartz

In 1815, Jean-Baptiste Biot showed that when polarized light passed through an organic liquid or solution, it could be rotated clockwise or counterclockwise²⁸.

In 1844, Eilhard Mitscherlich, a German scientist, examined the sodium ammonium salts of both enantiomerically pure and racemic tartaric acid. At that time, the main source of optically pure tartaric acid was potassium bitartrate, which is abundant in the sediments from fermenting wine. Often, another form of tartaric acid, “racemic acid” (Latin *racemus* meaning “bunch of grapes”), was found in wine barrels. Mitscherlich found that the crystals from enantiomerically pure and racemic sodium ammonium tartrate were identical in crystalline form, except that upon dissolution the former rotated polarized light whereas the latter did not^{29,30}.

Little was done after Biot’s discovery of optical activity until 1848, when Louis Pasteur began work on a study of crystalline tartaric salts derived from wine. By crystallizing a concentrated solution of sodium ammonium tartrate tetrahydrate below 27 °C, Pasteur made the surprising observation that two distinct kinds of crystals precipitated. Furthermore, the two kinds of crystals were non-superimposable mirror images and were related in the same way that a right-hand is related to a left-hand. Working carefully with tweezers, Pasteur was able to separate the crystals into two populations of crystals, one of right-handed crystals and one of left-handed crystals like those represented in the figure 1.7. Although the original sample, a 50:50% mixture of right- and left-handed crystals, was optically inactive, solution of the crystals from each of

the sorted population were optically active and their specific rotations were exactly equal but opposite sign^{31,32}.

Pasteur explained his results by speaking of the molecules themselves, saying that, “There is no doubt that [in the dextro tartaric acid] there exists an asymmetric arrangement having a non-superimposable image. It is no less certain that the atoms of the levo acid have precisely the inverse asymmetric arrangement”. Pasteur just has established the bases of chirality and achieved the first chiral separation and proved that racemic salt is a 1:1 mixture of left- and right-handed sodium ammonium tartrate tetrahydrate^{33,34} (Figure 1.7).

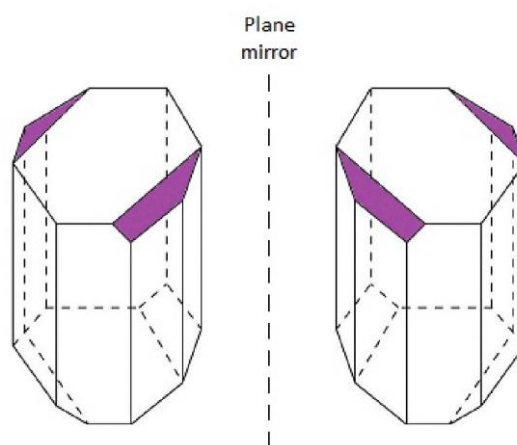


Figure 1.7. Levorotatory and Dextrorotatory Sodium ammonium tartrate tetrahydrate crystals

Today, we would describe Pasteur’s work by saying that he had discovered isomers having identical physical properties, such as melting point and boiling point but differ in the direction in which their solution rotate plane-polarized light.

3.1.2. Definition of chirality

Stereoisomers are isomers that differ in spatial arrangement of atoms, rather than order of atomic connectivity. One of their most interesting type of isomer is the mirror-image stereoisomers, a non-superimposable set of two molecules that are mirror image of each other. The existence of these molecules are determined by the concept known as chirality. The word "chiral" was derived from the Greek word for hand, because our hands display a good example of chirality since they are non-superimposable mirror images of each other.

For a most general definition of chirality: the geometry of a rigid object (or spatial arrangement of points or atoms) of being non-superimposable on its mirror-image; such an object has no symmetry element of the second kind (a centre of inversion, a mirror plane or a roto-inversion). If the object is superimposable on its mirror-image, the object is achiral. For example, our hands are chiral, but two flasks (Erlenmeyer) are achiral³⁵ (Figure 1.8).

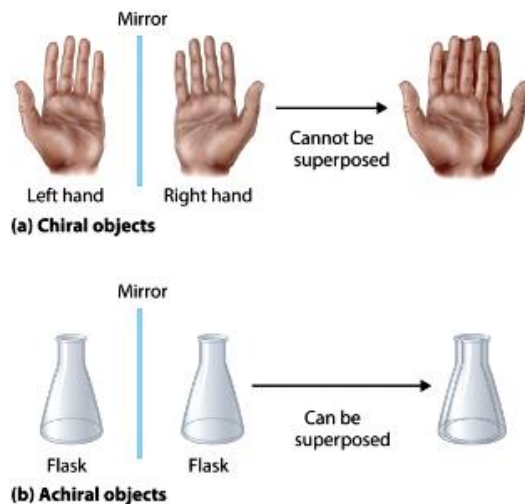


Figure 1.8: Chiral objects (hands) and achiral objects (flasks) (adapted from reference 35).

3.1.3. Stereogenic centre and stereoisomers

First, one must understand the concept of spatial arrangement to understand stereoisomerism and chirality. Spatial arrangement of atoms concerns how the different atomic elements are situated (located) in the space. Once a bond is rotated by even one degree in any three-dimensional spatial arrangement, it could give possibility to different molecular arrangements and such molecules may have different optical properties.

The designation depends on the difference in atomic weight of the four substituents of the chiral atom (chiral centre). A carbon atom that is bonded to four different atoms or groups loses all symmetry and is often referred to as an asymmetric carbon or a stereogenic centre (Figure 1.9).

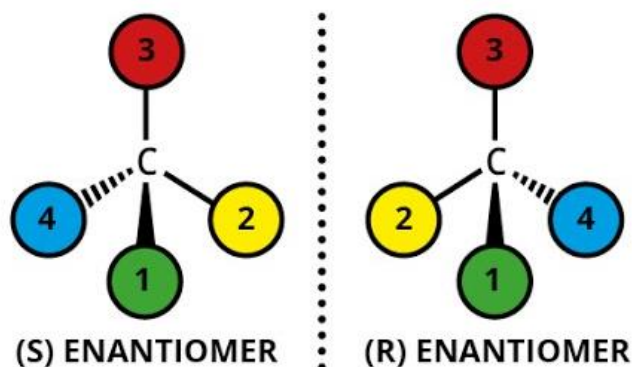


Figure 1.9: Stereogenic centre representation

The configuration of such molecular unit is chiral, and the structure may exist in either a right-handed configuration or a left-handed configuration (mirror image of each other). The chiral centre (or multiple chiral centres) can have either (*R*) (Rectus) or (*S*) (Sinister) label as edited

by Cahn, Ingold, and Prelog to design the two stereoisomers. Fischer projections are used to describe chirality of sugars and amino acids. Depending on the position of the substituent with the highest priority, enantiomers are noted **D** or **L**. This type of configurational stereoisomerism is termed enantiomorphism, and the non-identical, mirror-image pair of stereoisomers that result are called enantiomers.

3.1.3.1. Enantiomers

The term enantiomorph was introduced by Pierre Curie³⁶ in 1894. The word comes from Ancient Greek “enantios” and “meros” respectively meaning “opposite” and “part”. Enantiomers are molecular entities which are mirror-images of each other and non-superimposable. These enantiomers have the same physical properties except for their opposite rotatory effect on light polarization; such compounds are therefore described as optically active, with specific terms for each enantiomer based on the direction: a dextrorotatory compound rotates light a clockwise (+) direction whereas a levorotatory compound rotates light in a counter-clockwise (–) direction.

For illustrations, L and D sodium ammonium tartrate tetrahydrate crystals are enantiomers and a 1:1 mixture of both enantiomers is called ‘racemate’. Most of the amino acids, in our organism, exist only as L-enantiomers and sugars exist only as D-enantiomers. This phenomenon whereby compounds closely related in structures (families) have identical absolute configurations is known as homochirality³⁷.

It is interesting that our hands serve as an example to describe chirality, but most people are only able to use one of their hands to write. Similarly, this is true with chiral biological molecules and interactions. Just like your left hand will not fit properly in your right glove, one of the enantiomers of a molecule may not work the same way in your body.

The smell receptors in the nose are a striking example of the effect of chirality. A famous example is limonene (depicted in Figure 1.10). The (*R*)-enantiomer smells like orange whereas the (*S*)-enantiomer smells like lemon³⁸.

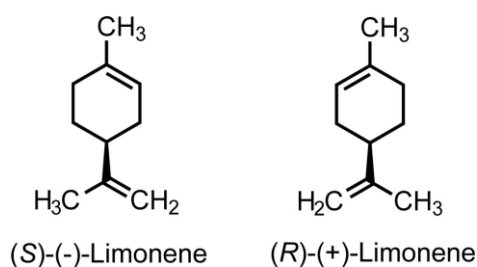


Figure 1.10. Enantiomers of limonene

3.1.3.2. Diastereomers

If two molecules, having more than one chiral centre, are stereoisomers (same molecular formula, same connectivity, different arrangement of atoms in space) but are not enantiomers, then they are diastereomers by default. It means that at least one but not all the chiral centres are opposite in a pair of diastereomers. In other words, stereoisomers that are not mirror images of each other are diastereomers. The relation between the four stereoisomers of threose³⁹ with two chiral centres is shown in Figure 1.11.

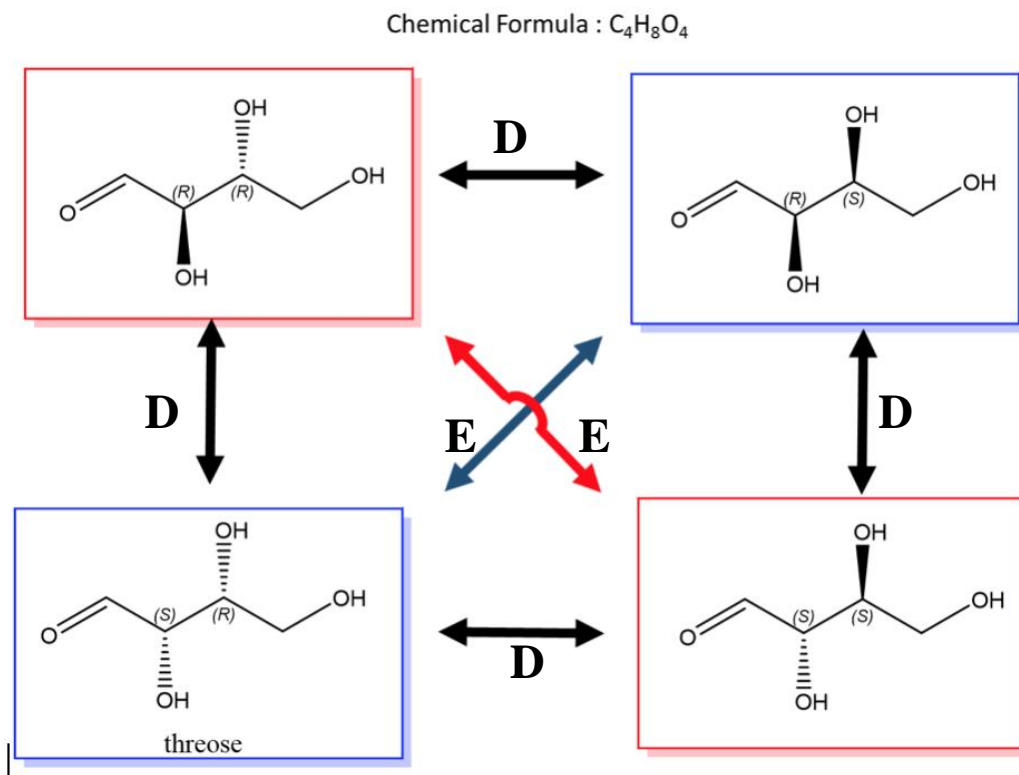


Figure 1.11. Relation between the four stereoisomers of threose with two stereogenic centres (**D** for diastereomer pairs and **E** for enantiomer pairs) of threose.

3.1.3.3. Atropisomers

Atropisomerism (from the Greek atropos, meaning ‘not turning’) refers to the restricted rotation of a single bond, which effectively locks the configuration into a ‘minus’ (**M**) or ‘plus’ (**P**) isomer (depicted in Figure 1.12), and in many cases may be visualised as a ‘helicity’⁴⁰. Vladimir Prelog defined atropisomers as stereoisomers “due to the so-called secondary structure, i.e. hindered rotation around single bonds”⁴¹. The chirality is not up to the conformation of the molecule but up to its configuration.

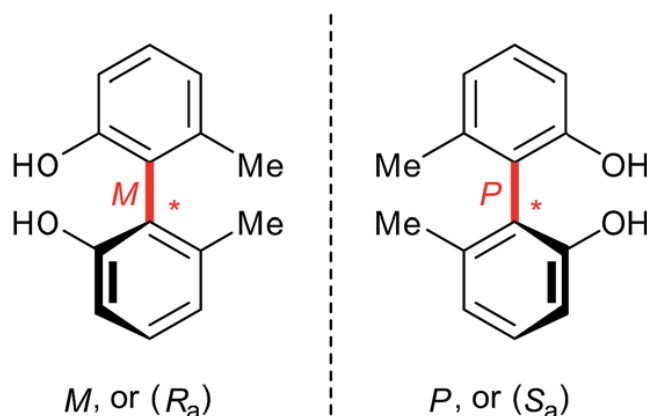


Figure 1.12³⁸. Restricted rotation about a biaryl bond, giving rise to (M) and (P) atropisomers, with alternate nomenclature of R_a and S_a respectively (subscript a indicating axial chirality), with highest priorities assigned to the ortho hydroxyl groups.

3.2. THERMODYNAMICS OF CHIRAL SYSTEMS

The equation 1.5, known as Gibb's phase rule, is the basis of the phase diagram building. Thermodynamically, for a system of n components at equilibrium state, the intensive variables such as temperature, pressure and chemical composition are the same in all phases. However, for equilibria between enantiomers, the intensive variables are linked by an additional equation. Indeed, the two enantiomers have the same chemical potential. Thus, modification of the Gibbs' phase rule is required and the Gibbs-Scott phase rule⁴² must be applied (equation 1.7).

$$V = C + C'/2 + 2 - \phi - \phi'/2 \quad (1.7)$$

Where C and ϕ stand for non-symmetrical components and non-symmetrical phases and C' and ϕ' stand for symmetrical components and symmetrical phases.

Representation of the thermodynamic phase equilibria of chiral systems using phase diagrams deserve attention to better understand the domain of stability of a chiral system. Crystallization procedures of chiral systems require a good knowledge of the behaviour of the two enantiomers regarding melting (binary phase diagrams) and solubility in a given solvent (ternary phase diagrams). Overviews and comprehensive details of identified phase diagrams encountered for these systems of enantiomers were widely described by Jacques *et al.*⁴³, Coquerel⁴⁴ and Lorenz⁴⁵.

3.2.1. Binary phase diagrams of racemic mixtures

There are many possibilities for a racemic mixture to form condensed phases. Firstly, to simplify, let us consider that partial solid solutions and solid-solid transitions are absent. Three possibilities exist for racemic mixture conglomerate, racemic compound and solid solutions (Figure 1.13).

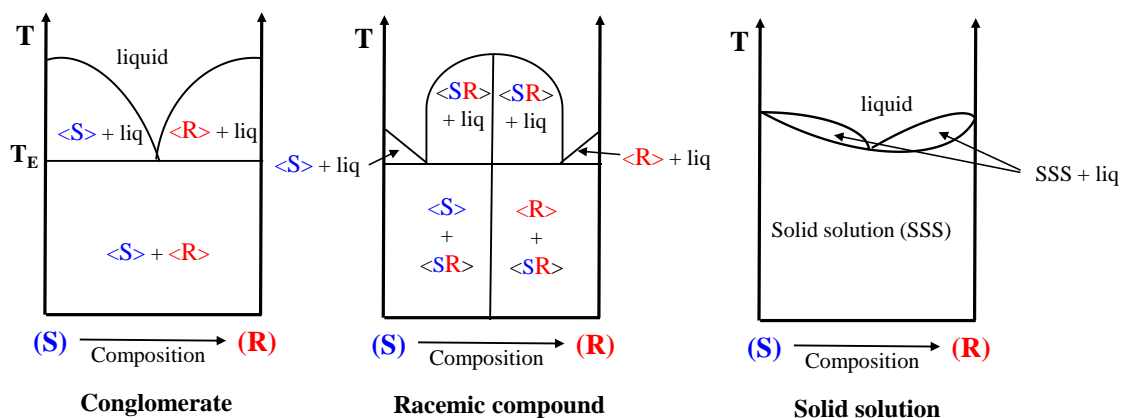


Figure 1.13: Fundamental types of binary solubility phase diagrams for chiral systems in absence of partial solid solution and solid-solid transition (T_E : eutectic temperature; liq: liquid).

- Conglomerate (5-10% of the pair of enantiomers)⁴⁶: the two enantiomers crystallize separately, as in a physical mixture. The binary phase diagram of a conglomerate consists in a eutectic invariant and it is symmetric because of the similarity of physico-chemical properties of the pure enantiomers. Below the eutectic temperature, the solid phase is composed of crystals of pure enantiomer whatever the composition of the mixture and thus there is a full chiral discrimination in the solid state.
- Racemic compound (90-95% of the racemic species): there is a defined compound formed by a stoichiometric mixture of the two enantiomers. In the solid state there is a mixture of the racemic crystals and crystals of the pure enantiomer ($\langle R \rangle$ or $\langle S \rangle$, depending on the composition of the system). This $\langle RS \rangle$ compound exhibits a congruent melting temperature which can be higher (as it is the case in the example of Figure 1.13) or lower than the pure enantiomer melting temperature.
- Total solid solutions ($<1\%$): crystals composed of the two enantiomers which are randomly distributed inside the structure. Each crystal is representative of the composition of the system, whatever its composition. The chiral discrimination is almost impossible in this case; only few cases of preferential enrichment were described in the literature⁴⁷.

These three cases are not the only ones to exist and mixtures of them are frequently observed. A part of the molecules of one enantiomer is substituted by the other enantiomer preventing the total discrimination at the solid state. A mixed situation between the conglomerate and the total solid solutions exists i.e. conglomerate with partial solid solutions. In that case, a part of the molecules of one enantiomer in its crystal structure is substituted by the other enantiomer preventing a full chiral discrimination in the solid state. A typical example will be widely

developed in the chapter 3. Many other possibilities can be encountered, as mixed situations between a conglomerate and a racemic compound, or eutectoid or peritectoid transitions both for pure enantiomer and racemic compound⁴⁸.

3.2.2. Ternary phase diagrams of racemic mixtures

The behaviour of a mixture of two crystalline compounds and a solvent can be visualized and explained by means of a ternary phase diagram. A ternary phase diagram shows how this mixture of components behaves thermodynamically. The ternary isotherms (the solvent is liquid, and the enantiomers are solid at the considered temperature) related to the three cases encountered in absence of partial solid solution and solid solid-transition^{49,45} are depicted in figure 1.14.

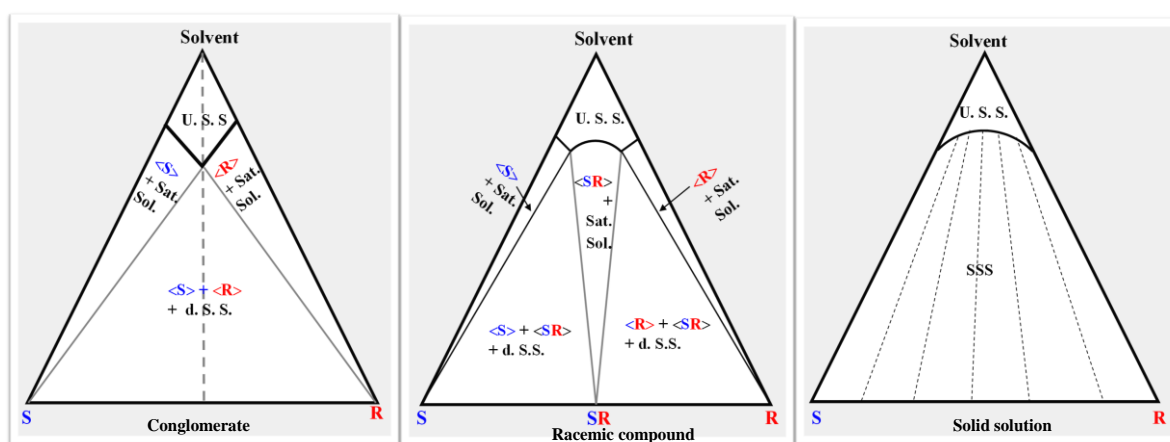


Figure 1.14: Fundamental types of ternary solubility phase diagrams for chiral systems in absence of partial solid solution and solid-solid transition (U.S.S. indicates under saturated solution; d.S.S.: double saturated solution and S.S.S.: indicates saturated solid solution).

- The isothermal sections of the three-dimensional representation associated with a conglomerate is divided into four domains. The monophasic domain (U.S.S.) is composed by an undersaturated liquid phase and is located at the solvent apex of the triangle. Two symmetrical domains exist in which a solid phase composed by crystals of a pure enantiomer is in equilibrium with a saturated liquid (domains: $\langle S \rangle + \text{sat. sol.}$ and $\langle R \rangle + \text{sat. sol.}$). The fourth domain is a three-phase domain in which a double saturated solution is in equilibrium with the two solid phases (domain: $\langle S \rangle + \langle R \rangle + \text{d.S.S.}$). The dashed line connecting the solvent corner with the binary chiral system (“eutectic line”) indicates the eutectic composition.
- The isotherm associated with a racemic compound is divided into six domains. The domains (U.S.S.), $\langle S \rangle + \text{sat. sol.}$ and $\langle R \rangle + \text{sat. sol.}$ are the same as in the ternary phase diagram of the conglomerate (respectively a liquid phase, pure crystals of (S), in

equilibrium with a saturated liquid, and pure crystals of (*R*), in equilibrium with a saturated liquid). The racemic compound is present in three domains: $\langle SR \rangle + \text{sat. sol.}$, $\langle S \rangle + \langle SR \rangle + \text{d.S.S.}$ and $\langle R \rangle + \langle SR \rangle + \text{d.S.S.}$. The former is a biphasic domain composed by the racemic compound in equilibrium with a saturated liquid while the two latter are three-phase domains in which the racemic compound is in equilibrium with crystals of a pure enantiomer and a double-saturated solution. The locations of these domains are the key data for the enantiomeric separation from a racemic compound.

- The isotherm associated with a complete solid solution exhibits only two domains. The monophasic domain (U.S.S.) is composed by a liquid phase and is located at the solvent apex of the triangle. The domain (SSS) is a biphasic domain: the solid phase is in equilibrium with a saturated liquid. The composition of both phases in equilibrium is linked by tie lines represented by dashed lines in the diagram.

In contrast to the binary chiral systems, solvates can occur as additional solid phases in the solubility phase diagrams. When a solvate directly crystallizes, the main question remains: Is there any conglomerate solvate crystallizable⁵⁰? For this reason and since polymorphism might be solution-mediated (thus, providing polymorphic varieties), solid-phase analysis should always accompany solubility measurements to avoid wrong allocation of solubility values to solid phases. This type of ternary phase diagrams is not underlined in this manuscript but Coquerel⁵¹ has fully detailed these possibilities.

3.3. CRYSTALLOGRAPHY OF CHIRAL MOLECULES

The best way of designating the chirality of the crystals is to know their space groups obtained by X-ray crystallographic analysis. It is important to distinguish the chirality of the molecule itself and the chirality of the crystalline structure in which the molecule crystallizes. Chiral molecules are usually present either in enantiomerically pure or racemic mixture form. When the space group of the single crystal of a compound is chiral, the crystal is designated to be chiral. As mentioned in Section 1.2.2., the order of the symmetry operation determines the crystal class. Crystals can be classified into three crystal structure types regarding their point groups⁵²⁻⁵⁴.

- Centrosymmetric (achiral) structures (**CA**) which correspond to point groups: $\bar{1}$, $2/m$, mmm , $4/m$, $4/mmm$, $\bar{3}$, $\bar{3}m$, $6/m$, $6/mmm$, $m\bar{3}$ and $m\bar{3}m$.
- Non-centrosymmetric achiral structures (**NA**) for point groups: m , $mm2$, $\bar{4}$, $4mm$, $\bar{4}2m$, $3m$, $\bar{6}$, $6mm$, $\bar{6}m2$ and $\bar{4}3m$.

- Non-centrosymmetric chiral structures (NC) associate with point groups: 1, 2, 222, 4, 422, 3, 32, 6, 622, 23 and 432.

Enantiomers, indeed conglomerates⁹, can only crystallize in the NC type and 95% of them belong to one of the four space groups $P2_12_12_1$, $P2_1$, $C2$ and $P1$.

For Racemic compounds, they can crystallize in any of these crystal structure types (CA, NA or NC) even though 95% of the known cases crystallize in centrosymmetric space groups i.e. CA type. In centrosymmetric racemic compounds, the predominant space groups⁵⁴ (95%) are: $P2_1/c$, $C2/c$, $Pbca$ and $P\bar{1}$. However, non-centrosymmetric racemic compounds (NA) like DL-Allylglycine⁵⁴ represent a certain proportion (4.5-5%), mainly placed in space groups $Pna2_1$, $Pca2_1$, Cc and Pc . Racemic compounds crystallizing in chiral space groups (NC, mainly $P2_12_12_1$ and $P2_1$) named kryptoracemic compounds have been also reported^{43,55,56,47}. Their occurrence is estimated by Flack⁴¹ to be only 0.02% of the other cases.

For solid solutions, rare cases are reported in the literature, but they can crystallize in all space groups^{57,58}.

Molecules impose some restrictions in the formation of crystalline structure from chiral or achiral molecules. For example, for non-racemic enantiomeric mixtures, chiral crystal structures should be permitted whereas achiral crystal structures should be forbidden (Table 1.3)⁵³.

Table 1.3: Crystallographic data of the formation of chiral and achiral crystal structures (stat. for statistical; adapted from reference 53).

		Achiral Structure		Chiral Structure
		CA	NA	NC
Racemic compound (90-95%)	Structure	Permitted	Permitted	Permitted
	Proportion (%)	~ 95	4.5-5	0.02
	Dominant SG	$P2_1/c$; $C2/c$, $Pbca$; $P\bar{1}$	$Pna2_1$; $Pca2_1$; Cc ; Pc	$P2_12_12_1$; $P2_1$
Conglomerate (5-10%)	Structure	Forbidden	Forbidden	Mandatory
	Proportion (%)	0	0	100
	Dominant SG			$P2_12_12_1$, $P2_1$, $C2$; $P1$
Solid Solutions (<1%)	Structure	Permitted	Permitted	Permitted
	Proportion (%)	No stat. data	No stat. data	No stat. data
	Dominant SG	No stat. data	No stat. data	No stat. data

The choice of resolution methods of the racemic mixtures depends on the racemic species (crystallographic crystal system, solubility, stability) and the ratio time to reach pure enantiomer/cost of the method. The separation of the two enantiomers by crystallization is made easier when the compound crystallizes as a stable conglomerate. However, conglomerates are not prevalent in nature, but some simulation works for conglomerate forming systems (salt formation, multicomponent crystals) are the object of research for many research groups.

Chiral compounds synthesized from achiral starting materials and reagents are generally racemic (i.e. a 50:50% mixture of enantiomers called racemic mixture). Separation of racemic compounds into their component enantiomers is a process called resolution. Several techniques are available for researchers to resolve a racemic mixture. Among these techniques, some are described in the following paragraphs.

PART 4: RESOLUTION OF RACEMIC MIXTURES

4.1. CHROMATOGRAPHIC RESOLUTION

Chromatographic separation of compounds is a method based on the difference between their affinities with the stationary phase (column material) and the mobile phase (eluent)⁵⁹. It means that a racemic mixture can only be separated on a chiral column or on an achiral column with a chiral eluent.

The two most commonly used chromatographic methods to produce pure enantiomers are batch chromatography and Simulating Moving Bed (SMB), and the choice is very much dependent on the time constraints and the quantities needed.

For preparative separation, SMB chromatography is an attractive method used in industry. It consists of switches between identical columns in order to simulate a column of infinite length in which each enantiomer moves in opposite directions⁶⁰. However, the chiral SMB chromatography is not often the best alternative to separate a racemic mixture because of its investment cost. This method is thus used if the other methods fail. It is worth noting that it can be used in combination to crystallization to increase the productivity⁶¹.

4.2. DIRECT RESOLUTION

Crystallization methods such as preferential crystallization (PC) are still competitive since the end of the 20th century, when Secor and then Jacques and collaborators started looking at its systematic application. Direct crystallization leads to the complete conversion of a racemic mixture into a single enantiomer. The prerequisite being the crystallization of the racemic mixture as a conglomerate.

Once a conglomerate forming system is established, the following chiral resolution methods can be employed to separate the racemic mixture into its enantiomers.

4.2.1. Preferential crystallization (PC)

PC consists in alternating a stereoselective crystallization of the two enantiomers out of a racemic mixture. The precise mechanism and full details on each mode have been described by Collet *et al.*⁶² and by Coquerel⁶³.

A schematic representation of the different steps of PC can be summarized as represented in Figure 1.15 and its different modes are more detailed in the chapter 3.

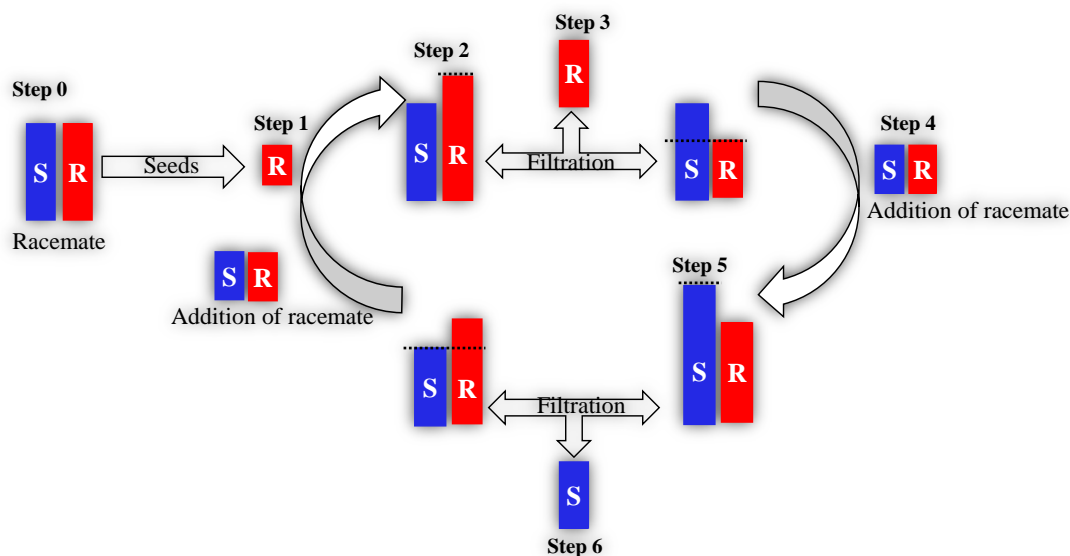


Figure 1.15: Schematic representation of the different steps of preferential crystallization (PC)

The resolution starts with a racemic mixture in a solvent (step 0) which is artificially biased in the (*R*)-enantiomer (step 1) and heated to dissolution. The mixture is cooled to supersaturation of both enantiomers. The enantiomer with the highest concentration, (*R*) (step 2), will start to crystallize first and its concentration will return to the saturation point. The (*R*)-enantiomer is collected by filtration before the supersaturated (*S*)-enantiomer starts to crystallize (step 3). Racemic mixture, with the same weight, as the (*R*)-enantiomer collected in step 3, is added and the mixture is heated to dissolution (step 4). Note that the resulting situation is the same, but mirror imaged to the one resulting from step 1. Again, the mixture is cooled to supersaturation of both enantiomers and now the (*S*)-enantiomer crystallizes (step 5). The amount of crystals collected after filtration is the same as the amount of racemic mixture added in the previous step (step 6). Subsequently, racemic mixture is added, and the mixture is heated to dissolution, resulting in the same situation as was obtained after step 1. The system can be run for several cycles (usually from 30 to 100), when the system is too much disturbed by the impurities accumulated by the recycle of the mother liquor a start over with a fresh racemic mixture is necessary.

However, several reasons could account for a severe limited entrainment effect down to a complete failure. Some of them are highlighted in the chapter 3 and really alter the PC performances. As a rule of thumb, only circa 50% of the conglomerates can be efficiently resolved by preferential crystallization because of these limitations.

4.2.2. Deracemization

Deracemization process can be defined as a conversion of a racemic mixture of chiral molecules into a single enantiomer. Sometimes maximum yield of chiral resolution is limited to 50 % (diastereomeric resolution and preferential crystallization). However, this limitation can be overcome if the compound can change its handedness in solution (racemization). An example of such a process is through spontaneous symmetry breaking, which was first discovered by Havinga who obtained enantiopure crystals from a supersaturated solution in which the compound is racemized⁶⁴.

Further examples were illustrated by Kondepudi, Soai and in 2005 by Viedma⁶⁵ who showed that it is possible to completely break the symmetry of a racemic mixture of D- and L-crystals of NaClO₃ by using a continuous grinding technique in suspension (NaClO₃ is achiral in solution but crystallizes in the chiral space group *P2₁3*).

Stirring a grinding media in contact with a suspension (solution-solid equilibrium) can lead to a complete conversion into one of the single enantiopure solid phase. This process known as attrition-enhanced deracemization of an achiral compound was later extended by Noorduyn and co-workers to chiral amino acid derivatives^{66,67}. Several works have illustrated these experiments by combining grinding with temperature cycling⁶⁸. Grinding the slurry of crystals with glass beads promotes dynamic dissolution and crystallization processes that result in the conversion of one solid enantiomer into the other. And the temperature cycling leads also into a partial dissolution and crystal re-growth^{69,70}. Combining both processes could enhance the deracemization rate.

4.3. DIASTEREOMERIC RESOLUTION

Diastereomers have different physical properties, and this fact is used to achieve resolution of racemic mixtures. Reaction of a racemic mixture with an enantiomerically pure chiral reagent gives a mixture of diastereomers, which can be separated. This is known as resolution by diastereomeric salt formation or Pasteurian resolution or even ‘classical’ resolution⁷¹. The easiest way to do this is by crystallization providing that the least soluble diastereomer crystallizes out of the solution selectively. By crystallizing the salts from a proper solvent, high diastereomeric excess (*de*) can often be found in the precipitated salts. Reversing the first reaction then leads to the separated enantiomers plus the recovered resolution reagent.

Many kinds of chemical and physical reactions may be used to achieve the diastereomeric intermediates needed for separation. Chemical reactions of enantiomers are normally not so dramatically different, but a practical distinction is nevertheless possible.

PART 5: INTRODUCTION TO NONLINEAR OPTICS

5.1. GENERALITIES

Nonlinear optics (NLO) is the branch of optics that describes the effects of light in media in which the dielectric polarization responds nonlinearly to the electric field of the light. This phenomenon is only observed at very high light intensities such as those provided by pulsed lasers. The coherent radiation at a few discrete frequencies can be produced by laser devices as in solid-state lasers or with narrow range of tunability as in dye lasers. Many applications require frequencies that are not readily available from such laser sources. The most effective way of converting a fundamental laser frequency to other frequencies, either to higher or lower frequencies, is harmonic generation or parametric oscillation in NLO crystalline media⁷².

5.1.1. Origin of optical nonlinearity

Nonlinear optics is the effect in which, light of a fundamental wavelength is transformed to light of a new wavelength. The creation of light of new wavelength comes from the interaction between the source of light and the electrons of a crystal. The electrons in a crystal are bound in a potential well, which acts like a spring, holding the electrons to lattice point in the crystal. If an external force pulls an electron away from its equilibrium position, the spring pulls it back with a force proportional to the displacement. The spring's restoring force increases linearly with the electron displacement from its equilibrium position. In an ordinary optical material, the electrons oscillate about their equilibrium position at the frequency of this electronic field. According to the fundamental law of physics an oscillation charge will radiate at its frequency of oscillation; hence, these electrons in the crystal "generate" light at the frequency of the light wave. If the light passing through the material is intense enough, its electric field can pull the electrons so far that the restoring force is no longer proportional to the displacement and, then, it becomes nonlinear. The electrons are roughly thrown rather than pulled back smoothly and they oscillate at frequencies other than the driving frequency of the light wave. These electrons radiate at the new frequencies, generating the new wavelength of light⁷³⁻⁷⁷.

5.1.2. Theoretical explanation of nonlinear optics

A medium exhibiting nonlinear optical property is a crystal composed of molecules with asymmetric charge distributions arranged in the crystal in such a way that a polar orientation is maintained throughout the crystal.

The charged particles in dielectric medium are bound together. When an electric field is applied, they are displaced slightly from their equilibrium positions. This small movement of positive charges in one direction and negative charges on the other, results in a collection of induced

electric dipole moments⁷⁸. Oscillation of those dipoles due to interaction with the electromagnetic radiation results in themselves acting as sources of electromagnetic radiation. For small values of the electric field associated with the radiation, the induced polarization P , which is the electric dipole moment per unit volume of the medium, is linear with the field⁷⁹.

$$P = \epsilon_0 \chi E \quad (1.8)$$

Where χ is the linear susceptibility of the material, E is the electric field vector, ϵ_0 is the electrical permittivity of vacuum.

At high fields, the polarization becomes independent of the field and the susceptibility becomes field dependent. Therefore, this nonlinear response is expressed by writing the induced polarization as a power series of the field.

$$P = \epsilon_0 \{ \chi^{(1)}E + \chi^{(2)}E \cdot E + \chi^{(3)}E \cdot E \cdot E + \dots \} = P_L + P_{NL} \quad (1.9)$$

Where $\chi^{(1)}$ is the linear susceptibility tensor corresponding to the linear polarisation P_L , $\chi^{(n)}$ are the nonlinear susceptibilities of the medium ($n = 2, 3, \dots$) giving rise to the nonlinear polarization P_{NL} .

The coefficients of $\chi^{(1)}$, $\chi^{(2)}$ and $\chi^{(3)}$ give rise to numerous optical effects⁸⁰ listed in Table 1.4. $\chi^{(1)}$ is the linear term responsible for materials linear optical properties like refractive index, dispersion, birefringence, absorption. $\chi^{(2)}$ is the quadratic term which corresponds for example to the second harmonic generation in non-centrosymmetric materials. $\chi^{(3)}$ is the cubic term responsible for the third harmonic generation, as stimulated Raman scattering, phase conjugation and optical stability.

In equations containing nonlinear terms, a product of two or more oscillating fields gives oscillation at combination of frequencies and therefore the equation (1.9) can be expressed in terms of frequency as:

$$P(\omega_0) = \epsilon_0 \{ (\chi^{(1)}(\omega_0; \omega_1) \cdot E(\omega_1) + \chi^{(2)}(\omega_0; \omega_1, \omega_2) \cdot E(\omega_1) \cdot E(\omega_2) + \chi^{(3)}(\omega_0; \omega_1, \omega_2, \omega_3) \cdot E(\omega_1) \cdot E(\omega_2) \cdot E(\omega_3) + \dots \} \quad (1.10)$$

Table 1.4: Optical effects of nonlinear materials

Order	Tensor	N° of Coefficients	Effects	Applications
1	$\chi^{(1)}$	9	Refraction, Absorption	Lens, Microscope
2	$\chi^{(2)}$	27	SHG ($\omega; \omega; 2\omega$) Sum frequency generation ($\omega_1 \pm; \omega_2; \omega_3$) Pockels effects ($\omega; 0; \omega$)	Laser source Laser pointer, Optical parametric oscillators Electro-optical modulators
3	$\chi^{(3)}$	81	Four wave mixing phase gratings ($\omega_1; \omega_2; \omega_3; \omega_4$) Kerr effect Optical amplitude	Raman Coherent spectroscopy, Real time holography Ultra-high-speed optical gates Amplifiers, choppers etc.

5.1.3. Quadratic nonlinear phenomena

The susceptibility coefficients decrease rapidly with increasing order. Consequently, in most cases, only the linear and quadratic terms of equation (1.10) give rise to significant effects.

If two monochromatic optical fields, with frequencies ω_1 and ω_2 and amplitudes E_1 and E_2 respectively, are applied to a medium with non-vanishing second-order susceptibility $\chi^{(2)}$, the induced dipole response will contain, in addition to the ordinary linear response terms at frequencies ω_1 and ω_2 , a nonlinear response P_{NL} proportional to $\chi^{(2)}E_1E_2$, with spectral components at $\omega_1 \pm \omega_2$. These frequencies can be obtained from the propagation equations.

Let us assume that the two travelling waves are given by the two equations (1.11) and (1.12).

$$E_1(t, z) = E_1 \cos(\omega_1 t + k_1 z) \quad (1.11)$$

$$E_2(t, z) = E_2 \cos(\omega_2 t + k_2 z) \quad (1.12)$$

The second order nonlinearity term is given by:

$$P_{NL} = \epsilon_0 \chi^{(2)} E^2 \quad (1.13)$$

Equations (1.11) and (1.12) in (equation (1.13) gives:

$$P_{NL} = \epsilon_0 \chi^{(2)} [E_1^2 \cos^2(\omega_1 t + k_1 z) + E_2^2 \cos^2(\omega_2 t + k_2 z) + 2E_1 E_2 \cos(\omega_1 t + k_1 z) \cos(\omega_2 t + k_2 z)] \quad (1.14)$$

Or

$$P_{NL} = \epsilon_0 \chi^{(2)} \{E_1^2 [\cos 2(\omega_1 t + k_1 z)] + E_2^2 [\cos 2(\omega_2 t + k_2 z)] + E_1 E_2 \cos [(\omega_1 + \omega_2)t + (k_1 + k_2)z] + E_1 E_2 \cos [(\omega_1 - \omega_2)t + (k_1 - k_2)z]\} \quad (1.15)$$

Thus, the polarization consists of number of components with different frequencies. The different components of nonlinear polarization generate electromagnetic waves having frequencies different from those of the incident ones.

In a medium, several types of second-order nonlinear optical effects can experimentally be observed. Sum frequency generation (SFG) or difference frequency generation (DFG), in which two initial beams generate a new beam with the sum or difference of the optical frequencies of the initial beams. Second harmonic generation (SHG) is a special case of SFG for which the two initially interacting waves exhibit the same frequency ($\omega_1 = \omega_2 = \omega$) and will be developed in the following section.

5.2. SECOND HARMONIC GENERATION (SHG)

5.2.1. Principle of SHG

In SHG, a wave of angular frequency ω (wavelength λ), electric amplitude $E(\omega)$ and wave vector k_ω passing through a material generates a second harmonic wave of angular frequency 2ω (wavelength $\lambda/2$) and wave vector $k_{2\omega}$. The amplitude of the second harmonic electric field $E(2\omega)$ varies with the distance travelled through the medium due to the continuous exchange of energy between the fundamental and the second harmonic wave. The SHG is schematically represented in Figure 1.18.

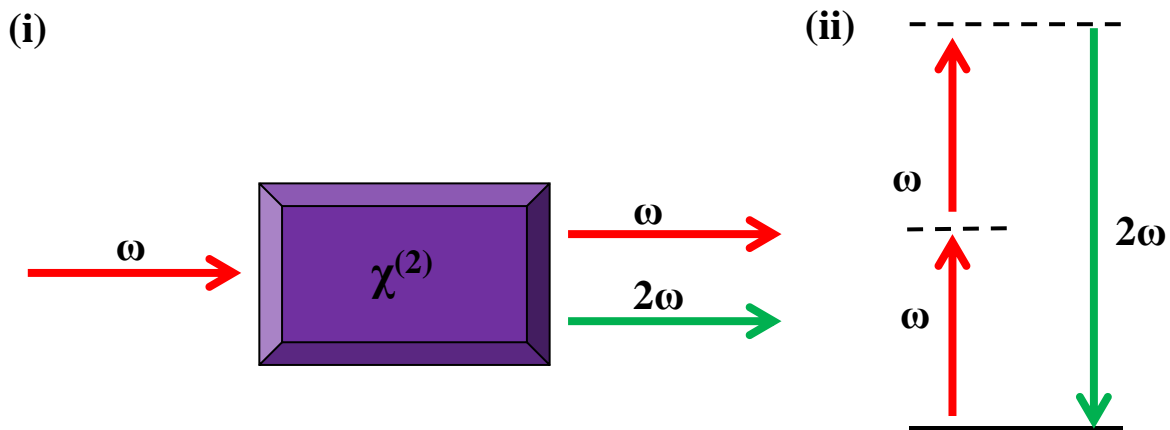


Figure 1.16: Geometry (i) and energy-level diagram (ii) description of SHG

Among the nonlinear optical phenomena, the second harmonic generation (frequency doubling) is the most important one, because this process provides significant tool for the conversion of near infrared laser light from diode laser into visible light in the field of optical image storage. The Second Harmonic Generation (SHG) was first observed by Franken and co-workers⁸¹ in 1961 which marked the birth of nonlinear optics as a new discipline in the area of laser matter interaction. Franken observed that the light at $\lambda = 347.15$ nm could be generated when a quartz crystal was irradiated with light at $\lambda = 694.3$ nm obtained from a ruby laser.

5.2.2. Requirements for SHG

5.2.2.1. Non-centrosymmetry

In equation (1.10), the odd orders of $\chi^{(n)}$ are orientationally independent but the even ones vanish in a centrosymmetric environment. Hence, for centrosymmetric materials (conventional liquid, gases, amorphous solids, centrosymmetric crystals) all components of $\chi^{(2)} = 0$. Therefore, an important criterion for a material to exhibit SHG is that it should be a **non-centrosymmetric material**. This can be illustrated by the following equations.

If we consider an electric field given by equation (1.16) which is incident on a material, the resultant second order polarization is given by equation (1.17).

$$E(t, z) = E(\omega) \cos(\omega t + kz) \quad (1.16)$$

$$P_{NL}(t, z) = \chi^{(2)} [E(t, z)]^2 \quad (1.17)$$

If the medium is centrosymmetric and thus possesses inversion symmetry, we can also write

$$-P_{NL}(t, z) = \chi^{(2)} [-E(t, z)]^2 = \chi^{(2)} [E(t, z)]^2 \quad (1.18)$$

Equations (1.17) and (1.18) can be simultaneously true only if the polarization field is zero. Therefore, $\chi^{(2)}$ is zero for a centrosymmetric medium and no SHG will occur. Thus, only non-centrosymmetric crystals and macromolecular assemblies which are fairly ordered to form large non-centrosymmetric structures (e.g. collagen or myosin) can generate SHG.

Moreover, even in non-centrosymmetric crystalline materials, the intrinsic symmetry of the physical properties decreases the number of the independent tensor components. Among those, Neumann principle⁸² and Kleinman permutation rules⁸³ impose some restrictions.

5.2.2.2. Neumann principle

Neuman's principle formulated already in the 19th century stated that the symmetry elements of any physical property of a crystal must include all the symmetry elements of the point group of the crystal. This principle may be illustrated by considering the optical indicatrix of a crystal, which is an ellipsoid. If the medium is invariant with respect to a three-fold, a four-fold or a six-fold rotation (as in a trigonal, tetragonal or hexagonal crystal, for instance), its optical

indicatrix must also be invariant with respect to the same operation, according to Neumann's principle. Thus, it results that SHG is not possible in **432**-point group.

5.2.2.3. Kleinman symmetry rules

In off-resonance studies of oriented bulk media, ultrathin surface films and interpretation of nonlinear optical measurements are routinely simplified by the assumption of Kleinman symmetry⁸³. Simply stated, Kleinman symmetry is defined as the interchangeability of all n indices in the rank n tensor $\chi^{(n)}$ describing the macroscopic nonlinear polarizability of a system arising explicitly from the absence of dispersion⁸⁴⁻⁸⁶. These “non-resonant” conditions studied by Kleinman (Kleinman 1962) lead to reduce to 10 (instead of 27) the number of independent coefficients in the second order tensor $\chi^{(2)}$. These restrictions impose that all the $\chi^{(2)}$ coefficients in the point groups **422** and **622** vanish.

Finally, SHG should not be observable for crystals belonging to these three-point groups (432, 422 and 622) which reduce the number of possible crystal systems.

A statistical estimation of molecular structures crystallizing in such point group is summed up in Table 1.5. It was found that it represents only 2.41% of non-centrosymmetric structures reported in the CCDC database⁸⁷.

Table 1.5: Statistical estimation of structures crystallizing in point group 422, 432 and 622 according to the CCDC database.

422			432		622	
Space group	P422	7	P432	5	P622	5
	P4 ₂ 12	46	P4 ₁ 32	36	P6 ₁ 22	186
	P4 ₁ 22	56	P4 ₂ 32	5	P6 ₂ 22	45
	P4 ₁ 2 ₁ 2	1377	P4 ₃ 32	27	P6 ₃ 22	86
	P4 ₂ 22	6	F432	22	P6 ₄ 22	30
	P4 ₂ 2 ₁ 2	120	F4 ₁ 32	24	P6 ₅ 22	141
	P4 ₃ 22	47	I432	21		
	P4 ₃ 2 ₁ 2	1156	I4 ₁ 32	20		
	I422	43				
	I4 ₁ 2 ₁ 2	70				
Total/% NC CSD	2922/1.97		160/0.11		493/0.33	

However, it is important to mention that, Kleinman symmetry restriction has failed in hyperpolarizability measurements by hyper-Rayleigh scattering; in electric field-induced

second harmonic (EFISH) generation measurements^{88,89} but also in classical SHG measurements. In fact, many compounds crystallizing in 422 and 622 point group classes have proven to exhibit a positive SHG signal and it seems that this restriction is the exception rather than the rule for organic solids at the incident wavelength of 1064 nm^{90,91}.

5.2.3. Conversion efficiency

In a mathematical point of view, the propagation of light through a medium can be given by the equation (1.19).

$$\nabla^2 E - \mu_0 \epsilon_0 \frac{\partial^2 E}{\partial t^2} = \mu_0 \frac{\partial^2 P}{\partial t^2} \quad (1.19)$$

With μ_0 is the permeability of the free space.

By resolving the propagation equation for waves travelling in one direction, we can lead to the relation of the conversion efficiency when the phase vectors of the input and generated beams match^{76,92}.

The conversion efficiency harmonic noted η is defined as the converted intensity $I(2\omega)$ with respect to the incident intensity $I(\omega)$ sent through the material. It is given by the equation (1.20).

$$\eta = \frac{I(2\omega)}{I(\omega)} = \gamma^2 l^2 \text{sinc}^2\left(\frac{\Delta k l}{2}\right) \quad (1.20)$$

Where $\gamma^2 = \frac{\chi^{(2)^2 \omega^2}{2n_{2\omega}^2 n_{2\omega} c^3 \epsilon_0}$ is the hyper-polarizability; l is the distance travelling through the crystal, ω is the fundamental frequency, n_{ω} and $n_{2\omega}$ are the refractive indexes at frequency ω and 2ω respectively, c is the speed of light and $\Delta k = \frac{2\omega}{c}(n_{2\omega} - n_{\omega})$ is the phase mismatch.

5.2.4. Phase matching conditions

The phase mismatch⁹³ is expressed as follows:

$$\Delta k = \frac{2\omega}{c}(n_{2\omega} - n_{\omega}) \quad (1.21)$$

If the generated second harmonic waves add up coherently ($\Delta k = 0$), the SHG intensity increases quadratically with the travelled distance l and the nonlinear medium is called **phase matchable (PM)**. It requires that the relation $2k(\omega) = k(2\omega)$ where $k(\omega) = \frac{\omega n(\omega)}{c}$ is fulfilled.

If $\Delta k \neq 0$, the function oscillates⁷⁶ and the second harmonic intensity reaches a maximum value for $l = nL_c$ where $n = 1, 3, 5, \dots$ with L_c expressed as follows:

$$L_c = \frac{\pi}{|\Delta k|} = \frac{\lambda}{4|n_{2\omega} - n_{\omega}|} \quad (1.22)$$

The **coherence length L_c** is defined as the distance in the crystal for which both waves are in phase. In numerous materials, the coherence length has been evaluated to few micrometers⁷⁴.

For an efficient energy transfer to occur, the polarized wave and the second harmonic wave must remain in phase. For $\Delta k = 0$; the two waves remain in phase i.e. $n_{2\omega} = n_{\omega}$; the SHG signal is maximum and is simply related to the square of the distance **L**.

However, the generation of a new wave at frequency 2ω can also occur spontaneously with the destruction of the fundamental wave at frequency ω ⁸⁰. This is due to the dispersion (the velocity of a wave changes with the wavelength), the second harmonic waves and the fundamental waves are not in phase ($\Delta k \neq 0$). The energy cannot only be transferred from the fundamental field towards the second harmonic field, but also from the second harmonic field towards the fundamental field (destructive interference). The nonlinear medium is then called **non-phase-matchable (NPM)**. For normal dispersion, the refractive index increases with respect to the frequency. This makes difficult to achieve the phase matching conditions⁹⁴ (see Figure 1.17)⁷⁴.

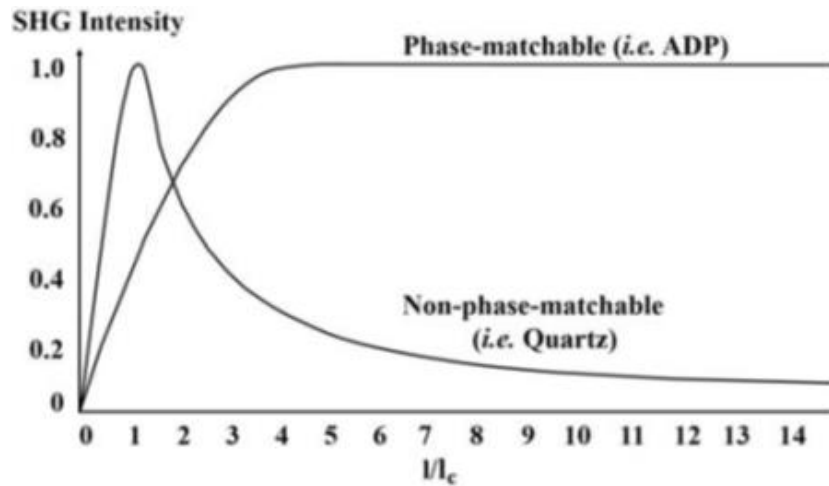


Figure 1.17: Schematic representation of different particle-size dependences for phase-matchable and non-phase matchable materials (adapted from reference 74).

5.3. CLASSIFICATION OF NONLINEAR OPTICAL MATERIALS

The NLO materials can be classified into three different categories as inorganic, organic and semi-organic or metal-organic materials.

5.3.1. Inorganic NLO materials

Inorganic materials are covalent and ionic bulk materials in which the optical nonlinearity is a bulk effect. It is always easier to synthesize inorganic materials which have high melting point, high degree of chemical inertness, high thermal and mechanical stabilities. The inorganic NLO materials have some advantages like highest bulk electrical susceptibility but on the other hand these materials suffer from disadvantages like absorption in the visible region, poor response time and degradative photorefractive effects, low laser damage threshold ($\sim 10 \text{ MW cm}^{-2}$) and poor optical transparency⁹⁵. Potassium dihydrogen phosphate, ammonium dihydrogen phosphate and lithium iodate are for example appropriate infrared NLO materials.

5.3.2. Organic NLO materials

Organic materials are molecular materials that consist of chemically bonded molecular units interacting in the bulk media through weak interactions (van der Waals, hydrogen bonds) or ionic bonds. The organic molecules which contain both conjugated bonds and acceptor group on one side and a donor group on the other side are known as nonlinear optical (NLO) materials⁹⁶. Urea derivatives, 4-methoxy benzaldehyde- N-methyl 4-stilbazolium tosylate (MBST) have high NLO properties^{74,97}.

The organic nonlinear optical materials have advantages such as high second order nonlinear optical coefficient, great resistance to damage in the laser beam, birefringent nature facilitating phase-matching and the possibility to chemically ‘engineer’ molecular properties. However, the limitations of these organic materials are the poor physicochemical stability, low hardness.

5.3.3. Semi-organic materials

Semi-organic compounds share the properties of both organic and inorganic compounds. They are organic based materials in which the polarizable part is an organic molecule which is stoichiometrically bonded with an inorganic ion. L-arginine phosphate monohydrate and L-arginine fluoride are excellent semi-organic materials with nonlinearity and high conversion efficiency^{98,99}. The approach of combining the high nonlinear optical coefficients of the organic molecules with the excellent physical properties of the inorganic materials has been found to be overwhelmingly successful in recent years. Hence, recent search is concentrated on semi-organic materials due to their large nonlinearity, high resistance to laser induced damage, low angular sensitivity and good mechanical hardness.

5.3.4. Organo-metallic NLO crystals

The metal-organic crystals form a new class of materials under semi-organics. Compared to organic molecules, metal complexes offer a large variety of structures, and a diversity of electronic properties by the coordinated metal centre. Tri-allyl thiourea zinc chloride and zinc thiourea chloride are complexes of organo-metallics all owing large nonlinearity, high laser damage threshold, low UV-cut off and good mechanical properties^{100,101}.

5.4. APPLICATIONS OF NLO CRYSTALS

Several works have been done to improve the optical, mechanical characteristics and damage thresholds far higher than the classical crystals¹⁰². High NLO coefficient, wide phase matching angle and high laser damage threshold are very important for a non-centrosymmetric crystal for device applications. KDP (or even DKDP where part of the hydrogen is substituted by deuterium to limit the threshold of damage due to internal Raman emission) crystal are suitable

for higher harmonic generation of huge laser systems for nuclear fusion experiments (large crystal size and high laser damage threshold). Potassium titanyl phosphate (KTP) crystal is a useful nonlinear optical crystal to get efficient green light by the frequency doubling of Nd:YAG laser.

Several researches conducted in nonlinear optics have shown that the electron donor-acceptor-systems exhibit the greatest anharmonicity¹⁰³ with organic compounds reaching SHG intensity several orders of magnitude higher than usual inorganic non-centrosymmetric crystals¹⁰⁴.

In the following, a chapter will be dedicated to the search of organic compounds which could secure non-centrosymmetric crystallographic structure from a centrosymmetric material.

PART 6 : CONCLUSION

The aim of this chapter was to introduce to the reader the different physical properties of the crystalline solid and to refresh important concepts that help to understand the development of the following chapters.

Since Pasteur separated the right- and left-handed of sodium ammonium tartrate tetrahydrate crystals into two populations of homochiral crystals, several techniques have been developed to give life to the chiral discrimination of solid-state materials.

Chiral solid materials can be organized in three different crystal structures and among them conglomerate forming systems. Conglomerate being a physical mixture of crystals corresponding to a chiral space group makes possible the use of Second Harmonic Generation (SHG) for a solid-state discrimination. The technique has its advantages and its drawbacks. The principle, the responses and the limitation of the technique are revisited herein.

The main interest of the technique lies in the fact that in centrosymmetric structures all the elements of the second order tensor are zero. This is the case for most of racemic compounds which are thus expected to be non-SHG materials. Conversely, crystallized samples exhibiting SHG must be composed of non-centrosymmetric crystals. Therefore, crystallized derivatives of a racemic mixture exhibiting a SHG positive effect are likely to crystallize as a conglomerate.

REFERENCES

- (1) Dekker, A. J. *Chapter 1 in Solid State Physics*; Macmillan Publishers India Ltd: Delhi-India, 1981.
- (2) Donth, E.-J. *The Glass Transition: Relaxation Dynamics in Liquids and Disordered Materials*; Springer Science & Business Media: Halle Germany, 2013.
- (3) Atawa, B.; Correia, N. T.; Couvrat, N.; Affouard, F.; Coquerel, G.; Dargent, E.; Saiter, A. Molecular Mobility of Amorphous N-Acetyl- α -Methylbenzylamine and Debye Relaxation Evidenced by Dielectric Relaxation Spectroscopy and Molecular Dynamics Simulations. *Phys. Chem. Chem. Phys.* **2019**, *21* (2), 702–717.
- (4) Zachariasen, W. H. The Atomic Arrangement in Glass. *J. Am. Chem. Soc.* **1932**, *54* (10), 3841–3851.
- (5) Janssen, T.; Birman, J. L.; Koptsik, V. A.; Senechal, M.; Weigel, D.; Yamamoto, A.; Abrahams, S. C.; Hahn, T. H. Report of a Subcommittee on the Nomenclature of N-Dimensional Crystallography. I. Symbols for Point-Group Transformations, Families, Systems and Geometric Crystal Classes. *Acta Crystallogr. Sect. A Found. Crystallogr.* **1999**, *55* (4), 761–782.
- (6) Vippagunta, S. R.; Brittain, H. G.; Grant, D. J. W. Crystalline Solids. *Adv. Drug Deliv. Rev.* **2001**, *48* (1), 3–26.
- (7) Brittain, H. G. *Structural Aspects of Polymorphism*, H. G. Brit.; Marcel Dekker, Ed.; New York -USA, 1999.
- (8) Konig, A.; Mermin, N. D. Screw Rotations and Glide Mirrors: Crystallography in Fourier Space. *Proc. Natl. Acad. Sci.* **2002**, *96* (7), 3502–3506.
- (9) Belsky, V. K; Zorkii, P. M. Distribution of Homomolecular Crystals by Crystal Types and Structural Classes. *Acta Cryst* **1977**, *A33*, 1004–1006.
- (10) Eupen, J. T. H. Van; Elffrink, W. W. J.; Keltjens, R.; Bennema, P. Polymorphism and Migratory Chiral Resolution of the Free Base of Venlafaxine . A Remarkable Topotactical Solid State Transition from a Racemate to a Racemic Conglomerate. *Cryst. Growth Des.* **2008**, *8* (1), 71–79.
- (11) Courvoisier, L.; Mignot, L.; Petit, M. N.; Coquerel, G. Combined Effect of Polymorphism and Process on Preferential Crystallization: Example with (\pm)-5(4'-Methylphenyl)-5- Methylhydantoin. *Org. Process Res. Dev.* **2003**, *7* (6), 1007–1016.
- (12) Yeh, P. and; Yariv, A. Theory of Bragg Fiber. *J. Opt. Soc. Am.* **1978**, *68* (9), 1196–1201.
- (13) Langford, J. I.; Louër and D Scardi P. Effect of a Crystallite Size Distribution on X-Ray

- Diffraction Line Profiles and Whole-Powder-Pattern Fitting. *Appl. Crystallogr.* **2000**, *33*, 964–974.
- (14) Roelands, C. P. M.; Roestenberg, R. R. W.; Ter Horst, J. H.; Kramer, H. J. M.; Jansens, P. J. Development of an Experimental Method to Measure Nucleation Rates in Reactive Precipitation. *Cryst. Growth Des.* **2004**, *4* (5), 921–928.
- (15) Coquerel, G. Crystallization of Molecular Systems from Solution: Phase Diagrams, Supersaturation and Other Basic Concepts. *Chem. Soc. Rev.* **2014**, *43* (7), 2286–2300.
- (16) Ostwald, W. Studien Über Die Bildung Und Umwandlung Fester Körper. *Zeitschrift für Phys. Chemie* **1897**, *22U* (1), 289–330.
- (17) Mullin, J. M. *Crystallization*, Butterworth.; Elsevier Inc.: Oxford, UK, 2001.
- (18) Polte, J. Fundamental Growth Principles of Colloidal Metal Nanoparticles - a New Perspective. *CrystEngComm* **2015**, *17* (36), 6809–6830.
- (19) McCabe, W. L.; Smith, J. C. and Harriott, P. *Unit Operations of Chemical Engineering*, fifth.; McGraw-Hill, Inc.: New Delhi, India, 1993.
- (20) Kondepudi, D. K.; Sabanayagam, C. Secondary Nucleation That Leads to Chiral Symmetry Breaking in Stirred Crystallization. *Chem. Phys. Lett.* **1994**, *217* (4), 364–368.
- (21) Volmer, M. Über Gerichtetes Kristallwachstum. *Zeitschrift für Phys.* **1922**, *9*, 193–196.
- (22) Burton, W. K.; Cabrera, N.; Frank, F. C. The Growth of Crystals and the Equilibrium Structure of Their Surfaces. *Philos. Trans. R. Soc. A Math. Phys. Eng. Sci.* **2006**, *243* (866), 299–358.
- (23) Bennema, P. Spiral Growth and Surface Roughening: Developments since Burton, Cabrera and Frank. *J. Cryst. Growth* **1984**, *69* (1), 182–197.
- (24) Gibbs, J. W. On the Equilibrium of Heterogeneous Substances. *Trans. Connect. Acad. Arts Sci.* 343–524 & 108–248.
- (25) Stumm, W.; Morgan, J. J. *Aquatic Chemistry; an Introduction Emphasizing Chemical Equilibria in Natural Waters.*; Wiley-Interscience: New York, USA, 1970.
- (26) Freeze, R. A.; Cherry, J. A. Chemical Properties and Principles. In *Groundwater*; Prentice Hall Inc., 1979; pp 80–139.
- (27) Haüy, R. J. *Traité de Minéralogie*; Chez Louis, Ed.; Libraire: Paris-France, 1801.
- (28) Biot, J. B. Phénomène de Polarisation Successive Observe Dans Les Fluides Homogènes. *Bull. Soc. Philomath.* **1815**, 190–192.
- (29) E. Mitscherlich, E.; Biot, J. B. *A Note Sent by E. Mitscherlich to J. B. Biot and Presented*

- to the French Académie Des Sciences; 1844.*
- (30) Sah, Y.; Krishna, J. G. Optical Properties of an Isotropic Optically Active Medium at Oblique Incidence. *J. Opt. Soc. Am. A* **2000**, *18* (6), 1388–1392.
- (31) Wainer, I. W. *Drug Stereochemistry: Analytical Methods and Pharmacology.*; CRC Press: New York, USA, 1993.
- (32) Pasteur, L. *The Asymmetry of Natural Occuring Compounds (Two Lectures given to The Chemical Society of Paris, 1860), Translated by G.M. Richardson, in The Foundations of Stereochemistry; 1901.*
- (33) Pasteur, L. Mémoire de L. Pasteur Sur La Relation Qui Peut Exister Entre La Forme Cristalline et La Composition Chimique et Sur La Cause de La Polarisation Rotatoire. *C. R. T.* **1848**, *26*, 535–539.
- (34) Pasteur, L. Recherches de L. Pasteur Sur Les Relations Qui Peuvent Exister Entre La Forme Cristalline, La Composition Chimique et Le Sens de La Polarisation, Rotatoire. *C. R. T.* **1849**, *28*, 477–478.
- (35) Bruice, P. *Organische Chemie*; Pearson: Santa Barbara, 2011; p pp 191-192.
- (36) Curie, P. Sur La Possibilité d'existence de La Conductibilité Magnétique et Du Magnétisme Libre. *J. theor. Appl.*, **1894**, *3* (1), 415–417.
- (37) Mason, S, F. Origins of Biomolecular Handedness. *Nature* **1984**, *311*, 19–23.
- (38) Smyth, J. E.; Butler, N. M.; Keller, P. A. A Twist of Nature-the Significance of Atropisomers in Biological Systems. *Nat. Prod. Rep.* **2015**, *32* (11), 1562–1583.
- (39) Campbell, M. K.; Farrell, S. O. Carbohydrates. In *Biochemistry*; Belmont CA 94002, USA, 2006; p pp 434.
- (40) Prelog, V. Chirality in Chemistry. *J. Mol. Catal.* **1976**, *1* (3), 159–172.
- (41) Flack, H, D. Chiral and Achiral Crystal Structures. *Helv. Chem. Acta* **2003**, *86*, 905–921.
- (42) Scott, R. L. Modification of the Phase Rule for Optical Enantiomers and Other Symmetric Systems. *J. Chem. Soc. Faraday Trans. 2 Mol. Chem. Phys.* **1977**, *73* (3), 356–360.
- (43) Jacques, J .; Collet, A.; Wilen, S. H. *Enantiomers, Racemates and Resolutions*, 3rd ed.; Kriger Pub. Co: Malabar Florida, USA, 1994.
- (44) Coquerel, G. Review on the Heterogeneous Equilibria between Condensed Phases in Binary Systems of Enantiomers. *Eur. PMC* **2000**, *5*, 481-98.
- (45) Lorenz, H.; Seidel-Morgenstern, A. Processes to Separate Enantiomers. *Angew. Chemie - Int. Ed.* **2014**, *53* (5), 1218–1250.

- (46) Sheldon, R. A. *Chirotechnology: Industrial Synthesis of Optically Active Compounds*; Marcel Dekker, Ed.; New York -USA, 1993.
- (47) Lyssenko, K. A.; Kostyanovsky, R. G.; Torbeev, V. Y.; Antipin, M. Y.; Kharybin, O. N. Lamellar Racemic Twinning as an Obstacle for the Resolution of Enantiomers by Crystallization: The Case of Me(All)N + (CH₂ Ph)Ph X - (X = Br, I) Salts . *J. Phys. Chem. B* **2003**, *107* (48), 13523–13531.
- (48) Tamura, R.; Fujimoto, D.; Lepp, Z.; Misaki, K.; Miura, H.; Takahashi, H.; Ushio, T.; Nakai, T.; Hirotsu, K. Mechanism of Preferential Enrichment, an Unusual Enantiomeric Resolution Phenomenon Caused by Polymorphic Transition during Crystallization of Mixed Crystals Composed of Two Enantiomers. *J. Am. Chem. Soc.* **2002**, *124* (44), 13139–13153.
- (49) Coquerel, G. Thermodynamic Predictions of Physical Properties - Prediction of Solid Solutions in Molecular Solutes Exhibiting Polymorphism. *Chem. Eng. Technol.* **2006**, *29* (2), 182–186.
- (50) Wacharine-Antar, S.; Levilain, G.; Dupray, V.; Coquerel, G. Resolution of (±)-Imeglimin-2,4-Dichlorophenylacetate Methanol Solvate by Preferential Crystallization. *Org. Process Res. Dev.* **2010**, *14* (6), 1358–1363.
- (51) Coquerel, G. Solubility of Chiral Species as Function of the Enantiomeric Excess. *J. Pharm. Pharmacol.* **2015**, *67* (6), 869–878.
- (52) Galland, A.; Dupray, V.; Berton, B.; Morin-Grognet, S.; Sanselme, M.; Atmani, H.; Coquerel, G. Spotting Conglomerates by Second Harmonic Generation. *Cryst. Growth Des.* **2009**, *9* (6), 2713–2718.
- (53) Dupray, V. Recrystallization of Enantiomers from Conglomerates. In *Recrystallization*; Sztwiertnia, P. K., Ed.; InTech, 2012.
- (54) Dalhus, B.; Görbitz, C. H. Non-Centrosymmetric Racemates: Space-Group Frequencies and Conformational Similarities between Crystallographically Independent Molecules. *Acta Crystallogr. Sect. B Struct. Sci.* **2000**, *56* (4), 715–719.
- (55) Fábíán, L.; Brock, C. P. A List of Organic Kryptoracemates. *Acta Crystallogr. Sect. B Struct. Sci.* **2010**, *66* (1), 94–103.
- (56) Brock, C. P.; Schweizer, W. B.; Dunitz, J. D. On the Validity of Wallach's Rule: On the Density and Stability of Racemic Crystals Compared with Their Chiral Counterparts. *J. Am. Chem. Soc.* **2001**, *113*, 9811–9820.
- (57) Brandel, C.; Petit, S.; Cartigny, Y.; Coquerel, G. Structural Aspects of Solid Solutions

- of Enantiomers. *Curr. Pharm. Des* **2016**, 22, 4929–4941.
- (58) Matsuura, T.; Koshima, H. Introduction to Chiral Crystallization of Achiral Organic Compounds: Spontaneous Generation of Chirality. *J. Photochem. Photobiol. C Photochem. Rev.* **2005**, 6 (1), 7–24.
- (59) Beesley, T, E and Scott, R, P, W. *Chiral Chromatography*; John Wiley & Sons Inc: New York, USA, 1999.
- (60) Andersson, S and Allenmark, S, G. Preparative Chiral Chromatographic Resolution of Enantiomers in Drug Discovery. *J. Biochem. Biophys. Methods* **2002**, 54 (1–3), 11–23.
- (61) Kaspereit, M. Separation of Enantiomers by a Process Combination of Chromatography and Crystallization, OVG Magdurg, 2006.
- (62) Collet, A.; Brienne, M. J.; Jacques, J. Optical Resolution by Direct Crystallization of Enantiomer Mixtures. *Chem. Rev.* **1980**, 80 (3), 215–230.
- (63) Coquerel, G. Topic in Current Chemistry. In *Novel Optical Resolution Technologies*; Springer GmbH: Berlin, Heidelberg, 2006; Vol. 269, pp 1–51.
- (64) Havinga, E. Spontaneous Formation of Optically Active Substances. *BBA - Biochim. Biophys. Acta* **1954**, 13 (C), 171–174.
- (65) Viedma, C. Chiral Symmetry Breaking during Crystallization: Complete Chiral Purity Induced by Nonlinear Autocatalysis and Recycling. *Phys. Rev. Lett.* **2005**, 94 (6), 3–6.
- (66) Kaptein, B .; Noorduyn, W. L.; Meekes, H.; Van Enckevort, W. J. P.; Kellogg, R. M.; Vlieg, E. Attrition-Enhanced Deracemization of an Amino Acid Derivative That Forms an Epitaxial Racemic Conglomerate. *Angew. Chemie - Int. Ed.* **2008**, 47 (38), 7226–7229.
- (67) Noorduyn, W, L. et al. Emergence of a Single Solid Chiral State from a Nearly Racemic Amino Acid Derivative. *J. Am. Chem. Soc.* **2008**, 130, 1158–1159.
- (68) Belletti, G.; Meekes, H.; Rutjes, F. P. J. T.; Vlieg, E. Role of Additives during Deracemization Using Temperature Cycling. *Cryst. Growth Des.* **2018**, 18, 6617–6620.
- (69) Breveglieri, F.; Maggioni, G. M.; Mazzotti, M. Deracemization of NMPA via Temperature Cycles. *Cryst. Growth Des.* **2018**, 18 (3), 1873–1881.
- (70) Oketani, R.; Hoquante, M.; Brandel, C.; Cardinael, P.; Coquerel, G. Practical Role of Racemization Rates in Deracemization Kinetics and Process Productivities. *Cryst. Growth Des.* **2018**, 18 (11), 6417–6420.
- (71) Leeman, M. Resolutions of Racemates by Crystallization Additives and Attrition, University of Groningen, University of Groningen, 2009.

- (72) He, G. S.; Cui, Y.; Bhawalkar, J. D.; Prasad, P. N.; Bhawalkar, D. D. Intracavity Upconversion Lasing within a Q-Switched Nd:YAG Laser. *Opt. Commun.* **1997**, *133* (1–6), 175–179.
- (73) Franken, P. A.; Ward, J. F. Optical Harmonics and Nonlinear Phenomena. *Rev. Mod. Phys.* **1963**, *35* (1), 23–39.
- (74) Kurtz, S. K.; Perry, T. T. A Powder Technique for the Evaluation of Nonlinear Optical Materials. *J. Appl. Phys.* **1968**, *39* (8), 3798–3813.
- (75) Shen, Y. R. *The Principles of Nonlinear Optics*; Wiley- Interscience: New York, USA, 1984.
- (76) Williams, D. J. Organic Polymeric and Non-Polymeric Materials with Large Optical Nonlinearities. *Angew. Chemie Int. Ed. English* **1984**, *23* (9), 690–703.
- (77) Caroline, M. L.; Sankar, R.; Indirani, R. M.; Vasudevan, S. Growth, Optical, Thermal and Dielectric Studies of an Amino Acid Organic Nonlinear Optical Material: L-Alanine. *Mater. Chem. Phys.* **2009**, *114* (1), 490–494.
- (78) Dimitriev V, G. *Handbook of Nonlinear Optical Crystals*; Springer: Berlin, Heidelberg, Germany, 1999.
- (79) Nalwa, H. S.; Miyata, S. *Nonlinear Optics of Organic Molecules and Polymers*; CRC Press. Inc.: New York, USA, 1997.
- (80) Manley, J. M.; Rowe, H. E. Nonlinear Elements- General Energy Relations *. *Proc. IRE* **1954**, 904–913.
- (81) Franken, P. A.; Hill, A. E.; Peters, C. W.; Weinreich, G. Generation of Optical Harmonics. *Phys. Rev. Lett.* **1961**, *7* (4), 118–119.
- (82) Nye, J. F. *Physical Properties of Crystals: Their Representation by Tensors and Matrices*; Clarendon Press: Great Britain, 1985.
- (83) Kleinman, D. A. Theory of Second Harmonic Generation of Light. *Phys. Rev.* **1962**, *128* (4), 1761–1775.
- (84) Sauter, E. G. *Nonlinear Optics*; John Wiley & Sons, Inc.: New York, USA, 1996.
- (85) Boyd, R. W. *Nonlinear Optics*; Academic Press: San Diego, USA, 2003.
- (86) Rottwitt K and Tidemand-Lichtenberg P. *Nonlinear Optics. Principles and Applications*; CRC Press. Inc.: Finland, 2015.
- (87) Clevers, S. Prototyping of In-Situ Optical Methods to Characterize Organic Molecular Crystals, University of Rouen-France, 2014.
- (88) Wortmann, R.; Krämer, P.; Glania, C.; Lebus, S.; Detzer, N. Deviations from Kleinman

- Symmetry of the Second-Order Polarizability Tensor in Molecules with Low-Lying Perpendicular Electronic Bands. *Chem. Phys.* **1993**, *173* (1), 99–108.
- (89) Hubbard, S. F.; Petschek, R. G.; Singer, K. D.; DSidocky, N.; Hudson, C.; Chien, L. C.; Henderson, C. C.; Cahill, P. A. Measurements of Kleinman-Disallowed Hyperpolarizability in Conjugated Chiral Molecules. *J. Opt. Soc. Am. B* **1998**, *15* (1), 289.
- (90) Dailey, C. A.; Burke, B. J.; Simpson, G. J. The General Failure of Kleinman Symmetry in Practical Nonlinear Optical Applications. *Chem. Phys. Lett.* **2004**, *390* (1–3), 8–13.
- (91) Zhao, H. J.; Zhang, Y. F.; Chen, L. Strong Kleinman-Forbidden Second Harmonic Generation in Chiral Sulfide: La₄InSbS₉. *J. Am. Chem. Soc.* **2012**, *134* (4), 1993–1995.
- (92) Rentzepis, P. M.; Giordmaine, J. A.; Wecht, K. W. Coherent Optical Mixing in Optically Active Liquids. *Phys. Rev. Lett.* **1966**, *16* (18), 792–794.
- (93) Andrews, D. L.; Allcock, P.; Demidov, A. A. Theory of Second Harmonic Generation in Randomly Oriented Species. *Chem. Phys.* **1995**, *190* (1), 1–9.
- (94) Yuan, L. Second Harmonic Generation as a Complementary Technique for Characterization of Powdered Organics, University of Rouen-Normandie, 2018.
- (95) Fan, Y. X.; Eckardt, R. C.; Byer, R. L.; Route, R. K.; Feigelson, R. S. AgGaS₂infrared Parametric Oscillator. *Appl. Phys. Lett.* **1984**, *45* (4), 313–315.
- (96) F Zernike, J. E. M. *Applied Nonlinear Optics*; Wiley: New York, USA, 1973.
- (97) Yuan, L.; Clevers, S.; Couvrat, N.; Cartigny, Y.; Dupray, V.; Coquerel, G. Precise Urea/Water Eutectic Composition by Temperature-Resolved Second Harmonic Generation. *Chem. Eng. Technol.* **2016**, *39* (7), 1326–1332.
- (98) Monaco, S. B.; Davis, L. E.; Velsko, S. P.; Wang, F. T.; Eimerl, D. Synthesis and Characterization of Chemical Analogs of L-Arginine Phosphate. *J. Cryst. Growth* **1987**, *85*, 252–255.
- (99) Haja Hameed, A. S.; Anandan, P.; Jayavel, R.; Ramasamy, P.; Ravi, G. Synthesis, Growth and Characterization of Nonlinear Optical Material: L-Arginine Fluoride. *J. Cryst. Growth* **2003**, *249* (1–2), 316–320.
- (100) Warren, L. F. New Development in Semi-Organic Nonlinear Optical Crystals in Electronic Materials. *Proc. 4th Inter. SAMPE Electron. Conf.* **1990**, *4*, 388.
- (101) Sun, H. Q.; Wang, X. Q.; Cheng, X. F.; Gong, C. R.; Zhou, M.; Xu, H. Y.; Wei, X. C.; Luan, C. N.; Pan, D. Y.; Li, Z. F.; Shi, X. Z. A Novel Metal-Organic Coordination Complex Crystal: Tri-Allylthiourea Zinc Chloride (ATZC). *Cryst. Res. Technol.* **2005**,

- 40 (9), 882–886.
- (102) Shadrivov, I. V. Nonlinear Guided Waves and Symmetry Breaking in Left-Handed Waveguides. *Photonics Nanostructures - Fundam. Appl.* **2004**, 2 (3), 175–180.
- (103) Chemla, D, S. *Nonlinear Optical Properties of Organic Molecules and Crystals*; Academic Press Inc.: London, UK, 2012.
- (104) Kaino, T.; Tomaru, S. Organic Materials for Nonlinear Optics . *J. Adv. Mater.* **1993**, 5 (3), 172–178.

**CHAPTER 2: DEVELOPMENT OF *IN SITU* SHG SET-UP AND ITS
APPLICABILITY FOR CHIRAL COMPOUNDS**

PART 1 : INTRODUCTION

In the framework of the chiral resolution by crystallization and the screening of conglomerates, DSC and XRPD analyses are commonly used to characterize the compounds of interest for the SMS laboratory and its industrial partners. However, these techniques suffer some limitations (notably a low detection threshold) and need the availability of both racemic mixture and pure enantiomer to characterize the racemic species.

One decade ago, the SMS laboratory has developed a sensitive characterization technique based on the nonlinear optical phenomenon of SHG to differentiate non-centrosymmetric crystals from centrosymmetric crystals¹. Several conglomerates have already been spotted using this second harmonic generation (SHG) technique¹⁻³ which requires only the racemic mixture. However, the experimental set-up developed by the laboratory only allowed the screening of dry solid forms. It is a limiting factor as interesting conglomerates may exist only in equilibrium with their mother liquor (because of one or several of the following reasons: non-congruent solubility, solvates with an efflorescent character, solvates that are hydrolyzed by moistures, CO₂ sensitive solid, etc.)⁴. Thus, the improvement of the SHG set-up has to be pursued to analyze the solid phases in suspension and in equilibrium with their mother liquor.

SHG was already used to follow *in situ* the crystallization of a non-centrosymmetric crystal from a supersaturated solution⁵⁻⁷ (to measure the induction time of non-centrosymmetric crystal systems; with the difficulty to regulate the experimental conditions due to the use of capillaries) and the temperature-resolved SHG was used to probe the structural purity and to tackle the structural purification of organic products⁸.

In this chapter, after recalling the principle of the conglomerate prescreening by SHG, we will present the work performed to design the new *in situ* set-up that allows us to track the crystallization of non-centrosymmetric crystals at an early stage by combining the SHG technique with a batch cooling crystallizer. The *in situ* SHG technique is further used for the monitoring of solid-solid phase transitions providing one of the two varieties crystallizes in a non-centrosymmetric space group. The advantages and limitations of the techniques are discussed.

PART 2: PRINCIPLE OF SCREENING OF CONGLOMERATE FORMING SYSTEM BY SHG

To achieve an efficient separation of a racemic mixture by direct crystallization, chiral discrimination in the solid state must be complete (e.g. the racemic mixture has to crystallize as a stable conglomerate). Jacques, Eliel and Wilen (1994)⁹ have described in detail the concept of enantiomers, racemic compounds and their resolutions. As said before only 5 to 10% of the enantiomer pairs crystallize as conglomerates¹⁰. When the compound of interest does not crystallize itself as a conglomerate, a screen of conglomerate derivatives is necessary³. This screening for conglomerate forming system is usually performed by numerous attempts to crystallize salts (if the molecule bears acidic or basic moiety), co-crystals and/or solvates.

Various methods can be used to spot conglomerates during the screening. The main techniques are described as follows.

2.1. CLASSICAL TECHNIQUES

2.1.1. Comparison of spectroscopic data

The techniques are mainly X-Ray Powder Diffraction (XRPD), Solid-State Nuclear Magnetic Resonance (SS-NMR), Infra-Red (IR), Near Infra-Red (NIR) and Raman spectroscopies. These analyses require that both: the pure enantiomer and the racemic mixture must be accessible. The comparison of spectroscopic data between the pure enantiomer and racemic mixture provides information about the nature of the racemic mixture. These methods are practically the most reliable used techniques. However, a complete solid solution (in which there is a single solid phase, *i.e.* a single crystal packing) can be mistaken with a conglomerate as its crystal packing is only slightly modified by the substitution of an enantiomer by the other¹¹. Comparing spectroscopic data of the racemic mixture and enantiomer can thus sometimes be difficult or misleading³.

2.1.2. Thermal behaviour analyses

Differential Scanning Calorimetry (DSC) is also a reliable analytical method to spot 'ideal' conglomerates. If the melting point difference between the pure enantiomer and racemic mixture is in the range 20-35 °C, a conglomerate might be expected¹⁰. The melting point of the pure enantiomer should be higher than the conglomerate. If the melting point of the racemic mixture is higher than that of the pure enantiomer, a racemic compound is *a priori* expected. However, this characterization technique is hardly applicable to conglomerate solvates and thermally unstable compounds.

2.1.3. Solubility data

From the solubility studies, a conglomerate forming system can be predicted. The method consists in slurring crystals with ca. 5% of enantiomeric excess in a minimum volume of an appropriate solvent. The resulting optical purity will give 0% of enantiomeric excess (at the eutectic composition) for a conglomerate while the eutectics of racemic compounds will always be higher than 0% of enantiomeric excess¹².

2.2. SECOND HARMONIC GENERATION (SHG) TECHNIQUE

To assess organic crystalline materials, non-linear techniques particularly second harmonic generation (SHG) deserve attention because of its efficiency and reliability in characterization. Second harmonic generation allows to quickly (within seconds) short out non-centrosymmetric phases and centrosymmetric phases.

2.2.1 Principle of SHG pre-screening

In conglomerates, molecules compulsory organize in chiral crystalline structures (thus non-centrosymmetric). Conversely, racemic compounds are prone to adopt centrosymmetric crystalline structures. Consequently, a method that detects the absence of inversion of symmetry in crystals obtained from racemic mixtures will be able in most cases to detect conglomerates. This is the case of SHG as described in Chapter 1, Part 5.

2.2.2. Experimental Powder-SHG set-up

When a high-power laser (in our experimental set-up a Q-switched pulsed laser with a wavelength of 1064 nm which delivers 300 mJ pulses of 5 ns duration) interacts with a non-centrosymmetric material, it gives rise to a new wave at half of the fundamental wavelength (i.e. 532 nm) (Figure 2.1). This nonlinear optical process is called Second Harmonic Generation and is observable only for non-centrosymmetric crystals.

To spot conglomerate, the SHG signal generated by the crystalline powder samples placed in wells (diffused light) is collected into an optical fibre (0.5 nm of core diameter), directed onto the entrance slit of a spectrometer (Ocean Optics) and recorded through the boxcar integrator. The typical time duration of communication with the detector is circa in the order of milliseconds. The laser sends pulses at a frequency of 10 Hz (i.e. one pulse every 100 ms) and is relatively stable in energy (energy fluctuation ranging typically between 1-3% depending on the incident intensity). The energy fluctuations of the incident beam are determined thanks to a detector placed behind the mirror and that allows the detection of a small part (0.06%) of the incident beam intensity¹³. The SHG intensity depends on the square of the fundamental

(incident) beam intensity but only one part of the total SHG signal emitted by the sample is collected by the optical fibre.

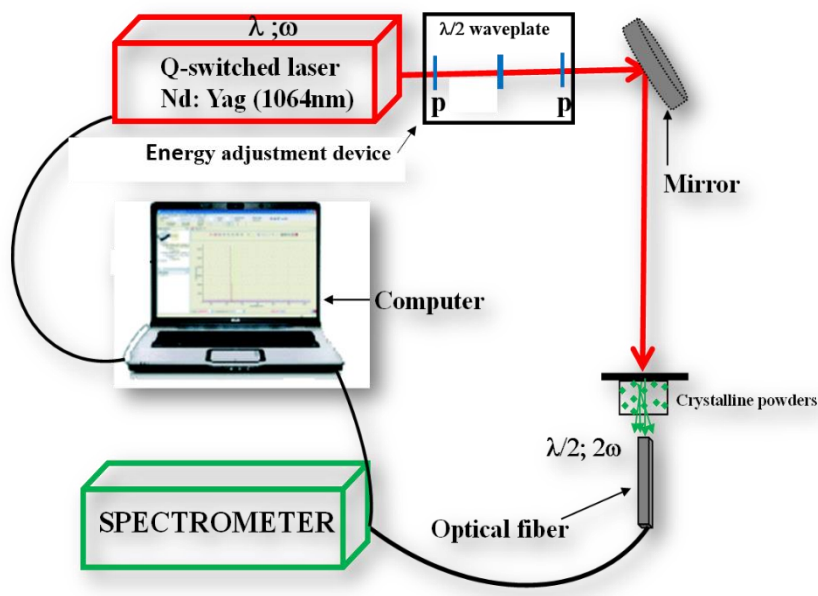


Figure 2.1: Principle of Second Harmonic Generation (SHG, powder set-up)

2.2.3. SHG responses

Evaluation of the nature of a racemic mixture, conglomerate or not by using SHG, requires a small quantity only of the racemic mixture (a few mg typically). The advantage of this technique compared to classical techniques is that comparison between the SHG response of the racemic mixture and the pure enantiomer is not needed. Therefore, the conglomerate screening can be undertaken even when the pure enantiomer is not available or when the particles are too small for direct tests (single crystal not available). Spotting conglomerates by SHG technique avoids waste of time and materials even though the method exhibits some drawbacks.

The SHG spectrum for the α -quartz (reference sample) and the SHG response for chiral organic materials are represented in Figure 2.2. The intensity signal of the racemic sample is usually normalized with the intensity of the reference sample (α -quartz, 45 μm average sizes). SHG signal is considered as negligible (negative response) when its intensity is less than 1% of the signal of the reference sample. Furthermore, it is important to note that the intensity of the SHG signal is quadratic to the initial SHG light. So, the uncertainty of the SHG signal was estimated at ca. 9% due the deviation of the initial laser beam¹⁴.

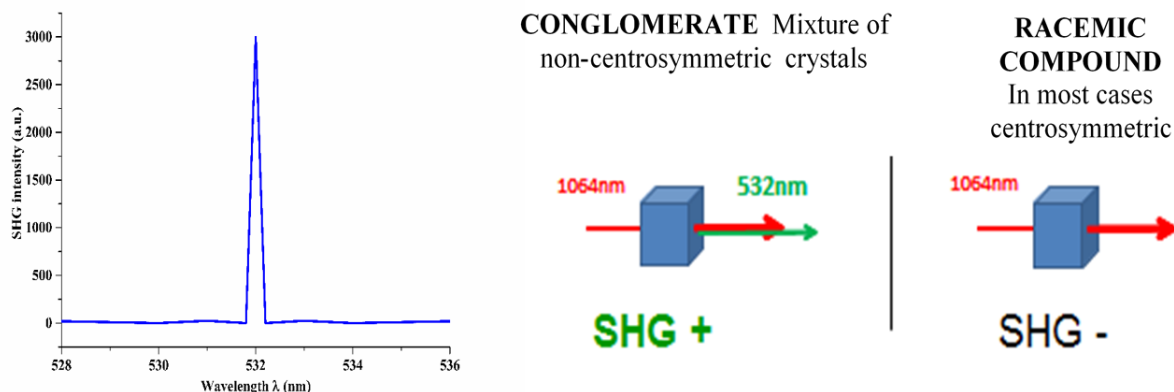


Figure 2.2: SHG spectrum for the α -quartz (reference sample) (left) and schematic SHG response for chiral organic compounds (right)

However, SHG technique displays two major disadvantages. These are mainly related to the properties of the second order tensor $\chi^{(2)}$ of the NLO material:

- (i) A non-detected SHG positive racemic mixtures can be due to:
 - A $\chi^{(2)}$ parameter that is too small (i.e. a low hyperpolarizability of the molecule);
 - Absorption at the wavelength of irradiation (e.g. 1064 nm) or at the wavelength of the re-emitted radiation (e.g. 532 nm);
 - Amorphous sample.
- (ii) False-negative: A non-active SHG space group. Indeed, some chiral space groups are SHG inactive¹⁵ (those related to point groups 422, 622 and 432).

However, these highly symmetrical groups are poorly represented among organic materials.

False-positive response can occur:

- For racemic compounds crystallizing in a non-centrosymmetric space group, e.g. $Pca2_1$ (not frequent);
- For racemic compounds crystallizing in a chiral space group, e.g. $P2_1$ (rare kryptoracemic compounds);
- If the sample is composed of too fine particles.

SHG can also be an alternative technique to assign the space group of chiral organic molecules because of the number of wrong structures in the CSD estimated at circa 3% of published crystal structures¹⁶. The presence or not of an inversion centre is usually a source of error for a correct crystal structure resolution (dilemma between centrosymmetric or non-centrosymmetric space group).

2.2.4. Detection of SHG signal in suspension (*in situ*)

The conglomerate occurrence is only 5-10% of organic compounds. The latter proportion corresponds to stable conglomerates which are mostly stable under ambient conditions. We know that interesting non-centrosymmetric crystals may exist only in equilibrium with their mother liquor because of their efflorescent and non-congruent characters⁴. Only a few works deal with search of solvates at low temperature which could increase the number of conglomerates. Therefore, the development of the SHG technique for suspended samples is necessitated to highlight such chiral organic materials. The development of this new configuration of the SHG is the subject of the following paragraph of this manuscript.

PART 3: FEASIBILITY STUDY

The SHG technique can suffer from limitations in term of detection threshold due to absorption and/or scattering of the fundamental and second harmonic beams by the liquid and the amount of the crystalline phase in the liquid phase (suspensions). In order to establish the possibility to design a new SHG set-up, preliminary tests have been carried out using the crystalline α -quartz in suspension in various solvents.

3.1. DETECTION OF SHG SIGNAL FOR NON-CENTROSYMMETRIC CRYSTALS IN SUSPENSION

3.1.1. Choice of α -quartz as a reference

The crystalline structure of α -quartz is non-centrosymmetric. It is the first crystal in which the SHG activity was observed by Franken¹⁷. That is why, often in the literature, nonlinear optical surveys compare the values of the SHG signal given by the compound of interest with the SHG given by the α -quartz¹⁸. This standard material generates a relatively moderated SHG signal compared to other nonlinear optical (NLO) compounds¹⁹. Consequently, the α -quartz is a good candidate to test the detection threshold and the reliability of the new SHG set-up²⁰. This aspect is developed in the following through several tests in order to define the parameters of the measurement. We established that the crystalline α -quartz (reference sample) has a particle size distribution centred on an average value of ca. 45 μm (by laser granulometry measurements).

3.1.2. Preliminary tests

Experiments were conducted using the classical powder-SHG set-up (Figure 2.1). It consists of weighing certain amounts of α -quartz in vials, filed with 2 ml of selected solvents and placed in wells. The SHG signal of α -quartz [50 and 100 mg] in 2 ml volume scale of the chosen solvent were prepared and the ratio between the SHG intensity of the α -quartz with and without solvent is reported in Table 2.1.

Table 2.1: Ratio of the SHG intensity^a of crystalline α -quartz with and without solvent

Mass of α -quartz (mg)	Solvent	I _{ref} (quartz) (counts)	I (quartz + solvent) (counts)	I / I _{ref} (%)
50	water	1474	270	18.3
	ethanol	1411	198	14.0
	chloroform	1430	142	9.9
	toluene	1472	41	2.8
100	Water	1823	461	25.2
	ethanol	1812	351	19.4
	chloroform	1841	164	8.9
	toluene	1811	92	5.1

^aI_{ref}: the intensity of the reference sample; I intensity

The SHG activity of the crystalline α -quartz with and without solvent recorded shows that the intensity of the signal varies depending (obviously) on the amount of crystalline phase and the volume of the solvent but also on the nature of the solvent (e.g. refractive index and absorption coefficient).

These first examples provide an overview of the efficiency of the SHG signal when we are tracking non-centrosymmetric crystals in suspension. The experimental tests illustrate the possibility to detect SHG activity of a non-centrosymmetric crystal in equilibrium with its mother liquor even though the collected SHG signal can decrease down to 90% of the SHG intensity from dry powder samples. Moreover, a certain variability of the SHG activity can be observed if the medium of crystallization changes (nature and/or volume of solvent).

3.2. SHG INTENSITY DEPENDENCIES

3.3.1. Influence of the amount of crystalline phase

The influence of the amount of crystalline phase on the SHG intensity was illustrated using the following approaches.

Experience was conducted in the same volume scale of 2 ml of different solvents for different amounts of crystalline α -quartz [20; 50; 100 mg] in a vial. The results summarized in Figure 2.3 showed that the SHG intensity increases by increasing the amount of crystalline phase in the suspension. The test highlighted the dependence of the SHG signal on the amount of crystalline phase in the suspension for a same volume but also on the solvent nature (refractive index and absorption coefficient) since the evolution of the intensity of the SHG signal with the mass of the crystalline compound is clearly different for different solvents.

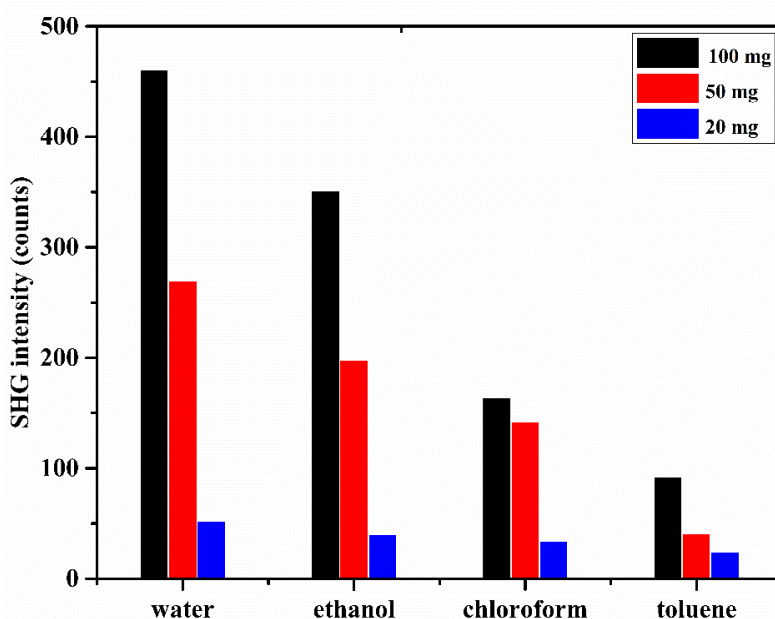


Figure 2.3: Influence of the amount of crystalline α -quartz in suspension (2 ml scale) on the SHG signal

3.3.2. Influence of the nature of solvent

Solvents can be classified by their refractive index and absorption coefficient when light passes through them. By measuring the SHG signal generated by a non-centrosymmetric material in equilibrium with its mother liquor, the nature of the solvent particularly the absorption coefficient of the liquid at the fundamental and daughter wavelengths should be taken into account.

Since crystalline α -quartz is a birefringent material i.e. having two refractive indexes at each wavelength ($\lambda = 1064$ nm and at $\lambda = 532$ nm). For $\lambda = 1064$ nm, the refractive index of the ordinary ray is 1.5469 and 1.5561 for the extraordinary ray. For $\lambda = 532$ nm, the refractive index of the ordinary ray is 1.5341 and 1.5429 for the extraordinary ray.

However, for the following, we consider the ratio of refractive indexes between those of crystalline α -quartz and those of the chosen solvent. For the crystalline α -quartz, the mean refractive index value ($n_{\text{ref}} = 1.5385$) at $\lambda = 532$ nm is taken between the ordinary ray and extraordinary ray. For those of the selected solvents (water, ethanol, chloroform and toluene), their values were taken at the second harmonic wavelength as given in the refractive index database.

Herein, we just focused on the influence of the refractive index and absorption coefficient of the solvents at $\lambda = 532$ nm (Second harmonic wavelength) on the SHG effect generated by the crystalline phase in suspension. The suspension is composed for a first experiment of a mass of 20 mg of α -quartz + 2 ml of solvent and for a second experiment of 100 mg of α -quartz + 2 ml of solvent in different vials. For each prepared vial, the SHG intensity is recorded.

3.3.2.1. Refractive index

The influence of the refractive index of the chosen solvent at $\lambda = 532$ nm on the SHG signal of the crystalline α -quartz is reported as given in Figure 2.4.

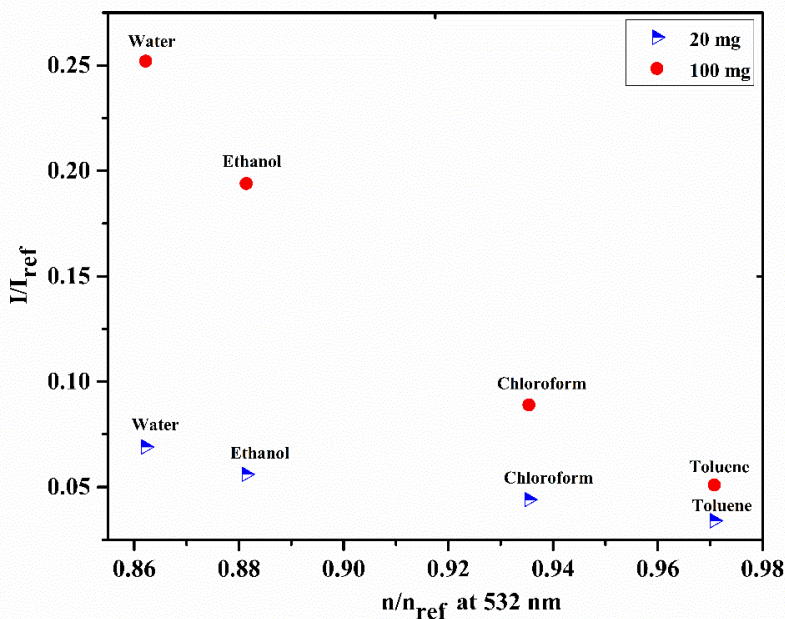


Figure 2.4: Influence of the refractive index of the solvent at 532 nm on the SHG signal of the crystalline α -quartz in suspension (refractive index data collected from Refractive index database).

Results show that the refractive index of the solvent should not be too close to those of the solid phase i.e. when the refractive index of the solvent is approached those of the crystalline α -quartz, the SHG response of the material in suspension decreases. Thus, in this particular case, water should be preferred than other solvents to collect a maximum SHG signal of the α -quartz in suspension.

3.3.2.2. Absorption coefficient

For the same experiments, the influence of the absorption coefficient is also highlighted. The results of the SHG intensity versus the absorption coefficient (data from the Refractive index database) of the solvent is reported in Figure 2.5.

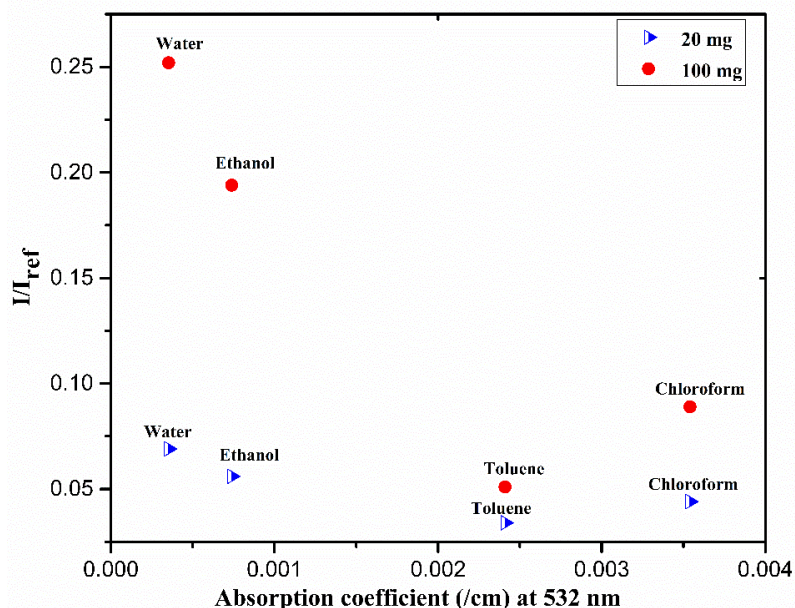


Figure 2.5: Influence of the absorption coefficient of the solvent at 532 nm on the SHG signal of the crystalline α -quartz in suspension (absorption coefficient data collected from Refractive index database).

The higher, the solvent absorption coefficient, the lower the SHG intensity collected except in the case of chloroform in this study. This discrepancy might be due to its high viscosity. Indeed, the solid phase was stagnated in the bottom (detection window) even though the vial was agitated, thus a more significant SHG signal was collected despite its high absorption coefficient at 532 nm) compared to the other suspensions. It is better to choose a solvent with having a small absorption coefficient at 532 nm to monitor the crystallization by *in situ* SHG.

3.3. CONCLUSION OF THE FEASIBILITY STUDY

The SHG activity of a non-centrosymmetric crystal in suspension is difficult to evaluate. Indeed, besides the volume and nature of the solvent, the intensity of the SHG signal depends on various parameters such as the particle size, crystallinity of the sample, phase matchability (SHG signal increases with respect to the crystal size) of the crystals, density...

Nevertheless, this preliminary study gave interesting indications that turned out to be useful for the design of the new set-up.

Indeed, the experimental results obtained with the reference (quartz) showed that:

- The SHG signal intensity increases with the amount of crystalline solid phase in suspension.
- The volume of liquid phase should be as small as possible.
- The refractive index of the liquid should not be too close to the one of the solid phases.
- The absorption coefficient of the liquid phase at the working wavelengths (1064 nm and 532 nm) should be moderated.

- The viscosity of the liquid phase should not be too high because it can prevent the sedimentation of the sample close to the optical window and thus limit the detection of the SHG signal.

In conclusion, even though the SHG activity of a non-centrosymmetric crystal in suspension decreases drastically compared to the signal from the dried powder, crystals in suspension can still give measurable SHG signal. Thus, spotting non-centrosymmetric crystals in suspension seems feasible with an *in situ* SHG set-up.

PART 4: EXPERIMENTAL SHG SET-UP FOR *IN SITU* MEASUREMENTS

4.1. DESCRIPTION OF THE SET-UP AND PRINCIPLE OF THE MEASUREMENTS

After the period devoted to the choice, the manufacturing and/or the acquisition of the adequate equipment, the implementation of the set-up was achieved. SHG technique combined (connected) with a batch cooling crystallizer was named *in situ* SHG technique. We can recall that the main motivation is to track conglomerate forming-systems in equilibrium with their mother liquor and to follow the phase change between centrosymmetric and non-centrosymmetric phases or vice-versa. The schematic representation of the *in situ* SHG set-up is displayed in Figure 2.6. A picture of the experimental SHG set-up is shown in Appendix II, Figure A. II- 1.

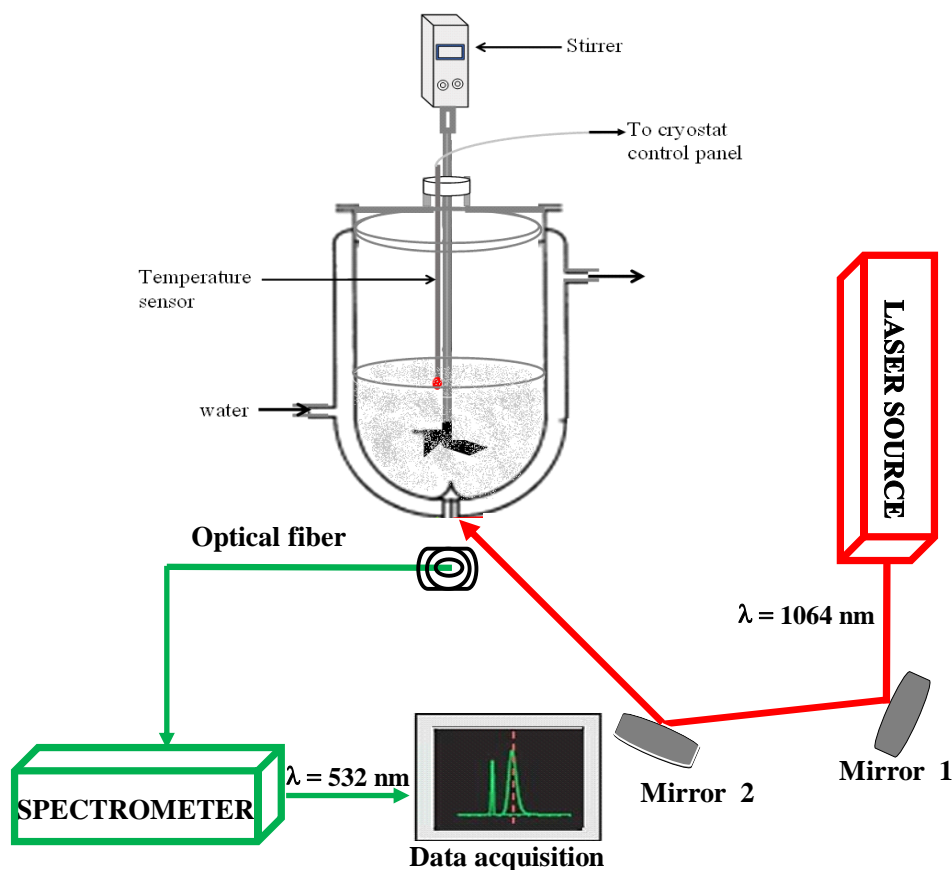


Figure 2.6: Schematic view of SHG set-up equipped with a batch cooling crystallizer: *in situ* SHG

The batch cooling crystallization operations are carried out in a double jacketed reactor of a volume of ca. 200 ml with a speed-controlled mechanical stirrer. The dedicated reactor is designed with a thin bottom to enable the optical fiber to collect the generated SHG signal. The reactor is placed in a cryo-thermostatic bath and the temperature inside the reactor is controlled using an internal Pt100 probe. A NL300 series laser is used as the laser source with

characteristics similar to the one used in the conventional set-up (Q-switched pulsed laser operating at 1064 nm and delivering 300 mJ of 6 ns duration). Measurements are performed in reflection geometry, i.e., the backward SHG signal at 532 nm (green light) generated by the non-centrosymmetric crystal in suspension is collected into an optical fiber (0.5 nm of core diameter), directed onto the entrance slit of a spectrometer (Ocean Optics) and recorded through the boxcar integrator. The generated new light is scattered in all directions and only a fraction of the emitted light passing through the cone of the optical fibre is detected. Nevertheless, the recorded SHG signal is high enough to indicate the presence or absence of non-centrosymmetric crystals in the mother liquor. The intrinsic sensitivity of SHG to symmetry properties and molecular orientation makes it well-suited for tracking the possible rearrangements arising as crystallization progresses. *In situ* SHG provides a sensitive mean to detect crystal formation at early stages for crystals containing a non-centrosymmetric unit cell.

The software Oceanview is used to collect the detected SHG signal. It gives a plot of the SHG signal intensity versus the wavelength. The mean SHG intensity is first expressed in counts then in percentage by normalizing it to the maximum SHG intensity generated from the dried solid phase.

4.2. SELECTION OF CRYSTALLIZATION SYSTEMS

The challenge is to monitor crystal formation at the earliest possible stages for crystal systems that could serve as an alert and be useful in tracking non-centrosymmetric crystals (e.g. metastable conglomerates). The *in situ* SHG technique seems to allow quantification of the SHG activity of crystalline materials in equilibrium with their mother liquor in the limit detection of 10% of the intensity from the dried powder sample.

We have first selected the crystallization of potassium dihydrogen phosphate (KDP, SHG efficiency material) before extending to the crystallization of organic crystal systems.

PART 5: CRYSTALLIZATION OF POTASSIUM DIHYDROGEN PHOSPHATE (KDP) MONITORED BY *IN SITU* SHG

5.1. REASONS OF THE CHOICE

Potassium dihydrogen phosphate has been proven to be a nonlinear efficient material over the years^{21,22}. Several nonlinear techniques (Ruby or Q-Switched laser) and associated methods (dispersion effects, mixing of light beams in crystals, etc.)^{23,24} have been tested using KDP.

Additionally, the KDP is easily available and its crystallization from water is easy and fast. One can also obtain large particle size which is interesting as KDP is a phase matching material, SHG intensity increases with particle size.

All these benefits suggest that KDP is a good candidate to ensure that the *in situ* SHG set-up is operating accurately.

5.2. EXPERIMENTAL CONDITIONS

A supersaturation slightly greater than one is usually enough to induce a crystallization²⁵. Four different supersaturated solutions of KDP; solid form purchased from Sigma Aldrich ($\beta = 1.03$; 1.04; 1.05 and 1.07) were prepared in purified water at 20 °C (the solubility of KDP in water at 20 °C is 18.93 wt%).

For each performed run the solution was cooled down from 20 °C to 0 °C at the cooling rate 1K min⁻¹ to create a highly supersaturated solution and induce the crystallization of KDP at 0°C within few minutes.

The SHG data are collected every 2 minutes starting from 0 to 60 min (the time zero being taken when the cooling from 20 °C to 0 °C started -see Figure 2.7-), thus enabling to follow the crystallization of KDP inside the reactor during the cooling to 0 °C and subsequent isotherm at this temperature.

5.3. RESULTS AND DISCUSSION

The variation of the SHG intensity over time for the four slightly supersaturated solution ratios is reported in Figure 2.7. The SHG intensity of KDP in suspension was normalized to the SHG intensity of KDP in powder.

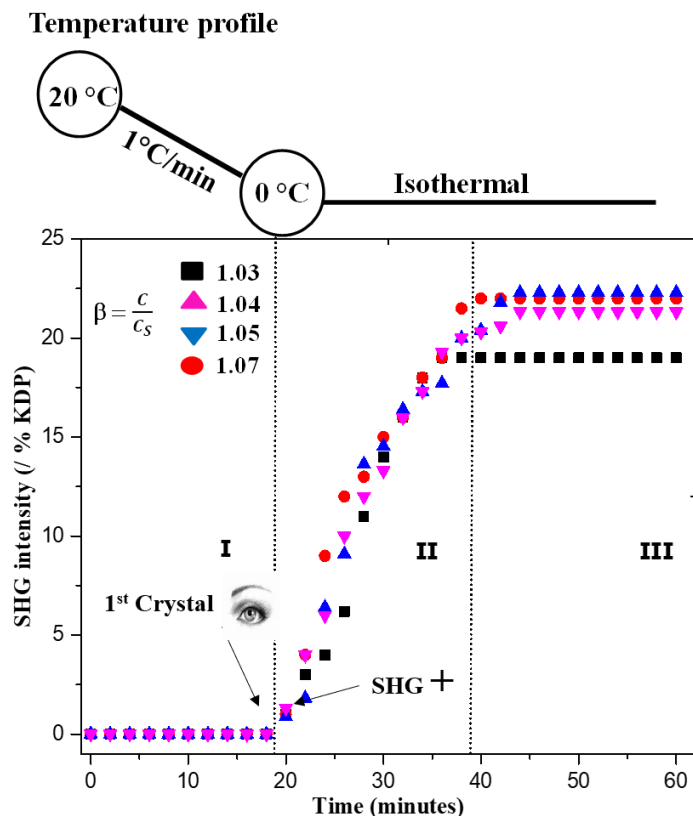


Figure 2.7: Crystallization of potassium dihydrogen phosphate for different supersaturated solution ratios monitored by *in situ* SHG technique. The SHG intensities are normalized by using KDP in powder

The results show that each performed run can be divided into three domains depending on the recorded SHG intensity starting from zero (no nuclei) to ca. 23% of the maximum SHG intensity of KDP (powder).

Domain I (no SHG signal detected) corresponds to the supersaturated solution: the system goes from slightly supersaturated (at 0 minute) to highly supersaturated solution (at ca. 18 minutes) while the system is cooled down. The first crystals appeared (detectable by eye) at ca. 19 minutes but due to SHG signal crystal size dependence, the SHG signal was not detectable. Crystal sizes of average value of [45-100 μm] seem necessary to generate a SHG signal detectable by the set-up by referring to the average particle size in the case of α -quartz.

Domain II (SHG signal is positive and sharply increases): Nucleation has already occurred, the crystal growth started after ca. 20 minutes and the number and size of particles increase while the crystallization progresses, inducing the increase of the SHG intensity. The temperature of the batch is stabilized; the crystal growth reaches its maximum rate. KDP crystals in suspension generate their highest SHG activity combining particle size and amount of KDP in suspension.

Domain III (SHG signal maximum and constant): No additional crystal growth, the SHG signal is at its maximum intensity and the system returns to the equilibrium. Thus, the experiment can be ended because there is no more variation on the SHG signal.

The experimental data obtained from the crystallization of KDP confirm the preliminary results obtained from crystalline α -quartz in suspension. The results are consistent with Lecaptain⁵ data for the measurement of the induction time of KDP crystallization using SHG technique. In our work, we use the same principle of SHG technique as Lecaptain to test the KDP efficiency for *in situ* SHG monitoring. The only difference between those studies is in the experimental conditions (shape of the reactor, temperature control, supersaturation ratio, volume scale etc.). The study gives a good indication on the possibility to track non-centrosymmetric organic crystals in solution as shown earlier by Lecaptain for α -lactose.

5.4. CONCLUSION AND POSSIBILITY TO EXTEND TO CHIRAL ORGANIC SYSTEMS

The reliability of the experimental *in situ* SHG set-up was tested by using inorganic materials (Quartz and KDP) which are efficient for SHG generation. The results highlighted the possibility of SHG technique to be used to track non-centrosymmetric crystals in their mother liquor. To extend the possibility of the set-up, the test is exemplified through the case studies of some organic salts crystallizing as polymorphs.

In situ monitoring of the time evolution of a reaction has become a standard tool in controlling crystal morphology and crystal size distribution, particularly in the pharmaceutical industry. In our work, the *in situ* SHG monitoring can give a rapid response on the racemic species nature while crystallization progresses.

PART 6: INVESTIGATION OF A PHASE TRANSITION BY *IN SITU* SHG FOR CHIRAL COMPOUNDS

6.1. INTRODUCTION ON POLYMORPHIC PHASE CHANGE

Most of the organic substances exist in solid state as polymorphs, pseudo-polymorphs (solvates) or amorphous forms. The physicochemical properties of active pharmaceutical ingredients (APIs) are key factors to the development of appropriate dosage forms²⁶ and those crucially depend on the solid form present.

Differential scanning calorimetry (DSC) and X-ray diffraction (XRD) are the common techniques used to determine the thermodynamic relationships between different phases: enantiotropic and monotropic transitions between polymorphs, solvation/desolvation and amorphization/recrystallization processes^{25,27}. These techniques emphasize the characterizations, knowledge of thermodynamic and kinetic parameters that determined the temperature stability domain for storage condition and dosage form.

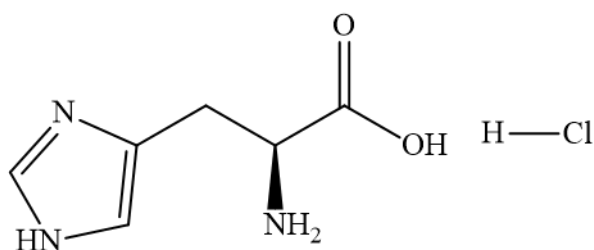
In this work, we aim at evaluating the applicability of *in situ* SHG set-up for tracking phase transitions, two compounds were studied:

- Histidine monohydrochloride, to monitor the three-phase transition between the hydrate and dihydrate forms of this compound.
- Imeglimin propionate to monitor the eutectoid transitions between the conglomerate and the racemic compound.

6.2. HISTIDINE MONOHYDROCHLORIDE HYDRATE (S)

6.2.1. Histidine monohydrochloride

DL-2-amino-3-(1H-imidazol-4-yl) propanoic acid monohydrochloride or histidine monohydrochloride (scheme 1) is an amino acid commercially available. The compound exists in two different hydrated forms.



Scheme 1: Histidine monohydrochloride

6.2.2. Histidine monohydrochloride hydrate (s)

Histidine monohydrochloride can crystallize either as a monohydrate or a dihydrate depending on the temperature of the crystallization.

The resolution of DL-histidine monohydrochloride by crystallization was first demonstrated by Duschinsky^{28,29}, who separated the isomers by seeding supersaturated aqueous solutions containing an excess of one or the other antipode. This is consistent with the existence of a conglomerate forming-system. However, racemic histidine monohydrochloride crystallizes in water at 20 °C as a dihydrate while at higher temperatures (45 °C and above) as a monohydrate. According to Duschinsky, the racemic compound which is stable at low temperature changes to a conglomerate between 40 and 55 °C. The ternary isotherms of the histidine hydrochlorides were determined in water at 25, 35 and 45 °C by Jacques and Gabard³⁰. It was confirmed that a racemic compound is formed at 25 and 35 °C and the data obtained at 45 °C reveal the formation of a conglomerate. It was clearly shown by Jacques *et al.*³¹ that the transition temperature at which the racemic compound decomposes is quite close to 45 °C. The crystal structures of histidine monohydrochloride have been resolved by Donohue and Caron³² (1964) for the monohydrate and Bennett *et al.*³³ (1970) for the dihydrate.

Finally, it was shown by Jacques *et al.* that histidine monohydrochloride crystallizes at 45 °C and above, as a conglomerate (monohydrate, $P2_12_12_1$, space group) and as a racemic compound (dihydrate, $P2_1/a$, space group) at low temperatures.

6.2.3. Salt formation and characterizations

6.2.3.1. Salt formation

DL and L-histidine monohydrochloride monohydrate were purchased from Sigma Aldrich with a purity grade better than 99% and were used without any further purification. DL-histidine monohydrochloride dihydrate was crystallized from an equimolar ratio of DL-histidine and hydrochloride acid in aqueous solution at room temperature. The solution obtained was stirred well at room temperature using a controlled magnetic stirrer (500 rpm) to yield a homogenous mixture of solution. Then the solution was left to evaporate at room temperature up to crystallization. The collected solid was gently ground and analysed by using classical SHG, XRPD and DSC.

6.2.3.2. Powder-SHG technique

For the commercial DL and pure L-enantiomer of the monohydrate, the SHG response was positive but with a very weak intensity compared to the intensity of the reference sample (< 1% / quartz).

For DL-histidine monohydrochloride dihydrate, the crystallized solid phase gave no SHG signal, as expected for a centrosymmetric crystal.

6.2.3.3. XRPD measurements

The XRPD measurements performed on the commercial and crystallized histidine monohydrochloride salts are reported in Figure 2.8.

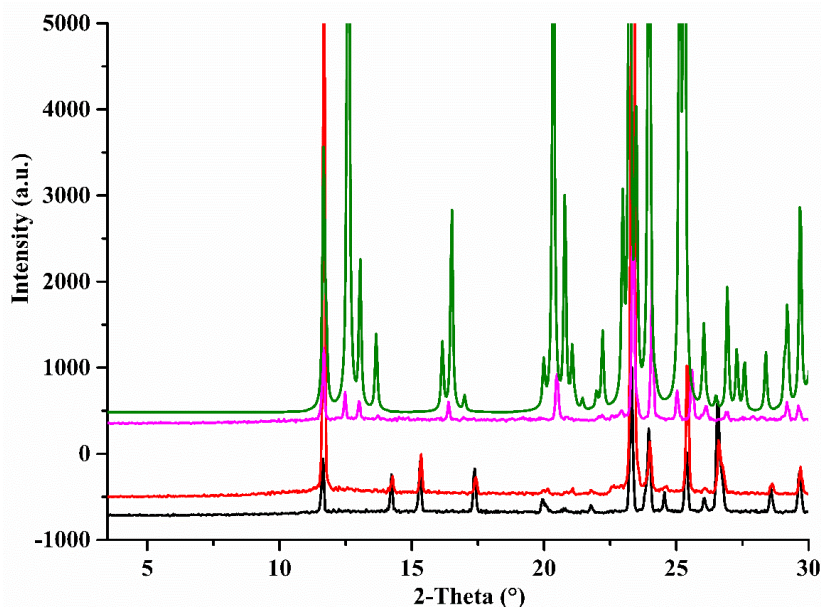


Figure 2.8: XRPD patterns of DL (black) and L (red) histidine monohydrochloride monohydrate and experimental (pink) and calculated (green) DL-histidine monohydrochloride dihydrate

The XRPD patterns of commercial DL (black) and L- (red) histidine monohydrochloride monohydrate are identical and confirm the conglomerate nature of the monohydrate form ($P2_12_12_1$, space group) even though their SHG intensities are weak.

The calculated (green) and experimental (pink) XRPD patterns of DL-histidine monohydrochloride dihydrate are similar with some shifted peaks. A single crystal of the racemic mixture dihydrate was analysed by single crystal X-ray diffraction (SC-XRD) and gave the same crystallographic data as those reported by Bennett *et al*³³.

6.2.3.4. DSC and TGA-DSC analyses

DSC analyses were performed on each form of the histidine monohydrochloride and the results are reported in the Figure 2.9.

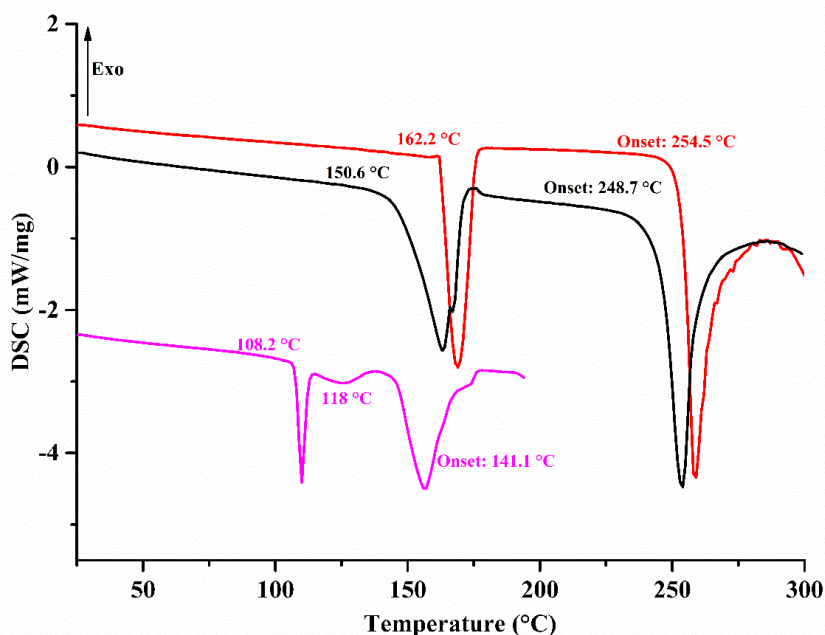


Figure 2.9: DSC curves of histidine monohydrochloride: experimental DL dihydrate (pink), commercial DL (black) and L (red) monohydrate

For the commercial monohydrate, two endothermic events appear: one at 150.6 °C and the other at 248.7 °C for DL-histidine monohydrochloride (respectively at 162.2 °C and 254.5 °C for L-histidine monohydrochloride) corresponding to dehydration and melt (followed by decomposition), respectively. The dehydration (loss of mass of 7.82% corresponds to circa one water molecule) on both DL and L monohydrate samples was confirmed by TGA-DSC analysis. For the DL-dihydrate, DSC analysis displays two events: one endothermic event at 108.2 °C assigned to the dehydration and one endothermic event at 141.1 °C assimilated to the melt. In between, an undetermined endothermic event at 118 °C (probably a loss of mass due to the lattice water). TGA-DSC analysis performed on the DL-dihydrate confirms the loss of 13.73% of mass equivalent to circa two water molecules at 107.3 °C.

6.2.3.5. *In situ* SHG analyses

The classical powder-SHG analysis revealed that the SHG efficiency of DL-histidine monohydrochloride monohydrate is very weak. Furthermore, as demonstrated in Table 2.1, the SHG intensity of a non-centrosymmetric crystal decreases when the latter is in equilibrium with its mother liquor (suspension). This fact could constitute an issue for the monitoring of the polymorphic phase change between the monohydrate and dihydrate forms.

A suspension of the commercial DL histidine monohydrochloride monohydrate was prepared in purified water at room temperature and submitted to the *in situ* SHG analysis. For different concentration rates, no SHG signal was detected and the complete conversion to the dihydrate

phase took at least 24 hours. The absence of SHG signal in the suspension was probably due to the weakness of the SHG signal of histidine monohydrochloride monohydrate powder.

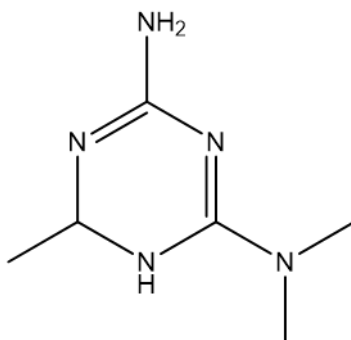
6.2.4. Conclusion

Histidine monohydrochloride exhibits different crystal structures for different amount of water and crystallization temperatures. The DL-monohydrate salt crystallizes in the non-centrosymmetric, $P2_12_12_1$, space group and the DL-dihydrate salt in the centrosymmetric, $P2_1/a$, space group. This makes this binary system theoretically suitable to be analysed by *in situ* SHG. However, experimentally, the weakness of the SHG signal generated by the monohydrate conglomerate powder prevented the study of the phase transition in suspension by *in situ* SHG. Consequently, the level of SHG efficiency of a non-centrosymmetric crystal is a critical parameter for the monitoring by *in situ* SHG technique of a phase change. A non-centrosymmetric phase for which powder-SHG is already weak would hardly give a detectable signal by *in situ* SHG. Thus, the weakness of the SHG signal constitutes one of the drawbacks of the *in situ* SHG technique.

6.3. IMEGLIMIN PROPIONATE

Imeglimin: commonly named in the SMS laboratory “Merck base”, has the chemical name: (R) 1,6-dihydro-N,N,6-trimethyl-1,3,5-triazine-2,4-diamine (Scheme 2) and belongs to the family of dihydro-1,3,5-triazine derivatives. This family of compounds have pharmaceutical interests such as anti-malarial activity, herbicide or insecticide^{34,35}.

(R)-imeglimin hydrochloride salt, an active pharmaceutical ingredient (API, patented by POXEL-Merck KGaA) reduces the level of glucose in blood and is used to cure the diseases caused by insulin resistance³⁶.



Scheme 2: Imeglimin

Levilain et co-workers³⁷ have identified and characterized three solid phases of imeglimin propionate and have resolved the crystal structure of the conglomerate phase. The crystal structures of the racemic compound and hydrate phases were not yet solved.

Imeglimin propionate is a suitable candidate to test the reliability and applicability of our *in situ* SHG set-up.

6.3.1. Salt formation and characterizations

6.3.1.1. Salt formation

For this work, the pure enantiomer of imeglimin was not available to crystallize the enantiomeric salt, but XRPD data of the (-) imeglimin propionate previously obtained by Levilain were used for the comparison of XRPD data obtained from the racemic mixture salt.

The crystallization of (\pm) imeglimin propionate (Scheme 3) was carried out:

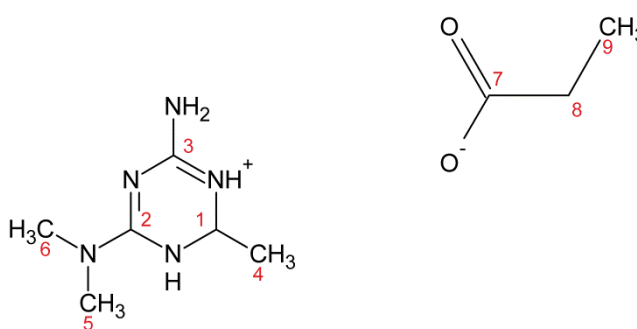
- In isopropyl alcohol at 11 °C (conditions reported by Levilain *et al.* to obtain the conglomerate by spontaneous crystallization): Phase I).

For a 1:1 ratio reaction between (\pm) imeglimin and propionic acid, the parameters of crystallization of the phase I are summarized in Table 2.2.

Table 2.2: Parameters of crystallization of conglomerate phase of imeglimin propionate

(\pm) imeglimin propionate	Conglomerate
Mass of (\pm) imeglimin (g)	3.990
Volume of propionic acid (ml)	1.918 (1.0 equivalent)
Mass of isopropyl alcohol (g)	20.044 (g)
Crystallization temperature (°C)	11

- In ethanol at 70 °C with fast evaporation in a ventilated oven (conditions reported for racemic compound formation: Phase II).
- In ethanol at room temperature by slow evaporation (our own conditions for hydrated phase formation: Phase III).



Scheme 3: Imeglimin propionate with labelled carbons

6.3.1.2. Solid state NMR analyses

The formation of (\pm) imeglimin propionate was confirmed by solid state nuclear magnetic resonance (ss-NMR) measurements for the Phase I and Phase II. The NMR spectra (despite 2

extra peaks for Phase II, indicated by black arrows) of imeglimin propionate were superimposable (Figure 2.10).

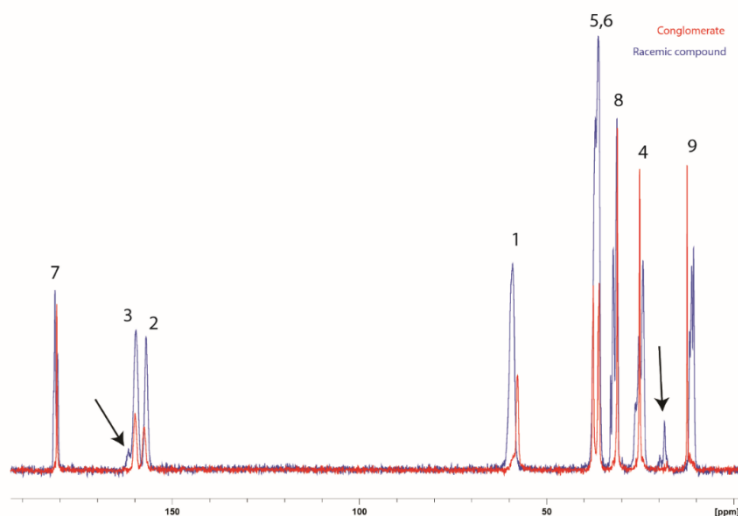


Figure 2.10: Superposition of spectra of racemic compound (blue) and conglomerate (red) of imeglimin propionate at rotation frequency of 25 kHz. (Black arrows indicate extra peaks in the racemic compound).

The spectral line for Phase II exhibits 2 peaks (indicated by black arrow) which are not present in the spectral line for Phase I. A recrystallization in ethanol solution was performed to exclude the hypothesis of presence of impurities for Phase II, but the two peaks were still present in the new spectral line. Some solvent (or something else) could be expected (even though we performed ss-NMR analysis with a solid sample) for Phase II but only its crystal structure will allow to compute completely the chemical shifts.

The crystallized solids were further characterized by classical techniques (i.e. SHG, XRPD and DSC).

6.3.1.3. Powder-SHG technique

The classical SHG (in powder) analyses revealed that Phase I gave a strong SHG signal (826% / quartz) in agreement with the formation of a conglomerate. More surprisingly, Phase II gave a positive but relatively weak SHG signal (9% / quartz) which is not expected for a racemic compound. Phase III exhibited no SHG signal.

Since a positive SHG signal was obtained for Phase II, a non-centrosymmetric space group was suspected for the racemic phase even though racemic compounds crystallizing in a non-centrosymmetric crystal exist but their number is rather limited³⁸.

This hypothesis was reinforced by SHG microscopy observations of the crystalline powder spread on a glass microscope slide. Emission of light (in yellow) was observed for each crystal which banned the possibility for Phase II of a contamination of the sample by a non-

centrosymmetric impurity. Thus, SHG microscopy indicates (Figure 2. 11) that conglomerate (a) and racemic compound (b) of imeglimin propionate have a positive SHG activity, indeed both are constituted of non-centrosymmetric crystals.

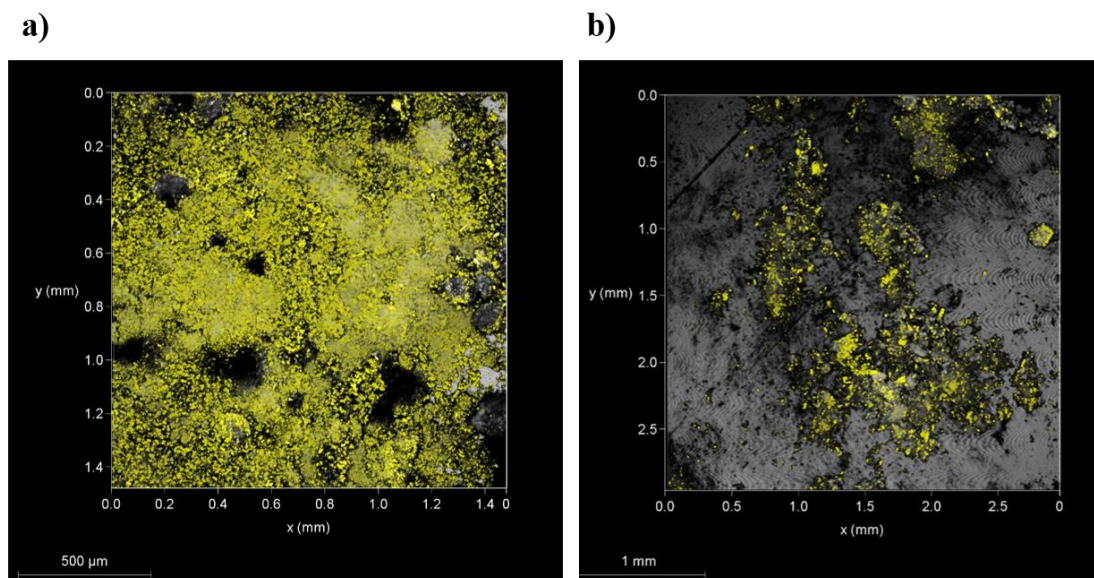


Figure 2.11: SHG microscopy on conglomerate a) and racemic compound b) of imeglimin propionate

6.3.1.4. XRPD measurements

Characterization of the crystallized phases were also performed by using XRPD measurements and the XRPD patterns of the different phases of imeglimin propionate are reported in Figure 2.12.

The perfect superimposition of the experimental XRPD patterns of Phase I (red) and (-) enantiomer (green) confirms the conglomerate nature of the imeglimin propionate racemic mixture.

A single crystal of sufficient size and quality was obtained from crystallization of the enantiomeric salt (reported by Levilain *et al.*). The crystal structure of the conglomerate was resolved and revealed that the (-) imeglimin propionate enantiomer crystallizes in the non-centrosymmetric crystal system: hexagonal, $P6_5$ space group. Thus, the conglomerate phase crystallizes in the non-centrosymmetric crystal system with, either $P6_5$ (n° 170), space group for (-) enantiomer or $P6_1$ (n° 169), space group for (+) enantiomer.

The superimposition of the experimental (green) and calculated (blue) XPRD patterns from the (-) enantiomer sample indicates that the analysed crystal was representative of the bulk sample.

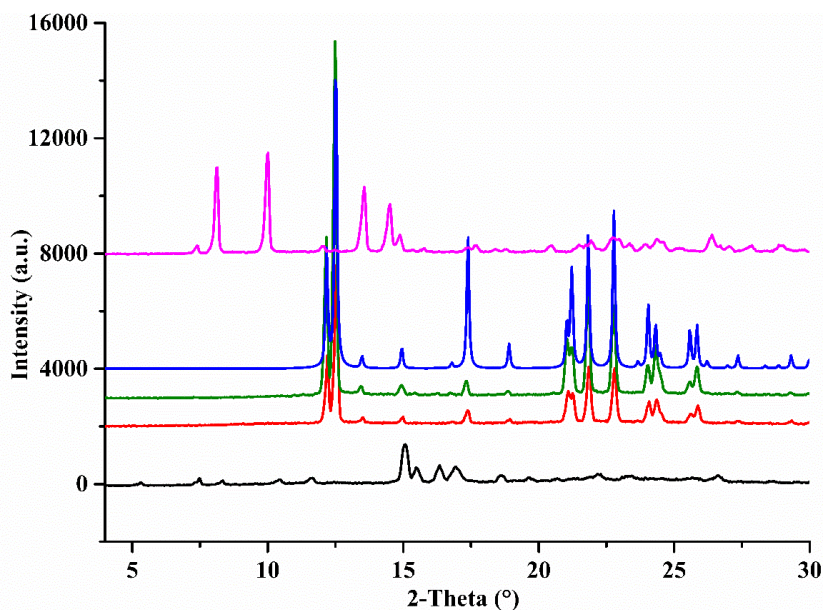


Figure 2.12: XRPD patterns of imeglimin propionate: experimental (black) racemic compound; experimental (red) conglomerate; experimental (green) and calculated (blue) (-) enantiomer; experimental hydrate solid solution (pink).

The XRPD pattern of Phase II (black) is different from that of the conglomerate (Phase I). As the ss-NMR analysis evidenced the propionate salt for both samples (even though two unidentified peaks were present in the spectra of Phase II, see Figure 2.10), Phase I and Phase II correspond to different solids of racemic imeglimin propionate (conglomerate and racemic compound).

The XRPD pattern of hydrate phase is also different from those of the conglomerate (Phase I) and the racemic compound (Phase II). Moreover, Levilain³⁷ has shown that XRPD patterns of racemic hydrate and its corresponding (-) enantiomer hydrate have similarities with peak shifts and their solubility studies revealed small differences. Therefore, he concluded that the hydrate phase likely crystallizes as a complete solid solution^{11,39}.

Several attempts for different methods (slow evaporation, cooling crystallization) at different temperatures were used to grow single crystals of the racemic compound and the hydrate solid solutions. However, single crystals of sufficient size and quality were not obtained. The crystal structure determination using X-ray powder diffraction pattern was also impossible due to the poor intensities and resolution of the peaks in their X-ray diffractions patterns.

6.3.1.5. DSC and TGA-DSC analyses

DSC analyses (Figure 2.13) revealed a single endothermic peak at 211.8 °C (onset) for the conglomerate (Phase I) and at 208.6 °C (onset) for the racemic compound (Phase II), attributed to their melting. DSC curves of the racemic compound and conglomerate did not show any

thermal event which could be associated to a polymorphic transition. For the hydrate phase, DSC analyses gave three endothermic events at 57.2 °C (dehydration) at 183.2 °C (unidentified event) and at 206.9 °C (onset melting).

TGA-DSC analysis (Figure 2.14) was used to confirm the presence of one water molecule in the crystal structure of the hydrate phase. Figure 2.8 shows the profile of mass loss of 7.54% corresponding to the loss of one water molecule at 56.9 °C.

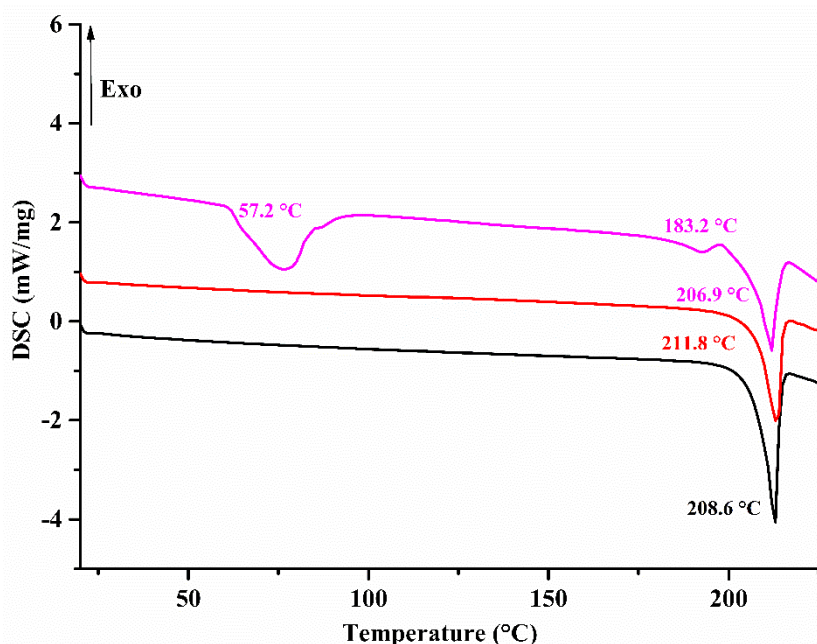


Figure 2.13: DSC curves of racemic compound (black), conglomerate (red) and monohydrate solid solutions (pink) of imeglimin propionate

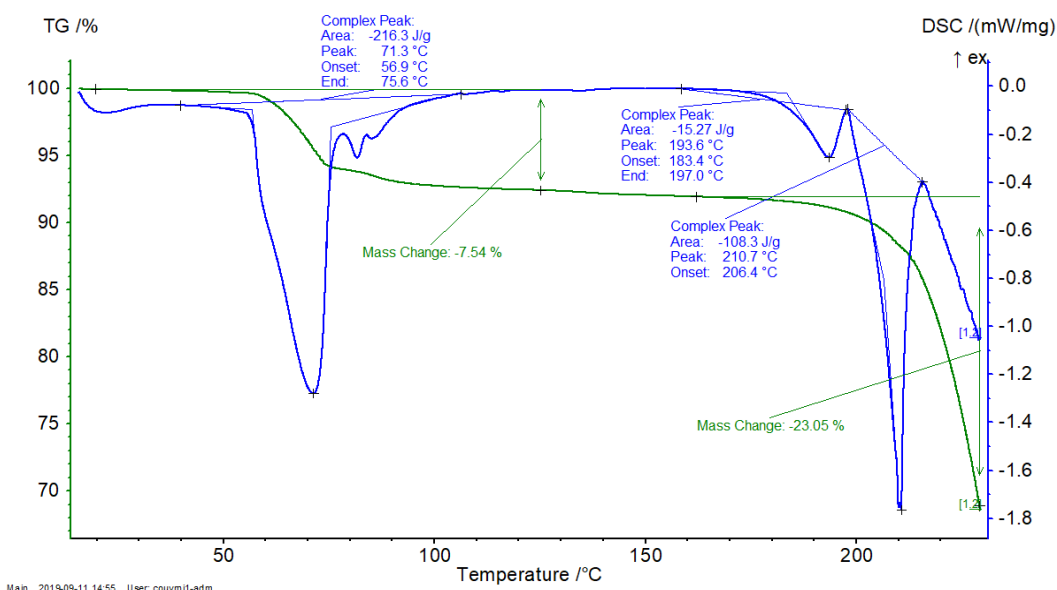


Figure 2.14: TGA-DSC analysis of the monohydrate solid solutions of imeglimin propionate

6.3.2. Relative stability of the phases

Regarding their melting temperature, the conglomerate (Phase I) was suspected to be more stable than the racemic compound (Phase II). However, relative stability temperature tests were performed and revealed that the conglomerate phase is metastable at room temperature and above. To check the occurrence of the polymorphic change, a suspension of the conglomerate was prepared in ethanol under magnetic stirring at room temperature. After ten days, the conglomerate was completely converted into the racemic compound. The solid of the suspension was sampled every two days and analyzed by XRPD measurements and the polymorphic change was confirmed by the comparison of their XRPD patterns (see section 6.3.4, Figure 2.17).

The same protocol was used to suspend under magnetic stirring the racemic compound in ethanol at 11 °C (temperature of crystallization of the conglomerate) but the racemic compound remains unchanged after one month. The temperature of the suspension was maintained at lower temperature (7 °C) but no change was observed on the racemic compound for several days.

Consequently, the conglomerate and the racemic compound phases of imeglimin propionate seem to be in a monotropic relationship⁴⁰ with the racemic compound as the stable phase, and the conglomerate as the metastable phase at all temperatures.

The solubility variations of the two phases were studied in ethanol solution for different temperatures.

6.3.3. Solubility studies

The solubility of racemic compound and conglomerate phases of imeglimin propionate was measured in ethanol using the classical evaporation method. A suspension of each phase was prepared in ethanol for different temperatures and let under stirring during several hours. Then the suspension was filtered, and the saturated solution was weighed, then evaporated and dried at room temperature. The solubility is calculated by dividing the mass of the recovered powder by the mass of the saturated solution. Hereafter, each reported value of the solubility is the mean value of three measurements (with the errors) and is expressed in weight percent (wt%). We checked that the solid-solid transition did not occur during the solubility measurement (verification of the solid phase by XRPD after filtration). Figure 2.15 displays the solubility variation over temperature of the racemic compound and conglomerate phases.

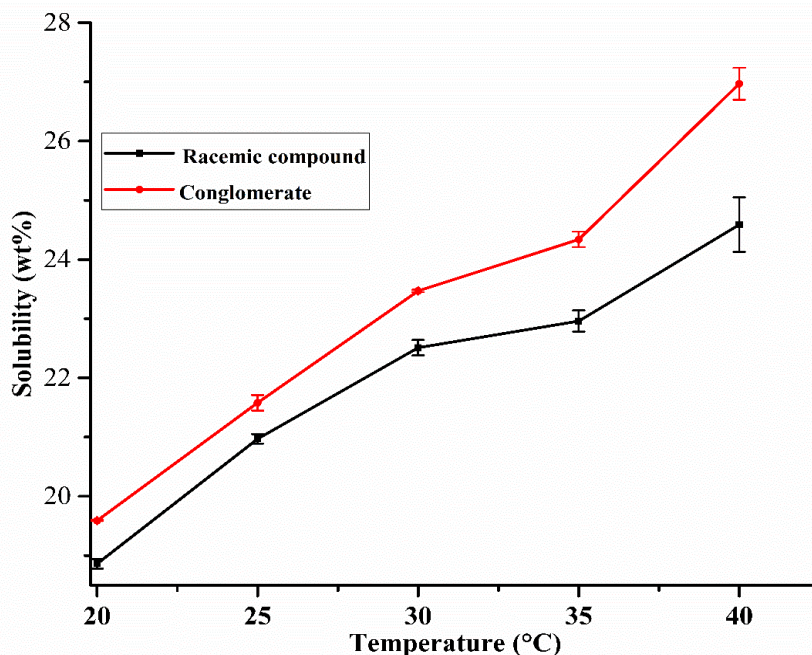


Figure 2.15: Solubility curves of racemic compound (black) and conglomerate (red) phases of imeglimin propionate in ethanol solution.

The solubility of the conglomerate in ethanol is systematically higher than that of the racemic compound in the range of temperature investigated, thus confirming its metastable character in a monotropic relationship with the racemic compound, the stable form (the most stable form at a given temperature and pressure is the least soluble in a given solvent at the same temperature and pressure).

6.3.4. Phase change monitored by *in situ* SHG

We have confirmed that imeglimin propionate crystallizes in three forms (e.g. conglomerate, racemic compound and monohydrate solid solutions) which have different physicochemical and physical characteristics (morphology, density, solubility, melting point, etc.). Several common techniques such as differential scanning calorimetry, temperature-resolved X-ray diffraction were used to identify and characterize this system.

Herein, we propose a complementary experimental method (i.e. *in situ* SHG) that could be used to follow the three-phase transition since at least one phase exhibits a non-centrosymmetric crystal structure. In the following, we monitor the phase change between the conglomerate and the racemic compound of imeglimin propionate.

We have shown that the conglomerate (powder-SHG intensity: 826% / α -quartz) is metastable and that the racemic compound (powder-SHG intensity: 9% / α -quartz) is stable for all temperatures through a monotropic relationship under atmospheric pressure. Under these conditions, the known irreversible solid-solid transition from the conglomerate to the racemic

compound of imeglimin propionate could occur within few days as shown above (section 6.3.2). In this studied system, the two phases are non-centrosymmetric crystals but show drastically different SHG response as powder samples (almost two orders of magnitude in percentage of α -quartz intensity). Therefore, it is possible to follow the phase change by following the evolution with time of the SHG intensity measured for a suspension of the conglomerate at a given temperature. In parallel, periodic sampling of the suspension and analysis by XRPD can be performed to identify the phases present in the suspension during the monitoring.

As we know that the intensity of the SHG signal is sample and solvent dependent, we have prepared a suspension with a large amount of solid 33% above the solubility limit of the conglomerate in ethanol solution (25 ml scale).

The experiment was carried out in the batch cooling crystallizer described in section 4.1, the reactor was completely sealed to avoid evaporation of the solvent during the monitoring.

The suspension was maintained at constant temperature (i.e. 40 °C, herein) under mechanical stirring and the intensity of the SHG signal was daily collected and recorded every two hours up to complete transformation of the conglomerate into racemic compound. The SHG intensity recorded over time is normalized with the SHG intensity of the pure metastable conglomerate (maximum value in the suspension) and expressed in percentage. The results of three runs (same experimental conditions) are reported in Figure 2.16.

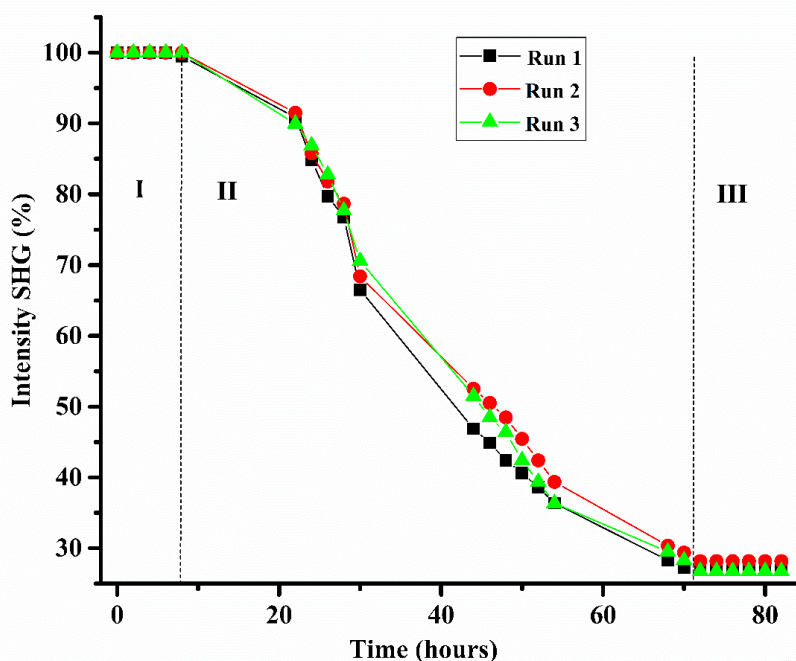


Figure 2.16: Phase transition between the conglomerate and racemic compound of imeglimin propionate monitored at 40 °C by *in situ* SHG.

The monitoring by *in situ* SHG of the phase change can be divided into three different domains depending on the SHG intensity of the suspension recorded over the time:

- (i) **Domain I** where no variation on the SHG signal is observed. The metastable conglomerate is the only phase present in the suspension, thus the SHG signal is at its maximum value (100%).
- (ii) **Domain II** where the intensity of the SHG signal of the suspension is decreasing i.e. the suspension is not composed only of the conglomerate. The metastable phase (conglomerate) starts to convert into the stable phase (racemic compound) which has a weaker SHG efficiency. This decrease gradually occurs from ca. 10 hours up to nearly 72 hours confirming a slow rate of solid-solid transition between the metastable and stable phases at this temperature (40 °C).
- (iii) **Domain III** where no variation on the SHG signal occurs anymore, the intensity measured remains constant (i.e. only the stable phase is present in the suspension).

The experimental parameters such as the temperature and stirring rate remained constant, the phase transition occurred after a certain time once the energy barrier is overcome. The rate of phase transition for imeglimin propionate is poor i.e. at least three days were necessary to completely transform the conglomerate into the racemic compound for a batch of 25 ml scale, with an amount of solid 33% above the solubility limit, at 40 °C, and stirring rate of 250 rpm. For each run, samples were taken at $t = 44$ and 80 hours (domain II and III) in the suspension to identify the phases present at that time. For each sample, the collected solid was analyzed by XRPD (Figure 2.17)

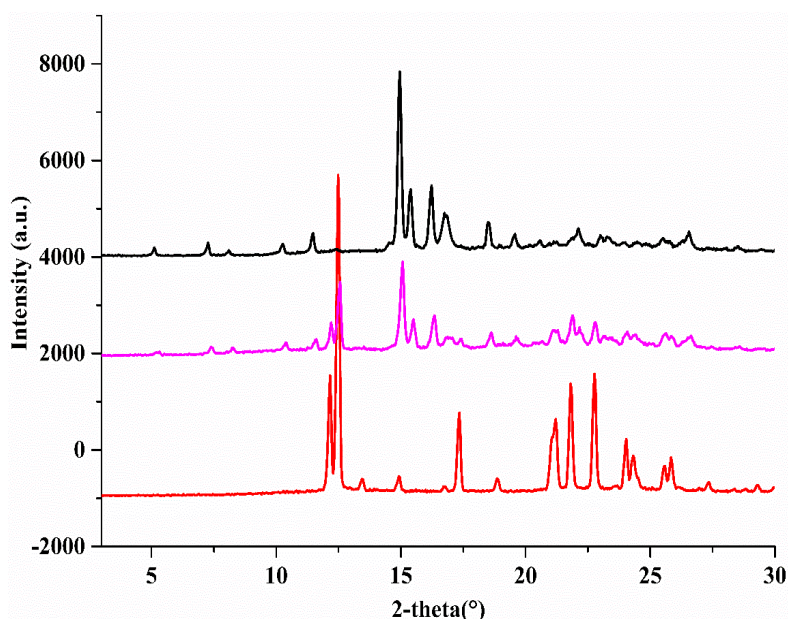


Figure 2.17: XRPD patterns of conglomerate (red; at $t = 0$ hour), mixture (pink at $t = 44$ hours) and racemic compound (black; at $t = 80$ hours) imeglimin propionate.

The XRPD patterns of collected solids confirm that at $t = 44$ hours (pink), the suspension is composed of the mixture of conglomerate and racemic compound and at $t = 80$ hours (black), the racemic compound only is present in the suspension. These results are in perfect agreement with the variation of the SHG intensity of the suspension recorded over time.

Another challenge was to evaluate the rate of solid-solid transition as a function of the temperature. So, with the same experimental parameters (25 ml volume scale and 250 rpm), a fourth run was performed at 35 °C and the results displayed in Figure 2.18. The fourth run was chosen at lower temperature to prevent evaporation of the solvent during crystallization. The variation of the SHG intensity versus time was plotted for the monitoring at 35 °C and 40 °C.

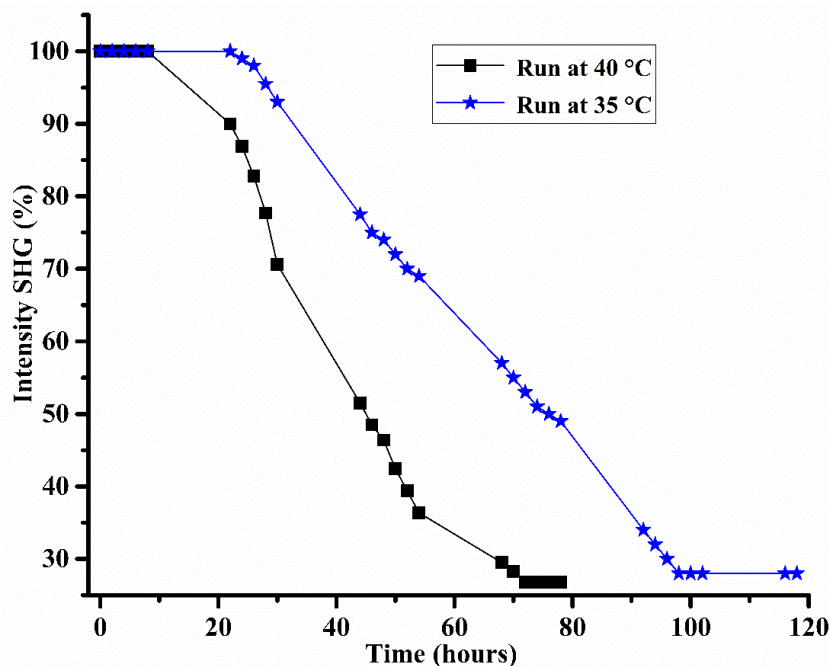


Figure 2.18: Phase transition between the conglomerate and racemic compound of imeglimin propionate monitored at 35 °C (blue) and 40 °C (black) by *in situ* SHG.

At 35 °C, the conversion of the metastable to stable phases takes more time than at 40 °C. Consequently, the higher the temperature at which the monitoring is performed, the fastest the complete transformation of the conglomerate into the racemic compound of imeglimin propionate. The elevation in temperature enhances the molecular motion and helps to overcome the energy barrier.

6.3.5. Conclusion

The conversion from the conglomerate (metastable) to the racemic compound (stable) has a slow kinetics which can be increased at higher temperatures. The large difference in SHG intensity of the two forms, although both non-centrosymmetric, is enough to discriminate the different solids and unambiguously allowed to monitor the phase transformation by *in situ* SHG.

These observations provide compelling evidence for the ability of *in situ* SHG to directly monitor solid-solid transition by means of measuring SHG signal of crystalline non-centrosymmetric phases. However, in the case in which a small difference in SHG intensity exists between the two forms, the identification of the solids by XRPD will be necessary.

PART 7 : CONCLUSION AND PROSPECTS

We have implemented a technique based on second harmonic generation to track non centrosymmetric crystals at the early stages of crystal formation. The developed technique named *in situ* SHG has been successfully tested to track non-centrosymmetric crystal in equilibrium with their mother liquor.

Through the investigation of KDP crystal formation, the *in situ* monitoring demonstrates the versatility of the SHG technique. The results allowed to extend the applicability of the *in situ* monitoring to chiral organic compounds crystallizing with at least one non-centrosymmetric crystal phase.

The *in situ* SHG has been used to monitor the solid-solid transition between two organic crystal phases having both a positive SHG activity. The monotropic conversion from conglomerate to racemic compound of imeglimin propionate at 35 °C necessitated minimum four days for a 25 ml volume scale. The rate of solid-solid transition is slow for imeglimin propionate but is increased at higher temperature.

The technique provides the screening of non-centrosymmetric crystals in suspension and direct evidences the polymorphic transition in such crystals. A SHG signal greater than 5-10% of the α -quartz SHG intensity could be detected without ambiguity in suspension²². This level of detection allows to be sure that the crystal in equilibrium with its mother liquor is non-centrosymmetric when the SHG signal is detected. Nevertheless, it should be noted that a threshold SHG efficiency of the material is required to be tested in suspension as shown by the example of histidine monohydrochloride.

Evaluation of the SHG signal is rather complex when the crystallization progresses because the SHG intensity is sample and solvent dependent but can be normalized with the intensity (powder-SHG on the chosen compound). Although it is sometimes possible to differentiate two solids by their SHG intensities (i.e. conglomerate and racemic compound of imeglimin propionate) but a XRPD analysis may be nonetheless necessary to identify the phase present in suspension for a small difference in their SHG intensities.

Clearly, through this study, progress has been made in development of methods to use second harmonic generation technique for tracking metastable conglomerates at the early stages of crystal formation. This is a new direction to find new conglomerate forming systems (even metastable) and to increase their proportion which is nowadays on the average less than 10% of the pairs of enantiomers for crystalline racemic mixtures. Additionally, efforts should be concentrated to the determination of threshold volume scale that could allow to detect a SHG

signal in suspension if the latter exists. That will contribute to reduce misinterpretation of absence of SHG signal for unknown candidates. Furthermore, the study of crystallization kinetic parameters would be envisaged to have information on the existence in time of conglomerate during crystallization from solution.

REFERENCES

- (1) Galland, A.; Dupray, V.; Berton, B.; Morin-Grognon, S.; Sanselme, M.; Atmani, H.; Coquerel, G. Spotting Conglomerates by Second Harmonic Generation. *Cryst. Growth Des.* **2009**, *9* (6), 2713–2718.
- (2) Dupray, V. Recrystallization of Enantiomers from Conglomerates. In *Recrystallization*; Sztwiertnia, P. K., Ed.; InTech, 2012.
- (3) Mbodji, A.; Gbabode, G.; Sanselme, M.; Couvrat, N.; Leeman, M.; Dupray, V.; Kellogg, R. M.; Coquerel, G. Family of Conglomerate Forming Systems Composed of Chlocyphos and Alkyl-Amine. Assessment of Their Resolution Performances by Using Various Modes of Preferential Crystallization. *Cryst. Growth Des.* **2019**, *19*, 5173–5183.
- (4) Wacharine-Antar, S.; Levilain, G.; Dupray, V.; Coquerel, G. Resolution of (\pm)-Imeglimin-2,4-Dichlorophenylacetate Methanol Solvate by Preferential Crystallization. *Org. Process Res. Dev.* **2010**, *14* (6), 1358–1363.
- (5) LeCaptain, D. J.; Berglund, K. A. Applicability of Second Harmonic Generation for in Situ Measurement of Induction Time of Selected Crystallization Systems. *J. Cryst. Growth* **1999**, *203* (4), 564–569.
- (6) Kissick, D. J.; Wanapun, D.; Simpson, G. J. Second-Order Nonlinear Optical Imaging of Chiral Crystals. *Annu. Rev. Anal. Chem.* **2011**, *4*, 419–437.
- (7) Hall, V. J.; Simpson, G. J. Direct Observation of Transient Ostwald Crystallization Ordering from Racemic Serine Solutions. *J. Am. Chem. Soc.* **2010**, *132* (39), 13598–13599.
- (8) Clevers, S.; Simon, F.; Dupray, V.; Coquerel, G. Temperature Resolved Second Harmonic Generation to Probe the Structural Purity of M-Hydroxybenzoic Acid. *J. Therm. Anal. Calorim.* **2013**, *112* (1), 271–277.
- (9) Eliel, E. L.; Wilen, S. H. *Stereochemistry of Organic Compounds*; J Wiley & Sons Inc., Ed.; New York, USA, 1994.
- (10) Collet, A.; Brienne, M. J.; Jacques, J. Optical Resolution by Direct Crystallization of Enantiomer Mixtures. *Chem. Rev.* **1980**, *80* (3), 215–230.
- (11) Chion, B.; Lajzerowicz, J.; Bordeaux, D.; Collet, A.; Jacques, J. Structural Aspects of Solid Solutions of Enantiomers. The 3-Hydroxymethyl- and 3-Carboxy-2,2,5,5-Tetramethylpyrrolidinyl 1-Oxyl Systems as Examples. *J. Phys. Chem.* **1978**, *82* (25), 2682–2688.
- (12) Klusmann, M.; Iwamura, H.; Mathew, S. P.; Wells, D. H.; Pandya, U.; Armstrong, A.;

- Blackmond, D. G. Thermodynamic Control of Asymmetric Amplification in Amino Acid Catalysis. *Nature* **2006**, *441* (7093), 621–623.
- (13) Simon, F.; Clevers, S.; Dupray, V.; Coquerel, G. Relevance of the Second Harmonic Generation to Characterize Crystalline Samples. *Chem. Eng. Technol.* **2015**, *38* (6), 971–983.
- (14) Yuan, L.; Clevers, S.; Couvrat, N.; Cartigny, Y.; Dupray, V.; Coquerel, G. Precise Urea/Water Eutectic Composition by Temperature-Resolved Second Harmonic Generation. *Chem. Eng. Technol.* **2016**, *39* (7), 1326–1332.
- (15) Dougherty, J, P and Kurtz, S, K. (1976). 9, 145. *J. Appl. Crystallogr.* **1976**, *9*, 145–158.
- (16) Baur, W, H. How to Avoid Unnecessarily Low Symmetry in Crystal Structure Determinations. *Acta Cryst* **1986**, *B42*, 95–111.
- (17) Franken, P. A.; Hill, A. E.; Peters, C. W.; Weinreich, G. Generation of Optical Harmonics. *Phys. Rev. Lett.* **1961**, *7* (4), 118–119.
- (18) Delfino, M. A Comprehensive Optical Second Harmonic Generation Study of the Non-Centrosymmetric Character of Biological Structures. *J. Biol. Phys.* **1978**, *6* (3–4), 105–117.
- (19) Nikogosyan, D, N. *Nonlinear Optical Crystals: A Complete Survey*; Springer Science & Business Media, 2006.
- (20) Clevers, S. Prototyping of In-Situ Optical Methods to Characterize Organic Molecular Crystals, University of Rouen-France, 2014.
- (21) Kleinman, D. A. Theory of Second Harmonic Generation of Light. *Phys. Rev.* **1962**, *128* (4), 1761–1775.
- (22) Kurtz, S. K.; Perry, T. T. A Powder Technique for the Evaluation of Nonlinear Optical Materials. *J. Appl. Phys.* **1968**, *39* (8), 3798–3813.
- (23) Giordmaine, J. A. Mixing of Light Beams in Crystals. *Phys. Rev. Lett.* **1962**, *8* (1), 19–20.
- (24) Maker, P. D.; Terhune, R. W.; Nisenoff, M.; Savage, C. M. Effects of Dispersion and Focusing on the Production of Optical Harmonics. *Phys. Rev. Lett.* **1962**, *8* (1), 21–22.
- (25) Coquerel, G. Crystallization of Molecular Systems from Solution: Phase Diagrams, Supersaturation and Other Basic Concepts. *Chem. Soc. Rev.* **2014**, *43* (7), 2286–2300.
- (26) Giron, D. Investigations of Polymorphism and Pseudo-Polymorphism in Pharmaceuticals by Combined Thermoanalytical Techniques. *J. Therm. Anal. Calorim.* **2001**, *64* (1), 37–60.

- (27) Hu, Q. Y.; Shu, J. F.; Cadien, A.; Meng, Y.; Yang, W. G.; Sheng, H. W.; Mao, H. K. Polymorphic Phase Transition Mechanism of Compressed Coesite. *Nat. Commun.* **2015**, *6*.
- (28) Greenstein, J. P. The Resolution of Racemic α -Amino Acids BY. *Adv. proteins Chem.* **1954**, 121–202.
- (29) Secor, R. M. RESOLUTION OF OPTICAL ISOMERS BY CRYSTALLIZATION PROCEDURES. **1968**.
- (30) Jacques, J and Gabard, J. Etude Des Mélanges Des Antipodes Optiques. Diagrammes de Solubilité Pour Les Divers Types de Racemiques. *Bull. Soc. Chim. Fr* **1972**, 343.
- (31) Jacques, J .; Collet, A.; Wilen, S. H. *Enantiomers, Racemates and Resolutions*, 3rd ed.; Kriger Pub. Co: Malabar Florida, USA, 1994.
- (32) Donohue, J.; Caron, A. Refinement of the Crystal Structure of Histidine Hydrochloride Monohydrate. *Acta Crystallogr.* **1964**, *17* (9), 1178–1180.
- (33) Bennett, I.; Davidson, A. G. H.; Harding, M. M.; Morelle, I. The Crystal Structure of DL -Histidine Hydrochloride Dihydrate . *Acta Crystallogr. Sect. B Struct. Crystallogr. Cryst. Chem.* **1970**, *26* (11), 1722–1729.
- (34) Lowe, G. . ‘Dihydrofolate Reductase Inhibitors’, WO/2001/053276., 2001.
- (35) Howard, N.;Leslie, M. E.; Pollard, E. J. Novel 1, 2-Dihydro-s-Triazines", US3287366, 1966.
- (36) Moinet, G.;Cravo, Doare, L.; Kergoat, M.; Mesangeau, D. ‘Dihydro-1,3,5- Triazine Amine Derivatives and Their Therapeutic Uses’, WO2001055122, 2001.
- (37) Levilain, G. Development and Improvement of Resolution Methods by Direct Crystallization. PhD dissertation, University of Rouen-France, 2010.
- (38) Dalhus, B.; Görbitz, C. H. Non-Centrosymmetric Racemates: Space-Group Frequencies and Conformational Similarities between Crystallographically Independent Molecules. *Acta Crystallogr. Sect. B Struct. Sci.* **2000**, *56* (4), 715–719.
- (39) Lajzerowicz, J.; Chion, B.; Lajzerowicz, J. Two Dimensional Order in a Solid Solution of Molecules of Opposite Chirality. *J. Chem. Phys.* **1981**, *74* (6), 3500–3509.
- (40) Martins, D.; Sanselme, M.; Houssin, O.; Dupray, V.; Petit, M. N.; Pasquier, D.; Diolez, C.; Coquerel, G. Physical Transformations of the Active Pharmaceutical Ingredient BN83495: Enantiotropic and Monotropic Relationships. Access to Several Polymorphic Forms by Using Various Solvation-Desolvation Processes. *CrystEngComm* **2012**, *14* (7), 2507–2519.

**CHAPTER 3: CHIRAL RESOLUTION OF CHLOCYPHOS VIA ITS
SALT DERIVATIVES**

PART 1: INTRODUCTION

Chlocyphos is the trivial name of a member of a family of phosphoric acids designed and introduced in 1985 by ten Hoeve and Wynberg¹. These cyclic phosphoric acids were the first “family” to be investigated in the resolution technique now known as Dutch Resolution^{2,3}. The enantiomers of chlocyphos are of great interest as several cyclic phosphoric acids, including phencyphos and anicyphos, are used as effective resolving agents in preparing optically pure amines^{1,4} (ephedrine, valine etc.). Diastereomeric salt formation process^{5,6} is often used to resolve these phosphoric acids but this method can present failure due, for example, to the formation of an oil, a gel or a solid solution^{7,8}. Furthermore, this method does not always fit with industrial needs (i.e., low cost, high enantiomeric excess and high productivity). An attractive alternative method is to perform preferential crystallization⁹ (PC) which could be in favourable cases a reliable and inexpensive process to resolve the racemic mixture into its enantiomers. PC consists in isolating pure enantiomers by alternating crystallization with no need for addition of any chiral agent. PC does not alter the global molecular symmetry of the system. However, it requires that the racemic mixture crystallizes in an equimolar mixture of enantiopure crystals, i.e. a stable conglomerate.

Leeman¹⁰ and co-workers have reported the resolution by PC of a compound from the same family of phosphoric acids: phencyphos. Indeed, phencyphos monohydrate crystallizes as a conglomerate and its resolution by PC was successful. It was thus logical to apply this method of entrainment to the resolution of chlocyphos.

Racemic chlocyphos crystallizes, as will be shown further, as a racemic compound. Thus, to achieve resolution by PC, chlocyphos derivatives (salt or co-crystal) that exhibit a full chiral discrimination in the solid state (e.g. conglomerate forming system) must be found. Moreover, these derivatives must not display epitaxial behaviour and/or other complications that can frustrate a resolution by PC¹¹.

In this chapter, we report first the thermal and structural characterizations of both racemic mixture and (*S*)-enantiomer of chlocyphos. The search for conglomerate forming systems among a series of more than twenty salts formed by combining chlocyphos (a strong acid) with strong bases or alkyl amines in 1:1 ratio is also reported. SHG¹² is firstly used to preselect the non-centrosymmetric crystallized phases. Then for the SHG spotted compounds, both pure enantiomer and racemic mixture samples are submitted to additional characterizations such as DSC and X - ray powder diffraction mainly. Crystal structures of the salts are determined by

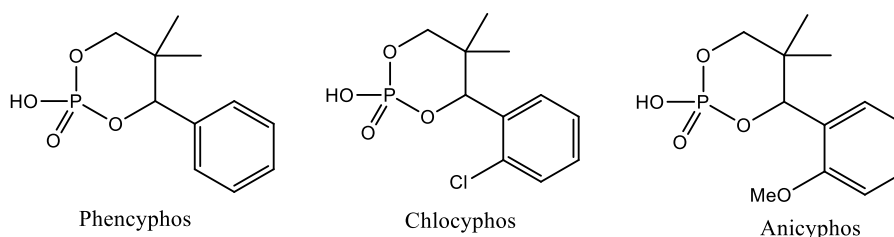
SC-XRD and the strong tendency of chlocyphos alkyl-amine salts to crystallize as conglomerates with similar crystal packing arrangements is highlighted. Through careful analysis of their crystal and molecular structures, a trend with respect to alkyl amine moiety length starting from ethyl to cyclohexyl can be established.

Then, PC through its different modes^{13,14} (SIPC, AS3PC and ASPreCISE) is performed at small scale on the spotted conglomerates of chlocyphos alkyl amine salt derivatives and the results are discussed in terms of enantiopurity level and yield.

PART 2: CHLOCYPHOS

2.1. CYCLIC PHOSPHORIC ACIDS

The trivial names of these cyclic phosphoric acids shown in scheme 1 were suggested by Michel Leeman in 2009^{6,10} even though they were described many years before by Wynberg and co-workers¹. This family of phosphoric acids has been proven to be excellent resolving agents¹⁵. These strong acids easily form crystalline salts even with weak bases which make them suitable for conglomerate screening.



Scheme 1

2.2. CHLOCYPHOS: THERMAL AND STRUCTURAL CHARACTERIZATIONS

4-(2-chlorophenyl)-5,5-dimethyl-2-hydroxy-1,3-dioxaphosphorinane 2-oxide or chlocyphos ($C_{11}H_{14}ClO_4P$), a white crystalline solid, was kindly provided by Syncom BV with a purity grade better than 99%. Chlocyphos is practically insoluble in water and most of the organic solvents but soluble in polar solvents^{16,17} such as methanol, ethanol etc.

2.2.1. DSC analyses

A full characterization of the racemic and pure enantiomer of chlocyphos free acid was performed prior to considering derivatives.

The DSC analyses performed on chlocyphos display a single endothermic event at 219.5 °C (onset) for the racemic mixture and 232.2 °C (onset) for (*S*)-enantiomer samples corresponding to their respective melting point. Before completion of the fusion, a sharp exothermic phenomenon appears, interpreted as chemical degradation (Figure 3.1). Samples were weighed at the end of the DSC analyses and a large mass loss (ca. 42%) compared to the mass at the start of the measurement was observed for both racemic mixture and (*S*)-chlocyphos. Note also that, the crucible content turned to be burned (dark residual). Hence, chlocyphos likely degraded after the melt. No other extra thermal event corresponding to a polymorphic transition, an eutectoid, or peritectoid transformation or a desolvation has been observed for the starting compounds.

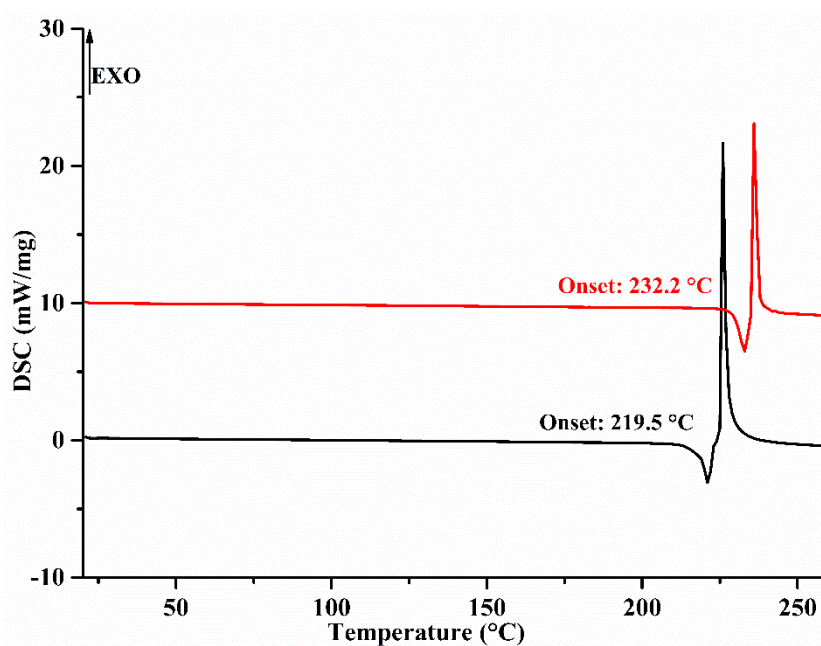


Figure 3.1: DSC curves of racemic (black) and (*S*)- (red) chlocyphos

2.2.2. XRPD measurements

The absence of a significant SHG signal emitted by the crystallized racemic mixture chlocyphos and the clear differences between the XRPD patterns of racemic mixture and (*S*)- enantiomer samples (Figure 3.2) indicate that racemic chlocyphos most likely crystallizes as a centrosymmetric racemic compound.

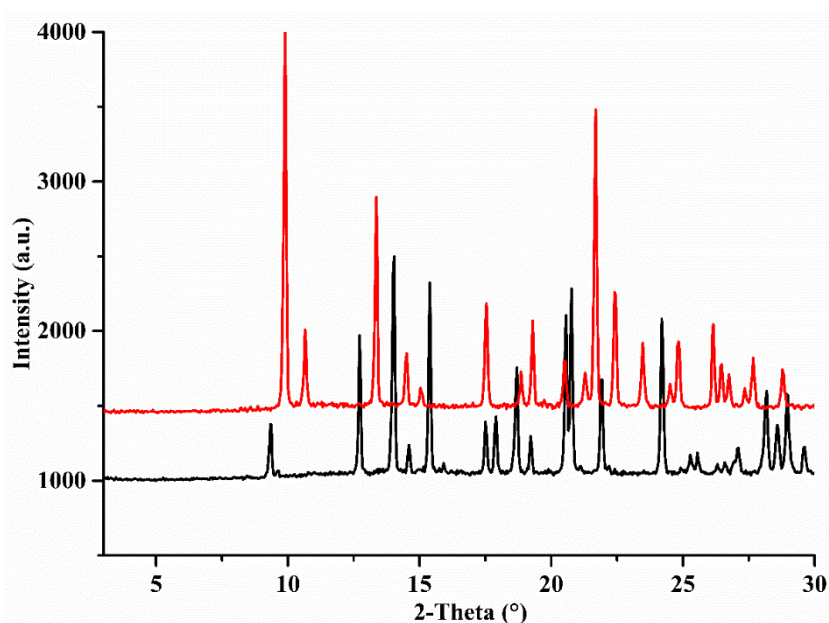


Figure 3. 2: XRPD patterns of racemic (black) and (*S*)- (red) chlocyphos

2.2.3. Crystal structure determination by SC-XRD

Crystal structure determination from single crystal data of the racemic sample was used to confirm the hypothesis of centrosymmetric racemic compound. Single crystals were grown by

slow evaporation of methanol solutions at room temperature and atmospheric pressure. After few days, single crystals (average size: 1-2 mm) were obtained from (*S*) and racemic crystallized batches and analysed by SC-XRD. All crystal structures were determined from single crystal diffraction on a SMART APEX diffractometer (with MoK α_1 radiation: $\lambda = 0.71073 \text{ \AA}$). The crystal structure of chlocyphos samples were solved at room temperature in the triclinic centrosymmetric *P*-1 space group for the racemic sample and in the chiral space group *P*2₁ for the (*S*)-enantiomer. Their crystallographic parameters are reported in Table 3.1.

Table 3.1: Crystallographic data of racemic mixture and (*S*)-chlocyphos

	racemic chlocyphos	(<i>S</i>)-chlocyphos
CSD number	1912257	1912259
Chem. Formula	[C ₁₁ H ₁₄ ClO ₄ P]	
MW / g.mol ⁻¹	276.64	
Temperature (K)	300	
Crystal system	Triclinic	Monoclinic
Space Group	<i>P</i> -1	<i>P</i> 2 ₁
Z, Z' (asymmetric units per unit cell)	2, 1	4, 1
<i>a</i> / Å	6.879 (3)	7.968 (1)
<i>b</i> / Å	9.415 (4)	7.234 (1)
<i>c</i> / Å	9.826 (4)	11.143 (2)
α / °	82.597 (7)	90.00
β / °	76.805 (6)	105.590 (3)
γ / °	80.685 (6)	90.00
<i>V</i> / Å ³	608.6 (4)	618.8 (2)
<i>d</i> _{calc} / g.cm ⁻³	1.510 (9)	1.485 (5)
Absorption coefficient μ (MoK α_1) / mm ⁻¹	0.445	0.437
N° reflexions unique / I>2 σ I	2424 / 1956	2470 / 2279
Final R1 / wR2 (I>2 σ I)	0.0452 / 0.1135	0.0349 / 0.0863
Final R1 / wR2 (all data)	0.0565 / 0.1197	0.0383 / 0.0888
Absolute structure (Flack) parameter	NA	-0.03 (7)

For racemic chlocyphos as for (*S*)-chlocyphos, the asymmetric unit is composed of one molecule of C₁₁H₁₄ClO₄P (Figure 3.3).

For racemic chlocyphos, the hydroxyl moiety establishes some hydrogen bonds (Table 3.2) that give rise to dimers (Figure 3.4). These dimers are interacting through π - π interactions and generate periodic bond chains spreading along *a* and *b* axes (Figure 3.5).

For (*S*)-chlocyphos, the molecules establish hydrogen bonds (Table 3.2) along *b* direction and give rise to periodic bond chains along this direction (Figure 3.6). The van der Waals

interactions ensure the cohesion of the crystal structure. The projection of the whole packing along *b* and *c* directions are displayed in Figure 3.7.

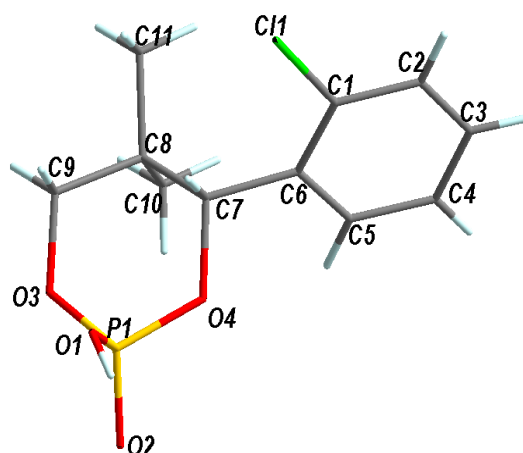


Figure 3.3: Asymmetric unit in labelled atoms representation for racemic and (*S*)-chlocyphos

Table 3.2: Hydrogen bonds characteristic lengths and angles^a of chlocyphos

	D-H...A	d(D-H) (Å)	d(H...A) (Å)	d(D...A) (Å)	<(DHA) (°)
Racemic	O(1)-H(1)...O(2) # ^a	0.82	1.75	2.571 (3)	177.4
(<i>S</i>)	O(1)-H(1)...O(2) # ^a	0.82	1.76	2.487 (2)	147.6

^asymmetric transformations used to generate equivalent atoms #: $-x+1, -y, -z+1$ (for racemic) and #: $-x+2, y+1/2, -z$ (for *S*)

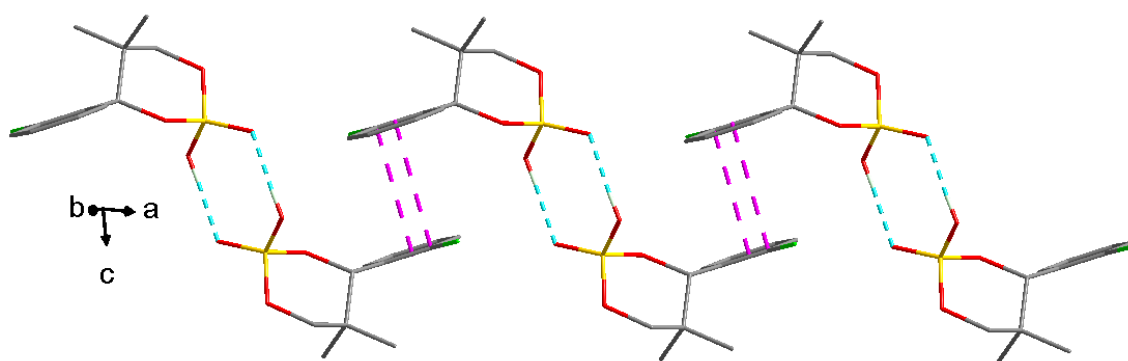


Figure 3.4: Molecular bond chains formed by hydrogen bonded dimers (dashed blue line) interacting through π - π interactions ($d \sim 3.6$ Å) (dashed pink lines) for racemic chlocyphos

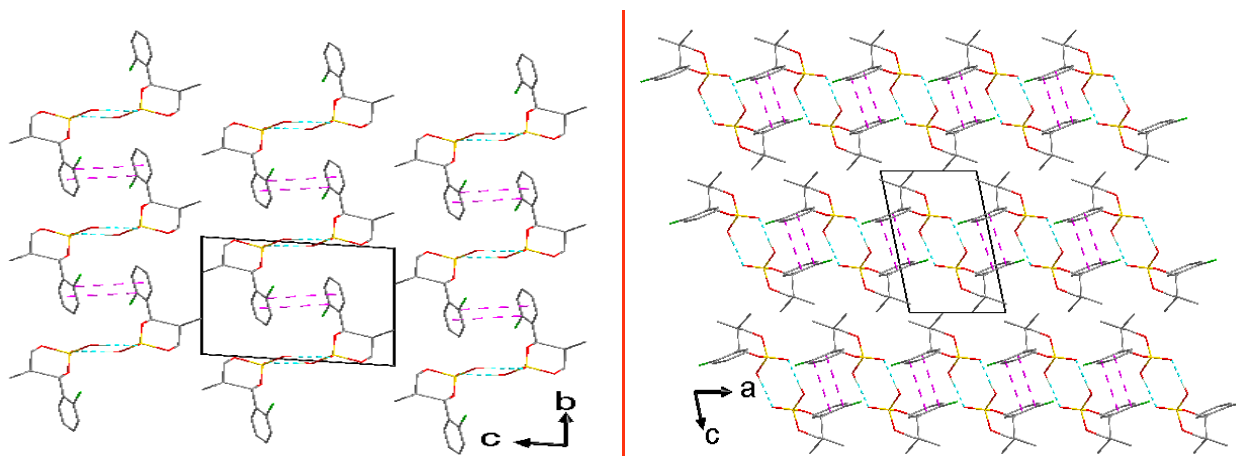


Figure 3.5: Periodic bond chain and projection of the whole packing along a (left) and b (right) axes. The black rectangle represents a unit cell for racemic chlocyphos.

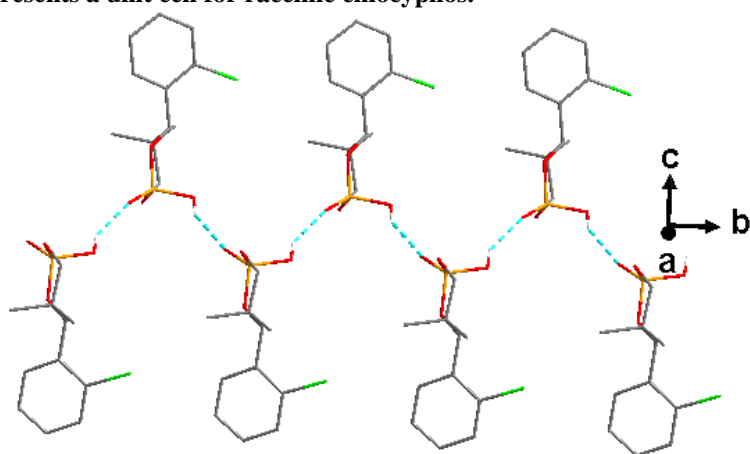


Figure 3.6: Molecular bond chains formed by hydrogen bonds (dashed blue line). van der Waals interactions ensure the cohesion of the crystal structure for (*S*)-chlocyphos.

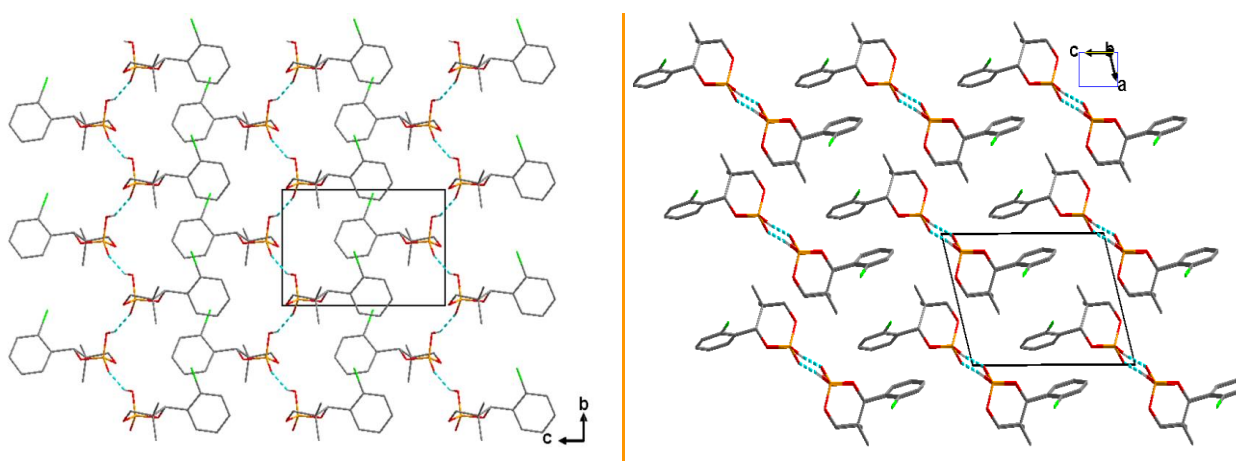


Figure 3.7: Periodic bond chain and projection of the whole packing along a (left) and b (right) axes. The black rectangle represents a unit cell for (*S*)-chlocyphos.

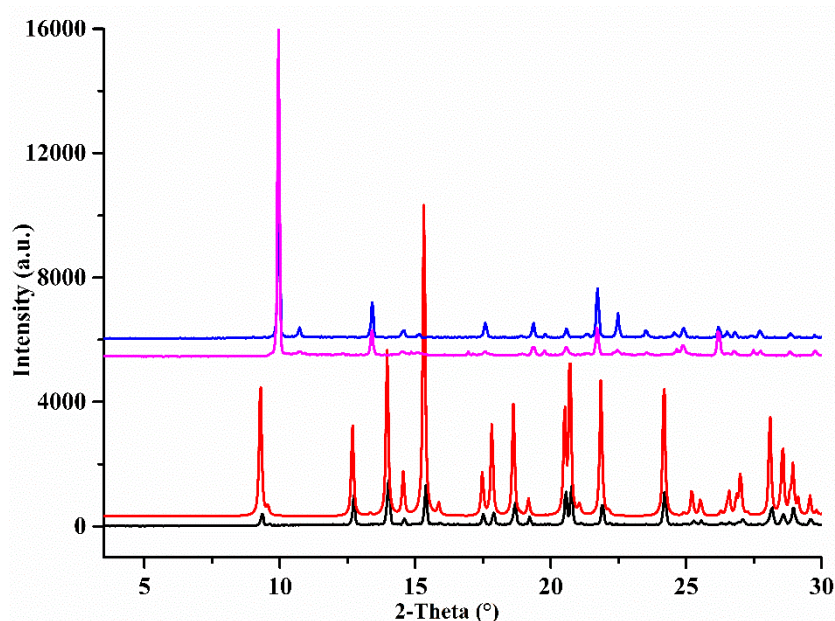


Figure 3.8: Calculated and experimental XRPD patterns for racemic (bottom) and (*S*)-chlocyphos (top). The calculated and experimental XRPD patterns obtained for racemic chlocyphos on one hand and (*S*)-chlocyphos on the other hand are identical (Figure 3.8).

This confirms that the chosen analysed crystals were representative of the bulk sample. Their crystal structures were deposited in the Crystallographic Structure Database (CSD) under the code number CCDC 1912257 for racemic and CCDC 1912259 for (*S*)-chlocyphos.

2.3. SOLUBILITY STUDIES OF CHLOCYPHOS

The solubility of chlocyphos was measured in different solvents using the classical evaporation method. A suspension of the racemic mixture was prepared in the chosen solvent at 20 °C and let under stirring during several hours. Then the suspension was filtered, and the saturated solution was weighed and then evaporated in a ventilated oven. The solubility expressed in weight percent (wt%) is calculated by dividing the mass of the recovered powder by the mass of the saturated solution. The results are summarized in Table 3.3.

Table 3.3: Solubilities of racemic chlocyphos in different solvents at 20 °C

N°	Solvent	Solubility (wt %)
1	MeCN	< 1
2	Water	< 1
3	MeOH	6.0
4	EtOH	3.9
5	IPA	2.7
6	DMF	18.1

Chlocyphos is soluble in all polar protic solvents (methanol, ethanol) and poorly soluble in polar aprotic solvents (acetonitrile).

We showed that chlocyphos crystallizes as a racemic compound. This is not compatible with a resolution by preferential crystallization. Logically, experiments were thus pursued to find derivatives crystallizing as conglomerates.

Due to the strong acidic function of chlocyphos, the choice for a derivative fell on salts rather than derivatives such as co-crystals for example. Indeed, cyclic phosphoric acids are strong acids ($pK_a = 2-3$) and they might be expected to form salts with strong bases, amines and amino acids.

PART 3 : CHLOCYPHOS SALTS**3.1. SALT FORMATION AND SHG RESPONSES**

Chlocyphos, strong bases (KOH, NaOH), amines and the polar protic solvents were used without further purifications. Chlocyphos salts were obtained from acid-base reactions by addition of 1 equivalent of pure base and 1 equivalent of chlocyphos in a polar solvent (e.g. methanol, ethanol or isopropyl alcohol) in a container placed in a thermostatic bath ($T = 30\text{ }^{\circ}\text{C}$) under magnetic stirring to ensure complete dissolution. Solutions were kept at room temperature during crystallization. The crystals were collected, dried at ambient temperature and analysed with the powder-SHG classical set-up.

Table 3.4: Salt formation and corresponding SHG responses

Acide	Amines	SHG signal	SHG Intensity (% of the signal of reference quartz sample)
Chlocyphos	Sodium hydroxide	-	< 1
	Ammonium hydroxide	-	< 1
	Potassium hydroxide	-	< 1
	Lithium hydroxide	-	< 1
	Strontium hydroxide	-	< 1
	Ethanolamine	-	< 1
	Triethanolamine	-	< 1
	Sarcosine	-	< 1
	Methylamine	-	< 1
	Ethylamine	+	4 (1)
	Diethylamine	-	< 1
	Triethylamine	-	< 1
	Propylamine	+	24 (1)
	Butylamine	+	20 (2)
	Isobutylamine	+	54 (3)
	Tert-butylamine	-	< 1
	Pentylamine	+	10 (2)
	Tert-pentylamine	-	< 1
	Hexylamine	+	10 (1)
	Cyclohexylamine	+	34 (2)
Octylamine	+	38 (1)	

(values in brackets are uncertainties calculated from three measurements)

SHG tests were performed on the various salts of the racemic mixture to preselect the non-centrosymmetric phases and further investigations were conducted on these preselected compounds (such as DSC, XRPD, SC-XRD) to establish if the crystallized racemic mixture is not only non-centrosymmetric but also chiral (conglomerate).

First trials involved strong bases such as sodium hydroxide, potassium hydroxide or ammonium hydroxide but none of these derivatives gave positive SHG response whatever the solvent used for the crystallization of the salt (methanol, ethanol or isopropyl alcohol). These salts were thus discarded. Conversely other trials with alkyl amines led to eight positive SHG responses highlighting the corresponding salts as potential conglomerates (Table 3.4). Thus, the study was focused on this family of compounds.

3.2. IDENTIFICATION OF CONGLOMERATES

3.2.1. Methylammonium chlocyphos

SHG response was negative for this compound but further analyses were pursued for methylammonium chlocyphos salt to understand why it bypasses the trend of alkyl amines to give a SHG positive response when combining with chlocyphos.

DSC analyses of the crystallized racemic salt showed two endothermic events at 78.1 °C and at 161.3 °C (onset) corresponding to dehydration followed by melt (Figure 3.9). After annealing at 80 °C overnight, the thermal analyses of the annealed racemic displayed one endothermic event at 198.5 °C (onset) corresponding to its melting point.

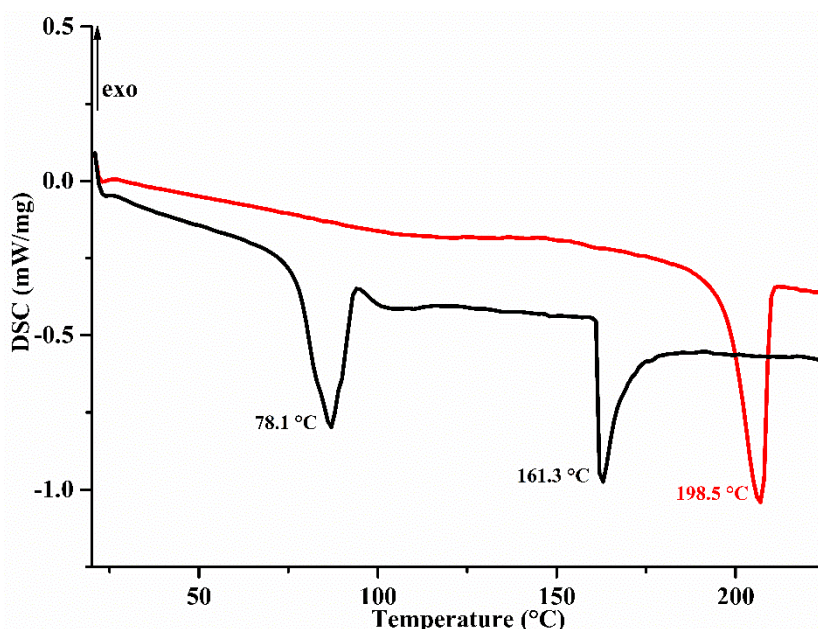


Figure 3.9: DSC curves of crystallized (black) and annealed (red, at 80 °C overnight) racemic methylammonium chlocyphos

The crystallized and annealed racemic methylammonium chlocyphos thus exhibit different solid phases and furthermore, SHG performed on the annealed (anhydrous) racemic methylammonium was also negative.

TGA-DSC analyses performed on the crystallized racemic salt indicated a mass loss of 4.19% of the total mass (Figure 3.10). The mass loss is less than the mass of one water molecule (which is ca. 5.53% of the total mass) but it confirms a reduction of the total mass of the salt which could be assimilated to dehydration.

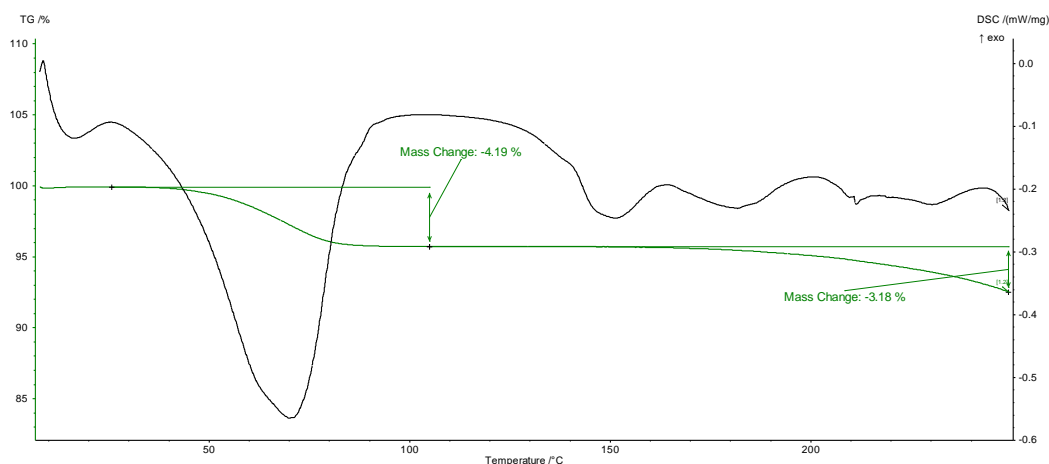


Figure 3.10: TGA-DSC analysis of crystallized racemic methylammonium chlocyphos

NMR analyses performed on the crystallized and the annealed salts show identical spectra for both phases because probably water molecules patterns could not be detectable in the NMR analysis (non-reported data).

Consistently with DSC measurements, XRPD measurements performed at room temperature for both crystallized and annealed salts show that their XRPD patterns are totally different (Figure 3.11).

Furthermore, XRPD measurements at different temperatures (TR-XRPD) were performed on the crystallized racemic salt. The results highlight two different XRPD patterns between 22 °C (room temperature) and 101 °C. A phase transition is observed starting at 40 °C and seems completed at 50 °C. Then, no change in the XRPD pattern is observed up to 101 °C and even when the sample is cooled back to 25 °C (Figure 3.12).

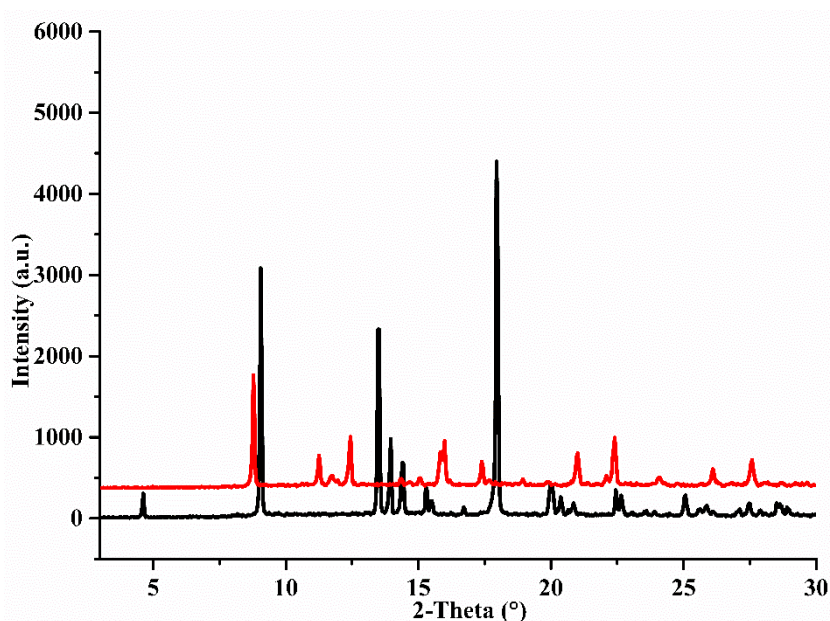


Figure 3.11: Crystallized (black) and annealed (red, at 80 °C overnight) XRPD patterns of racemic methylammonium chlocyphos

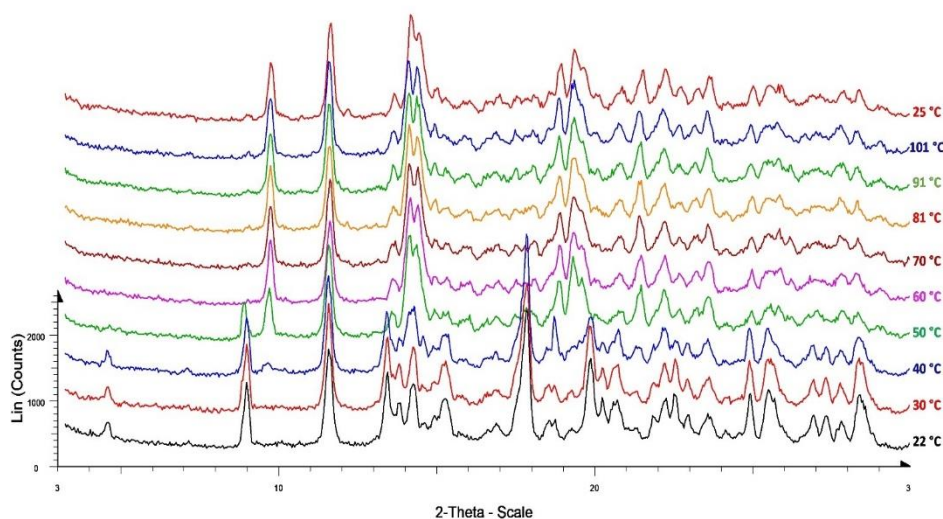


Figure 3.12: XRPD patterns of racemic methylammonium chlocyphos at different temperatures

Based on DSC, TGA-DSC and TR-XRPD measurements, the crystallized racemic methylammonium chlocyphos would crystallize as a racemic compound (hydrate). As the determination of its crystal structure is the better way to conclude and determine the fraction of water molecules, single crystals of racemic mixture methylammonium chlocyphos were grown and analysed by SC-XRD. The detailed crystal structure of methylammonium chlocyphos is presented in section 3.3 which is dedicated to the structural characterization of the various salts.

3.2.2. Ethylammonium chlocyphos

DSC analyses performed on the two ethylammonium chlocyphos samples showed one single endothermic event at 241.9 °C for racemic and at 274.9 °C for (*S*)-ethylammonium chlocyphos

(Figure 3.13). Thus, a difference of ca. 33 °C between the onset melting point of racemic and (*S*)- enantiomer samples is revealed, which is a common feature between a conglomerate-forming system and its pure enantiomers¹⁸.

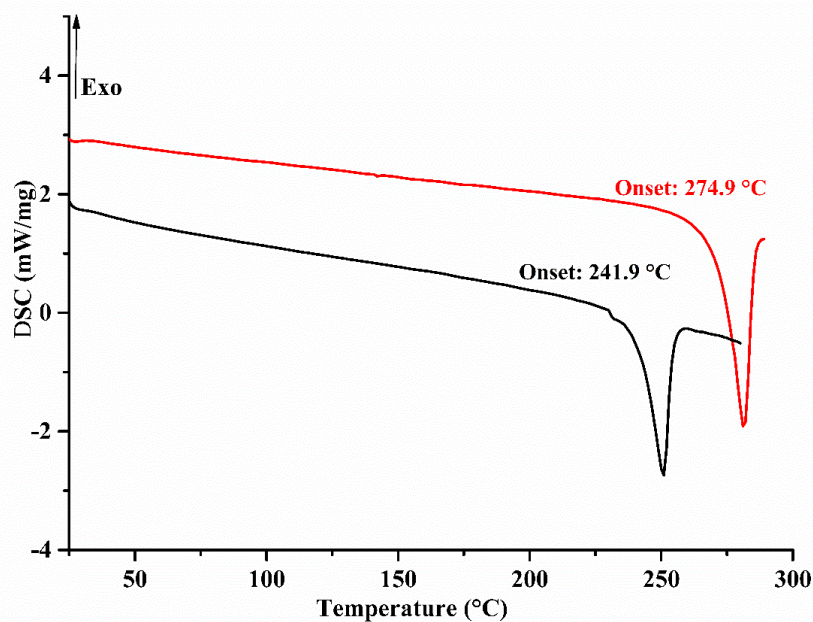


Figure 3.13: DSC curves of racemic (black) and (*S*)- (red) ethylammonium chlocyphos

Racemic ethylammonium chlocyphos salt gave a positive but relatively weak SHG signal. Similar XRPD patterns between racemic and (*S*)-ethylammonium chlocyphos were obtained at room temperature although with small angular shifts detected at 10° and in the range 20–30° in 2 θ (Figure 3.14). The shifted peaks observed in left- and right-hand sides from the XRPD patterns associated to the thermal and SHG results prompted us to envisage that the racemic mixture could crystallize as a conglomerate but with symmetrical partial solid solutions close to the enantiomer.

Numerous attempts to grow single crystals of sufficient size and quality of ethylammonium chlocyphos from the racemic mixture or mixtures of scalemic compositions failed. However, as spotting a conglomerate with partial solid solution is unusual, a thorough study of the phase diagram associated to this system was performed and will be presented in section 3.4.

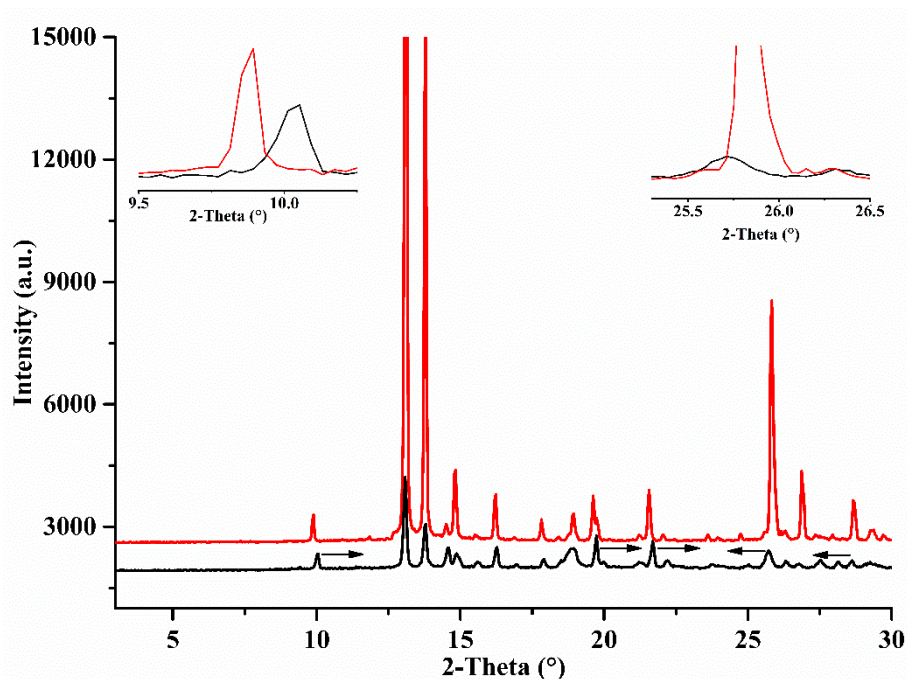


Figure 3.14: XRPD patterns of racemic (black) and (*S*)- (red) ethylammonium chlocyphos. The black arrows point the shifted peaks in left and right hands. The insets correspond to a zoom on the data at 10° (right hand shift) and at 25.8° (left hand shift).

3.2.3. Propylammonium chlocyphos

DSC analyses of each salt display at least two endothermic events at 154.7 °C and 182.5 °C (onset melting point) for racemic salt and at 197.3 °C and 223.1 °C (onset melting point) for (*S*)-propylammonium chlocyphos corresponding to their polymorphic transition temperatures and melting points respectively (Figure 3.15).

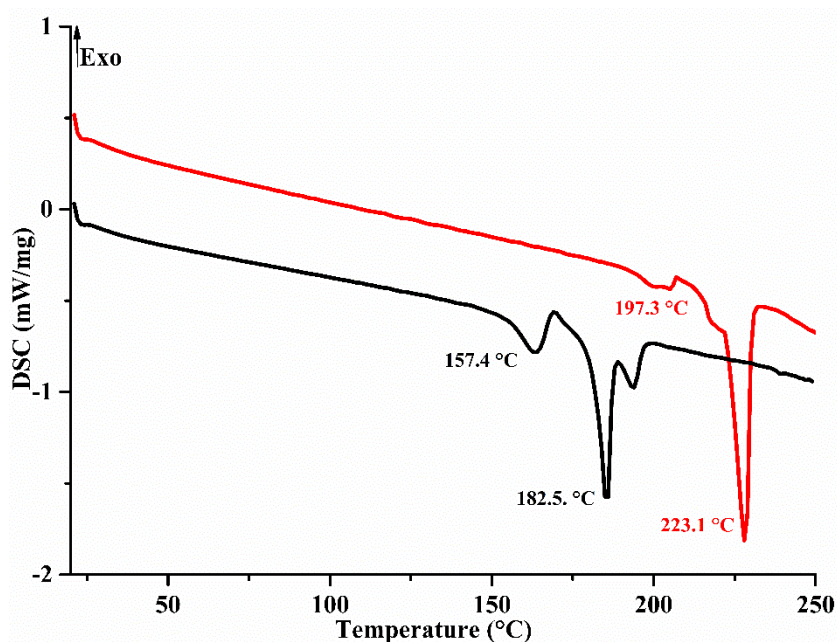


Figure 3.15: DSC curves of racemic (black) and (*S*)- (red) propylammonium chlocyphos

Propylammonium chlocyphos gave a positive SHG signal and a non-centrosymmetric crystal could be expected. However, XRPD patterns for racemic and (*S*)-enantiomer samples are totally different (Figure 3.16). Thus, temperature resolved (TR) XRPD measurements were performed for the racemic salt to help in the attribution of the multiple events observed on the thermograms (Figure 3.15).

TR-XRPD measurements highlighted several phase transitions but none of their X-ray pattern was superimposable to that of the enantiopure compound (Figure 3.17).

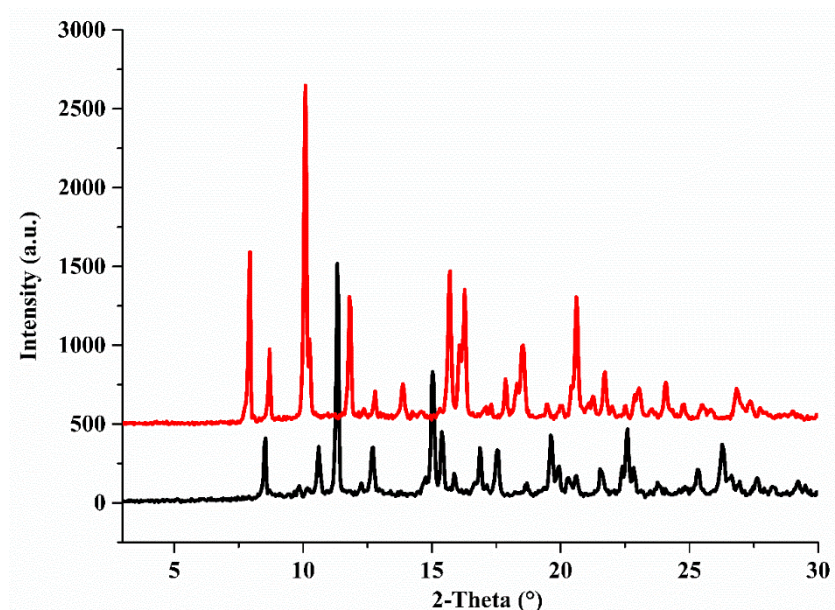


Figure 3.16: XRPD patterns of racemic (black) and (*S*)- (red) propylammonium chlocyphos

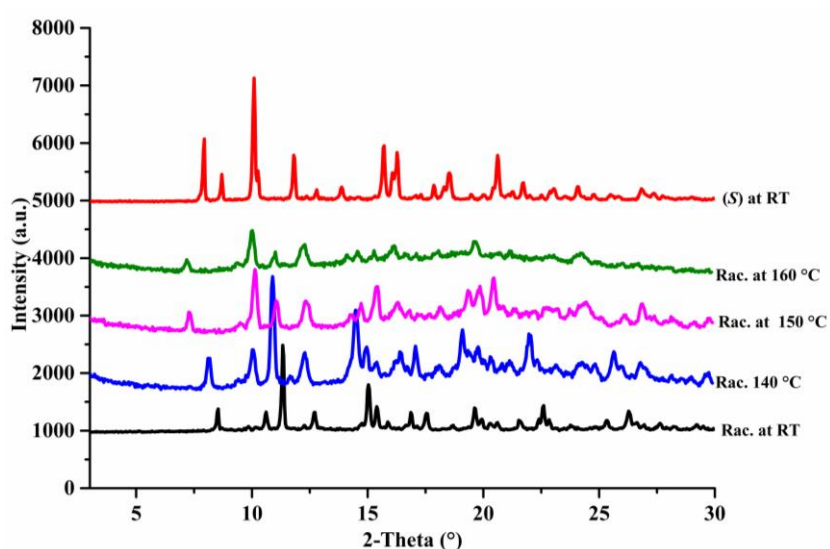


Figure: 3.17: XRPD patterns of propylammonium chlocyphos at different temperatures (RT: for room temperature, Rac.: for racemic mixture)

Finally, various solid phases of propylammonium chlocyphos were highlighted by the DSC analyses performed on the racemic and (*S*) salts. Those results point out the existence of several

crystalline phases (polymorphs or hydrated/solvated forms or racemic compound) for propylammonium chlocyphos. The phase behaviour of propylammonium chlocyphos is thus rather complex and requires further studies to understand more the behaviour of this compound. Nevertheless, single crystals of one racemic mixture form were obtained and analysed by SC-XRD (section 3.3.1).

3.2.4. Butylammonium, Isobutylammonium, Pentylammonium, Hexylammonium and Cyclohexylammonium chlocyphos

The DSC analyses performed on these compounds display a single thermal event either for the enantiomer or the racemic compounds (Figure 3.18) except for the cyclohexylammonium salt for which the melt is followed by a decomposition.

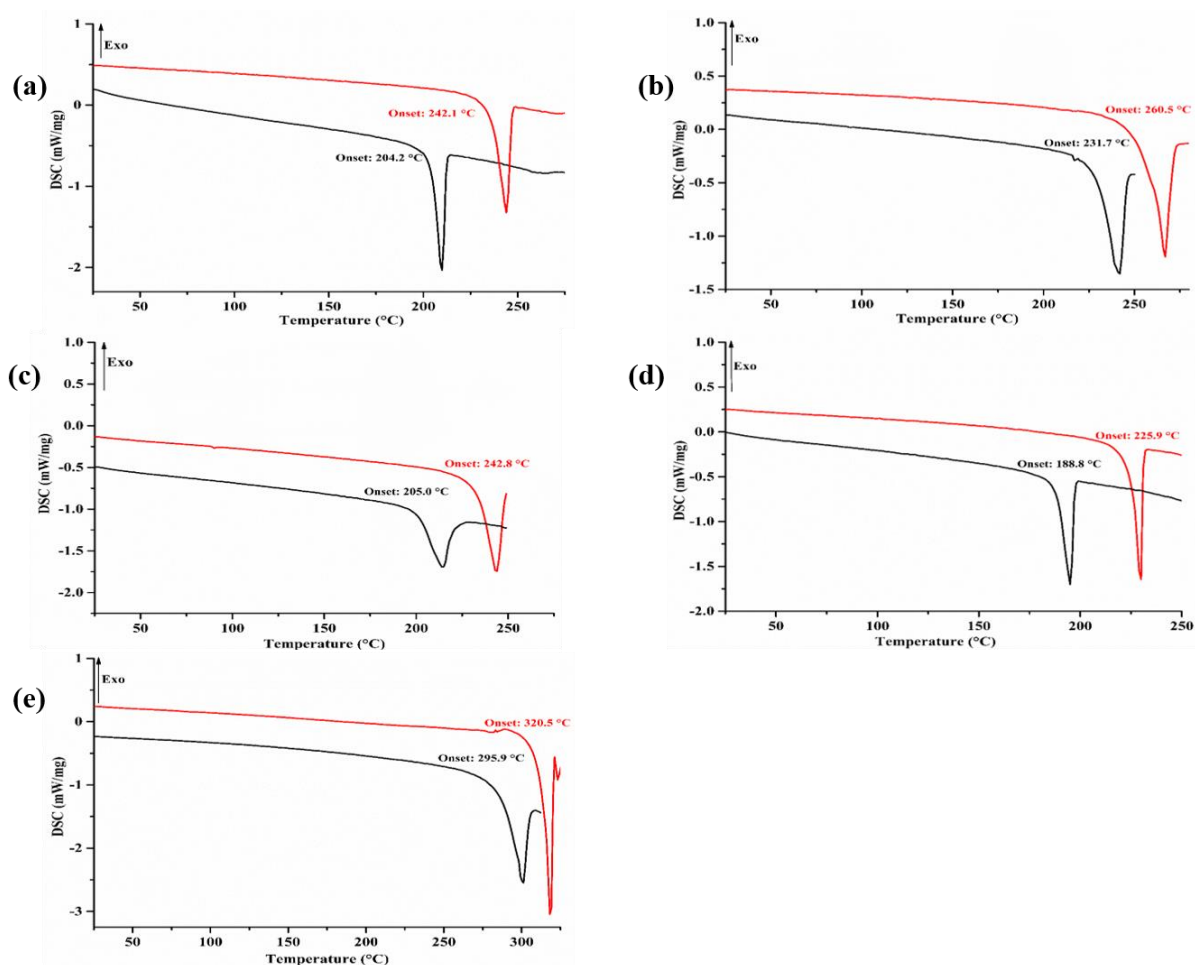


Figure 3.18: DSC curves of racemic (black) and (*R*)-(red) (a) Butylammonium, (b) Isobutylammonium, (c) Pentylammonium, (d) Hexylammonium and (e) Cyclohexylammonium chlocyphos.

DSC analyses for each salt derivative revealed that the difference between melting point of racemic mixture and pure enantiomer samples ranges between 25 and 38 °C (Table 3.5), which is a common feature between a conglomerate forming system and its pure enantiomers^{19,6}.

Table 3.5: Difference in the temperature of fusion (T_F) of enantiomer and racemic mixture chlocyphos salts

Salts	T_F (°C) Enantiomer	T_F (°C) Racemic mixture	ΔT_{exp} (°C)
Butylammonium	242.1	204.2	37.9
Isobutylammonium	260.5	231.7	28.8
Pentylammonium	242.8	205.0	37.8
Hexylammonium	225.9	188.8	37.1
Cyclohexylammonium	320.5	295.9	24.6

Concerning the XRPD analyses, for each salt, the XRPD patterns of racemic and pure enantiomer samples were found to be identical (i.e. perfectly superimposable) as reported in Figure 3.19.

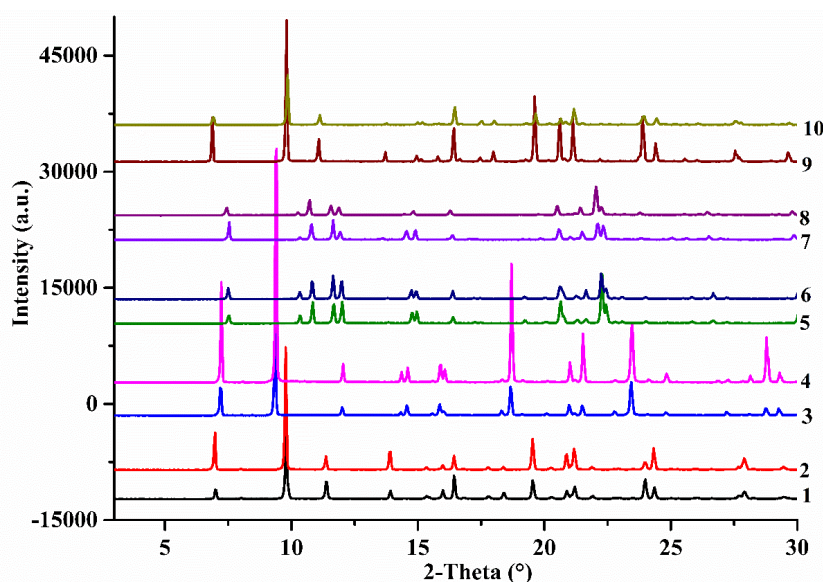


Figure 3.19: From bottom to top: XRPD patterns of racemic (1) and (*R*)- (2) Butylammonium, racemic (3) and (*R*)- (4) Isobutylammonium, racemic (5) and (*R*)- (6) Pentylammonium, racemic (7) and (*R*)- (8) Hexylammonium, racemic (9) and (*R*)- (10) Cyclohexylammonium chlocyphos.

Based on the results obtained from SHG pre-screening, XRPD and DSC measurements, we can conclude that butylammonium, isobutylammonium, pentylammonium, hexylammonium, and cyclohexylammonium chlocyphos would likely crystallize as conglomerate forming systems. Single crystals were grown to confirm these results by the determination of the crystal structure of these salts (Section 3.3.1).

3.2.5. Octylammonium chlocyphos

In the case of the octylammonium chlocyphos, DSC analyses for each salt display two endothermic events at 58.2 °C and at 142.3 °C (onset melt) for the racemic salt and at 138.9 °C and at 189.9 °C (onset melt) for (*S*) salt (Figure 3.20).

TGA-DSC analyses performed on the racemic salt indicate that the first endothermic event at 58.2 °C corresponds to dehydration i.e. a mass loss of one water molecule (ca. 4.01%) (Figure 3.21). The temperature difference of their melting point is circa 47.6 °C which is suitable for a conglomerate forming system. However, XRPD patterns at ambient temperature of racemic and (*S*)-octylammonium chlocyphos are totally different (Figure 3.22).

Even though, racemic octylammonium chlocyphos gave a strong SHG signal, the XRPD patterns of racemic and (*S*) salts are different. Several attempts to grow single crystals from the racemic mixture did not succeed. Conclusively, we can state that octylammonium chlocyphos likely crystallizes as a non-centrosymmetric crystal, probably a monohydrate racemic compound.

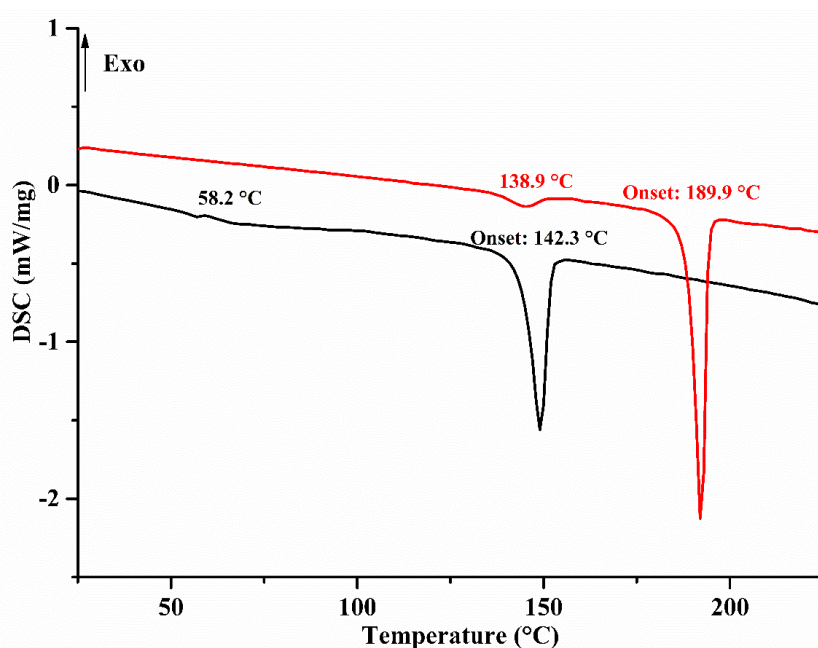


Figure 3.20: DSC curves of racemic (black) and (*S*)-(red) octylammonium chlocyphos

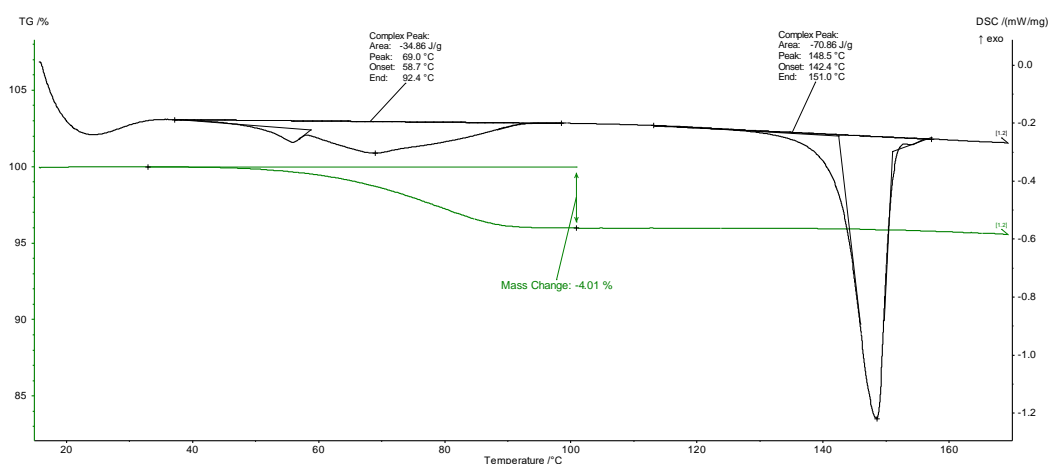


Figure 3.21: TGA (green curve) and DSC (black curve) analyses for racemic octylammonium chlocyphos

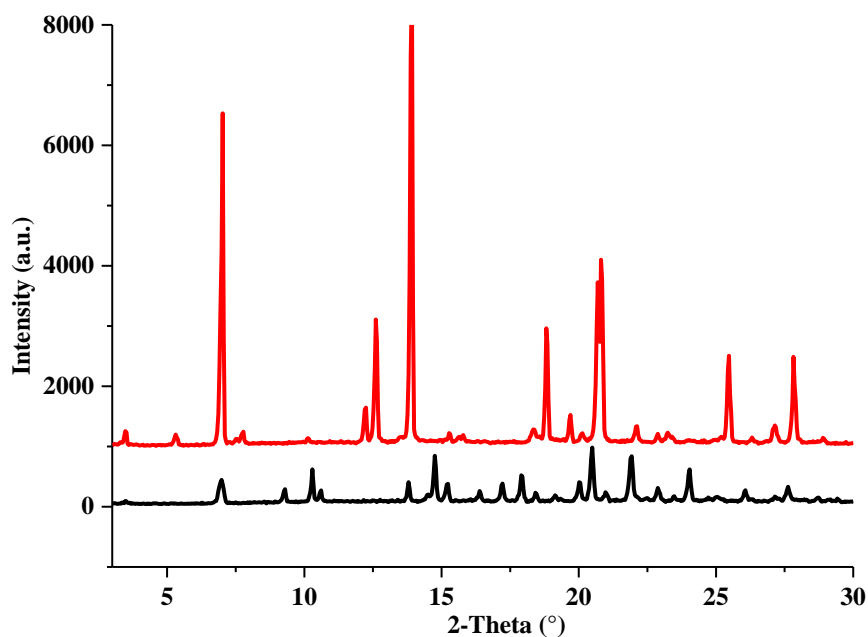


Figure 3.22: XRPD patterns of racemic (black) and (S)-(red) octylammonium chlocyphos

3.2.6. Calculation of the eutectic temperature for the conglomerate derivatives

Extra indications about the nature (conglomerate or not) of the spotted compound can be obtained using the Schroder-Van Laar (simplified) equations^{20,21} (equation 3.1). Indeed, this equation can be used to roughly calculate (using thermal data obtained for the pure enantiomer), the eutectic temperature at the eutectic composition ($x = 0.5$ mol) when the system is ideal ('stable' conglomerate).

$$\ln X = \frac{\Delta H_F}{R} \left(\frac{1}{T_F} - \frac{1}{T_E} \right) \quad (3.1)$$

Where $x = 0.5$ is the mole fraction at the eutectic composition; $R = 8.314 \text{ J mol}^{-1} \text{ K}^{-1}$ is the gas constant; ΔH_F (J mol^{-1}) and T_F (K) are the heat and temperature of fusion of the pure enantiomer; T_E (K) and $T_{\text{exp.}}$ (K) are the calculated and experimental eutectic temperatures; MW (g mol^{-1}) is the molecular weight of the salt.

The calculated and experimental eutectic temperatures at the eutectic composition are summarized in Table 3.6 for each salt derivative.

Table 3.6: summary of the calculation of the eutectic temperature for chlocyphos salts

Chlocyphos salts	Enantiomer (Thermal data)			Schroder Van Laar calculated value	Racemic mixture (Experimental value)
	T _F (K)	ΔH _F (J g ⁻¹)	MW (g mol ⁻¹)	T _E (K) / (°C)	T _{exp.} (°C)
Ethylammonium	548.05	180.6	321.73	519.79 / 246.6	241.9
Propylammonium	496.25	72.35	335.70	443.97 / 170.8	182.5
Butylammonium	514.95	104.60	349.78	476.32 / 203.2	204.2
Isobutylammonium	536.55	148.30	349.78	506.36 / 233.2	231.7
Pentylammonium	515.95	107.70	363.81	479.56 / 206.4	205.0
Hexylammonium	498.85	91.12	377.83	460.40 / 187.3	188.8
Cyclohexylammonium	586.95	309.70	375.82	570.35 / 297.2	295.9

(values in bold are consistent with Schroder-van Laar equations)

The uncertainties on the experimental values is ca. ± 2 °C within the experimental errors. Therefore, the calculated eutectic temperatures are in good agreement with the experimental values for butylamine, isobutylamine, pentylamine, hexylamine and cyclohexylamine derivatives which are expected to be stable conglomerates (equation 3.1. is applicable only for ‘ideal’ systems).

However, the difference between calculated and experimental temperatures is ca. 4.7 °C for ethylammonium chlocyphos and 11.7 °C for propylammonium chlocyphos.

For ethylammonium chlocyphos, the deviation from the ideal case could originate from the existence of a solid solution. This could be established by calculating the entropy of mixing of the two enantiomers in the liquid state as described in the equation (3.2), by Leclercq, Collet and Jacques^{22,23}.

$$-\Delta S_{liq}^m = \frac{\Delta H_A^F}{T_A^F} - \frac{\Delta H_R^F}{T_R^F} - \frac{\Delta H_A^F - \Delta H_R^F}{T_A^F - T_R^F} \ln \left(\frac{T_A^F}{T_R^F} \right) \quad (3.2)$$

with ΔS_{liq}^m , the entropy of mixing of the two enantiomers at the liquid state; ΔH_A^F and T_A^F , the enthalpy and temperature of fusion of the pure enantiomer and ΔH_R^F and T_R^F , the enthalpy and temperature of fusion of the racemic mixture.

Grant and co-workers²⁴ have used this thermodynamic approach to identify racemic species from thermal data and recently Bredikhin et al.²³ have underlined the presence of entropy anomaly in the melting of the two enantiomers of chiral drug timolol (another conglomerate

with partial solid solution). In the following, we use the same approach to verify the consistency between thermal data and the existence of a partial miscibility in the solid state for racemic ethylammonium chlocyphos system.

For an ideal conglomerate, the two enantiomers are perfectly immiscible in the solid state, their enthalpy of mixing is equal to zero. At the liquid state, the melting of the mixed enantiomers should be congruent, and their enthalpy of mixing is approximatively zero. Thus, the entropy of mixing will be constant, and the value is given by $R \ln 2$.

$$\Delta S_{liq}^m = R \ln 2 = 5.76 \text{ J mol}^{-1} \text{ K}^{-1} \quad (3.3)$$

For ethylammonium chlocyphos system, by replacing in equation (3.3) the experimental data obtained from DSC analysis, the entropy of mixing in the liquid state gives a value of $\Delta S_{liq}^m = 6.0 \pm 0.9 \text{ J mol}^{-1} \text{ K}^{-1}$. The value of $5.76 \text{ J mol}^{-1} \text{ K}^{-1}$ is within error the same as the experimental value of $6.0 \pm 0.9 \text{ J mol}^{-1} \text{ K}^{-1}$. So, unfortunately this does not allow us to conclude on the existence of a solid solution.

For propylamine derivative, the difference between the calculated and experimental values is due to the polymorphic phases of the racemic salt²².

Except for ethylammonium chlocyphos for which single crystals of sufficient size and good quality have not been obtained, the resolution of the crystal structures of the racemic mixture by SC-XRD have been performed to definitively conclude on the nature of the spotted compounds. As will be shown hereafter it revealed a family of conglomerate forming- systems formed between chlocyphos and alkyl-amine.

3.3. CRYSTAL STRUCTURE DETERMINATION BY SC-XRD

3.3.1. Butylammonium, Isobutylammonium, Pentylammonium, Hexylammonium, Cyclohexylammonium and Propylammonium chlocyphos.

3.3.1.1. Crystallographic data

For each derivative, the crystal structures have been determined by SC-XRD for the single crystal (average size 1-2 mm) obtained from the racemic mixture. All crystal structures were determined from single crystal diffraction on a SMART APEX diffractometer (with $\text{MoK}\alpha_1$ radiation: $\lambda = 0.71073 \text{ \AA}$). The crystallographic data are summarized in Table 3.7. As expected, every crystal phase corresponds to a chiral space group even for propylammonium salt.

Table 3.7: Crystallographic data* of the conglomerate derivatives

Alkyl-amine	Chlocyphos					
	Butyl	Isobutyl	Pentyl	Hexyl	Cyclohexyl	Propyl
Chem. Formula	[C ₁₁ H ₁₃ ClO ₄ P] [C ₄ H ₁₂ N]		[C ₁₁ H ₁₃ ClO ₄ P] [C ₅ H ₁₄ N]	[C ₁₁ H ₁₃ ClO ₄ P] [C ₆ H ₁₆ N]	[C ₁₁ H ₁₃ ClO ₄ P] [C ₆ H ₁₄ N]	[C ₁₁ H ₁₃ ClPO ₄] [C ₃ H ₁₀ N]
CSD number	1912254	1912255	1912258	1912271	1912256	1912822
MW / g.mol ⁻¹	349.78		363.81	377.83	375.82	335.7
Temperature (K)	300					
Crystal system	Monoclinic		Orthorhombic		Monoclinic	
Space group	P2 ₁ (n°4)		P2 ₁ 2 ₁ 2 ₁ (n°19)		P2 ₁ (n°4)	
Z, Z'	2, 1		4, 1		2, 1	
a / Å	11.282 (1)	11.436 (1)	7.0043 (6)	7.1595 (5)	11.355 (1)	11.427 (8)
b / Å	6.515 (7)	6.432 (8)	16.476 (1)	16.6398 (11)	6.5917 (7)	6.541 (5)
c / Å	12.958 (1)	12.819 (2)	17.303 (1)	17.3695 (12)	13.076 (1)	12.924 (9)
β / °	98.767 (2)	104.407 (2)	90	90	97.120 (2)	100.02 (1)
V / Å ³	941.4 (1)	913.3 (2)	1996.9 (3)	2069.3 (2)	971.2 (1)	951.4 (1)
N° reflexions unique / I>2σI	3513 / 2561	3297 / 2640	3809 / 2338	4206 / 3202	3933 / 3257	3746 / 835
Final R1/wR2 (I>2σI)	0.0517 / 0.1109	0.0496 / 0.1110	0.0689 / 0.1523	0.0585 / 0.1430	0.0462 / 0.0942	0.0799 / 0.1702
Final R1/wR2 (all data)	0.0735 / 0.1264	0.0649 / 0.1247	0.1142 / 0.1781	0.0781 / 0.1561	0.0570 / 0.1007	0.2893 / 0.2262
Absolute structure (Flack) parameter	-0.17 (10)	0.29 (9)	0.52 (16)	0.15 (14)	0.30 (1)	0.3 (2)

(*crystal structure determined from single crystal obtained from the racemic mixture)

For each salt, except the propylammonium salt, the calculated XRPD and experimental XRPD patterns match (reported in Appendix III, from Figure A. III-1 to Figure A. III-5), which means that the single crystals are representative of the bulk sample and confirm the conglomerate-forming system. However, several Flack¹⁹ parameters are not close to zero and cast some doubt (high uncertainties) about the enantiomeric purity of these phases. For instance, for pentylammonium chlocyphos, the Flack parameter is 0.52 (16) and raises the possibility of epitaxy between (*R*)- and (*S*)-enantiomers or even multi-epitaxy. Moreover, racemic pentylammonium chlocyphos could crystallize as a metastable racemic compound.

3.3.1.2. Crystal structures description

Whatever the two families of crystal structures (monoclinic *P*2₁, and orthorhombic *P*2₁2₁2₁), asymmetric unit is always composed by two entities: one deprotonated chlocyphos molecule and one protonated amine molecule as represented in Figure 3.23 for isobutylammonium

chlocyphos. Inside the asymmetric unit, strong interactions are established by ionic hydrogen bonds (Table 3.8) between the oxygen atom O (2) of anionic chlocyphos and the protonated amine N (1) of the amine cation (Figure 3.23) and are wrapped around a 2_1 screw axis and led to molecular bond chains spreading along **a** or **b** direction (Figure 3.24). Every ammonium moiety is connected to three chlocyphos anions: two are consecutive and form a single row (along **b** axis) and the third one (along **a** axis) connects to the adjacent row leading to double row periodic bond chains that build the crystal packing of isobutylammonium chlocyphos (Figure 3.25). These periodic bond chains are stacked along **c** direction, and the cohesions are ensured by van der Waals interactions between amine chains and π - π interactions between neighbouring chlocyphos benzyl rings.

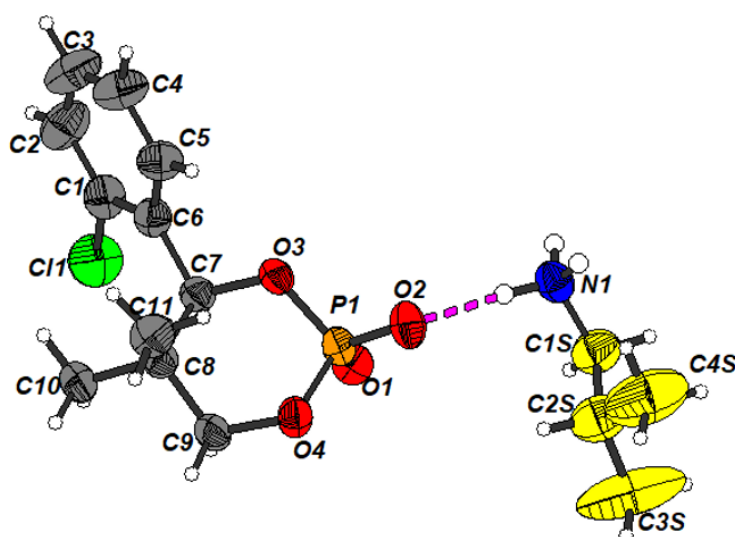


Figure 3.23: Asymmetric unit of racemic isobutylammonium chlocyphos, in thermal ellipsoidal representation with labelled atoms (pink dashed line represents the ionic hydrogen bond).

Table 3.8: Hydrogen bond characteristic lengths^a and angles of isobutylammonium chlocyphos

D-H...A	d(H...A) (Å)	d(D...A) (Å)	<(DHA) (°)
N(1)-H(1A)...O(2) #1	1.80	2.682 (4)	173.4
N(1)-H(1B)...O(1) #2	1.94	2.811 (3)	166.7
N(1)-H(1C)...O(1) #3	1.95	2.806 (4)	160.0

^aSymmetry operations used to generate equivalent atoms: #1: $x, y - 1, z - 1$; #2: $-x + 1, y - 1/2, -z + 1$; #3: $x, y, z - 1$.

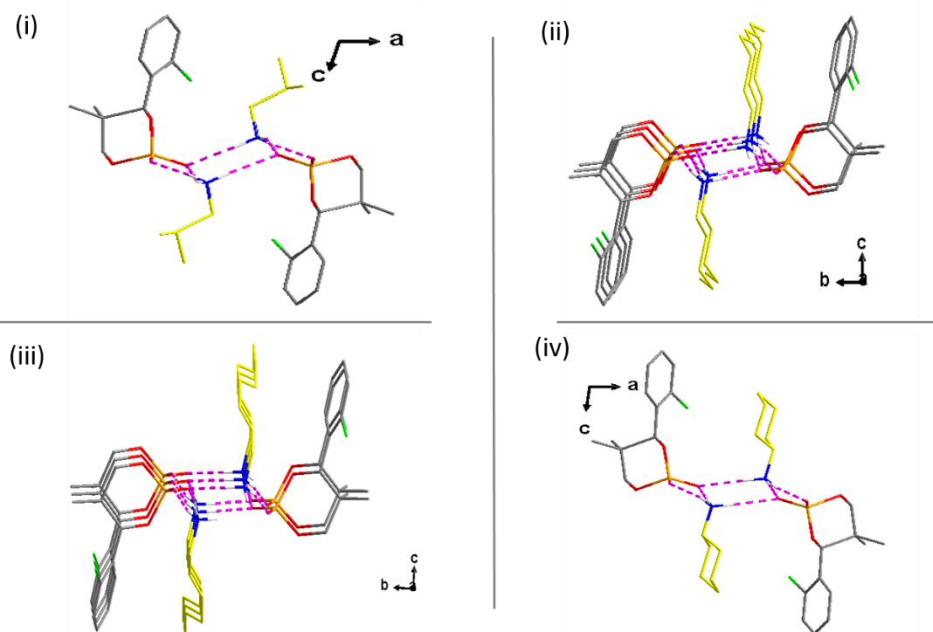


Figure 3.24: Periodic bond chains (PBC) around the 2_1 screw axis formed by the ionic hydrogen bonds of (i) Isobutylammonium, (ii) Pentylammonium, (iii) Hexylammonium and (iv) Cyclohexylammonium chlocyphos.

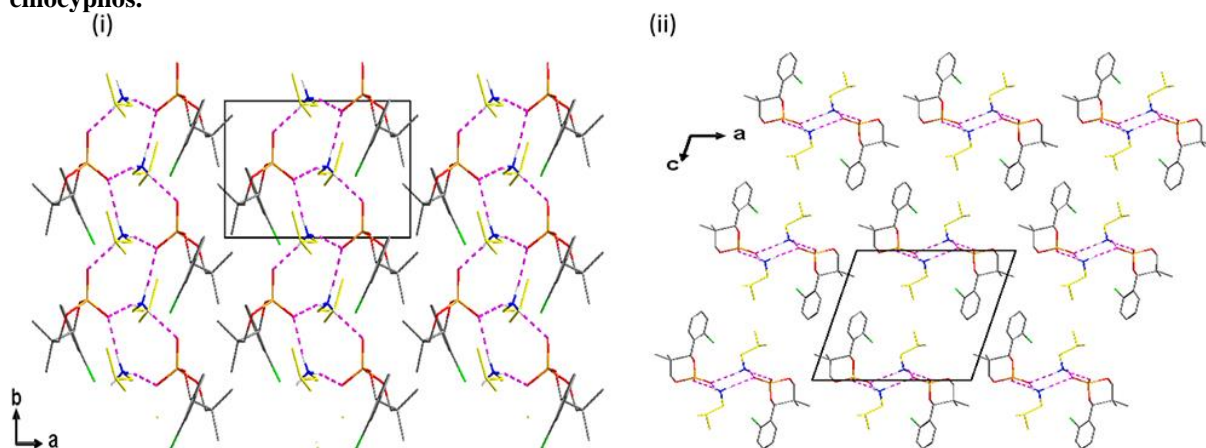


Figure 3.25: Double row periodic bond chains (hydrogen bonds represented in purple) and the projection of the whole packing along c (i) and b (ii) axes for isobutylammonium chlocyphos. The black rectangles represent a unit cell.

The crystal structures clearly show similarities for all conglomerate derivatives regardless of their space groups $P2_1$ or $P2_12_12_1$ (reported in Appendix III, from Figure A. III-8 to Figure A. III-13). The unit cell dimensions are closely related: **a**, **b**, and **c** parameters remain close for butylammonium, isobutylammonium, and cyclohexylammonium chlocyphos, which crystallize in the same space group $P2_1$. Similar observations can be noted for the unit cell parameters (**a**, **b**, and **c**) of the $P2_12_12_1$ structures for pentylammonium and hexylammonium chlocyphos. The hydrogen bond networks involving the heteroatoms in the molecular ribbon along **a** or **b** axes are identical. These characteristics lead to the same pattern of periodic bond chains and thus a clear homogeneity among the members of that family.

Propylammonium chlocyphos (with the $P2_1$ space group) has similar cell parameters and crystal structure packing even though its calculated and experimental XRPD patterns obtained from the racemic mixture are not identical (reported in Appendix III, Figure A. III-6). The quality of the analysed crystal obtained from racemic salt was not good (the number of unique reflections was 3748 and 835 with $I > 2\sigma I$). However, the crystal structure determined from SC-XRD data shows extensive analogies with those found for the longer alkyl amines. Thus, the crystal structure unambiguously proves the presence of a conglomerate among the different possible forms.

3.3.2. Methylammonium chlocyphos

3.3.2.1. Crystallographic data

From the single crystal data of the racemic mixture, methylammonium chlocyphos was proven to be a sesquihydrate salt crystallizing in the monoclinic centrosymmetric $C2/c$ space group. The crystallographic data reported in Table 3.9 confirm the SHG inactivity and highlight the hydrated character of the salt (1.5 water molecules: sesquihydrate).

Table 3.9: crystallographic data of racemic methylammonium chlocyphos (sesquihydrate)

Chem. Formula	$[C_{11}H_{13}ClO_4P] [CH_3NH_3]_{1,5} H_2O$
CSD number	1968943
MW / $g.mol^{-1}$	334.73
Crystal system	Monoclinic
Space group	$C2/c$ (n°15)
Z, Z' (asymmetric units per unit cell)	8,1
$a / \text{Å}$	41.447 (5)
$b / \text{Å}$	6.5284 (7)
$c / \text{Å}$	12.464 (1)
$\alpha / ^\circ$	90
$\beta / ^\circ$	105.655 (2)
$\gamma / ^\circ$	90
$V / \text{Å}^3$	3247.5 (6)
$d_{calc} / g.cm^{-3}$	1.369 (2)
F (000) / e^-	1416
Absorption coefficient μ (MoK α_1) / mm^{-1}	0.354
N° reflections unique / $I > 2\sigma I$	3312 / 2725
Final R1 / wR2 ($I > 2\sigma I$)	0.0518 / 0.1373
Final R1 / wR2 (all data)	0.0618 / 0.1474

3.3.2.2. Crystal structure description

The asymmetric unit of the racemic methylammonium chlocyphos sesquihydrate is composed of one and a half water molecules, one molecule of deprotonated chlocyphos, and one protonated molecule of methylamine (Figure 3.26). Inside the asymmetric unit, strong hydrogen bonds are established by ionic-hydrogen bonds (Table 3.10) between the oxygen atom O (3) of anionic chlocyphos and the protonated amine N (1) of the amine moiety for one hand and between the oxygen atom O (4) of anionic chlocyphos and the oxygen atoms O (w1 and w2) of the water molecules in the other hand and led to molecular bond chains through the ammonium moiety along **b** direction (Figure 3.27). These ribbons establish hydrogen bonds that generate molecular layer and lead to the periodic bond chains projected along **c** and **b** axes (Figure 3.28).

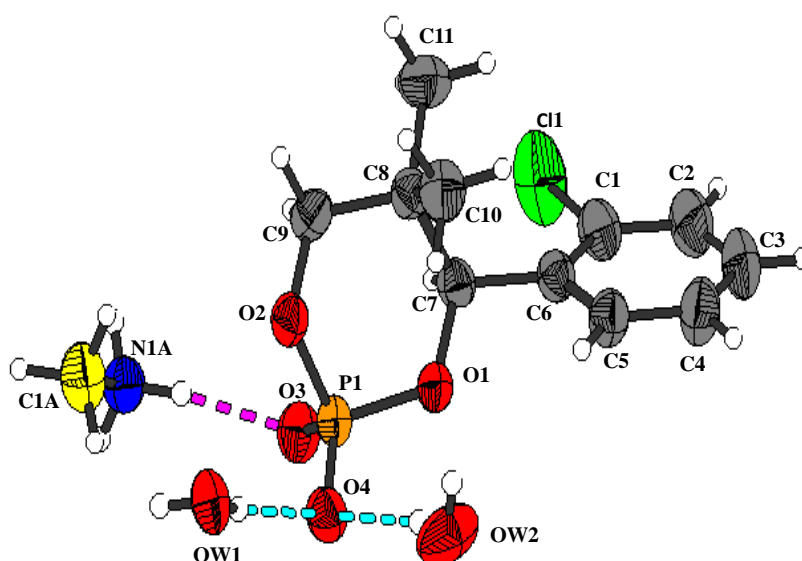


Figure 3.26: Asymmetric unit in thermal ellipsoidal representation with labelled atoms. The pink dashed line is ionic hydrogen bond.

Table 3.10: Ionic hydrogen bonds characteristics lengths and angles^a

D-H...A	d(D-H) (Å)	d(H...A) (Å)	d(D...A) (Å)	<(DHA) (°)
OW2-H(2O)...O (4)	0.68 (3)	2.10 (3)	2.773 (3)	169 (4)
N(1A)-H(1A5)...O (3)	0.89	1.87	2.750 (2)	169.6
N(1A)-H(1A6)...OW2 #2	0.89	1.89	2.764 (3)	165.8
N(1A)-H(1A4)...OW1 #1	0.89	1.96	2.835 (2)	168.8
OW2-H(3O)...O(3) #3	0.77 (3)	2.03 (3)	2.792 (3)	172 (3)
OW1-H(1O)...O(4) #4	0.81 (3)	1.93 (3)	2.7227 (19)	167 (3)

^asymmetry transformations used to generate equivalent atoms: #1: $x, y+1, z$; #2: $x, -y+2, z-1/2$; #3: $x, y-1, z$; #4: $-x+1, y, -z+1/2$.

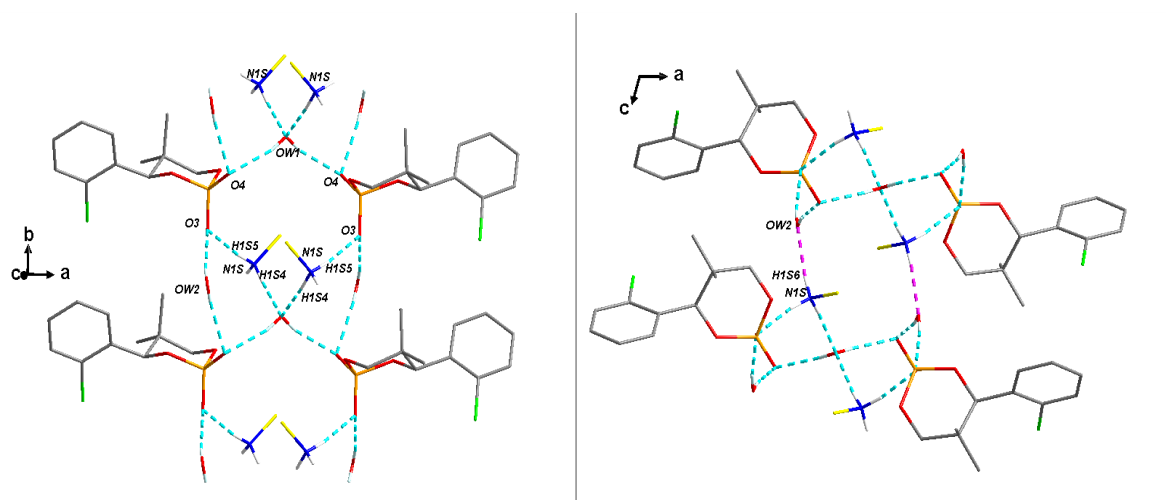


Figure 3.27: Molecular bond chain (left) and two consecutive molecular bond chains along b axis established by ionic hydrogen bonds (right)

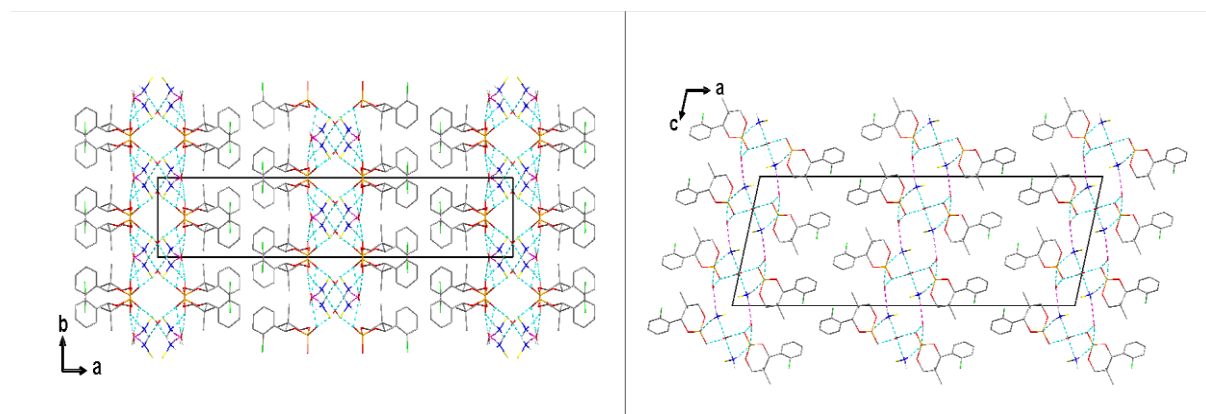


Figure 3.28: Periodic bond chains and the projection of the whole packing along c (left) and b (right) axes. The black rectangle represents a unit cell.

The experimental powder diffraction pattern obtained from the bulk, and the calculated powder pattern from the single crystal data show the representativeness of the analysed crystals (Figure 3.29). The crystal structure was deposited in the Crystallographic Structure Database (CSD) under the code number CCDC 1968943.

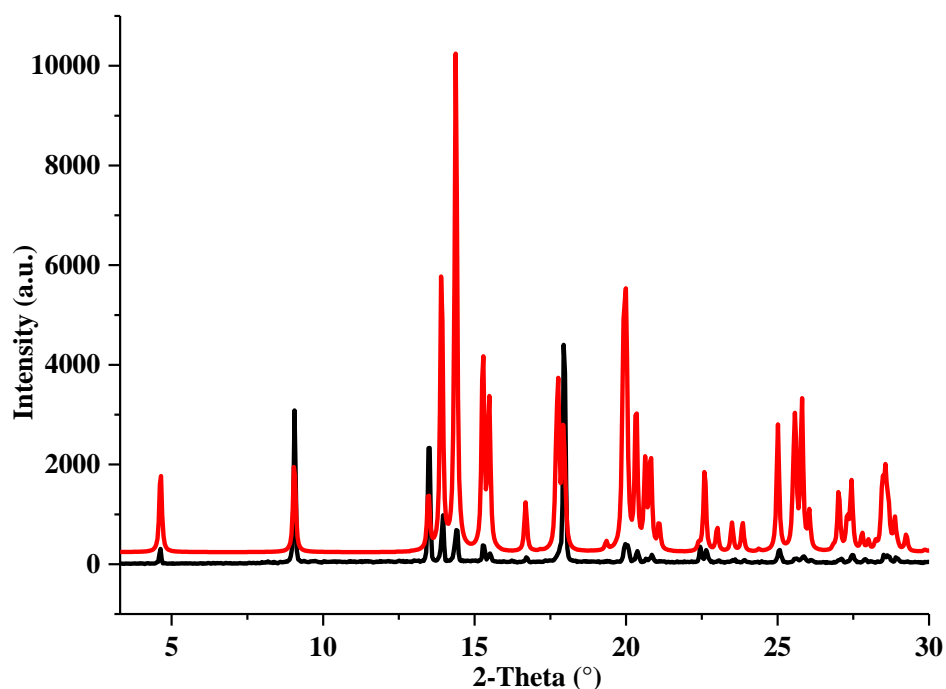


Figure 3.29: Calculated (red) and experimental (black) XRPD patterns of racemic methylammonium chlocyphos sesquihydrate.

3.3.3. Ethylammonium chlocyphos

3.3.3.1. Crystallographic data

Numerous attempts to grow single crystals of sufficient size and quality of ethylammonium chlocyphos from the racemic mixture failed. The reasons of this phenomenon remain unclear. Nevertheless, for this salt, it was hypothesised that the racemic mixture could crystallize as a conglomerate with partial solid solution close to the enantiomer. So, it can be speculated that compositional disorder (i.e. solid solution) inhibited the growth of large enough good quality crystals. This fact can be due to the presence of the counter enantiomer in the crystal lattice causing a high density of disorder/defects. This phenomenon has already been observed for other conglomerates with partial solid solutions^{25,26}.

Even so, the crystal structure has been determined by single crystal X-ray diffraction for pure enantiomers. Their crystallographic data, similar to those of the members of the alkylammonium chlocyphos family, are reported in Table 3.11.

Table 3.11: Crystallographic data of (*S*)- and (*R*)-ethylammonium chlocyphos

Enantiomer salt	(<i>S</i>)-enantiomer	(<i>R</i>)-enantiomer
Chem. Formula	[C ₁₁ H ₁₃ ClPO ₄]	[C ₂ H ₅ NH ₃]
CSD number	1968942	1968941
MW / g mol ⁻¹	321.73	
Crystal system	Orthorhombic	
Space group	P2 ₁ 2 ₁ 2 ₁ (n°19)	
Z, Z' (asymmetric units per unit cell)	4,1	
<i>a</i> / Å	6.5230 (5)	6.5205 (4)
<i>b</i> / Å	6.9313 (6)	6.9248 (5)
<i>c</i> / Å	36.119 (3)	36.100 (2)
α / °	90	90
β / °	90	90
γ / °	90	90
<i>V</i> / Å ³	1633.1 (2)	1630.03 (2)
<i>d</i> _{calc} / g.cm ⁻³	1.309 (2)	1.311 (2)
F (000) / e ⁻	680	680
Absorption coefficient μ (MoK α_1) / mm ⁻¹	0.343	0.344
N° reflections unique / I > 2 σ I	3329 / 2021	3320 / 2711
Final R1 / wR2 (I > 2 σ I)	0.0483 / 0.1042	0.0491 / 0.1319
Final R1 / wR2 (all data)	0.0838 / 0.1116	0.0613 / 0.1440
Absolute structure (Flack) parameter	-0.06 (1)	-0.06 (12)

Note that, concerning the anisotropic displacement parameters (ADP), they did not reveal any disorder in the crystal structure of the pure (*S*)- and (*R*)-ethylammonium chlocyphos^{25,27}. Indeed, when the disorder is refined on the terminal carbon atom of the ammonium cation, the adjacent carbon atom along the alkyl chain is no more anisotropically defined.

3.3.3.2. Crystal structure description

The hydrogen bond networks of (*S*)- and (*R*)-ethylammonium chlocyphos involving the heteroatoms in the molecular ribbon along **a** and **b** axes are also identical and analogical to the hydrogen networking of the other members of this family of conglomerates (Appendix III, Figure A. III-14 and Figure A. III-15). Their characteristics lead to the same pattern of periodic bond chains and thus a clear homogeneity among this family of conglomerates.

3.4. INVESTIGATION OF THE PARTIAL SOLID SOLUTION OF ETHYLAMMONIUM CHLOCYPHOS

Theoretically, the shape of the binary phase diagram of a conglomerate with partial miscibility in the solid state can be predicted by evaluating the minor/major differences in the XRPD patterns between the racemic and pure enantiomer samples. For the construction of the binary phase diagram, we have performed several DSC measurements to obtain: (i) the temperature and enthalpy of the eutectic transformation (ii) the end of melting for selected composition mixtures.

3.4.1. DSC measurements of different mixtures

Different mixtures of racemic mixture and (*S*)-ethylammonium chlocyphos were weighted, completely dissolved in isopropyl alcohol under magnetic stirrer and left at room temperature to recrystallize. Once all the solvent was evaporated, the dry solid was collected, crushed and gently ground using mortar and pestle to homogenize the (*R*) and (*S*) enantiomeric compositions of dispersed solids over the relevant range [50-100%]. The (*R*) and (*S*) enantiomeric compositions were calculated from the amount of racemic mixture (50% (*R*) + 50% (*S*)) and added pure (*S*) and expressed in terms of compositions of (*S*)- enantiomer (x%). For these measurements, ca. 9.00 ± 0.10 mg of samples with various enantiomeric compositions were prepared in a 25 μL closed aluminium crucible. A heating rate of 10 K min^{-1} was applied for all experiments in the 20-290 $^{\circ}\text{C}$ temperature range. Data obtained were evaluated using the Netzsch Proteus Thermal Analysis Software. For the pure crystalline phases, the melting temperature was taken from the onset temperature within the heat flux/temperature plot. For the composition mixtures, the eutectic melting temperature was taken from the appropriate onset temperature and peak values were used to determine the end of melting (liquidus line). DSC curves of ethylammonium chlocyphos of pure substances and intermediate enantiomeric compositions were reported in Figure 3.30.

The onset temperature and enthalpy at the eutectic composition and the peak temperature and the total enthalpy at the liquidus were accurately identified and recorded. However, the enantiomeric compositions between [90-99%] were not considered for these DSC analyses because only one single broad endothermal peak emerged at that range of composition mixtures due to the presence of mixed crystals. The DSC curves have been vertically shifted for clarity starting from the pure (*S*)-enantiomer (100%) toward the racemic composition (50%:50%).

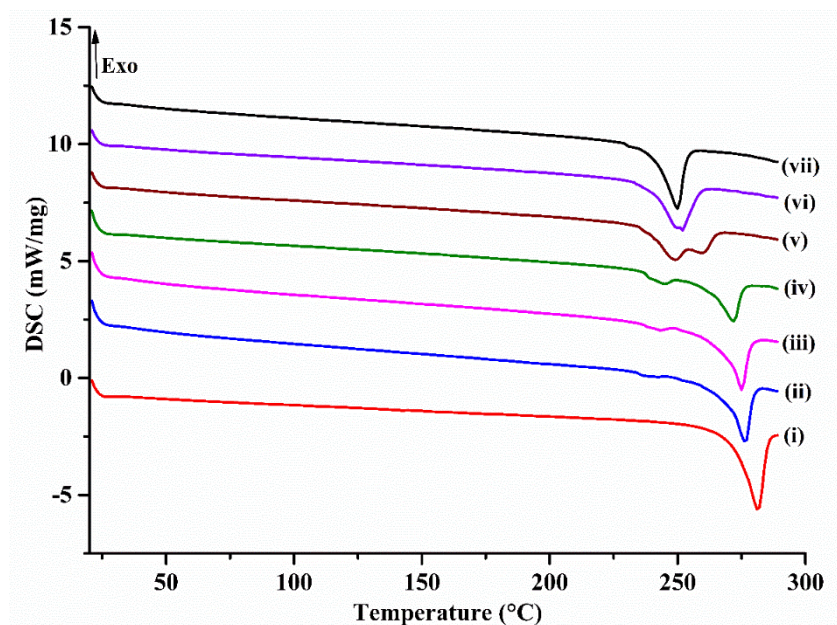


Figure 3.30: DSC curves of pure racemic, pure (*S*) and different enantiomeric compositions of ethylammonium chlocyphos: (i) (red), $x = 100\%$; (ii) (blue), $x = 87.6\%$; (iii) (pink), $x = 84.7\%$; (iv) (green), $x = 79.7\%$; (v) (brown), $x = 65.1\%$; (vi) (purple) $x = 57.2\%$ and (vii) (black), $x = 50.0\%$. DSC curves have been vertically shifted for clarity.

3.4.2. Construction of the binary phase diagram and Tammann graph

The binary phase diagram reported in Figure 3.31 was constructed from the DSC data obtained from the pure substances, the intermediate enantiomeric compositions [87.6; 84.7; 79.7; 65.1; 57.2%] and their corresponding symmetrical points with respect to the eutectic composition $x = 50.0\%$. The related Tammann graph (Figure 3.32) was constructed by plotting the eutectic enthalpy versus the enantiomeric compositions starting at the racemic composition $x = 50\%$. The linear regression fitting from the eutectic enthalpy over the enantiomeric composition indicates that the straight line intersects the abscissa axis at $x = 88 \pm 1\%$ (*S*-enantiomer composition). On Figure 3.32, the evolution of the total enthalpy of fusion above the composition 88% is not a straight line. This behavior is probably due to the loss of mass (ca. 2%) caused by the chemical degradation noted after the DSC measurements. However, this slight deviation from an ideal case did not prevent the plot of the Tammann graph (using eutectic enthalpy data extracted from the DSC curves) to determine the limits of composition of the solid solution. Consequently, the composition limits of the symmetrical monophasic domains could be proposed at: $12 \pm 1\%$ and $88 \pm 1\%$ in (*S*)- enantiomer composition.

Thermodynamically, the domain width of the solid solution limit was determined using DSC analyses. This domain of partial miscibility in the solid state can be furthermore evaluated by using XRPD patterns^{23,28}.

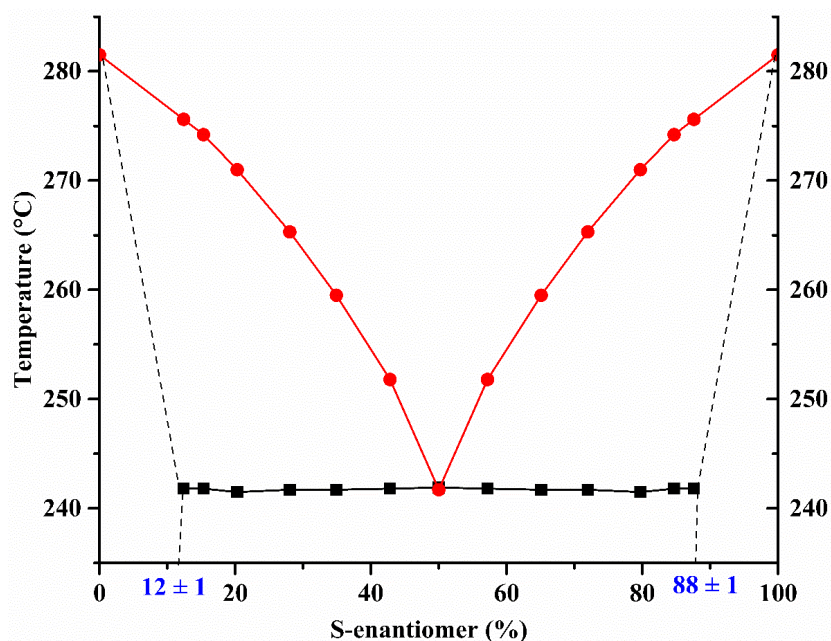


Figure 3.31: Experimental binary phase diagram of ethylammonium chlocyphos system. Red circles are the experimental temperatures of liquidus and red solid lines the corresponding liquidus line; black square are the experimental eutectic temperatures and the black solid line the corresponding eutectic invariant; black dashed lines represent the hypothetical solidus and solvus; the points $x = 12 \pm 1\%$ (left hand) and $x = 88 \pm 1\%$ (right hand) indicate the extreme limit of the eutectic invariant.

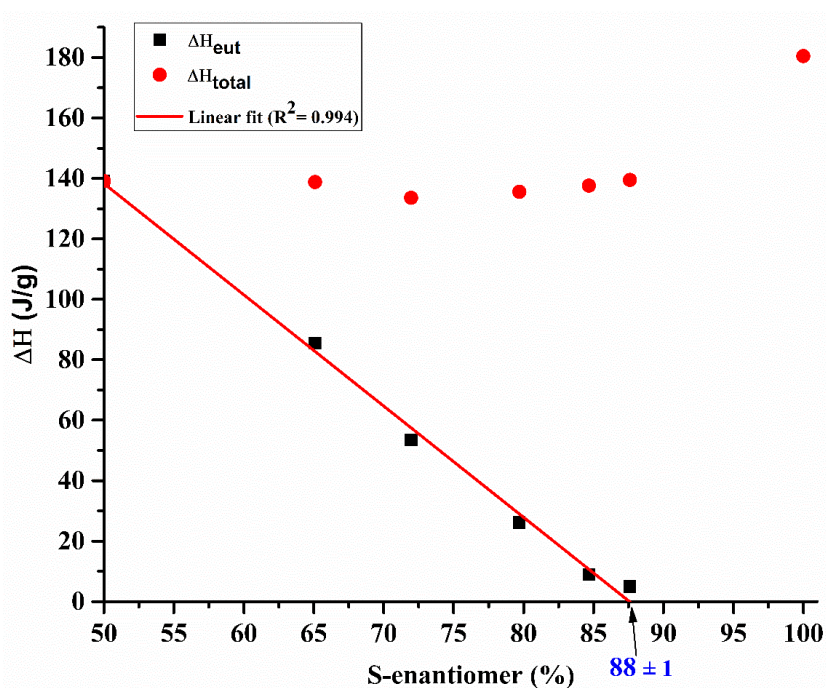


Figure 3.32: Tammann graph for the eutectic invariant between (*R*)- and (*S*)-ethylammonium chlocyphos: Red circles are the total enthalpy of fusion at the liquidus; black squares are the enthalpy of the eutectic transformation; red line is the linear regression fit ($R^2 = 0.994$) and $x = 88 \pm 1\%$ indicates the extreme limit of the eutectic invariant.

3.4.3. Investigation by XRPD measurements of the limit of the solid solution

This approach consists in analysing by XRPD, mixtures of different enantiomeric compositions to establish the limit of the solid solution domain. The evolution of the peak shifts, starting from

the pure enantiomer (100%) toward the intermediate enantiomeric compositions, could fix the boundary of the partial miscibility domain in the solid state.

As we already estimated the extreme limit ($x = 88 \pm 1\%$), we have then selected different enantiomeric compositions in the estimated solid solution and two-phase domains of the binary system. The various mixtures were prepared earlier as for the DSC analyses. Sodium chloride (ca. 5 mg NaCl) was used as internal standard (reference peak). For the XRPD measurements, the diffraction patterns were collected by steps of 0.02° (in 2-theta) over the angular range $8-40^\circ$, with a counting time of 1 second per step i.e. accumulated long-time acquisition measurements.

The XRPD patterns for different enantiomeric compositions of ethylammonium chlocyphos are reported in Figure 3.33. The black arrows indicate the peak shift positions in the XRPD patterns of ethylammonium chlocyphos.

For a more detailed visualization, some peaks of the XRPD patterns are magnified in Figure 3.34 and the left and right shifts are clearly highlighted.

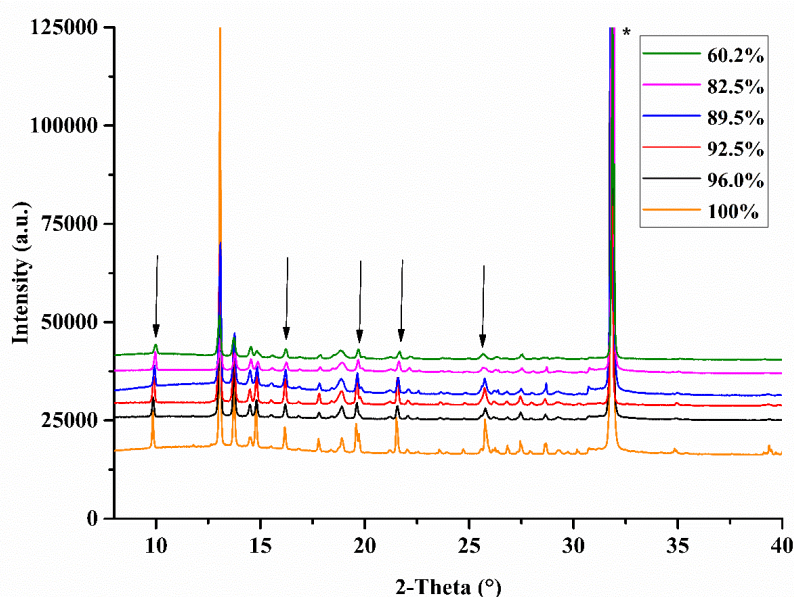


Figure 3.33: XRPD patterns of ethylammonium chlocyphos: Different composition mixtures + NaCl* (for calibration). Black arrows indicate the shifted peaks.

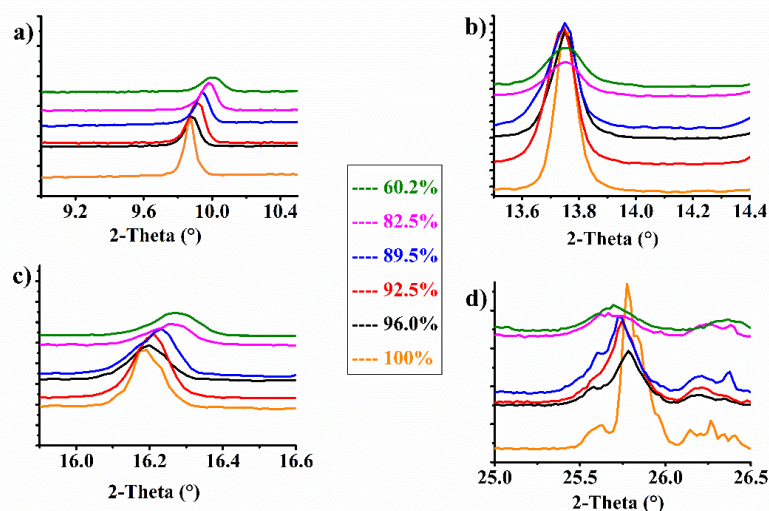


Figure 3.34: Magnified peaks of the XRPD patterns of ethylammonium chlocyphos for different enantiomeric compositions. a) and c) peak shifts at the right-hand side; b) no peak shift and d) peak shift at the left-hand side.

Figure 3.34a and Figure 3.34c point out peak shifts at right hand side and Figure 3.34d shows a peak shift at left hand side starting from the pure enantiomer ($x=100\%$; orange) toward the enantiomeric compositions chosen in the miscibility domain [$x = 96.0\%$ (black); $x = 92.5\%$ (red) and $x = 89.5\%$ (blue)]. These shifts vanish for the enantiomeric compositions in the non-miscibility domain [$x = 82.5\%$ (pink) and $x = 60.2\%$ (green)]. Additionally, in some peaks, no shift was observed whatever the enantiomeric compositions (e.g. magnified peak in Figure 3.34b).

These results show that the peak shifts correspond to a limited change of size of the unit cell (some cell parameters slightly change) upon incorporation of the other enantiomer in the miscibility domain. However, in the two-phase domain, the composition no longer changes and thus no peak shift can be observed by XRPD. Consequently, XRPD measurements serve to estimate the width of the miscibility domain at the temperature of measurement (i.e. room temperature).

The solid solution limit determined using XRPD measurements for different composition mixtures is comprised between compositions 89.5% and 82.5% in good agreement with the composition $88 \pm 1\%$ determined by using the Tammann plot. These results at room temperature are in good agreement with data obtained from DSC measurements which gives the extent of the miscibility domain at the eutectic temperature. It also implies that the limits in composition of the symmetrical monophasic domains do not evolve that much in a large temperature domain (from $20\text{ }^{\circ}\text{C}$ to $\sim 242\text{ }^{\circ}\text{C}$: the eutectic temperature). This has already been observed for another conglomerate with partial solid solutions²⁶.

3.5. TRENDS OF CONGLOMERATE FORMATION IN ALKYL-AMMONIUM CHLOCYPHOS SALTS

We showed that among the alkyl-ammonium chlocyphos family of salts:

- Racemic methylammonium chlocyphos crystallizes as a monoclinic centrosymmetric sesquihydrate ($C2/c$, space group).
- Racemic ethylammonium chlocyphos crystallizes as a conglomerate with limited partial solid solutions close to the pure enantiomer.
- Racemic propylammonium chlocyphos exhibits several polymorphic forms and among them a stable conglomerate ($P2_1$, space group).
- Racemic butylammonium, isobutylammonium, pentylammonium, hexylammonium and cyclohexylammonium chlocyphos crystallize as conglomerates and form a family of conglomerate derivatives ($P2_1$ or $P2_12_12_1$, space group).
- Racemic octylammonium chlocyphos crystallizes as a non-centrosymmetric crystal, probably a monohydrate racemic compound.

Thus, in this series of salt derivatives, conglomerates seem to be favoured rather than racemic compounds when the alkyl-amine moiety is long enough (starting from propyl chain). However, there is clearly a limit of the length of the alkyl chain (no conglomerate found for octylamine) and the types of amine (conglomerate favoured for primary amine but not for secondary or tertiary amine, see Table 3.4).

An explanation of this trend can be proposed if the greater thermal displacement of the terminal carbons of the alkyl-moiety is considered. Indeed, results presented in Table 3.12 reveal that there is a pocket in the crystal lattice that can accommodate alkyl-moieties. That was the reason that prompted us to successfully spot conglomerates with other amines with longer and bulkier chains (propyl, butyl, isobutyl, pentyl, hexyl, cyclohexyl).

Table 3.12: Isotropic displacement parameters^a of chlocyphos alkyl-amines

Isotropic displacement $U(\text{eq}) (\text{\AA}^2 \times 10^3)$	Propyl	Butyl	Isobutyl	Pentyl	Hexyl	Cyclohexyl
C(1A)	199 (8)	104 (2)	62 (1)	103 (2)	116 (2)	47 (1)
C(2A)	338 (16)	142 (3)	76 (2)	121 (3)	212 (5)	75 (1)
C(3A)	550 (40)	250 (7)	179 (5)	174 (4)	331 (10)	99 (2)
C(4A)	-	307 (10)	134 (3)	151 (3)	170 (3)	95 (2)
C(5A)	-	-	-	207 (6)	219 (5)	81 (1)
C(6A)	-	-	-	-	187 (4)	66 (1)

^a $U(\text{eq})$ is defined as one third of the trace of the orthogonalized U_{ij} tensor. Bolded values are more than double of the value of the first carbon atom linked to the nitrogen atom.

In the case of methylammonium chlocyphos, the alkyl-methyl molecule is probably too small; therefore, it is not large enough to fill (occupy) the entire crystal lattice of the derivative. To fulfil close and optimal intermolecular interaction requirements (for low energy packing), water molecules are incorporated to the unit cell, thus stabilizing a stable hydrated form.

The case of ethylammonium chlocyphos could first be considered as surprising as a “true” conglomerate would be expected in agreement with the positive SHG signal obtained from the racemic mixture. Moreover, usually, a rigid and stable packing of the molecule limits the possibility of molecular disorder often encountered in solid solutions^{26,29,30}. But, in the present case, the main cohesion interactions (i.e. H-bonds) in the crystal structure are located far from the chiral centre. Therefore, it may have only a limited effect on the crystal packing. The existence of a solid solution is thus possible^{31,32}. In addition, it was also reasonable to expect for ethylammonium chlocyphos, an intermediate crystal arrangement between those of the methylammonium and propylammonium chlocyphos.

Even though, the crystal structure of the limit of the solid solution could not be solved, the close similarities in crystal structures between the pure enantiomer of ethylammonium chlocyphos and the family of conglomerates described in the section 3.3.1 suggest that the hydrogen bond network would not be affected. Molecular arrangements (bond chains) formed between ammonium and chlocyphos are a constant in the family of salts made between chlocyphos and ammonium compounds. Thus, they are expected to remain constant in the solid solution. The bias might be how the molecular chains are arranged with themselves.

Through this study, we show that derivatives of chlocyphos alkyl-amines also constitute a family of conglomerates analogously to the derivatives of 5-aryl-5-alkyl hydantoins and 4-aryl-triazotyl ketones as reported in the literature^{33,34}. The optical resolution by preferential crystallization (PC) of these compounds was tested except for propylammonium, pentylammonium (multi-epitaxy) and ethylammonium chlocyphos for which the existence of partial solid solutions between the two enantiomers constitutes a factor that would have probably strongly limit the PC performances.

PART 4: RESOLUTION BY PREFERENTIAL CRYSTALLIZATION (PC)

Nowadays, diastereomeric salt formation is used to resolve chlocyphos. Because of the need to directly access to the pure enantiomer of chlocyphos, we set out to develop a fast and reliable method to crystallize chlocyphos. Preferential crystallization seems to be the most suitable method to access to the enantiopure crystals via its salt derivatives.

Once the conglomerate nature of the racemic chlocyphos derivative had been established, the efficiency of their chiral separation by PC was evaluated. It is indeed important to mention that, even if spotting a conglomerate is a prerequisite to the resolution of a chiral mixture by PC, several phenomena can prevent a productive entrainment effect³⁵.

It is common in the literature to consider that a PC process gives a productive and strong entrainment, if a yield better than 20%, a purity of the crude crops better than 90% ee without any purification and a final enantiomeric excess of the mother liquor better than 10% ee can be reached³⁶. In the following, the yield is defined as: $\text{Yield} = \frac{m_{\text{pure}} - m_{\text{seeds}}}{m_{(\pm)}} \times 100$ with:

- m_{pure} , the mass of pure enantiomer equal to the product of the mass of the crude crops and the optical purity (O.P) ($m_{\text{pure}} = m_{\text{crops}} \times \text{O.P}$)
- m_{seeds} , the mass of seeded crystals
- $m_{(\pm)}$, the initial mass of racemic mixture invested.

The strategy adopted was as follows: SIPC was run first systematically to test the entrainment effect for each derivative. If the performances were good, AS3PC was then attempted at larger scale (25 ml). Alternative variants such as ASPreCISE were adopted if SIPC did not work.

4.1. EXPERIMENTAL CONDITIONS

In our work, the following experimental conditions were taken for each selected mode to perform the PC.

4.1.1. Seeded Isothermal Preferential Crystallization (SIPC mode)

A 60 ml screw cap vial was used as a batch crystallizer and the experiments were performed at 25 ml scale. The temperature was controlled via a cryo-thermostat and the stirring was ensured with a magnetic bar (15 mm) at about 500 rpm.

An initial amount of racemic mixture (m_{\pm}) was totally dissolved in the chosen solvent at initial temperature (T_I) slightly higher than the temperature of dissolution of the total amount of racemic mixture (T_L) to obtain an undersaturated racemic solution. The racemic solution was then cooled to the filtration temperature (T_F), temperature in which the racemic mixture became supersaturated but should not crystallize within several hours (metastable zone). Thus, a small amount of pure enantiomer (m_{seeds}) was added to the solution so that the initial enantiomeric

excess (ee) of the resulting suspension was in the range 5-10%. The suspension was maintained at T_F during an optimized time to reach growth of the desired enantiomer without promoting the crystallization of the unwanted enantiomer. The crystals (m_{crops}) were then isolated by filtration. The mother liquor was collected and reused after addition of a mass of racemic mixture equivalent to the mass of the harvested solid. Then, when possible, alternating crystallizations of (*R*) and (*S*) were performed.

4.1.2. Auto Seeded Polythermic Programmed Preferential Crystallization (AS3PC mode)

Experiments performed in the AS3PC mode were carried out with similar equipment as for SIPC. Starting with a mass of racemic mixture (m_{\pm}) and an appropriate amount of solvent, a saturated solution of racemic mixture was formed at the initial temperature T_L (temperature of dissolution of the total amount of racemic mixture). A small amount of pure enantiomer (m_{seeds}) was then added to reach an ee in the range 5-10%. The suspension was heated to T_B defined as $\frac{1}{2}(T_{\text{Homo}} + T_L)$ where T_{Homo} stands for the temperature of homogenization (temperature of dissolution of the solute composed of the racemic mixture plus the enantiomer in excess). The suspension was subsequently cooled down to T_F during a temperature versus time ramp to promote secondary nucleation and growth of the desired enantiomer. The following steps (harvest by filtration and recycling of the mother liquor) are identical to the SIPC experiments.

4.1.3. Auto-Seeded Preferential Crystallization Induced by Solvent Evaporation (ASPreCISE)

The experimental process was performed in a 100 ml three-neck flask (supplied neck for N_2 gas, one neck for solvent evaporation and one neck for filtration) and temperature was accurately controlled by a cryo-thermostat.

In this particular mode the metastable zones depend on the solvent evaporation rate. Solvent evaporation can be stimulated by distillation of the solvent under reduced pressure or by means of an inert gas stripping (e.g., nitrogen).

The experimental process was performed in a 100 ml three-neck flask (supplied neck for N_2 gas, one neck for solvent evaporation and one neck for filtration) and temperature was accurately controlled by a cryo-thermostat. A small amount of pure enantiomer (seeded crystals) was added to the racemic saturated solution so that the initial enantiomeric excess was adjusted to circa 8%. Nitrogen gas was bubbled in the suspension to promote solvent evaporation. Volume variation from the initial volume was recorded versus time. The slurry was filtered off before primary nucleation of the unwanted enantiomer.

4.1.4. Solubility measurements

The solubility of each conglomerate was measured in different solvents using the classical evaporation method. A suspension of the conglomerate was prepared in the chosen solvent at a given temperature and let under stirring during several hours. Then the suspension was filtered, and the saturated solution was weighed and then evaporated in a ventilated oven at 50 °C. The solubility is calculated by dividing the mass of the recovered powder by the mass of the saturated solution. Hereafter, each reported value of the solubility is the mean value of three measurements and is expressed in weight percent (wt%).

4.1.5. Polarimetric measurements

The enantiomeric purities of the crops were determined by polarimetric measurements performed with a Jasco-P2000 and an Anton Paar-MCP5100 polarimeters (10 mg of powder dissolved in 2 ml of solvent, $\lambda = 546$ nm, $T = 20$ °C, tube length equal to $L = 10$ cm).

4.2. RESOLUTION OF BUTYLAMMONIUM CHLOCYPHOS

The difficulty to find an efficient process for the chiral resolution by PC was illustrated by preliminary tests performed in the classical SIPC mode on the salt formed with butylamine. Indeed, experiments led to very poor yield and low enantiomeric excess (non-reported data). As the first attempts to resolve butylammonium chlocyphos salt with SIPC mode have been unsuccessful, trials to work in the AS3PC mode were not undertaken for this salt. Preference was given to a resolution via the ASPreCISE mode. ASPreCISE was chosen as an alternative mode to perform the entrainment because of its capability to overcome the low variation of the solubility of the salt versus temperature³⁷ (from 1% to ca. 3% on a temperature range of 20 °C) in isopropyl alcohol, illustrated by Figure 3.35.

After solubility studies, a non-azeotropic mixture of acetone/ethanol (90/10 v%) was chosen at 10 ml scale experiments at 20 °C. The solubility of the racemic salt at 20 °C was found to be 4.80 wt% in the solvent mixture (acetone/ethanol).

The corresponding results are listed in Table 3.13. Six batches were independently performed in identical conditions except for the duration. Only single runs were tested and show a drop of the enantiomeric excess after 25 minutes. Even with these restrictions, after optimizing the duration of the run, a high enantiomeric excess was obtained (mean value circa 94.8% ee) without washing nor recrystallization. Nevertheless, the yield (9.55%) as well as the final enantiomeric excess of the mother liquor ($ee_f = 8.1\%$ ee) did not reach the expected yield values (20% and 10% ee respectively).

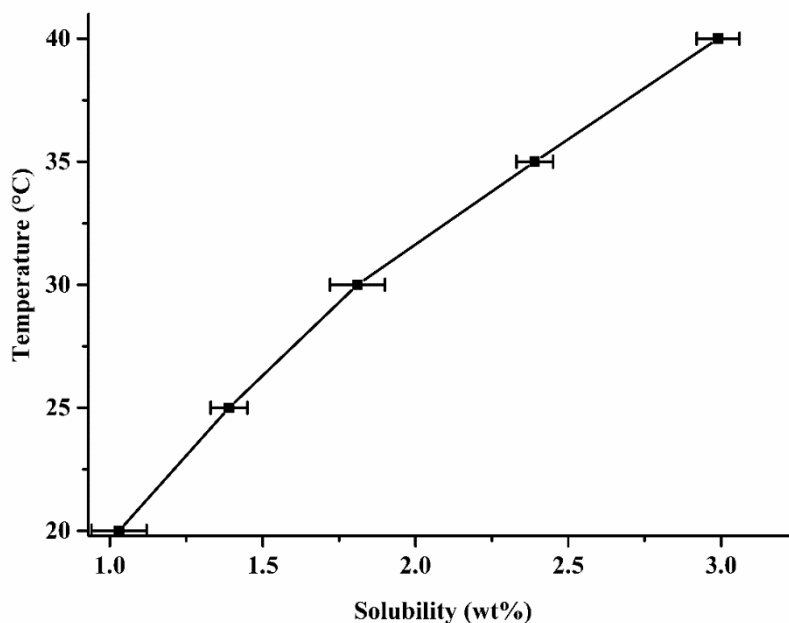


Figure 3.35: Solubility curve of racemic mixture butylammonium chlocyphos in isopropyl alcohol

Table 3.13: Initial conditions and results of ASPreCISE mode at 10 ml scale for butylammonium chlocyphos

m_{\pm} (g)	$m_{Ac/EtOH}$ (g)	m_{seeds} (g) / ee (%)	T_F (°C)
0.398	9.70	0.032 / +100	20

N°	Time(min)	m_{total} (g)	m_{crops} (g)	OP (%)	m_{pure} (g)	Yield (%)	ee _f (% ee)
A	46	0.430	0.105	+43.70	0.046	3.52	5.46
B	30	0.430	0.098	+63.45	0.062	7.54	7.23
C	25	0.430	0.058	+95.85	0.056	6.03	6.57
D	25	0.430	0.067	+96.37	0.064	8.04	7.44
E	25	0.430	0.083	+90.98	0.075	10.80	8.61
F	25	0.430	0.089	+96.10	0.085	13.32	9.67
Mean	25	0.430	0.074	+94.82	0.070	9.5	8.1

Notation: Ac = acetone; EtOH = ethanol; MeOH = methanol; IPA = isopropyl alcohol ee = enantiomeric excess; OP = optical purity, T_B = temperature of suspension; T_F = temperature of filtration ee_f = final enantiomeric

excess of mother liquor = $(\frac{m_{pure}}{2} + m_{\pm})$; **Calculation:** Mean value = runs (C+D+E +F)/4

4.3. RESOLUTION OF ISOBUTYLAMMONIUM CHLOCYPHOS

4.3.1. SIPC mode

The variation of racemic mixture solubility in ethanol solution versus temperature was determined (Figure 3.36). The solubility in ethanol at 20°C is 7.07 wt%. This condition was chosen to perform SIPC mode at 25 ml scale.

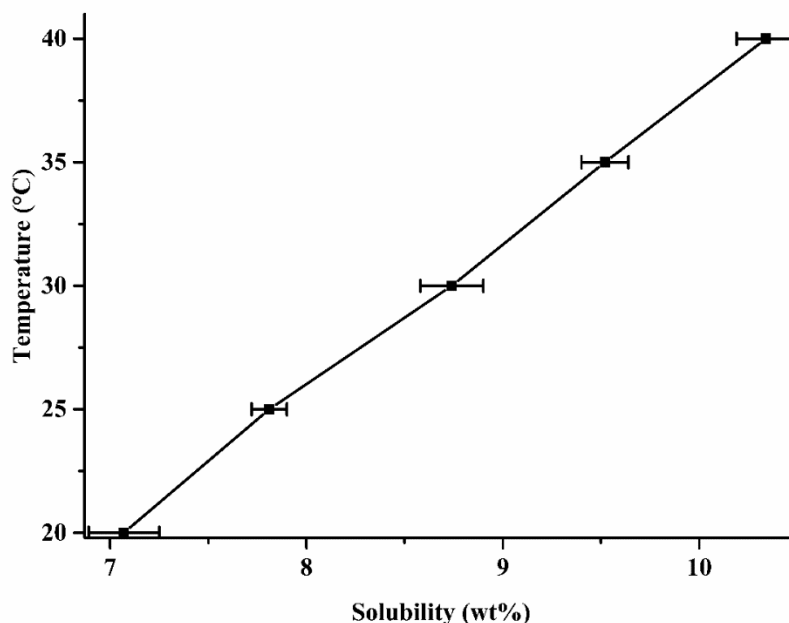


Figure 3.36: Solubility curve of racemic mixture isobutylammonium chlocyphos in ethanol

At the end of each single run the temperature of filtration was adjusted at 5 °C in SIPC mode. The mean value of the optical purity of the final product without any purification was 88% ee and a poor overall yield was obtained (ca. 6.8%). The experimental conditions and results are summarized in Table 3.14.

Table 3.14: Initial conditions and results of SIPC mode at 25ml scale

m_± (g) m_{EtOH}(g) m_{seeds} (g) / ee (%) T_F (°C)							
1.500 19.72 0.02 / ±100 5							
N°	Time(min)	m_{total} (g)	m_{cropl}(g)	OP (%)	m_{pure}(g)	Yield (%)	ee_f (% ee)
A	45	1.520	0.163	+64.81	0.106	5.75	3.41
B	42	1.520	0.143	+68.21	0.097	5.13	3.13
C	40	1.520	0.073	+90.43	0.066	3.07	2.15
D	38	1.520	0.156	-93.15	0.145	8.33	4.61
E	38	1.520	0.133	-83.84	0.111	6.07	3.55
F	38	1.520	0.122	-88.47	0.108	5.87	3.47
Mean	38	1.520	0.137	-88.49	0.121	6.8	3.9

Calculation: Mean value = runs (D+E+F)/3

4.3.2. AS3PC mode

As SIPC, AS3PC mode was performed at 25 ml scale while considering the solubility of the racemic salt at 35 °C to be 9.5 wt% as shown in Figure 3.36. The amount of seed crystals added to enrich the saturated racemic solution with initial ee was fixed at 5% of the initial mass of the racemic mixture. The initial conditions and results of AS3PC of isobutylammonium chlocyphos are reported in Table 3.15.

Table 3.15: Initial conditions and results of AS3PC mode for isobutylammonium chlocyphos at 25 ml scale

<table border="1"> <thead> <tr> <th>m_{\pm} (g)</th> <th>m_{EtOH} (g)</th> <th>m_{seeds} (g) / ee (%)</th> <th>T_B (°C)</th> <th>T_F (°C)</th> </tr> </thead> <tbody> <tr> <td>2.075</td> <td>19.72</td> <td>0.104 / -100</td> <td>36</td> <td>5</td> </tr> </tbody> </table>								m_{\pm} (g)	m_{EtOH} (g)	m_{seeds} (g) / ee (%)	T_B (°C)	T_F (°C)	2.075	19.72	0.104 / -100	36	5
m_{\pm} (g)	m_{EtOH} (g)	m_{seeds} (g) / ee (%)	T_B (°C)	T_F (°C)													
2.075	19.72	0.104 / -100	36	5													
N°	Time(min)	m_{total} (g)	m_{crops} (g)	OP (%)	m_{pure} (g)	Yield (%)	ee _f (% ee)										
A ₁	35	2.179	0.349	-60.10	0.210	5.11	4.82										
A ₂	33	0.349	0.340	+57.80	0.196	9.44	4.51										
A ₃	31	0.340	0.264	-86.24	0.138	6.65	3.22										
B ₁	27	2.179	0.235	-96.33	0.226	5.88	5.16										
B ₂	27	0.235	0.233	+77.98	0.182	8.77	4.20										
B ₃	27	0.233	0.239	-100.00	0.239	11.52	5.44										
B ₄	27	0.239	0.185	+91.74	0.170	8.19	3.93										
C ₁	27	2.179	0.293	-97.24	0.285	8.72	6.43										
C ₂	27	0.293	0.264	+98.85	0.261	12.58	5.92										
C ₃	27	0.264	0.206	-100.00	0.206	9.93	4.73										
C ₄	27	0.206	0.193	+94.95	0.185	8.91	4.27										
Mean	27	0.728	0.231	±94.65	0.220	9.3	5.0										

Calculation: Mean value = runs (B_i+C_i)/8 (i =1;2;3;4)

AS3PC mode improved the PC performances when compared to SIPC (i.e. reduced experimental time, mean enantiomeric excess of 95% ee and mean yield of 9.3%). Even if the solubilities at which the two process were performed (7.07 wt% at 20 °C for SIPC and 9.5 wt% at 35 °C for AS3PC modes) were different, the target yield (20%) could not be reached in both modes despite a large temperature window ($T_B = 36$ °C and $T_F = 5$ °C) for the auto-seeded process.

4.4. RESOLUTION OF HEXYLAMMONIUM CHLOCYPHOS

4.4.1. SIPC mode

To evaluate the performances of PC on hexylammonium chlocyphos, two modes (SIPC and AS3PC) were applied at 25 ml scale in isopropyl alcohol. The solubility in isopropyl alcohol at 20 °C is 10.62 wt% (Figure 3.37). these conditions were chosen to perform SIPC mode.

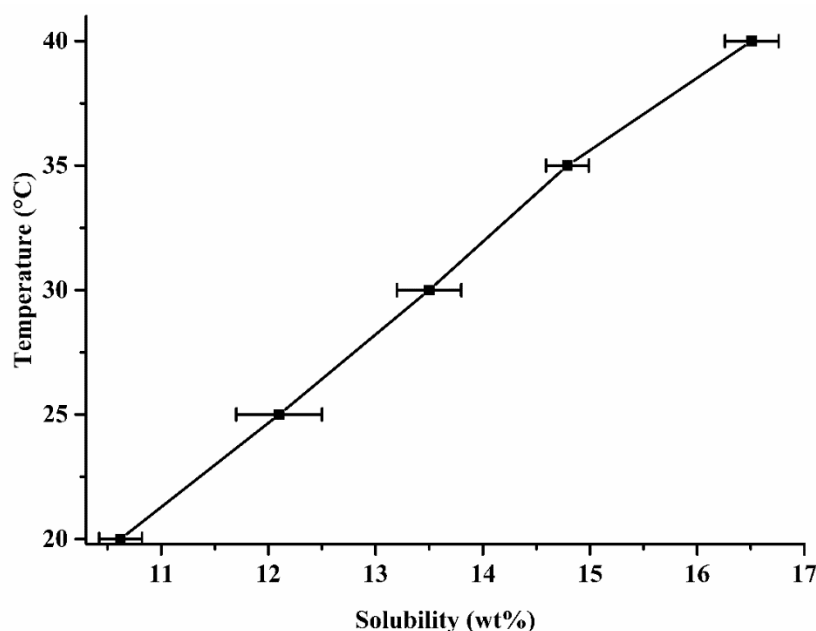


Figure 3.37: Solubility curve of racemic mixture hexylammonium chlocyphos in isopropyl alcohol

All experimental batches were carried out with the same amount of compound (2.335 g per batch) and suspension was prepared at 5 °C for SIPC experiments (50 mg of seeds) and at 25 °C for AS3PC experiments (90 mg of seeds).

At the end of each single run the temperature of filtration was adjusted at 5 °C in SIPC mode. The mean value of the optical purity of the final product without any purification was 75% ee and a poor overall yield was obtained (circa 2.65%). The experimental conditions and results are summarized in Table 3.16.

Table 3.16: Initial conditions and results of SIPC mode for hexylammonium chlocyphos at 25 ml scale

<table border="1" style="margin: auto;"> <tr> <th>m_{\pm} (g)</th> <th>m_{IPA} (g)</th> <th>m_{seeds} (g) / ee (%)</th> <th>T_{F} (°C)</th> </tr> <tr> <td>2.335</td> <td>19.65</td> <td>0.05 / +100</td> <td>5</td> </tr> </table>								m_{\pm} (g)	m_{IPA} (g)	m_{seeds} (g) / ee (%)	T_{F} (°C)	2.335	19.65	0.05 / +100	5
m_{\pm} (g)	m_{IPA} (g)	m_{seeds} (g) / ee (%)	T_{F} (°C)												
2.335	19.65	0.05 / +100	5												
N°	Time (min)	m_{total} (g)	m_{crops} (g)	OP (%)	m_{pure} (g)	Yield (%)	ee _f (% ee)								
A	37.5	2.385	0.240	+82.95	0.199	6.38	4.09								
B	38.5	2.385	0.257	+77.11	0.198	6.33	4.07								
C	38.5	2.385	0.130	+80.61	0.105	2.35	2.20								
D	37.5	2.365	0.116	+63.88	0.074	1.03	1.56								
E	37.5	2.355	0.173	+68.64	0.119	2.95	2.48								
F	37.5	2.355	0.091	+76.98	0.070	0.86	1.48								
Mean	37.8	2.372	0.168	+75.03	0.127	3.32	2.65								

Calculation: Mean value = runs (A+B+C+D+E+F)/6

4.4.2. AS3PC mode

Seven batches were performed by alternating the crystallization of (*R*) and (*S*) enantiomers and the results are collected in Table 3.17.

An in-situ focused beam reflectance measurement (FBRM- Mettler Toledo) particle counter has been also used to monitor the course of the auto-seeded process by measuring the particle number of chord lengths per unit time.

FBRM data (Figure 3.38) highlighted a small variation of the particle number counts during the process for the performed batches (high enantiomeric excess, ca. 96.9% ee) except for batch B₂ in which large number of small particles (ca. 230 counts) were generated. It indicates the presence of the counter enantiomer particles which reduced sharply the optical purity down to ca. 70% ee.

Table 3.17: Initial conditions and results of AS3PC mode for hexylammonium chlocyphos at 25 ml scale

<table border="1" style="margin: auto;"> <tr> <td>m_{\pm} (g)</td> <td>mIPA (g)</td> <td>m_{seeds} (g) / ee (%)</td> <td>T_B (°C)</td> <td>T_F (°C)</td> </tr> <tr> <td>2.335</td> <td>19.65</td> <td>0.09 / ± 100</td> <td>25</td> <td>5</td> </tr> </table>								m_{\pm} (g)	mIPA (g)	m_{seeds} (g) / ee (%)	T_B (°C)	T_F (°C)	2.335	19.65	0.09 / ± 100	25	5
m_{\pm} (g)	mIPA (g)	m_{seeds} (g) / ee (%)	T_B (°C)	T_F (°C)													
2.335	19.65	0.09 / ± 100	25	5													
N°	Time (min)	m_{total} (g)	m_{crops} (g)	OP (%)	m_{pure} (g)	Yield (%)	ee _F (% ee)										
A	23	2.425	0.240	-96.87	0.232	6.08	4.73										
B ₁	23	2.425	0.212	-85.94	0.182	3.94	3.75										
B ₂	23	0.212	0.177	+70.78	0.125	5.35	2.60										
B ₃	23	0.177	0.074	-99.23	0.073	3.21	1.54										
C ₁	23	2.425	0.213	-85.10	0.181	3.90	3.73										
C ₂	23	0.213	0.143	+96.87	0.138	5.91	2.87										
C ₃	23	0.143	0.081	-78.91	0.064	2.74	1.35										
Mean	23	1.146	0.163	± 87.67	0.142	4.4	2.9										

Calculation: Mean value = runs (A+B_i+C_i)/7 (i = 1;2;3)

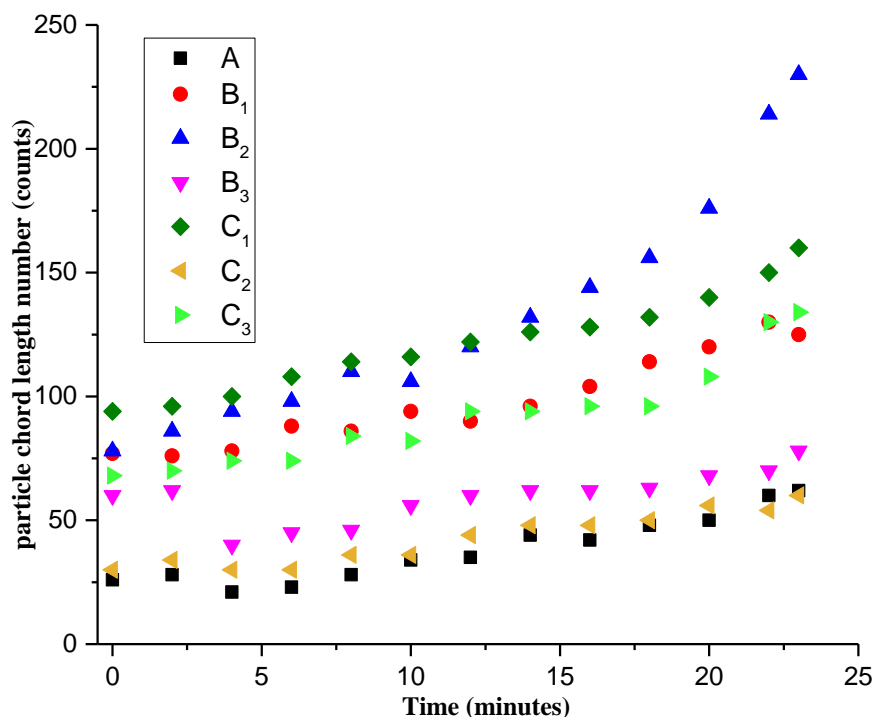


Figure 3.38: Particle chord length number versus time for AS3PC mode of hexylammonium chlocyphos

AS3PC mode versus SIPC mode applied to the hexylammonium derivative improved the resolution in terms of experimental time (23 minutes instead of 37.8 minutes), enantiomeric excess (87.67% ee instead of 75.03% ee) and yield (4.4% instead of 3.3%) (compare Table 3.16 and Table 3.17). The auto-seeded polythermal programmed preferential crystallization has proven its superiority to the classical isothermal process^{14,38} but reaching a high yield remains still challenging for these derivatives.

4.5. RESOLUTION OF CYCLOHEXYLAMMONIUM CHLOCYPHOS

For cyclohexylammonium chlocyphos salt, only AS3PC mode was applied. The solubility variation in methanol versus temperature is reported in Figure 3.39. The entrainment was performed at 40 °C with a corresponding solubility of 6.14 wt%. The initial conditions and results of twelve alternated PC batches are reported in Table 3.18.

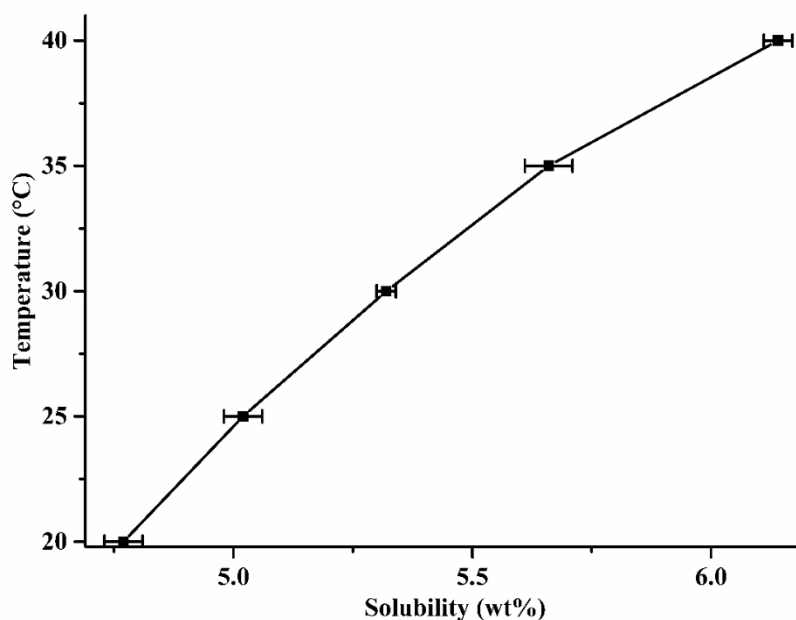


Figure 3.39: Solubility curve of racemic mixture cyclohexylammonium chlocyphos in methanol

Pure enantiomers (ca. 2.0 g) of cyclohexylammonium chlocyphos salt were collected with very high purity without any purification. Note that the last two batches were used for sampling to monitor the evolution of the rotatory power of the mother liquor (Figure 3.40) and led to a decrease of the optical purity and the yield. The obtained results have proven that a successful entrainment via AS3PC mode was performed with a high enantiomeric excess (ca. 92% ee, mean value) and a moderate yield (ca. 10.92%, mean value), the best achieved among the derivatives considered for the resolution by PC.

Table 3.18: Initial conditions and results of AS3PC mode of cyclohexylammonium chlocyphos at 25 ml Scale

m_{\pm} (g) m_{MeOH} (g) m_{seeds} (g) / ee (%) T_B (°C) T_F (°C)							
1.295 19.77 0.104 / -100 41 5							
N°	Time(min)	m_{total} (g)	m_{crops} (g)	OP (%)	m_{pure} (g)	Yield (%)	ee _f (% ee)
A ₁	45	1.399	0.261	-83.50	0.218	8.88	7.76
A ₂	40	0.261	0.200	+97.97	0.196	15.13	7.03
A ₃	40	0.200	0.194	-95.68	0.186	14.36	6.70
A ₄	40	0.194	0.149	+100.0	0.149	11.50	5.44
A ₅	40	0.149	0.125	-100.0	0.125	9.65	4.60
A ₆	40	0.125	0.124	+92.38	0.114	8.80	4.21
B ₁	40	1.399	0.195	-100.0	0.195	7.02	7.00
B ₂	40	0.195	0.215	+77.92	0.167	12.89	6.06
B ₃	40	0.215	0.177	-100.0	0.177	13.67	6.39
B ₄	40	0.177	0.198	+83.76	0.166	12.82	6.02
B ₅ *	40	0.198	0.153	-92.38	0.141	10.89	5.16
B ₆ *	30	0.153	0.094	+78.68	0.074	5.71	2.78
Mean	40	0.389	0.174	±91.85	0.159	10.9	5.7

Calculation: Mean value = runs (A_i+B_i)/12 (i =1;2;3;4;5;6) (*sampling batches)

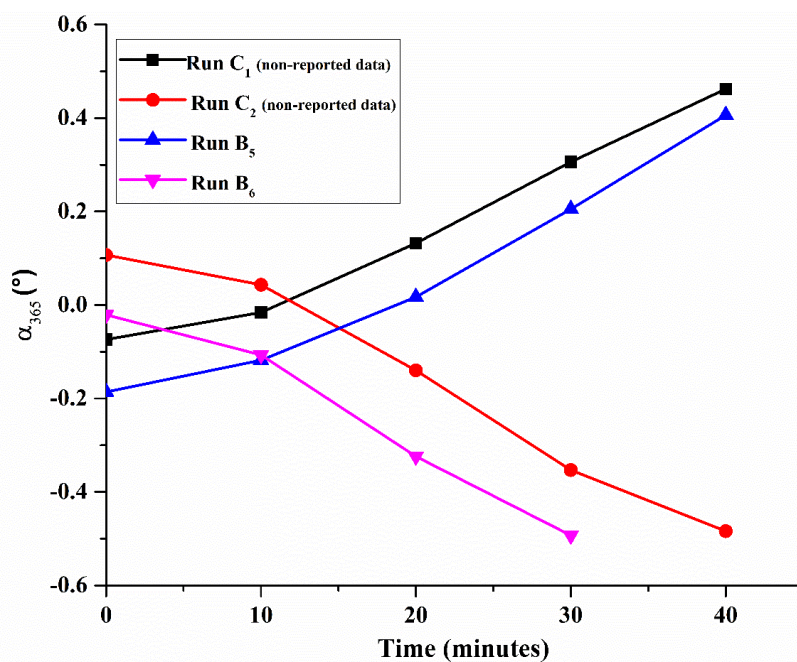


Figure 3.40: Evolution of the rotatory power of the mother liquor during AS3PC mode of cyclohexylammonium chlocyphos.

4.6. SUMMARY OF THE ENTRAINMENT PERFORMANCES

The PC performances of these conglomerates have been assessed via three modes SIPC, AS3PC and ASPreCISE and the results highlight the limitations of the process at 25 ml scale (Table

3.19). The best entrainment (AS3PC mode) to resolve the racemic mixture was achieved with cyclohexylammonium chlocyphos.

Table 3.19: summary of the entrainment performances

Chlocyphos alkyl-amine	PC mode	Mean OP (% ee)	Mean Yield (%)	Mean ee _r (% ee)	Absolute structure (Flack) parameter
Butyl	ASPreCISE	94.8	9.5	7.5	-0.17 (10)
Isobutyl	SIPC / AS3PC	88.5 / 94.6	6.8 / 9.3	3.4 / 5.0	0.29 (9)
Hexyl	SIPC / AS3PC	75.0 / 87.6	3.3 / 4.4	2.6 / 2.9	0.15 (14)
Cyclohexyl	AS3PC	91.8	10.9	5.8	0.30 (1)

Because a metastable racemic phase has been spotted at room temperature and the high value of the absolute structure parameter (Flack parameter = 0.52 (16)) of its conglomerate forming system, it was intentionally decided to not perform the chiral resolution of the pentylammonium chlocyphos.

4.7. PARAMETERS LIMITING THE PC PERFORMANCES OF CHLOCYPHOS DERIVATIVES

Several difficulties can be encountered when preferential crystallization is used to separate racemates. One or several of the following reasons could be suspected to cause the severe limitations of the PC performances for this family of conglomerates.

4.7.1. High value of Flack parameter

In fact, comparisons between Flack parameters and the performances of PC for these conglomerates suggest possible epitaxies and then possible multi-epitaxy or alternated growth between the two enantiomers (Table 3.19). Crystals of one enantiomer could grow on the surface of the other and lead to lamellar particles^{39,40} with (*R*)-(*S*) alternation despite the existence of a stable conglomerate. Epitaxial racemic conglomerate^{11,41–46} hamper the entrainment and lead to low yield.

4.7.2. Evidence of multi-epitaxy

To verify this possible epitaxy hypothesis, a single crystal grown from the racemic mixture of isobutylammonium chlocyphos was soaked in a saturated solution of (*S*)-isobutylammonium chlocyphos for 30 minutes according to a well-established procedure^{11,42,37}, but no partial dissolution of the immersed crystal was observed by optical microscopy. The α ratio < 2 (α = molar solubility of the racemic mixture (9.92×10^{-3} mol. L⁻¹) / molar solubility of the pure enantiomer (5.12×10^{-3} mol. L⁻¹) is not favourable for that type of demonstration.

To study the possible existence of the multi-epitaxy of isobutylammonium chlocyphos, we analysed by SHG (Second Harmonic Generation) technique, several mixtures with different enantiomeric excesses (0-100%) that were prepared in two different manners:

- physical mixtures of (*R*) and (*S*),
- recrystallized mixtures of (*R*) and (*S*) in ethanol by slow evaporation.

In order to homogenize the particle size distribution, these powder samples were gently ground by using mortar and pestle. The SHG intensities were normalized by using α -quartz (45 μm average size). The analyses show that the SHG intensity remains constant for the physical mixture whatever the enantiomeric excess. By contrast, the recrystallized samples show a maximum intensity for the racemic composition (Figure 3.41).

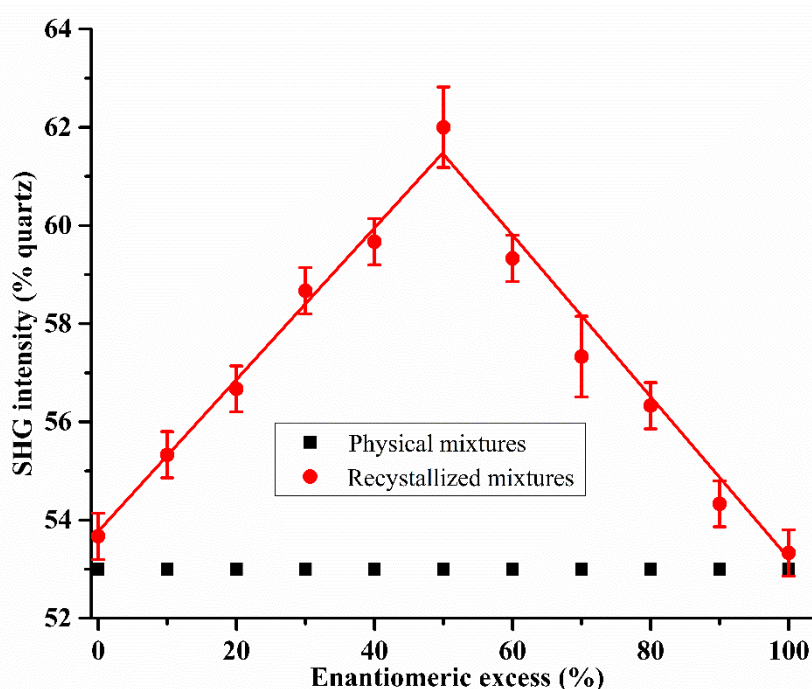


Figure 3.41: SHG efficiency normalized with α -quartz (45 μm average size) of physical mixture (black) and recrystallized mixtures with different enantiomeric excess (red) of isobutylammonium chlocyphos.

The difference between the SHG efficiency of the physical mixture and the recrystallized mixture for a same enantiomeric composition corresponds to the existence of microstructures between (*R*) and (*S*) crystals. It means that the dissolved enantiomer is likely to nucleate on the crystal of the opposite handedness during the crystal growth in the medium⁴⁷. This phenomenon induces the creation of a bi-dimensional interface between these two crystals of opposite chirality, and the resulting solid is not enantiomerically pure. This phenomenon is known as multi-epitaxy. Therefore, this structural behaviour leads to poorly enriched solid and could limit the PC performances.

4.7.3. The problem of insufficient solubility variation over temperature

The temperature dependence of the racemic mixture solubility has also a strong influence on the yield and should obviously be taken into account to analyse the PC performances of these salts. For these conglomerates, the slope (wt% K⁻¹) of the solubility versus temperature is low (see Figures 3.35; 3.36; 3.37 and 3.39) and thus, consistent with a poor productivity.

PC could also be limited by several other parameters like uncontrolled hetero nucleation of the antipode or presence of a metastable racemic compound. However, the XRPD analyses of the crops did not reveal any metastable racemic compound. The low productivity might also come from kinetics i.e. the stereoselective crystallization is very slow. In this case, the nucleation of the dissolved enantiomer occurs before a significant amount of the desired enantiomer has been crystallized. This limitation is, for instance, consistent with the results in AS3PC mode for hexylammonium chlocyphos salt. Indeed, for an initial racemic mixture mass of 2.335 g, we collect less than 0.25 g for a volume of 25 ml.

Hence, several features converge to justify a limited entrainment effect within this series of stable conglomerates.

PART 5. CONCLUSION AND PROSPECTS

Through this study, we have demonstrated that chlocyphos, crystallizing as a stable racemic compound (space group: $P-1$), forms with alkyl amine family a series of stable conglomerate salt derivatives. The SHG pre-screening technique pointed out seven salts as potential conglomerates. Their crystal structure, determined by SC-XRD, revealed among them, six derivatives as stable conglomerates in a large domain of temperature (i.e. room temperature to fusion). Interestingly, the salt with the smallest cation (ethylammonium chlocyphos) crystallizes as a conglomerate with partial solid solutions and the limits of its symmetrical monophasic domains were evaluated using binary phase diagram. This study features an interesting propensity between chlocyphos and alkyl-amines to form a family of conglomerates with close analogy between their crystal packings. There is a pocket in which various alkyl-amine chains can fit in without disturbing significantly the crystal packing.

Preferential crystallization is demonstrated to be feasible, but every derivative tested leads to a limited entrainment effect (enantiomeric excess of the mother liquor at the end of the entrainment (ee_f) does not exceed 10% ee). Consistently one can observe that: (i) several Flack parameters of crystals grown in racemic mixtures cast some doubts on the ability of those crystals to grow without epitaxy or heterochiral nucleation. This hypothesis is reinforced by the SHG intensity versus enantiomeric excess evolution of recrystallized samples; (ii) some metastable racemic compounds have been spotted which indicate that the energetic differences between the homochiral and the heterochiral interactions in the solid state are close; (iii) under moderate supersaturation the kinetics of stereoselective crystal growth is rather slow and for a high supersaturation there is a complete loss of stereoselectivity.

The homogeneity in the PC performances for the members of this family confirms a trend that has been observed on the few systematic studies among other families of conglomerate forming systems. Nevertheless, more investigations are necessary on homogeneous series of conglomerates to propose that early statement as a rule.

Reconsidering certain conditions, such as the choice of the solvent, the stereoselectivity during the crystal growth of pure enantiomers and the growth rate are necessary for a successful separation of enantiomers with PC. Associating these features with an additional online polarimeter (for the determination of optical purity of the solid and liquid phases) would possibly extend the advantageous operating mode for PC.

Screening racemizing agents for these stable conglomerates could also be suitable to achieve a fully chiral separation of enantiomers. Once, these conglomerates are racemized in solution

prior to the deracemization via temperature cycling (TCID), Viedma ripening or SOAT process.

REFERENCES

- (1) Hoeve, W. T.; Wynberg, H. The Design of Resolving Agents. Chiral Cyclic Phosphoric Acids. *J. Org. Chem.* **1985**, *50* (23), 4508–4514.
- (2) Nieuwenhuijzen, J. W. Resolutions with Families of Resolving Agents: Principles and Practice, University of Groningen, Netherlands, 2002.
- (3) Dalmolen, J. Synthesis and Application of New Chiral Amines in Dutch Resolution: Family Behaviour in Nucleation Inhibition, University of Groningen, Netherlands, 2005.
- (4) van der Haest, A. D.; Wynberg, H.; Leusen, F. J. J.; Bruggink, A. Towards a Rational Design for Resolving Agents. Part V: Substituent Effects in the Resolution of Ephedrine Using a Series of Cyclic Phosphoric Acids. *Recl. des Trav. Chim. des Pays-Bas* **1993**, *112* (3), 230–235.
- (5) Leusen, F. J. J. Crystal Structure Prediction of Diastereomeric Salts: A Step toward Rationalization of Racemate Resolution. *Cryst. Growth Des.* **2003**, *3* (2), 189–192.
- (6) Leeman, M. Resolutions of Racemates by Crystallization: Additives and Attrition., University of Groningen, Netherlands, 2009.
- (7) Christmann, M and Brase, S. . . , *Eds. II*, Eds. II.; Wiley-vch, 2012.
- (8) Sheldon, R. A. *Chirotechnology: Industrial Synthesis of Optically Active Compounds*; Marcel Dekker, Ed.; New York -USA, 1993.
- (9) Coquerel, G. Topic in Current Chemistry. In *Novel Optical Resolution Technologies*; Springer GmbH: Berlin, Heidelberg, 2006; Vol. 269, pp 1–51.
- (10) Leeman, M.; Querniard, F.; Vries, T. R.; Kaptein, B.; Kellogg, R. M. Phencyphos by Preferential Crystallization. *Org. Process Res. Dev.* **2009**, *13* (6), 1379–1381.
- (11) Gervais, C.; Beilles, S.; Cardinaël, P.; Petit, S.; Coquerel, G. Oscillating Crystallization in Solution between (+)- and (-)-5-Ethyl-5-Methylhydantoin under the Influence of Stirring. *J. Phys. Chem. B* **2002**, *106* (3), 646–652.
- (12) Kurtz, S. K.; Perry, T. T. A Powder Technique for the Evaluation of Nonlinear Optical Materials. *J. Appl. Phys.* **1968**, *39* (8), 3798–3813.
- (13) Levilain, G.; Coquerel, G. Pitfalls and Rewards of Preferential Crystallization. *CrystEngComm* **2010**, *12* (7), 1983–1992.
- (14) Wacharine-Antar, S.; Levilain, G.; Dupray, V.; Coquerel, G. Resolution of (±)-Imeglimin-2,4-Dichlorophenylacetate Methanol Solvate by Preferential Crystallization. *Org. Process Res. Dev.* **2010**, *14* (6), 1358–1363.
- (15) Nieuwenhuijzen, J. W.; Grimbergen, R. F. P.; Koopman, C.; Kellogg, R. M.; Vries, T.

- R.; Pouwer, K.; Van Echten, E.; Kaptein, B.; Hulshof, L. A.; Broxterman, Q. B. The Role of Nucleation Inhibition in Optical Resolutions with Families of Resolving Agents. *Angew. Chemie - Int. Ed.* **2002**, *41* (22), 4281–4286.
- (16) Sun, F.; Kang, H.; Zhang, K.; Liu, B.; Zhang, B. Solubility of Chlocyphos in Different Solvents. *Fluid Phase Equilib.* **2012**, *330*, 12–16.
- (17) Mbodji, A.; Gbabode, G.; Sanselme, M.; Couvrat, N.; Leeman, M.; Dupray, V.; Kellogg, R. M.; Coquerel, G. Family of Conglomerate Forming Systems Composed of Chlocyphos and Alkyl-Amine. Assessment of Their Resolution Performances by Using Various Modes of Preferential Crystallization. *Cryst. Growth Des.* **2019**, *19*, 5173–5183.
- (18) Jacques, J. ; Collet, A.; Wilen, S. H. *Enantiomers, Racemates and Resolutions*, 3rd ed.; Kriger Pub. Co: Malabar Florida, USA, 1994.
- (19) Flack, H. D.; Bernardinelli, G. Absolute Structure and Absolute Configuration. *Acta Crystallogr. Sect. A Found. Crystallogr.* **1999**, *55* (5), 908–915.
- (20) Schroder, I, Z. Über Die Abhängigkeit Der Löslichkeit Eines Festen. *J. Phys. Chem.* **1893**, *11*, 449–465.
- (21) Van Laar, J. J. Die Scmeltz - Oder Erstarrungskurven Bei Binaren Systemen, Wenn Die Feste Phase Ein Gemish (Amorphe Feste Losung Oder Mishkristalle) Der Beiden Komponentern Ist. *Z. Phys. Chem.* **1908**, *63*, 216–253.
- (22) Leclercq, M; Jacques, J and Collet, A. Mesure de La Stabilité Des Racemiques Vrais. *Tetrahedron* **1975**, *32*, 821–828.
- (23) Bredikhin, A. A.; Zakharychev, D. V.; Gubaidullin, A. T.; Fayzullin, R. R.; Pashagin, A. V.; Bredikhina, Z. A. Crystallization Features of the Chiral Drug Timolol Precursor: The Rare Case of Conglomerate with Partial Solid Solutions. *Cryst. Growth Des.* **2014**, *14* (4), 1676–1683.
- (24) Vippagunta, S. R.; Brittain, H. G.; Grant, D. J. W. Crystalline Solids. *Adv. Drug Deliv. Rev.* **2001**, *48* (1), 3–26.
- (25) Wermester, N.; Aubin, E.; Pauchet, M.; Coste, S.; Coquerel, G. Preferential Crystallization in an Unusual Case of Conglomerate with Partial Solid Solutions. *Tetrahedron Asymmetry* **2007**, *18* (7), 821–831.
- (26) Renou, L.; Morelli, T.; Coste, S.; Petit, M. N.; Berton, B.; Malandain, J. J.; Coquerel, G. Chiral Discrimination at the Solid State of Methyl 2- (Diphenylmethylsulfinyl)Acetate. *Cryst. Growth Des.* **2007**, *7* (9), 1599–1607.
- (27) Taratin, N. V.; Lorenz, H.; Kotelnikova, E. N.; Glikin, A. E.; Galland, A.; Dupray, V.;

- Coquerel, G.; Seidel-Morgenstern, A. Mixed Crystals in Chiral Organic Systems: A Case Study on (R)- and (S)-Ethanolammonium 3-Chloromandelate. *Cryst. Growth Des.* **2012**, *12* (12), 5882–5888.
- (28) Gbabode, G.; Negrier, P.; Mondieig, D.; Moreno, E.; ; Calvet, T.; Cuevas-Diarte, M. À. Fatty Acids Polymorphism and Solid-State Miscibility. Pentadecanoic Acid-Hexadecanoic Acid Binary System. *J. Alloys Compd.* **2009**, *469* (1–2), 539–551.
- (29) Chion, B.; Lajzerowicz, J.; Bordeaux, D.; Collet, A.; Jacques, J. Structural Aspects of Solid Solutions of Enantiomers. The 3-Hydroxymethyl- and 3-Carboxy-2,2,5,5-Tetramethylpyrrolidinyl 1-Oxyl Systems as Examples. *J. Phys. Chem.* **1978**, *82* (25), 2682–2688.
- (30) Lajzerowicz, J.; Chion, B.; Lajzerowicz, J. Two Dimensional Order in a Solid Solution of Molecules of Opposite Chirality. *J. Chem. Phys.* **1981**, *74* (6), 3500–3509.
- (31) Brandel, C.; Petit, S.; Cartigny, Y.; Coquerel, G. Structural Aspects of Solid Solutions of Enantiomers. *Curr. Pharm. Des* **2016**, *22*, 4929–4941.
- (32) Rekis, T.; Berziņš, A. On the Structural Aspects of Solid Solutions of Enantiomers: An Intriguing Case Study of Enantiomer Recognition in the Solid State. *CrystEngComm* **2018**, *20* (43), 6909–6918.
- (33) Tauvel et al. Structural Studies of Several Solvates Potassium Saltsof Tenatoprazole Crystallizing as Conglomerates. *J. Mol. Struct.* **2009**, *936*, 60–66.
- (34) Viedma, C.; Coquerel, G; Cintas, P. *Crystallization of Chiral Molecules. Handbook of Crystal Growth Fundamentals*, II.; Elsevier, 2015.
- (35) Gonella, S.; Mahieux, J.; Sanselme, M.; Coquerel, G. Spotting a Conglomerate Is Just Halfway to Achieving a Preparative Resolution by Preferential Crystallization. *Org. Process Res. Dev.* **2012**, *16* (2), 286–293.
- (36) Pasteur, L. Recherches de L. Pasteur Sur Les Relations Qui Peuvent Exister Entre La Forme Cristalline, La Composition Chimique et Le Sens de La Polarisation, Rotatoire. *C. R. T.* **1849**, *28*, 477–478.
- (37) Mahieux, J.; Sanselme, M.; Harthong, S.; Melan, C.; Aronica, C.; Guy, L.; Coquerel, G. Preparative Resolution of (\pm)-Bis-Tetralone by Means of Autoseeded Preferential Crystallization Induced by Solvent Evaporation (ASPreCISE). *Cryst. Growth Des.* **2013**, *13* (8), 3621–3631.
- (38) Courvoisier, L.; Petit, M. N.; Hedtmann, U.; Coquerel, G. Influence of the Process on the Mechanisms and the Performances of the Preferential Crystallization: Example with

- (±)-5-(4-Bromophenyl)-5-Methylhydantoin. *Chem. Lett.* **2001**, CL-010012, 364_365.
- (39) Kislyi, V. P.; Zubavichus, Y. V.; Babievsky, K. K.; Khrustalev, V. N.; Pivnitsky, K. K. Racemic Estrone Methyl Ether Is the Lamellar Conglomerate. *Mendeleev Commun.* **2019**, 29, 256–259.
- (40) Green, B. S.; Knossow, M. Lamellar Twinning Explains the Nearly Racemic Composition of Chiral, Single Crystals of Hexahelicene. *Science.* **1981**, 214, 795–797.
- (41) Kaptein, B. ; Noorduyn, W. L.; Meekes, H.; Van Enckevort, W. J. P.; Kellogg, R. M.; Vlieg, E. Attrition-Enhanced Deracemization of an Amino Acid Derivative That Forms an Epitaxial Racemic Conglomerate. *Angew. Chemie - Int. Ed.* **2008**, 47 (38), 7226–7229.
- (42) Toyokura, K.; Mizukawa, K.; Kurotani, M. Crystal Growth of L-SCMC Seeds in a DL-SCMC Solution of PH 0.5. In *CGOM3, Am.Chem. Soc.*; 1996; p 72.
- (43) Sadler, D. E.; Davey, R. J.; McEwan, D.; Williams, L. J.; Black, S. N. The Chiral Purity of a Triazolylketone Crystallised from Racemic Solutions. *J. Cryst. Growth* **2002**, 102 (1–2), 97–102.
- (44) Bellies, S.; Cardinael, P.; Ndzié, E.; Petit, S.; Coquerel, G. Preferential Crystallisation and Comparative Crystal Growth Study between Pure Enantiomer and Racemic Mixture of a Chiral Molecule: 5-Ethyl-5-Methylhydantoin. *Chem. Eng. Sci.* **2001**, 56 (7), 2281–2294.
- (45) Zbaida, D.; Lahav, M.; Drauz, K.; Knaup, G.; Kottenhahn, M. A Cyclic Continuous Process for Converting Conglomerates into Optically Pure Enantiomers by Crystallization and Dissolution with the Assistance of ‘Tailor-Made’ Polymers. *Tetrahedron* **2000**, 56 (36), 6645–6649.
- (46) Eupen, J. T. H. Van; Elffrink, W. W. J.; Keltjens, R.; Bennema, P. Polymorphism and Migratory Chiral Resolution of the Free Base of Venlafaxine . A Remarkable Topotactical Solid State Transition from a Racemate to a Racemic Conglomerate. *Cryst. Growth Des.* **2008**, 8 (1), 71–79.
- (47) Simon, F.; Clevers, S.; Gbabode, G.; Couvrat, N.; Agasse-Peulon, V.; Sanselme, M.; Dupray, V.; Coquerel, G. Enhanced Second Harmonic Generation from an Organic Self-Assembled Eutectic Binary Mixture: A Case Study with 3-Nitrobenzoic and 3,5-Dinitrobenzoic Acids. *Cryst. Growth Des.* **2015**, 15 (2), 946–960.

CHAPTER 4: GENERAL CONCLUSION AND PROSPECTS

The main objective of this PhD thesis was to develop an experimental method for screening conglomerate forming-systems in various media and at different temperatures.

To this end, we decide to modify an existing set-up based on the nonlinear optical phenomenon of second harmonic generation (which was initially dedicated to the study of dried powders) in order to allow the set-up to analyse the solid phase in suspension in different solvent.

Several steps were necessary to achieve this goal.

First, the influence of the liquid phase was evaluated through the investigation of crystalline α -quartz in equilibrium with various liquid phases. We showed that in these conditions, the detected SHG intensity depends on the amount of crystalline solid in equilibrium with the liquid phase but also on the volume, the refractive index and the absorption coefficient of the solvent of crystallization. The viscosity of the liquid phase is also to take account as a high viscosity can prevent the sedimentation of the solid phase near the detection window. All these preliminary results led to design and implement a new configuration of the SHG set-up: the *in situ* SHG allowing the detection of the SHG signal in a temperature-controlled batch crystallizer.

The reliability of the *in situ* SHG was then tested by monitoring the crystallization from aqueous solution of potassium dihydrogen phosphate (KDP) which is an inorganic material with a high SHG efficiency as demonstrated in several works^{1,2}. The results obtained from KDP crystal formation highlighted the possibility to use our *in situ* monitoring to track the crystallization of chiral organic compounds or more broadly non-centrosymmetric crystals at the early stages of the process (of course it should be kept in mind that the required condition for the SHG effect to be generated from a crystal is non-centrosymmetry^{3,4}).

According to the results obtained, the possibility to observe a SHG signal from a non-centrosymmetric crystal in equilibrium with its mother liquor necessitates a threshold SHG efficiency of the nonlinear material (e.g. SHG intensity > 5-10% / α -quartz).

The *in situ* SHG was further used to follow the crystal formation of two chiral organic compounds and more precisely the phase transition between a racemic compound and a conglomerate and vice-versa.

- For the first example of histidine monohydrochloride (compound crystallizing as pseudo-polymorph (hydrate) in two hydrated forms: monohydrate and dihydrate), the *in situ* SHG monitoring was not successful due to the low SHG signal (< 1% / α -quartz) of the histidine monohydrochloride monohydrate even though it crystallizes as a conglomerate.

- For the second example of imeglimin propionate crystallizing in three different phases, the *in situ* SHG analysis was applied to follow the transition between the conglomerate (Phase I) and the racemic compound (Phase II). The plot of the SHG intensity versus time exhibited three domains characterized by the presence of one or both solid phases in the suspension.

These results confirmed the potential of the *in situ* SHG to track conglomerates in suspension and to follow the phase transition with of course as an essential condition that one of the phases should be non-centrosymmetric. Furthermore, the strengths of the new SHG device developed herein are the possibility to modify the experimental conditions during the *in situ* monitoring by changing temperature, adding or mixing the solvent of crystallization. There is also the possibility to sample the system at all temperatures at any time to perform complementary measurements such as XRPD to further characterize the solid phase.

Unfortunately, no new metastable conglomerate has yet been detected using the developed *in situ* SHG. Moreover, the weakness of the SHG signal of a non-centrosymmetric crystal constitutes one of the limitations of the *in situ* SHG technique.

Future studies will focus on the search of new candidates to track (metastable or stable) conglomerates in equilibrium with their mother liquors. The experimental results of the *in situ* SHG monitoring of the solid phase transition at various isothermal conditions could also be processed to evaluate the converted fraction over the time during the crystallization and using the Kolmogorov-Johnson-Mehl-Avrami equation⁵⁻⁷ to obtain the activation energy of the molecular change from the Arrhenius equation^{8,9}. *In situ* precise evaluation of crystallization kinetic parameters would also be a significant added value to the technique, especially when dealing with metastable or even transient form (i.e. metastable or efflorescent conglomerates). Finally, a program based on a software (as in the classical-powder SHG technique) will be written for the *in situ* SHG set-up to treat a large number of SHG spectra and to automate the measurements¹⁰. The level of the SHG detection could also be improved by optimizing the collection of the SHG emitted signal.

The rest of the manuscript is focused on the characterization, the search and the resolution of conglomerate derivatives of chlocyphos which belongs to a family of chiral resolving agents. The crystal structure of its racemic mixture and pure enantiomers were resolved by SC-XRD for the first time. We established that chlocyphos crystallizes as a racemic compound (*P-I*, space group) and chlocyphos derivatives crystallizing as conglomerates via the formation of

alkyl-amine salts were screened using the classical SHG technique. The target was to tune the solids to total chiral discrimination that could be used to access to the pure enantiomer of chlocyphos by means of preferential crystallization.

A large survey of strong and weak bases (KOH, NaOH, LiOH, etc.) and amines were used in polar protic solvents to form derivatives that could be crystallized as conglomerate chlocyphos salts. The classical SHG pre-screening technique pointed out seven salts as potential conglomerates. Their crystal structure, determined by SC-XRD, revealed among them, six derivatives (with alkyl-amine) as stable conglomerates in a large domain of temperature (i.e. room temperature to fusion). The methylammonium chlocyphos salt crystallizing as a racemic compound (involved water molecules: sesquihydrate) seems that its alkyl-amine chain is not long enough to stabilize a crystal packing isostructural to that obtained for conglomerates of higher chain length (i.e. starting from propylammonium salt). The ethylammonium salt acts as link between the two distinct phase behaviours occurring as a function of alkyl amine chain length. Indeed, we proved that the salt with the smallest cation (ethylammonium chlocyphos) crystallizes as a conglomerate (as the six salts with longer alkyl chain) but, that is, allowing the presence of the counter enantiomer in the crystal structure of the other enantiomer. The limits of its symmetrical monophasic domains were evaluated by using binary phase diagram and further using XRPD measurements.

With a global view on all the members of the family of chlocyphos conglomerate salts with increasing chain length of alkyl amine moieties, there is a “elongated pocket”, starting from a critical chain length, in which various alkyl-amine chains can fit in (excluding the bulky tert-butyl group) and, these packings are flexible enough to adapt. Thus, we proposed that there are trends for alkyl-amine moieties to form with chlocyphos stable conglomerates.

Preferential crystallization was demonstrated to be feasible, but every derivative tested lead to a limited entrainment effect (enantiomeric excess of the mother liquor at the end of the entrainment (ee_f) does not exceed 10% ee). The PC performances are consistent with the existence of epitaxy (i.e. existence of microstructures as demonstrated) for the crystals grown from the racemic mixture (high value of Flack parameter), metastable racemic compounds and complete loss of stereoselectivity.

The homogeneity in the PC performances for the members of this family confirms a trend that has been observed on the few systematic studies among other families of conglomerate forming-systems. Nevertheless, more investigations are necessary on homogeneous series of conglomerates to propose that early statement as a rule.

One of the important results from this work is the propensity of alkyl-amine to form with chlocyphos stable conglomerates by increasing the length (up to a certain limit) of the alkyl-amine. This could be applicable to the phencyphos and anicyphos for future works to spot conglomerate derivatives of those compounds.

Another interesting result is the use of XRPD measurements to demonstrate the existence of partial solid solutions by evaluating the peak shifts over the enantiomeric composition. Moreover, the mechanism behind solid solutions is rather complex because its enantiomers are arbitrarily distributed within the crystallographic molecular sites. Further investigation would be needed to determine the crystal structure of the solid solution (additional trials of single crystal growth and crystal structure determination from X-ray powder data) and hence get some insights in the crystal packing of both enantiomers in the unit cell.

Even though, there were several parameters that have hampered the chiral resolution of these stable conglomerates, the PC performances were promising. So, for perspective works, investigating the racemization conditions of these chlocyphos conglomerate salts could allow their complete chiral separation via deracemization using Temperature cycling (TCID) or SOAT process.

REFERENCES

- (1) LeCaptain, D. J.; Berglund, K. A. Applicability of Second Harmonic Generation for in Situ Measurement of Induction Time of Selected Crystallization Systems. *J. Cryst. Growth* **1999**, *203* (4), 564–569.
- (2) Delfino, M. A Comprehensive Optical Second Harmonic Generation Study of the Non-Centrosymmetric Character of Biological Structures. *J. Biol. Phys.* **1978**, *6* (3–4), 105–117.
- (3) Kurtz, S. K.; Perry, T. T. A Powder Technique for the Evaluation of Nonlinear Optical Materials. *J. Appl. Phys.* **1968**, *39* (8), 3798–3813.
- (4) Franken, P. A.; Ward, J. F. Optical Harmonics and Nonlinear Phenomena. *Rev. Mod. Phys.* **1963**, *35* (1), 23–39.
- (5) Avrami, M. Kinetics of Phase Change. II Transformation-Time Relations for Random Distribution of Nuclei. *J. Chem. Phys.* **1940**, *8* (2), 212–224.
- (6) Avrami, M. Granulation, Phase Change, and Microstructure Kinetics of Phase Change. III. *J. Chem. Phys.* **1941**, *9* (2), 177–184.
- (7) Avrami, M. Kinetics of Phase Change. I: General Theory. *J. Chem. Phys.* **1939**, *7* (12), 1103–1112.
- (8) Bamford, C. H.; Tipper, C. F. H. *Reactions in the Solid State*; Elsevier: Amsterdam, 1980.
- (9) Connors, K. A. *Chemical Kinetics: The Study of Reaction Rates in Solution*; VCH Publishers, Inc: New York -USA, 1990.
- (10) Clevers, S. Prototyping of In-Situ Optical Methods to Characterize Organic Molecular Crystals, University of Rouen-France, 2014.

APPENDICES

APPENDIX I : EXPERIMENTAL CONDITIONS

1. X-Ray Powder Diffraction (XRPD)

XRPD measurements were carried out on a D8 Discover diffractometer (Bruker analytical X-ray Systems) with Bragg–Brentano geometry, in θ/θ reflection mode (Figure A. I-1). The instrument was equipped with a copper anticathode (40 kV, 40 mA, $K\alpha$ radiation: 1.5418 Å), and a Lynxeye linear detector.

- For the racemic and pure enantiomer samples, the diffraction patterns were collected by steps of 0.04 ° (in 2-theta) over the angular range 3-30°, with a counting time of 4 seconds per step.
- For the intermediate composition mixtures, the diffraction patterns were collected by steps of 0.02 ° (in 2-theta) over the angular range 8-40°, with a counting time of 1 second per step (2.5 hours, accumulated long-time acquisition). NaCl was used as internal standard. Its peak (indicates par * in the XRPD patterns) is taken as a reference peak to compare the peaks shifted for different composition mixtures [60.2-100%].

Powder samples were placed onto a flat frosted glass and analysed at room temperature.



Figure A. I-1: Photography of the XRPD used for this work

2. Single Crystal X-Ray Diffraction (SC-XRD)

The chosen crystal was stuck on a glass fibre and mounted on the full three-circle goniometer of a Bruker SMART APEX diffractometer (MoK α_1 radiation: $\lambda = 0.71073 \text{ \AA}$) with a CCD area detector (Figure A. I-2). The cell parameters and the orientation matrix of the crystal were preliminarily determined by SMART Software¹. Data integration and global cell refinement were performed with SAINT Software. Intensities were corrected for Lorentz, polarization, decay and absorption effects (SAINT and SADABS Softwares) and reduced to F_o^2 . The program package WinGX³ was used for space group determination, structure solution and refinement. The standard space group was determined from systematic extinctions and relative F_o^2 of equivalent reflections. The structure was solved by direct methods (SHEL-XS)⁴. Anisotropic displacement parameters were refined for all non-hydrogen atoms using (SHEL-XL⁵) available with the WinGX³ package. All hydrogen atoms were located from subsequent difference Fourier syntheses and fixed geometrically according to their environment with a common isotropic factor.



Figure A. I-2: Photography of the SC-XRD used for this work

- (1) SMART for WNT/2000 Smart software reference manual. 2001, 5, 622.
- (2) SAINT+ Saint Software reference manual. 1999, 6, 2.
- (3) Farrugia, L. J. WinGX suite for small-molecule single-crystal crystallography. *Appl. Cryst.* **1999**, 32, 837-838.
- (4) Altomare, A et al. Completion and refinement of crystal structures with SIR92. *Appl. Cryst.* **1993**, 26, 343-350.
- (5) Sheldrick, G. M. et al. SHELXL: High-resolution refinement. *Macro. Cryst.* **1997**, 277, 319-343.

3. Differential Scanning Calorimetry (DSC)

The DSC analyses were carried out on a Netzsch DSC 214 Polyma apparatus (Figure A. I-3) operating under a constant flow of helium. For these measurements, ca. 8.00 ± 0.10 mg or 9.00 ± 0.10 mg of samples with various enantiomeric compositions were prepared in a 25 μ L closed aluminium crucible. A heating rate of 5 K min^{-1} or 10 K min^{-1} was applied for all experiments in the 20-350 $^{\circ}\text{C}$ temperature range. Data obtained were evaluated using the Netzsch Proteus Thermal Analysis Software.

- For the pure crystalline phases, the melting temperature was taken from the onset temperature within the heat flux/temperature plot.
- For the composition mixtures, the eutectic melting temperature was taken from the appropriate onset temperature and peak values were used to determine the end of the melting at the liquidus line.



Figure A. I-3: Photography of the DSC apparatus used in this work

4. Thermogravimetric Analysis (TGA)-DSC

The mass composition (in water) were performed using a TGA-DSC NETZSCH STA 449 C instrument under a helium atmosphere (constant flow of 40 mL/min) (Figure A. I-4). Each DSC run was performed with few mg of a powdered sample (9.00 ± 0.05 mg) 25 μ L closed aluminium crucible. Measurements were carried out with heating/cooling rates of 5 K min^{-1}

in the of 20-200 °C. The Netzsch Proteus Thermal Analysis Software were used for data evaluating.



Figure A. I-4: Photography of the TGA-DSC apparatus used in this work

5. Polarimetry

An Anton Paar-MCP5100 (Figure A. I-5) is an automatic polarimeter for the analysis of the optical rotation of chiral substances. Each sample was prepared with $ca. 10.00 \pm 0.05$ mg of powder dissolved in 2 ml of solvent. The chosen standard wavelength is $\lambda = 365$ nm, standard temperature is typically $T = 20$ °C and the tube length (optical pathway) equal to $L = 10$ cm. The enantiomeric purities of the crops were determined from the optical rotation of the crops.



Figure A. I-5: Photography of the Polarimeter used in this work

6. Second Harmonic Generation Microscopy (SHGM)

The measurements were carried out by a laser scanning microscope set at 860 nm (Figure A. I-6). Powder samples were deposited in a glass microscope slide and imaged. The SHG signal emitted was collected with a bandpass filter.

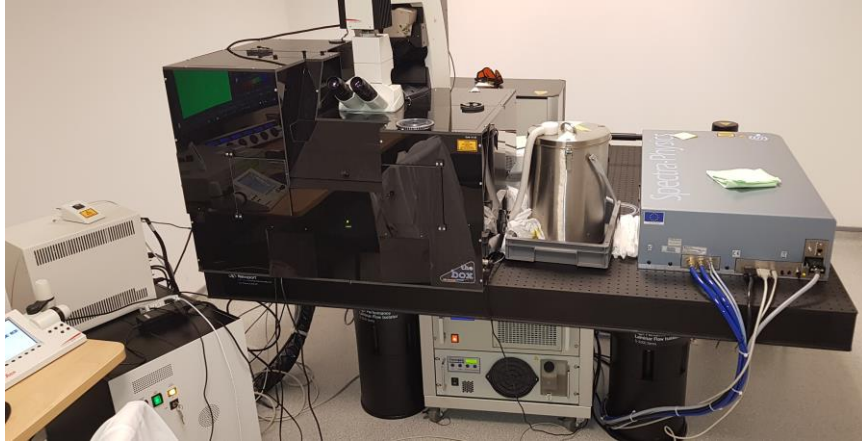


Figure A. I-6: Photograph of the SHG microscopy used in this work

APPENDIX II: DEVELOPMENT OF *IN SITU* MONITORING

In situ SHG set-up

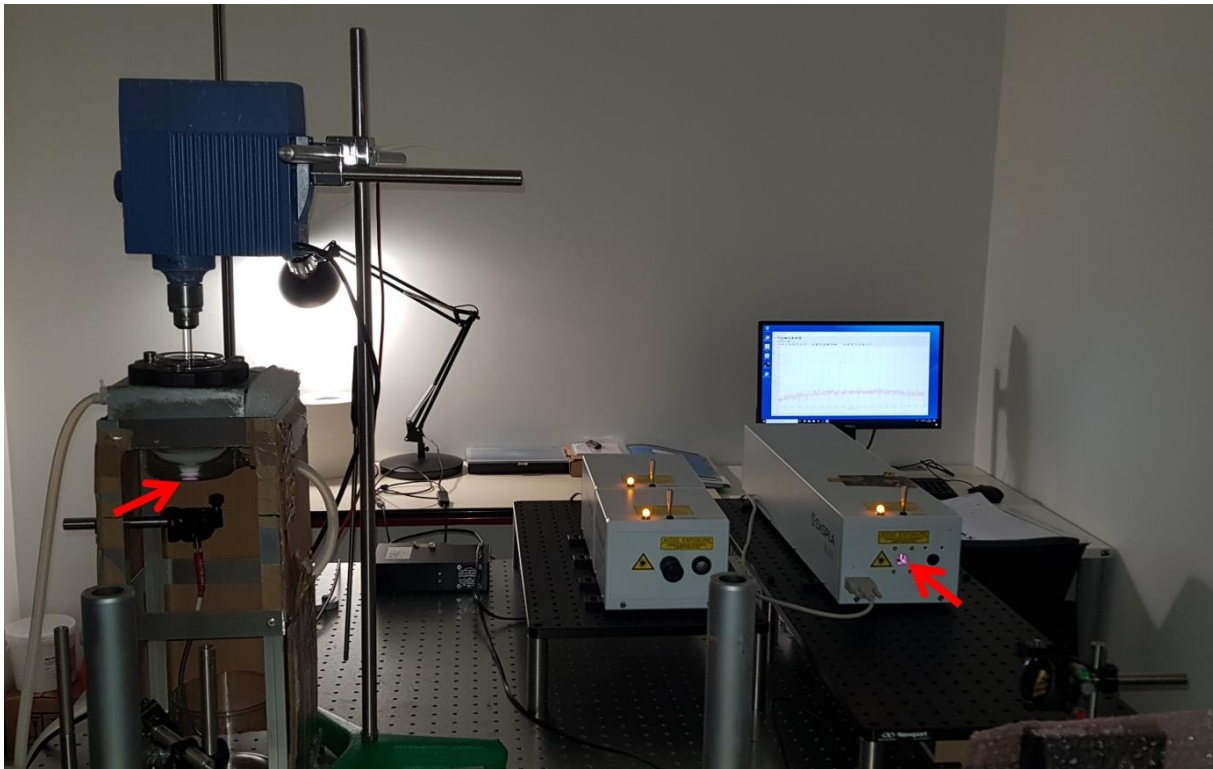


Figure A. II-1: Photograph of the *in situ* SHG set-up used in this work

APPENDIX III: CHLOCYPHOS SALTS

1. Calculated and experimental XRPD patterns

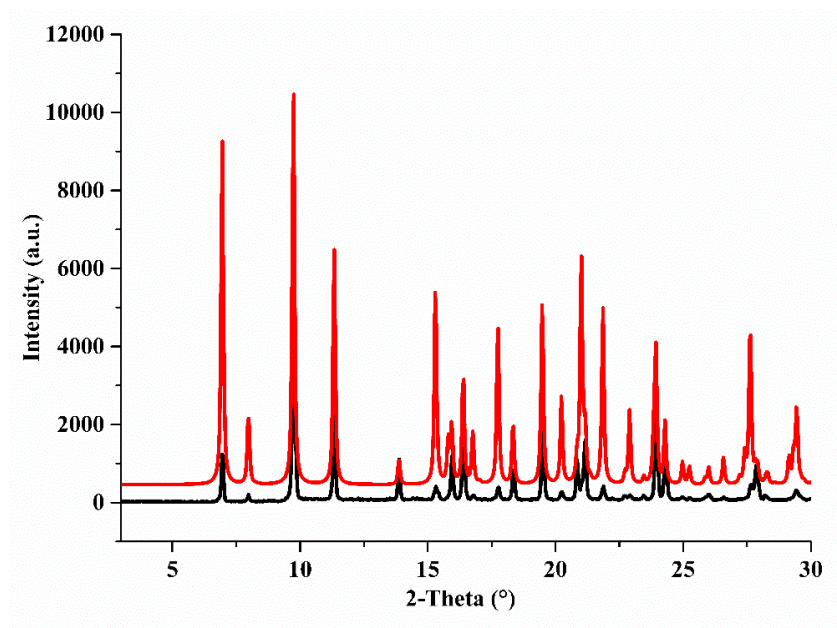


Figure A. III-1: Calculated (red) and experimental (black) XRPD patterns of racemic butylammonium chlocyphos.

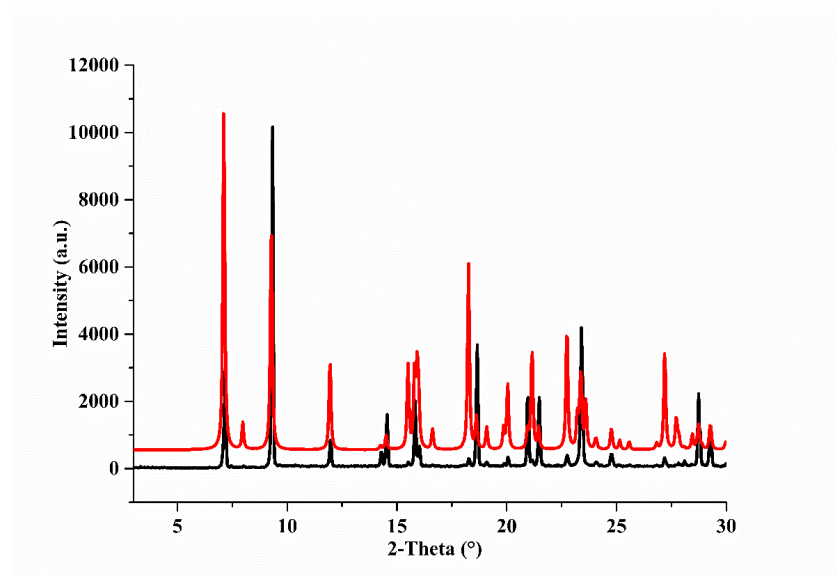


Figure A. III-2: Calculated (red) and experimental (black) XRPD patterns of racemic isobutylammonium chlocyphos

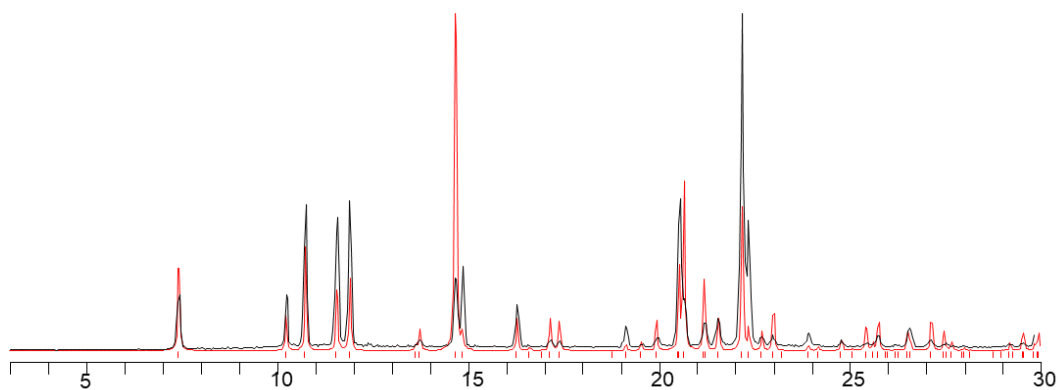


Figure A. III-3: Calculated (red) and experimental (black) XRPD patterns of racemic pentylammonium chlocyphos;

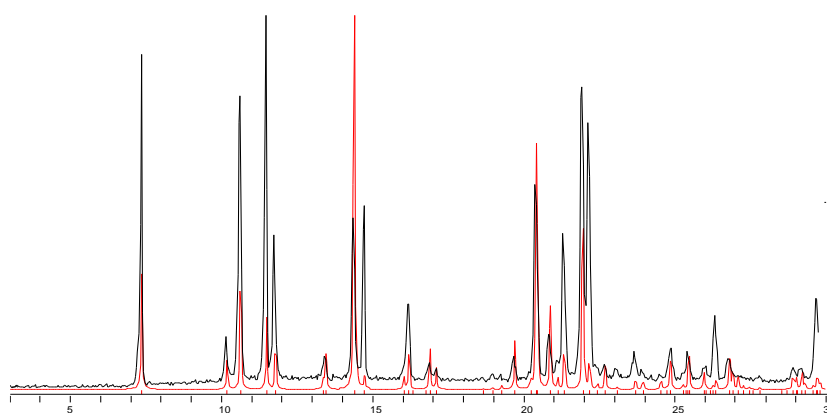


Figure A. III-4: Calculated (red) and experimental (black) XRPD patterns of racemic hexylammonium chlocyphos.

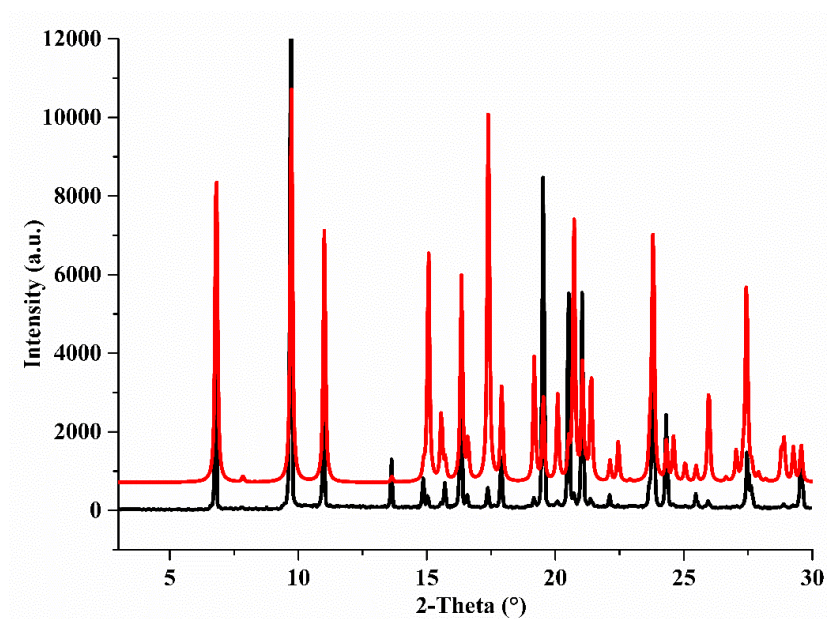


Figure A. III-5: calculated (red) and experimental (black) XRPD patterns of cyclohexylammonium chlocyphos.

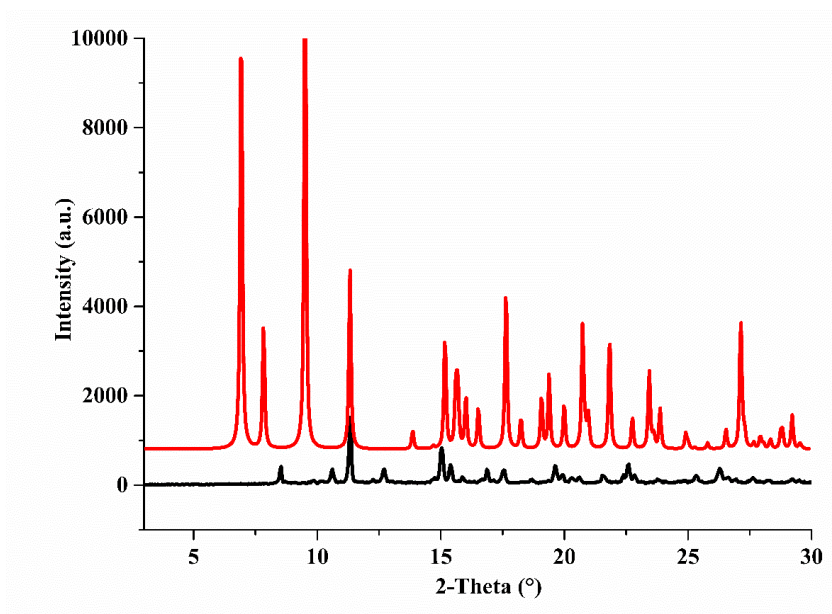


Figure A. III-6: Calculated (red) and experimental (black)XRPD patterns of racemic propylammonium chlocyphos.

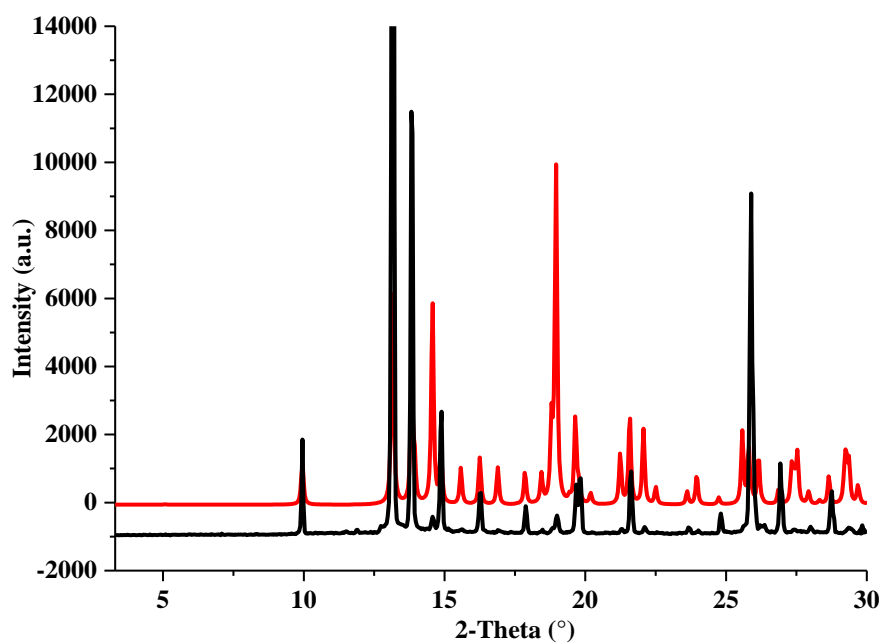


Figure A. III-7: Calculated (red) and experimental (black) XRPD patterns of (S)-ethylammonium chlocyphos.

2. Crystal structure packing

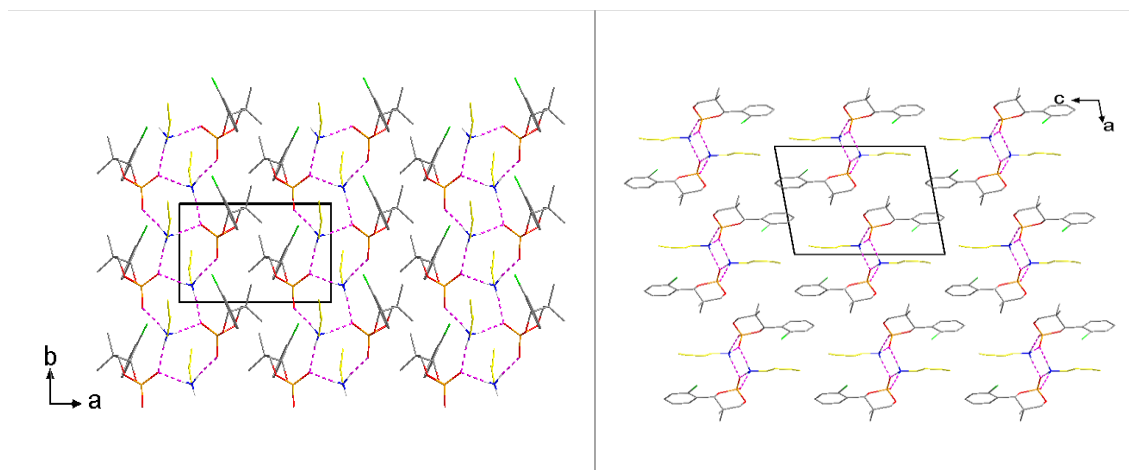


Figure A. III-8: Double row periodic bond chains (hydrogen bonds represented in purple) and the projection of the whole packing along c (left) and b (right) axes for butylammonium chlocyphos. The black rectangles represent a unit cell.

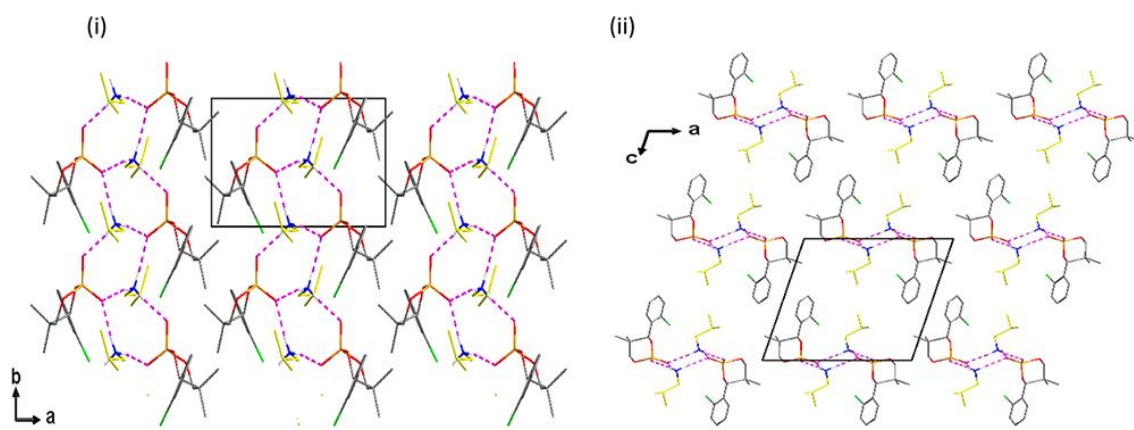


Figure A. III-9: Double row periodic bond chains (hydrogen bonds represented in purple) and the projection of the whole packing along c (left) and b (right) axes for isobutylammonium chlocyphos. The black rectangles represent a unit cell.

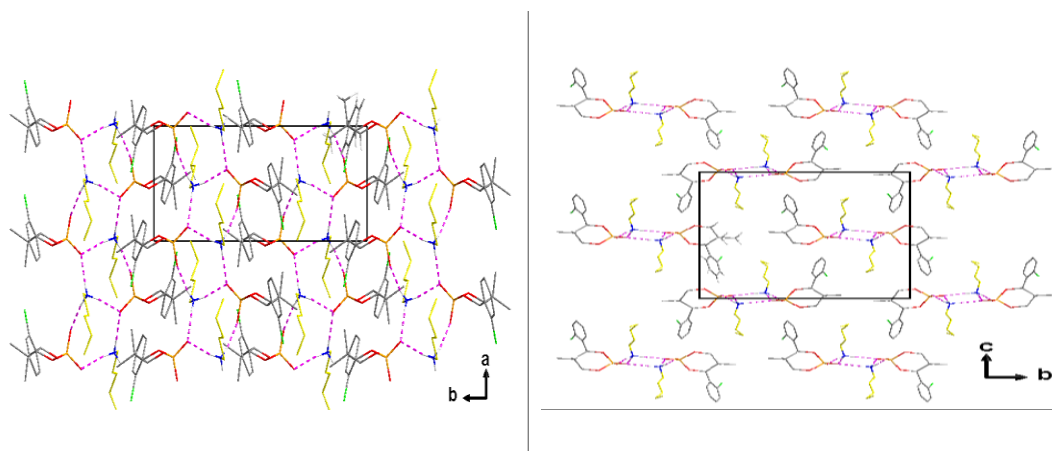


Figure A. III-10: Double row periodic bond chains (hydrogen bonds represented in purple) and the projection of the whole packing along c (left) and a (right) axes for pentylammonium chlocyphos. The black rectangles represent a unit cell.

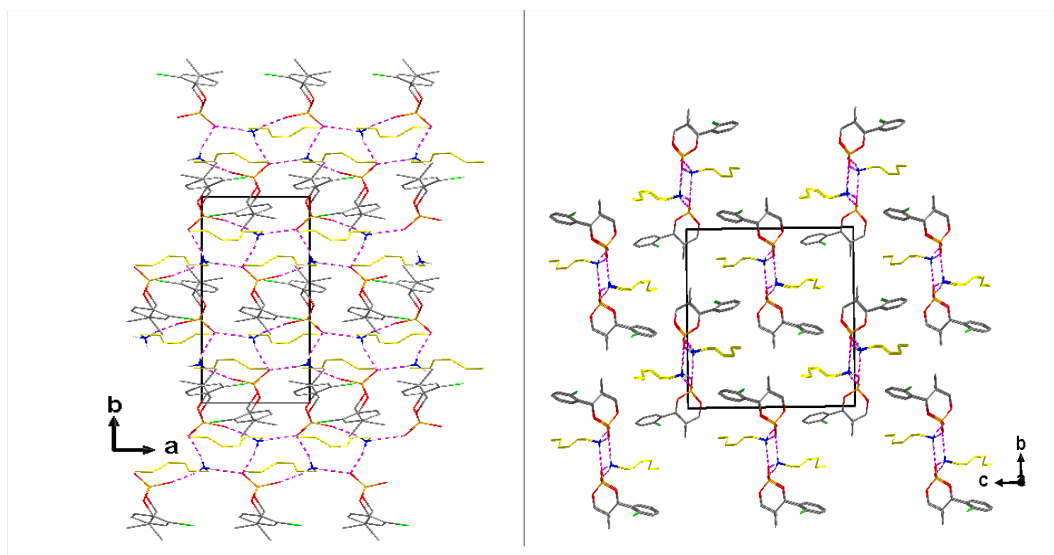


Figure A. III-11: Double row periodic bond chains (hydrogen bonds represented in purple) and the projection of the whole packing along c (left) and a (right) axes for hexylammonium chlocyphos. The black rectangles represent a unit cell.

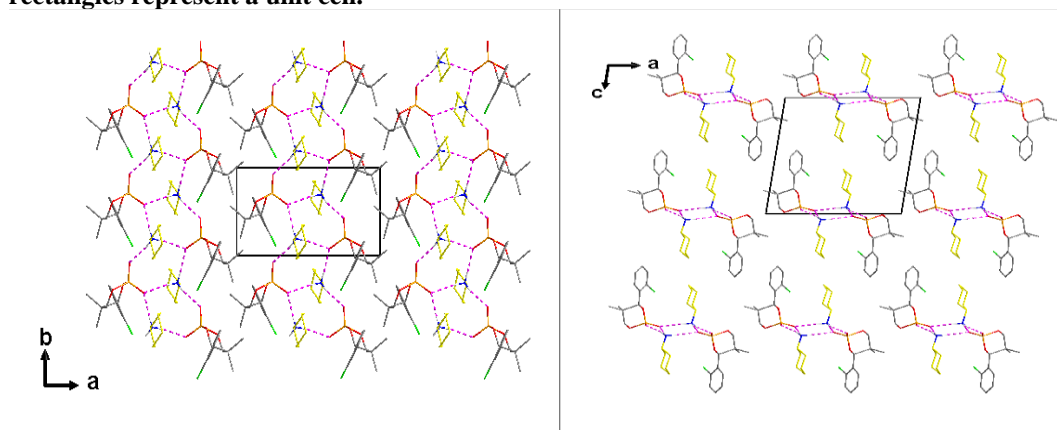


Figure A. III-12: Double row periodic bond chains (hydrogen bonds represented in purple) and the projection of the whole packing along c (left) and b (right) axes for cyclohexylammonium chlocyphos. The black rectangles represent a unit cell.

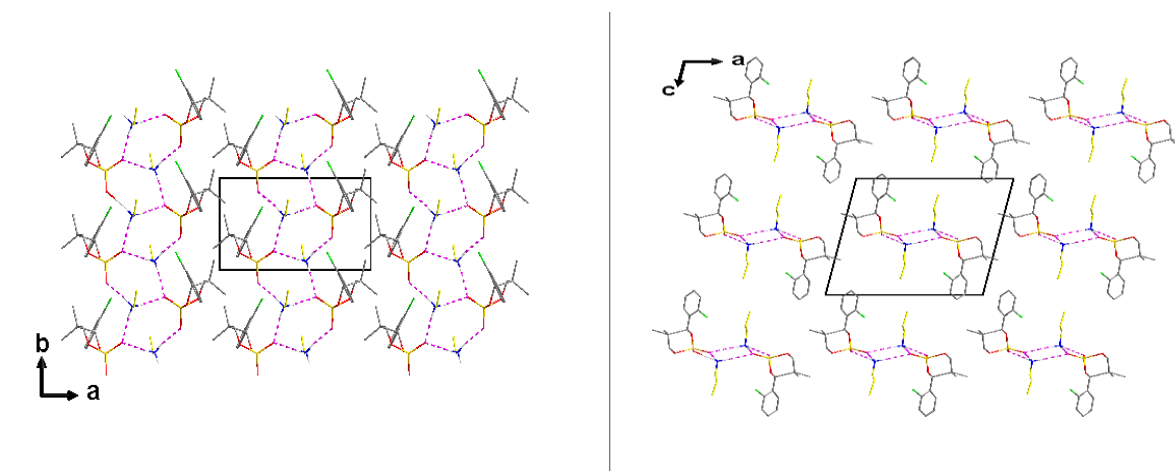


Figure A. II-13: Double row periodic bond chains (hydrogen bonds represented in purple) and the projection of the whole packing along c (left) and b (right) axes for propylammonium chlocyphos. The black rectangles represent a unit cell.

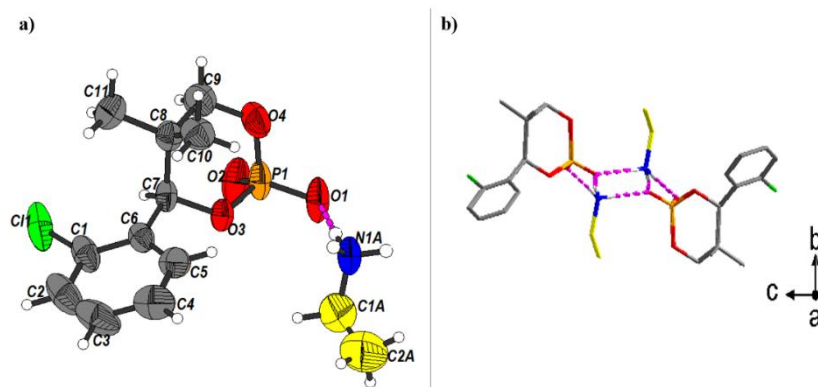


Figure A. III-14: a) Asymmetric unit of (*S*)-ethylammonium chlocyphos, in thermal ellipsoidal representation with labelled atoms and b) Periodic bond chains (PBC) around the 2₁ screw axis formed by the ionic hydrogen bonds. The pink dashed lines represent ionic hydrogen bonds.

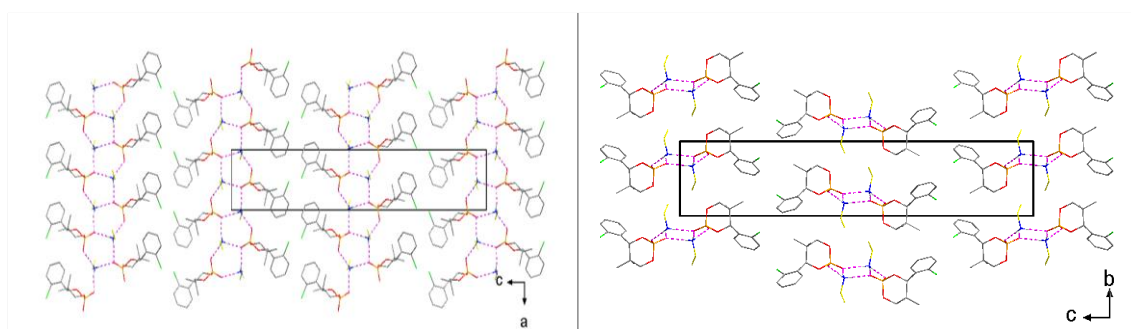


Figure A. III-15: Double row periodic bond chains and the projection of the whole packing along b (left) and a (right) axes for (*S*) and (*R*) ethylammonium chlocyphos. The black rectangles represent a unit cell.

3. Crystallographic data from the enantiopure salts

Enantiomer salt	(<i>R</i>)-butylammonium	(<i>R</i>)-pentylammonium
Chem. Formula	[C ₁₁ H ₁₃ ClO ₄ P] [C ₄ H ₁₂ N]	C ₁₁ H ₁₃ ClO ₄ P] [C ₅ H ₁₄ N]
MW / g mol ⁻¹	349.78	363.81
Crystal system	Monoclinic	Orthorhombic
Space group	<i>P</i> 2 ₁ (n°4)	<i>P</i> 2 ₁ 2 ₁ 2 ₁ (n°19)
Z, Z' (asymmetric units per unit cell)	2, 1	4, 1
<i>a</i> / Å	11.285 (2)	7.0145 (7)
<i>b</i> / Å	6.519 (1)	16.494 (1)
<i>c</i> / Å	12.978 (3)	17.312 (1)
α / °	90	90
β / °	98.733 (3)	90
γ / °	90	90
<i>V</i> / Å ³	943.7 (3)	2002.9 (3)
<i>d</i> _{calc} / g.cm ⁻³	1.231	1.206

F (000) / e^-	372	776
Absorption coefficient μ (MoK α_1) / mm^{-1}	0.302	0.287
N° reflections unique / $I > 2\sigma I$	3786 / 3272	4070 / 3045
Final R1 / wR2 ($I > 2\sigma I$)	0.0478 / 0.1175	0.0570 / 0.1376
Final R1 / wR2 (all data)	0.0548 / 0.1248	0.0771 / 0.1538
Absolute structure (Flack) parameter	-0.06 (8)	0.00 (12)

APPENDIX IV : SCIENTIFIC VALORISATION

1. Publications

Article I: Family of Conglomerate-Forming Systems Composed of Chlocyphos and Alkyl-amine. Assessment of Their Resolution Performances by Using Various Modes of Preferential Crystallization

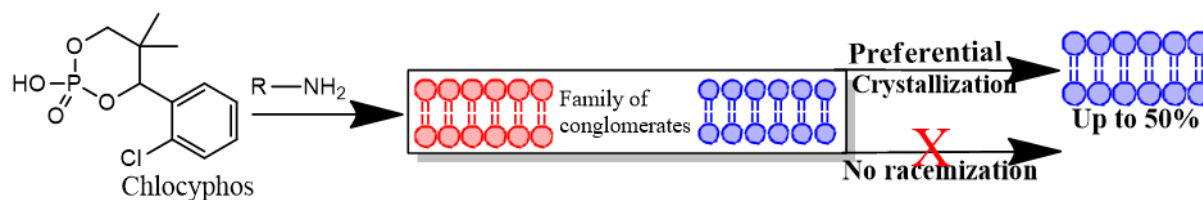


Volume: 19 (9), pp 5173-5183., 2019

[DOI.org/10.1021/acs.cgd.9b00568](https://doi.org/10.1021/acs.cgd.9b00568)

Aliou Mbodji, Gabin Gbabode, Morgane Sanselme, Nicolas Couvrat, Michel Leeman, Valérie Dupray, Richard M. Kellogg, and Gérard Coquerel.

Abstract:



The present study aimed at screening conglomerate derivatives of racemic chlocyphos (4-(2-chlorophenyl)-5,5-dimethyl-2-hydroxy-1,3,2-dioxaphosphorinane 2-oxide) and to perform enantiomeric separation by preferential crystallization. A list of more than 20 chlocyphos salt derivatives were characterized by various techniques (SHG, DSC, and X-ray powder diffraction). A family of salts formed with various alkyl amines crystallizing as conglomerates is evidenced. The first attempts to resolve these conglomerates by preferential crystallization at small scale were successful. The mitigated performances of these entrainments are discussed.

[Article II: Evidence of conglomerate with partial solid solutions in ethylammonium chlocyphos](#)

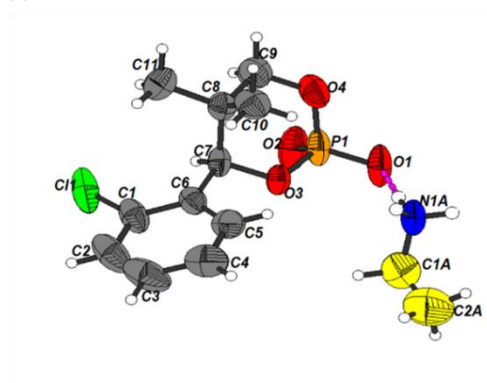
Volume : 20 (4), pp 2562-2569., 2020

DOI: <https://doi.org/10.1021/acs.cgd.9b01699>

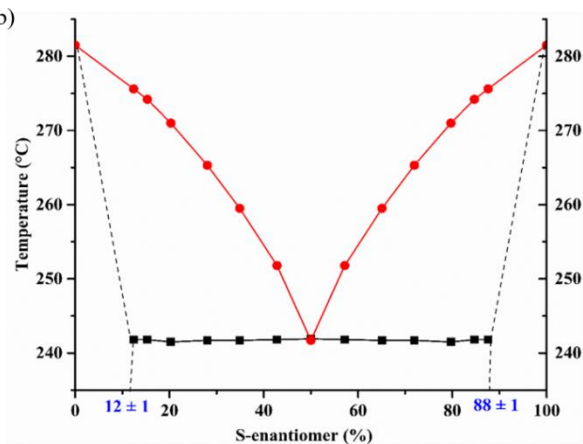
Aliou Mbodji, Gabin Gbabode, Morgane Sanselme, Yohann Cartigny, Nicolas Couvrat, Michel Leeman, Valérie Dupray, Richard M. Kellogg, and Gérard Coquerel.

Abstract:

(a)

(a): Asymmetric unit of (*S*)-ethylammonium chlocyphos

(b)



(b): Binary phase diagram of ethylammonium chlocyphos

Ethylammonium chlocyphos, which crystallizes as a conglomerate with partial solid solution behaviour, also belongs to a family of conglomerate derivatives wherein all the other members of that set lead to complete discrimination in the solid state. The construction of the binary phase diagram and Tammann graph between (*R*)- and (*S*)-ethylammonium chlocyphos serve to determine the limits of the symmetrical solid solutions at: $x = 12 \pm 1\%$ and $x = 88 \pm 1\%$ for the eutectic temperature. The comparison of the XRPD patterns of different composition mixtures of (*S*) and racemic samples confirms the partial miscibility in a similar range in composition at room temperature.

2. Oral communications

Oral I: An experimental conglomerate discovering method. CORE Workshop on Solid State Properties, 6-10 November 2017, Cluj Napoca, Romania.

Aliou Mbodji, Gabin Gbabode, Valérie Dupray, and Gérard Coquerel.

Oral II: Chlocyphos: Conglomerate forming derivatives (salts) for its resolution by preferential crystallization. CORE Summer School on Process Analytical Tools, 16-20 April 2018, Manchester, UK.

Aliou Mbodji, Gabin Gbabode, Valérie Dupray, and Gérard Coquerel.

Oral III: Propensity for Amine Family to Form Conglomerates with Chlocyphos and their Resolutions by Preferential Crystallization. CORE Workshop and Mid-term Review Meeting, 3-4 September 2018, Rouen, France.

Aliou Mbodji, Gabin Gbabode, Valérie Dupray, and Gérard Coquerel.

Oral IV: Applicability of Second Harmonic Generation (SHG) for *in situ* measurement of non-centrosymmetric crystals. CORE Workshop on Chirality in practice, 20-24 May 2019, Groningen, The Netherlands.

Aliou Mbodji, Gabin Gbabode, Valérie Dupray, and Gérard Coquerel.

Oral V: Applicability of Second Harmonic Generation (SHG) for *in situ* measurement of non-centrosymmetric crystals. CORE Workshop and Mini-Symposium on Deracemization of Chiral Compounds, 8-11 October 2019, Erlangen, Germany.

Aliou Mbodji, Gabin Gbabode, Valérie Dupray, and Gérard Coquerel.

3. Poster communications

Poster I: A new device for *in-situ* detection of conglomerate forming systems in suspension by Second harmonic generation. CORE summer school on Chiral Crystallization, Resolution & Deracemization, 3-7 July 2017, Nijmegen, The Netherlands.

Aliou Mbodji, Gabin Gbabode, Valérie Dupray, and Gérard Coquerel.

Poster II: Propensity for amine family to form conglomerates with chlocyphos and chiral separation of chlocyphos hexylamine by preferential crystallization. Solvay international workshop on chiral symmetry breaking at molecular level, 28-30 November 2018, Brussels, Belgium.

Aliou Mbodji, Gabin Gbabode, Morgane Sanselme, Michel Leeman, Valérie Dupray, Richard M. Kellogg, and Gérard Coquerel.

Poster III: Propensity for amine family to form conglomerates with chlocyphos and their resolutions by preferential crystallization BIWIC, 6-7 September 2018, Rouen-France.

Aliou Mbodji, Gabin Gbabode, Morgane Sanselme, Michel Leeman, Valérie Dupray, Richard M. Kellogg, and Gérard Coquerel.

Abstract

The objective of this research project is to develop a method that enables the identification of conglomerates rather than racemic compounds or solid solutions for their chiral resolution by crystallization. Then, evaluate the trends of conglomerate formation.

- The first part of the manuscript is specifically dedicated to the design and implementation of the *in situ* SHG set-up. The new SHG device allows to screen conglomerates in suspensions at various temperatures and in various solvents and to follow phase transition. The reliability of the experimental *in situ* SHG set-up was tested by using inorganic material (Quartz and KDP) which are efficient for SHG effects. The applicability of the method to chiral organic compounds was demonstrated by the study of the solid-solid transition between the conglomerate and the racemic compound phases of histidine monohydrochloride hydrate and imeglimin propionate.
- The second part concerns the characterization of the chiral compound chlocyphos, the search and identification of its conglomerate derivatives and their chiral separation by using preferential crystallization. Crystal structures of the chlocyphos salts are determined by SC-XRD and the strong tendency of alkyl-amine salts to crystallize as conglomerates with similar crystal packing is highlighted. Through careful analysis of their crystal and molecular structures, a trend with respect to alkyl amine moiety length starting from ethyl to cyclohexyl can be established. The elaboration of the binary phase diagram of conglomerate with partial solid solutions in ethylammonium chlocyphos is also investigated.

Résumé

L'objectif premier de cette thèse était de développer une méthode expérimentale qui permet d'identifier les conglomérats des composés racémiques ou des solutions solides pour leur séparation par voie de cristallisation. Ainsi évaluer des tendances de formation des conglomérats.

- La première partie est spécifiquement consacré à la conception et à l'installation de la génération de seconde harmonique (*in situ* SHG). Le nouveau dispositif de la SHG permettra de repérer des conglomérats en solution en variant les températures de cristallisation et de suivre les transformations entre phases auxquelles au moins une phase se cristallise dans un groupe d'espace non-centrosymétrique. La fiabilité de cette méthode expérimentale de SHG est testée en utilisant les composés inorganiques (Quartz et KDP) qui sont efficaces pour l'effet de la SHG. La transversalité de la

méthode pour les composés organiques chiraux a été démontrée par l'étude de la transition de phase entre le conglomérat et le composé racémique du monochlorhydrate hydraté d'histidine d'une part et du propionate de l'iméglimine d'autre part.

- La deuxième partie traite la caractérisation du composé chiral chlocyphos, de la recherche et de l'identification de conglomérats dérivés du chlocyphos et leur séparation chirale par voie de la cristallisation préférentielle. Les structures cristallines des sels du chlocyphos ont été résolues par la diffraction des rayons X sur monocristal (SC-XRD) et la tendance qui s'est dégagée est la formation de conglomérats avec les alkyle-amines à partir de l'éthyle jusqu'au cyclohexyle avec une similarité des structures cristallines. L'élaboration du diagramme de phase binaire du conglomérat avec une solution solide partielle du chlocyphos de l'éthylamine a été abordée.